PROCEEDINGS

SPACE TRANSPORTATION SYSTEM PROPULSION TECHNOLOGY CONFERENCE

APRIL 6 & 7, 1971

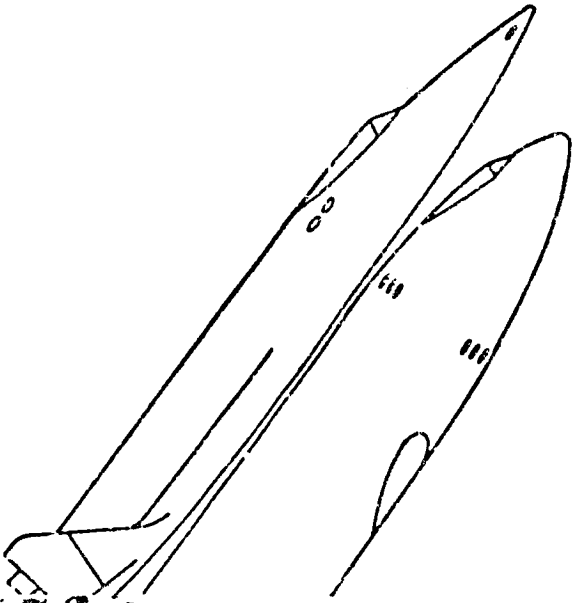

VOLUME I

MAIN PROPULSION

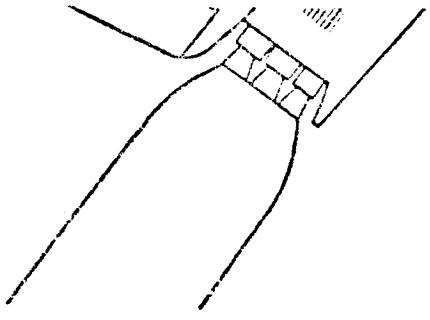

PROCEEDINGS
SPACE TRANSPORTATION SYSTEM
PROPULSION TECHNOLOGY CONFERENCE

APRIL 6-7, 1971

MARSHALL SPACE FLIGHT CENTER

VOLUME I

SESSION I MAIN PROPULSION J. THOMSON, CHAIRMAN

April 28, 1971

D'ETER K. HUZEL
N. AMER. ROCKWELL

DR. HERMAN WEIDNER
MSFC

KARL HEIMBURG
MSFC

THREE SAGES OF THE PROPULSION COMMUNITY

DR. WEIDNER SPEAKS TO A FULL HOUSE

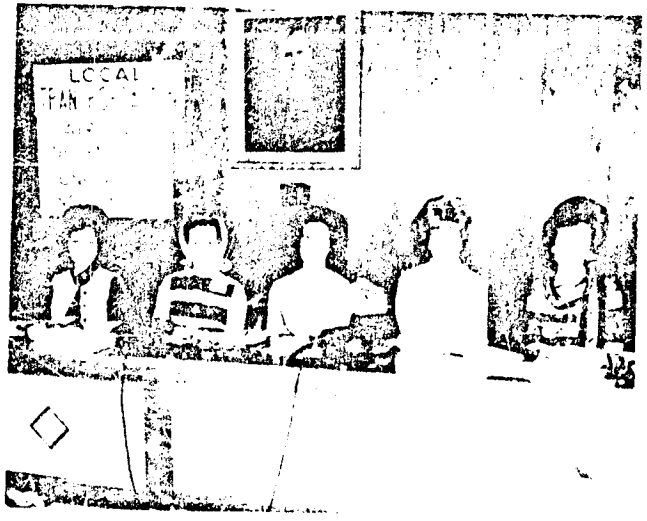

A PLEASING WELCOME TO ATTENDEES

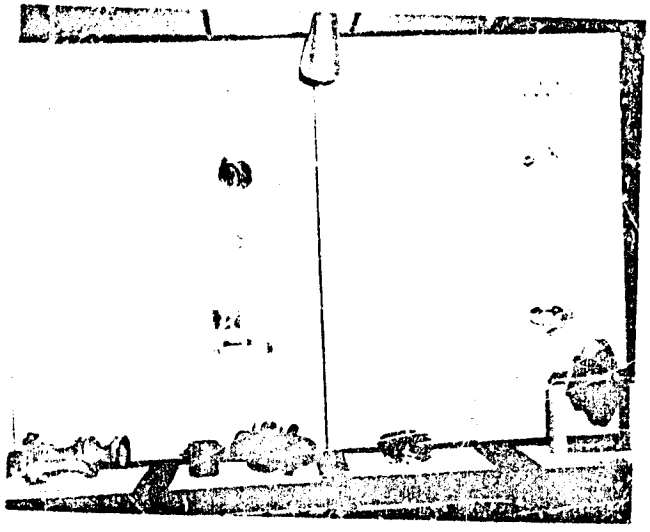

PUMP TECHNOLOGY FOR MAIN ENGINE

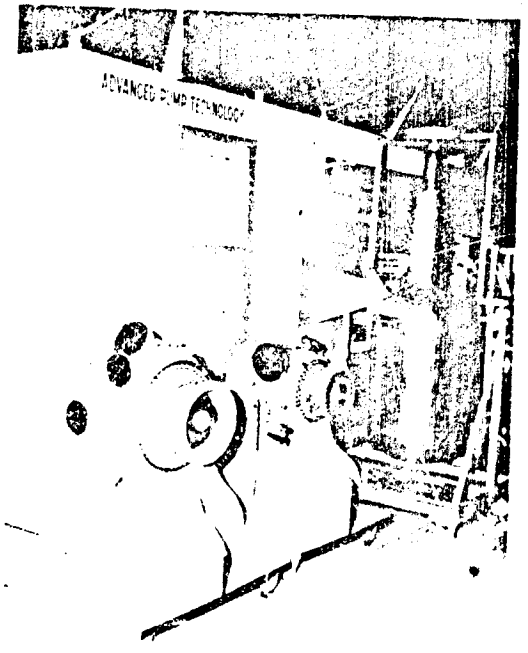

HIGH PRESSURE PUMP TECHNOLOGY
AND TANK-INSULATION RESEARCH

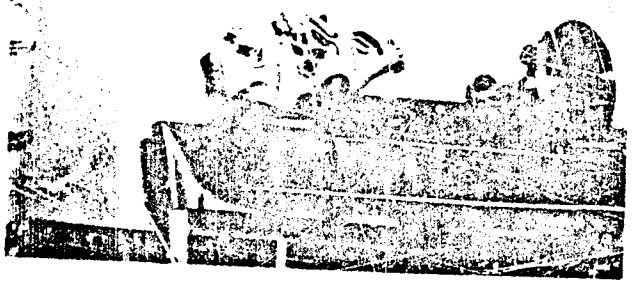

COMPONENTS FOR ACPS

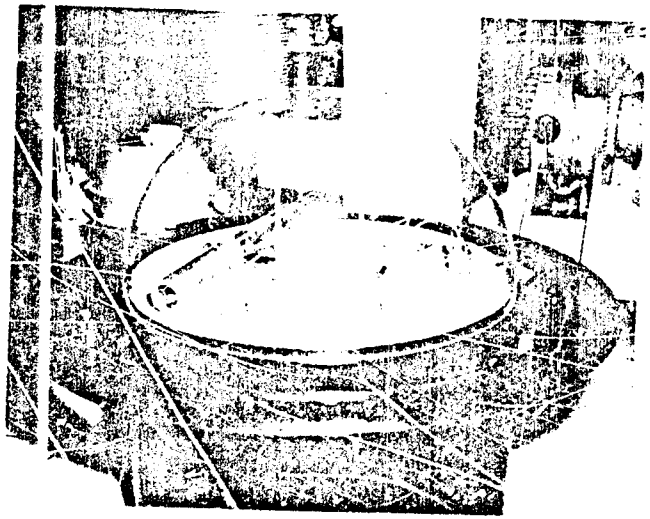

INSTRUMENTATION TECHNOLOGY FOR
SHUTTLE PROPULSION

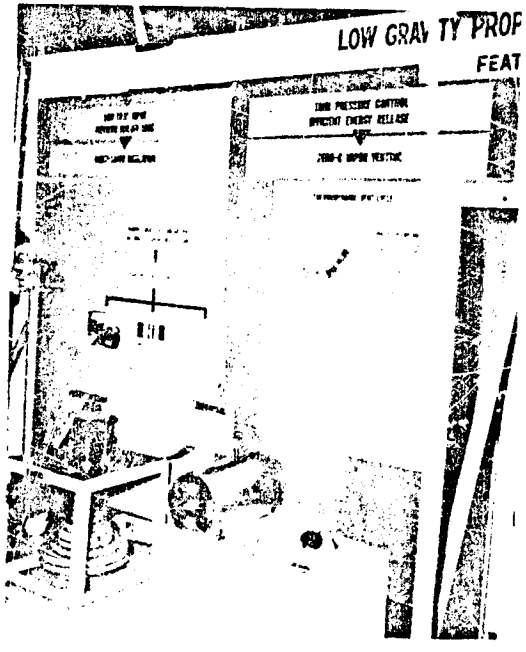

LOW GRAVITY PROPELLANT MANA GEMENT

PROPULSION TECHNOLOGY CONFERENCE PAPERS

VOLUME I MAIN PROPULSION

1.	"Final Results of the XLR-129 Program"	P&W
2.	"Two-Phase Flow LH_2 Pump Inducers"	Rocketdyne
3.	"Saturated LH_2 Turbopump Operation"	MSFC
4.	"Characteristics of Feed System Instabilities"	Martin Marietta
5.	"Combustion Oscillations Damping Devices"	P&W
6.	"Minimum Pressure Loss in High Velocity Flow Duct Systems"	S. R. I.
7.	"Engine Onboard Checkout System Study"	Martin Marietta
8.	"Low Frequency Analysis of Rocket Engines Using Compressible Propellants"	Aerojet
9.	"Titanium Pump Impeller Fabrication and Testing"	Rocketdyne
10.	"Advanced Thrust Chamber (Non-tubular)"	Rocketdyne
11.	"High Pressure Hydrogen Effects on Materials"	MSFC

VOLUME II AUXILIARY PROPULSION

1.	"Hydrogen/Oxygen ACPS Engines"	Rocketdyne
2.	"Hydrogen/Oxygen ACPS Engines"	Aerojet
3.	"High Pressure Reverse Flow ACPS Engine"	Bell
4.	"Space Shuttle ACPS Shutoff Valve"	Marquardt
5.	"Space Shuttle ACPS Shutoff Valve"	Rocketdyne
6.	"Ignition Devices for ACPS"	Aerojet
7.	"Spark and Auto Ignition Devices for ACPS"	Rocketdyne
8.	"Catalytic Ignition/Thruster Investigation"	TRW
9.	"Auxiliary Propulsion Subsystem Investigations"	MSFC
10.	"Injector Performance, Heat Flux and Film Cooling in O_2/H_2 Engines"	MSC
11.	"Auxiliary Propulsion Subsystem Definition Study"	TRW
12.	"Auxiliary Propulsion Subsystem Definition Study"	MDAC
13.	"Acoustic Cavity Use for Control of Combustion Instability"	Rocketdyne
14.	"Noncircular Injector Orifices and Advanced Fabrication Techniques"	Rocketdyne

PROPULSION TECHNOLOGY CONFERENCE PAPERS

VOLUME III AUXILIARY POWER UNIT AND AIRBREATHING PROPULSION

1.	"Auxiliary Power Unit Design Studies"	Airesearch
2.	"Auxiliary Power Unit Design Studies"	Rocketdyne
3.	"H_2 Fuel System Investigation"	G. E.
4.	"Booster and Orbiter Engine Studies"	P&W

VOLUME IV CRYOGENS

1.	"Orbital Cryogenic Acquisition and Transfer"	General Dynamics
2.	"Zero Gravity Incipient Boiling Heat Transfer"	Univ. of Michigan
3.	"Zero Gravity Propellant Transfer"	LeRC
4.	"Recent Developments in High Performance Insulation Purge Systems for Shuttle Application"	MDAC
5.	"Effect of Environment on Insulation Materials"	[illegible]
6.	"PPO Foam Internal Insulation"	General Dynamics
7.	"Internal Insulation Systems for LH_2 Tanks" and "Gas Layer and Reinforced Foam"	MDAC Martin Marietta
8.	"Shuttle Cryogen Technology Program"	MSFC

TABLE OF CONTENTS

VOLUME I

Jerry Thomson, Conference Chairman

Welcome

Good Morning Gentlemen.

I would like to officially open the Space Shuttle Propulsion Technology Conference and get on with our agenda and the business.

My name is Jerry Thomson of Marshall Space Flight Center; and I am the Chairman of the Propulsion Technology Working Group. I will serve as the Conference Chairman for the next two days.

There are some administrative matters and general information that I would like to present to you about the Conference, but first I would like to introduce the Director of Science and Engineering here at the Marshall Space Flight Center; a man very much at home in the field of propulsion. I'm sure most of you already know him. He is Dr. Herman K. Weidner -- Dr. Weidner, please.

[illegible] ADDRESS

Dr. [illegible] Acting Director Science & Engineering MSFC

[illegible] Perry,

Ladies and Gentlemen,

I would like to welcome you all this morning to the George C. Marshall Space Flight Center. We at this center have always been strongly propulsion oriented throughout our entire history and I feel it is very fitting, therefore, that we serve as the host center for this Propulsion Conference.

Our center Director, Dr. Eberhard Rees, was unable to avoid a schedule conflict and had to be away in Washington this week. He regrets that he cannot personally be here and extends his best wishes to this [illegible] in his behalf.

I am very pleased that so many of you were able to accept our invitation to attend this Space Shuttle Propulsion Technology Conference. While glancing over the list of conference participants, I find it to read pretty much like a "Who's Who" in the field of Rocket Propulsion. It represents an impressive cross section of competence in our field, from within NASA and the Department of Defense, from Industry and Universities, as well as from Foreign Countries.

I consider it a special honor to speak to you this morning. Having grown up in the propulsion field myself, I find many good old friends and many well known faces among you in the audience this morning. It brings back memories of many outstanding past accomplishments, which this same team - as it is represented here this morning - has been able to achieve together. The almost flawlessly executed Saturn/Apollo Lunar shots are only the latest and [illegible] example of such deeds. Propulsion people can rightfully claim their share of credit for these achievements.

Rocket propulsion is the most basic of all the disciplines and technologies which make up modern space flight. We cannot go anywhere in space without propulsion devices being brought into play. So it is for good reason that a Saturn/Apollo Space Vehicle designed to execute a variety of different and difficult maneuvers, as it sits ready on its launching pad at Cape Kennedy, is studded with the imposing total number of almost [illegible] individual thrusting devices, and systems of almost any kind, size, or function imaginable. All of them, I am happy to say, have performed very well and exactly as expected.

Within the past dozen years or so, this country has had a total of about 600 successful space flights to her credit. And propulsion devices did their thing in each and every one of them.

I mention these facts merely to point out that our professional specialty field - Space Propulsion - has come of age and has grown to be a dependable tool in our storehouse of engineering skills. All in all, a very impressive and proud record.

But this is no time to rest on our laurels. As of late, a new objective in the field of space transportation is making its even greater demands known. It is calling on the best talents of all of us to do better still. We are heavily banking on the results of your combined efforts and skills to furnish us with the firm technological basis so that we may commit ourselves, with good confidence, to new applications and concepts of advanced propulsive machinery.

It is the purpose then of this Space Shuttle Technology Conference to let us take stock of where we stand today in our efforts and to sense how much still remains to be done.

And I like to wish this conference much success in accomplishing this objective.

I do not want to close here this morning, without saying "Thank you" to all of you who have come, to Jerry Thomson who acts as the Chairman for the whole affair, and to the many session Chairmen and Speakers who have worked so diligently to make this conference possible.

Let me conclude, then, by recognizing one man who is with us here this morning. This man is Del Tischler, from NASA's office of Advanced Research and Technology. He has served for many years directing NASA's Technology efforts in the field of Chemical Propulsion. His leadership has contributed significantly to our past successes and to the state of our art today.

Lately, he has taken on a broader and even more important role in NASA, which is to plan and to pull together the totality of NASA's Shuttle Technology Program. A critically needed and a very difficult task.

I am sure that Del would want to make a few remarks of his own and place the objective of this conference into an even sharper focus.

Thank you,

Del Tischler, Director, Shuttle Technologies Office, NASA Headquarters

Thank you Dr. Weidner.

Good Morning, Gentlemen.

This conference on propulsion and its related area of cryogenic propellant handling is the third of a series of conferences sponsored by OART on the technology programs which support the development of the concept of a fully reusable Space Launch Vehicle.

It has been suggested that this vehicle be called a Space Plane rather than a Shuttle. Space Plane may be a dignified designation. No matter what you call it, its' ability to leave the confinement of the Earth's atmosphere is totally dependent on the performance of rocket equipment. And to do so in two stages (or less, for that matter) while carrying the thermal protection for reentry, the lifting surfaces for aerodynamic flight, and the wheels for landing as well as a crew compartment for human intelligence aboard, demands the utmost in performance of the hydrogen-oxygen-fueled rocket engines planned for this vehicle.

At the beginning of the Saturn/Apollo program such engines were inconceivable. The technological advances since then have created a pregnant situation in which birth of these engines is a matter of nourishment and time. Proposals to develop this equipment are due here in approximately two weeks. While the main engines are technologically in good shape their integration into the vehicle, which embodies propellant vessel, cargo carrier, reentry body, and aircraft, still constitutes a significant problem. The propellant feed lines in the booster stage, for example, contain a volume equivalent to the THOR Missile. Conditioning this bulk of propellants is a problem. The potential for POGO, in which on a La Grangian coordinate scale the pilots and the engines travel alternately in opposite directions, must be countered. Consider that the booster shrinks about a foot when propellants are put aboard and you begin to appreciate that the intra-vehicular motions are not of negligible magnitude.

Furthermore these vehicle stages need mechanisms for directional control, and in the orbiter, for translation between orbits. The problems of the Auxiliary Propulsion Systems and the orbit maneuvering system, both of which are fed high-pressure gaseous propellants from a low pressure liquid propellant tank source, cannot be regarded as proportional to the thrust of their combustors. Our experience with the generation of high pressure gas in flight and the use of gaseous combustion systems is extremely limited. And so there is a lot to learn, define, and verify about such systems in the next two years.

Finally both stages need to return to the launch/landing site. The orbiter gets there the long way, and can make it without airbreathing engines with sacrifice in maneuver and go-around capability at the landing site. The booster, however, will have to bore its way through 350 miles of atmosphere to get back to base. This job requires good airbreathing turbojet engines of large size.

Until these systems work, the Space Plane, or Shuttle, will go no where. Thus we can conclude that this conference will cover the most vital as well as challenging areas of work necessary to the Space Plane's successful operation.

To get on with it, may I promptly turn the business of running this show over to Jerry Thomson of MSFC, who has been chiefly responsible for organizing it.

Working Group Report

Jerry Thomson:

As you may have noted from the agenda this Conference is divided into five sessions. They are:

I.	Main Propulsion	J. Thomson, Chairman
II.	Auxiliary Propulsion	E. Jacobs, Chairman
III.	Airbreathing Propulsion	W. Stewart, Chairman
IV.	Auxiliary Power Unit	D. Beremand, Chairman
V.	Cryogens	C. Wood, Chairman

The last session, Cryogens is not a responsibility of the Propulsion Working Group; but falls under the Operations Working Group, chaired by Mr. Sam Beduingfield of KSC. Mr. C. Wood heads the Cryogens sub-group.

The last Propulsion Conference sponsored by the Propulsion Technology Working Group was held at Lewis Research Center in July, 1970. A great deal of the material presented at that conference covered "what we were going to do;" our conference today and tomorrow will present much on "what has been done." I believe that those of you who were present at that last Conference will be able to note that many significant achievements have been made since last July.

Before we get on with the technical presentation I would like to cover a few charts to show the structure of the Working Group.

(CHART 1) This chart shows the Propulsion Working Group and the other groups that make up the total group organized under Mr. Del Tischler of OART. These other groups have already held conferences such as we are today or will do so in the near future.

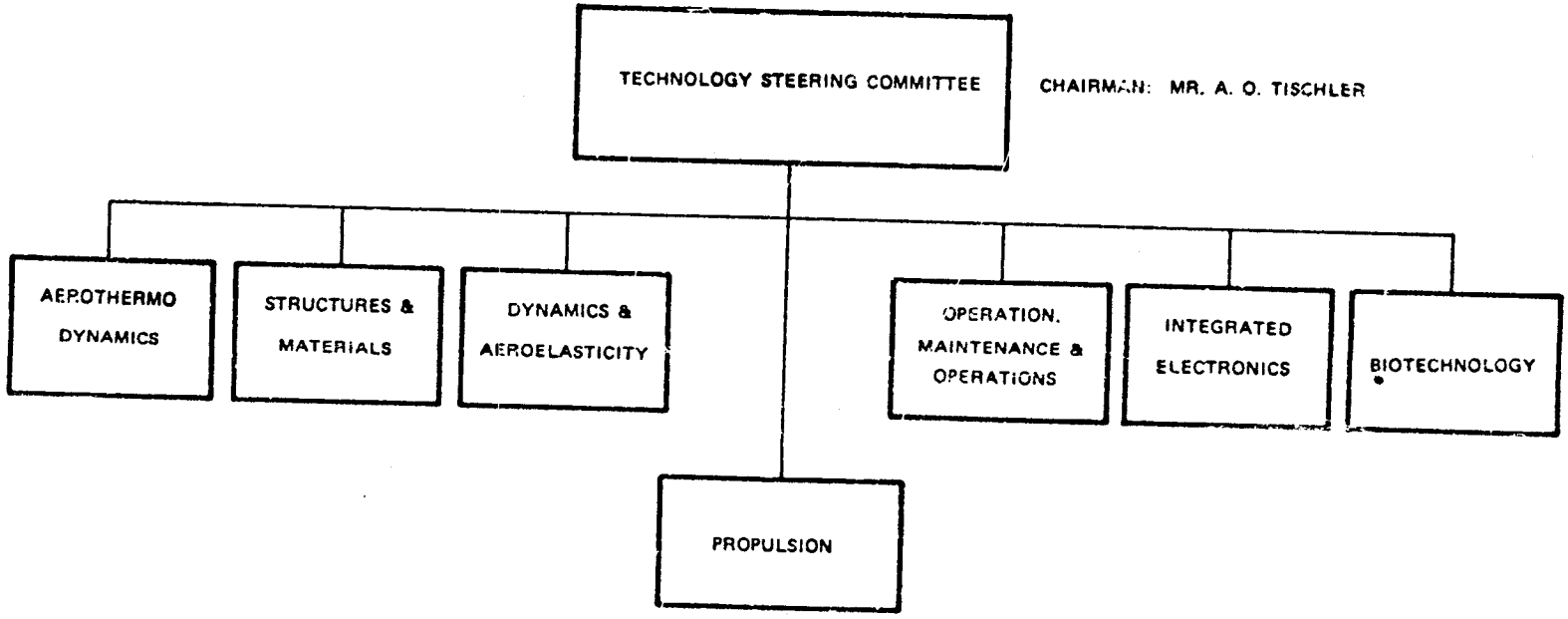

(TECHNOLOGY WORKING GROUPS)

(CHART 2) This shows the membership of the Propulsion Working Group. You will note among the members are representatives of various NASA field centers, Headquarters, and USAF. Special sub-groups have been established under Mr. Jacobs and Mr. Stewart for special emphasis on APS and Airbreathing.

ORGANIZATION CHART

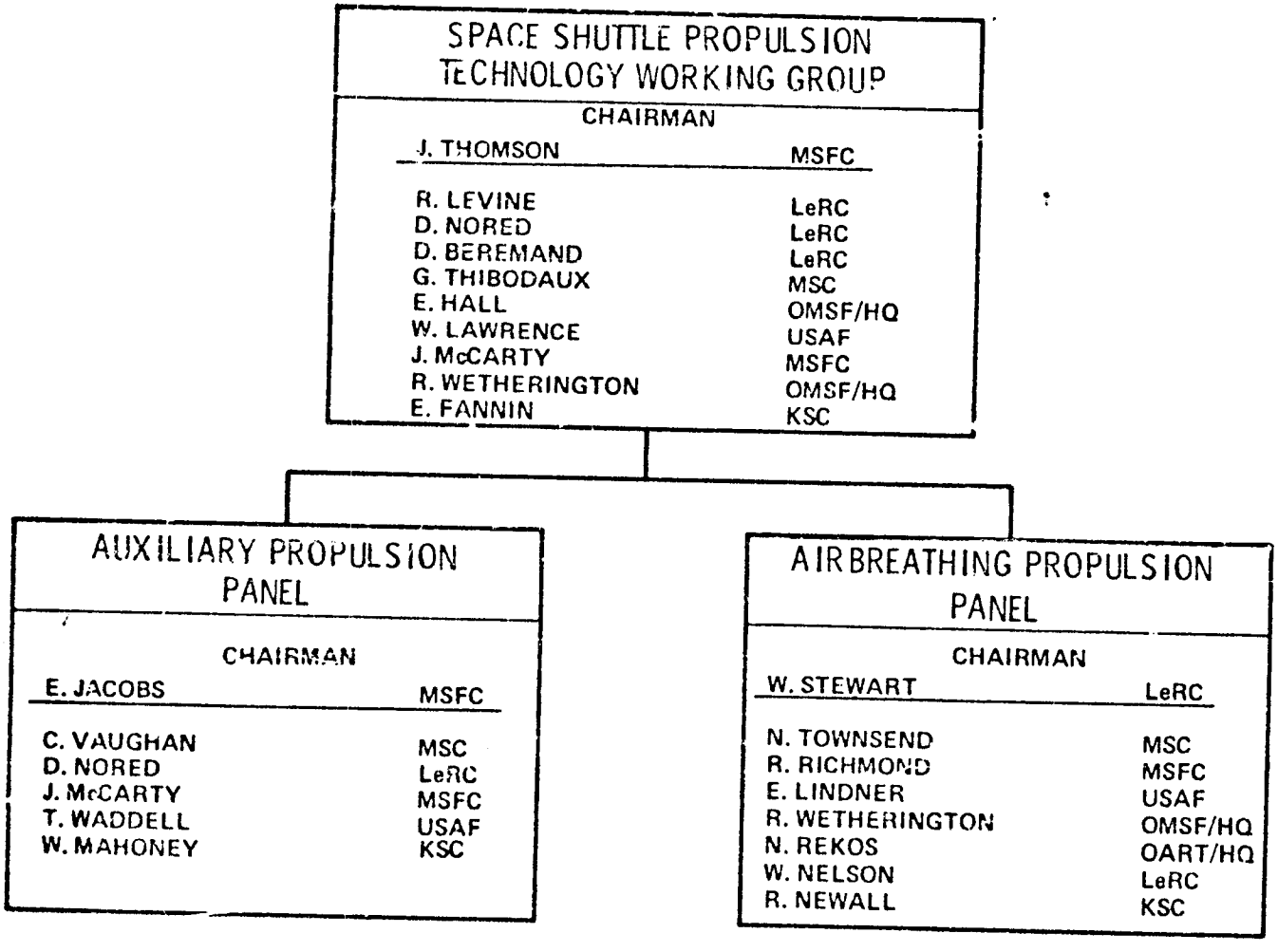

(CHART 3) This chart states the objectives of the Propulsion Group The job of getting the information to the user is accomplished by, in addition to Conferences such as here today, Quarterly reports published by the performing contractor or center which are distributed as directed by the Government, and Quarterly reports published by the Propulsion Working Group which contain under one cover a listing of all funded and planned tasks. The objective and status of each task is also shown. These reports are distributed within the NASA/USAF and a contractor version is given wide distribution to industry.

WORKING GROUP OBJECTIVES

- TO ORGANIZE UNDER ONE GROUP NASA/DOD PROPULSION EXPERTISE FOR THE PURPOSE OF ESTABLISHING AN INTEGRATED SPACE SHUTTLE PROPULSION TECHNOLOGY PLAN.

- PLAN SHALL IDENTIFY PROPULSION AREAS WHERE TECHNICAL ADVANCEMENTS ARE REQUIRED TO SATISFY THE VEHICLE REQUIREMENTS AND TO ESTABLISH THE NECESSARY TECHNOLOGICAL BASE.

- ASSURE THAT THE PLAN IS IMPLEMENTED IN AN EFFECTIVE MANNER AND THAT THE RESULTS ARE PROVIDED TO POTENTIAL USERS.

(CHART 4) This chart shows the funding available to the Propulsion Working Group. Note the decline in Main Propulsion funds for FY 71 and FY 72. For these years the Space Shuttle Main Engine Phase B studies were underway and were funded separately from technology. As you may know there are three study contractors (Aerojet, Rocketdyne, and Pratt & Whitney). The overall decline in FY 72 from that in FY 71 does not represent a recommendation from the Working Group, but is a result of "stretching the NASA budget."

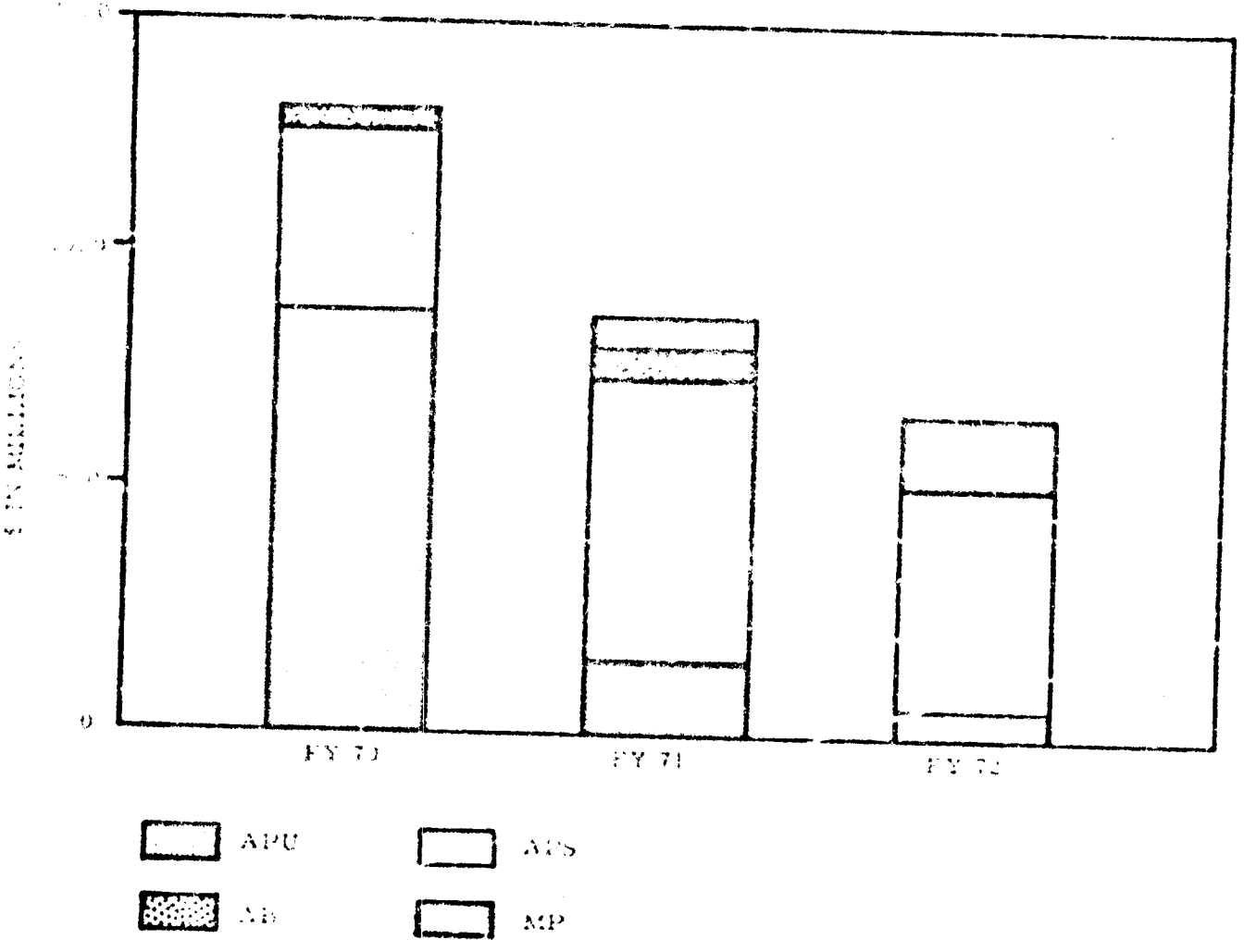
FY 70
FY 71
FY 72
APU
AFS
AB
MP

(CHART 5) This chart shows the various tasks which are currently listed as our Main Propulsion Program. It does not list all the completed tasks, nor the FY 72 tasks on which Request for Proposals are yet to be released. I would like you to note the reference schedule shown on the bottom line for the Space Shuttle Main Engine. Our tasks are all schedule-oriented, to be compatible with the Shuttle Program overall schedule needs. I believe the shuttle can not afford to count on technology which is not focused clearly on an availability date.

MAIN PROPULSION PROGRAM TASKS

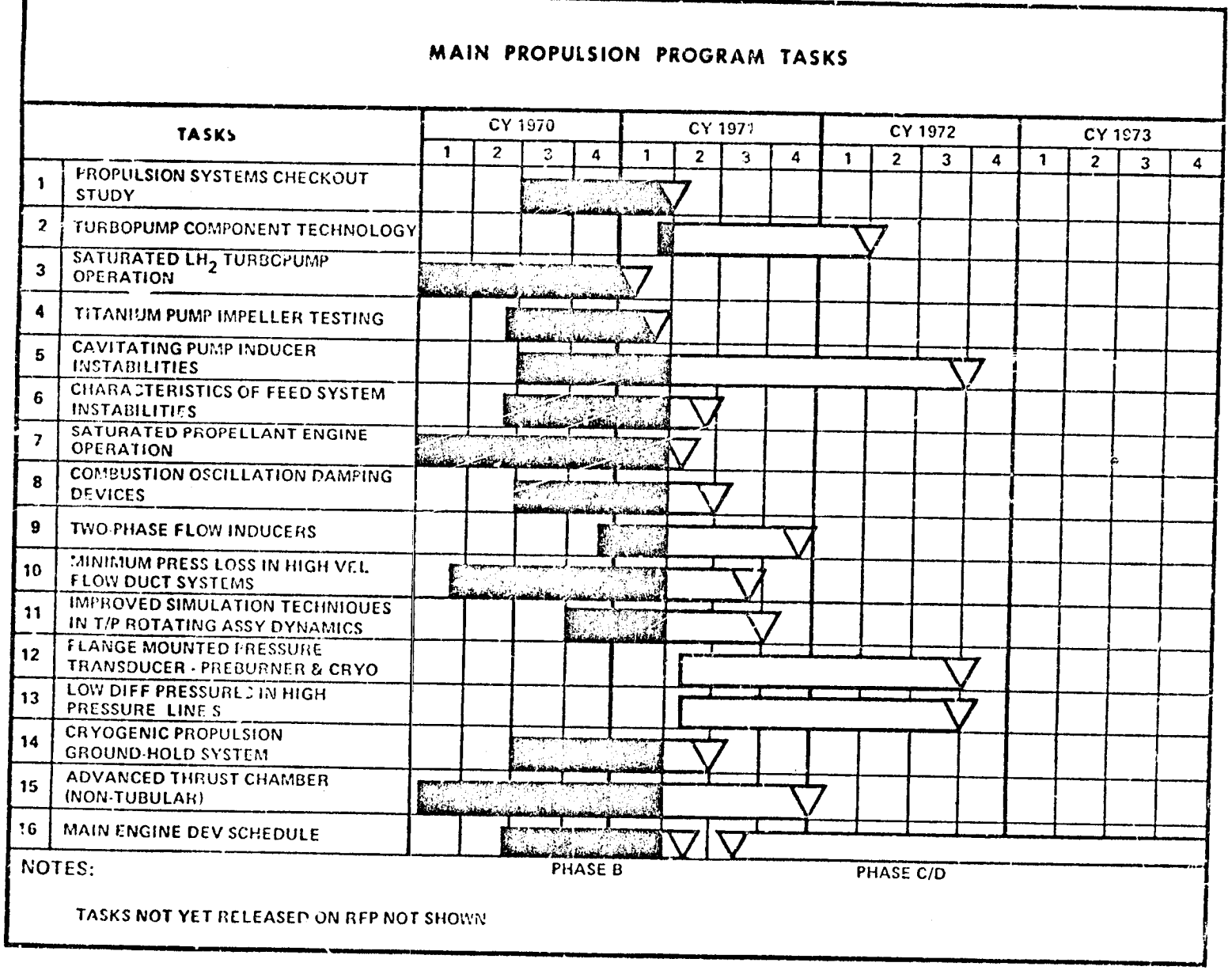

NOTES:

TASKS NOT YET RELEASED ON RFP NOT SHOWN

SESSION I

MAIN PROPULSION

J. THOMSON, CHAIRMAN

N7- 29577

"FINAL RESULTS OF XLR-129 PROGRAM"

R. R. ATHERTON

PRATT & WHITNEY AIRCRAFT

TECHNICAL MANAGER

CAPT. R. PROBST

USAF, ROCKET PROPULSION LABORATORY

FINAL RESULTS OF THE XLR129 PROGRAM

Pratt & Whitney Aircraft
Florida Research and Development Center
West Palm Beach, Florida

R. R. Atherton, Project Manager

Contract No. F04611-68-C-0002
United States Air Force - Rocket Propulsion Laboratory

ABSTRACT

This paper reviews the progress made on the XLR129-P-1 Reusable Rocket Engine Program conducted by Pratt & Whitney Aircraft under Air Force RPL sponsorship at the Florida Research and Development Center. The engine was designed to provide 250,000 pounds of thrust in vacuum with a high area ratio nozzle. The size was selected to provide meaningful data that could be scaled over the range of 100,000 to 1,000,000 pounds thrust. The design of all components and the engine system was completed. A full-scale engineering mockup of the demonstrator engine was also completed. Tests have been conducted on the preburner, the main case, and the fuel turbopump, which are reviewed and discussed. The assembly of two powerheads consisting of these components and tests on these powerheads are reviewed. The component reusability experience in this program is also reviewed. Component programs in specific areas with demonstrated reusability are: (1) wear life of critical moving components in valves, (2) fatigue life in turbopump bearings, (3) creep life of turbine blades, and (4) low cycle fatigue life of exhaust nozzle coolant passages. The design procedures and criteria that have been used for the XLR129-P-1 reusable rocket engine are based on those that have been used successfully for the design of commercial and military jet engines with proved durability and reliability.

CONTENTS

ILLUSTRATIONS

ILLUSTRATIONS
(con't)

II. XLR129-P-1 DEMONSTRATOR ENGINE

The advanced Development Program (ADP) for Pratt & Whitney Aircraft's XLR129-P-1 Reusable Rocket Engine was started on 6 November 1967 under contract from the Air Force Rocket Propulsion Laboratory. The overall objective of this program was to demonstrate the performance and mechanical integrity of a 250K oxygen/hydrogen reusable rocket engine. This demonstrator engine operates at high chamber pressure and uses the staged combustion engine cycle. The design and demonstration characteristics for the XLR129-P-1 demonstrator are shown in table I.

Nominal Thrust	250,000-lb vacuum thrust with area ratio of 166:1 244,000-lb vacuum thrust with area ratio of 75:1 209,000-lb sea level thrust with area ratio of 35:1
Minimum Delivered Specific Impulse Efficiency	96% of theoretical shifting I_s at nominal thrust; 94% of theoretical shifting I_s during throttling
Throttling Range	Continuous from 100 to 20% of nominal thrust over the mixture ratio range
Overall Mixture Ratio Range	Engine operation from 5.0:1 to 7.0:1
Rated Chamber Pressure	2740 psia
Engine Weight (With 75:1 Nozzle)	3520 lb (with flight-type actuators and engine command unit) 3380 lb (less flight-type actuators and engine command unit)
Expansion Ratio	Two-position booster-type nozzle with area ratios of 35:1 and 75:1
Durability	10 hours time between overhauls, 100 reuses, 300 starts, 300 thermal cycles, 10,000 valve cycles
Single Continuous Run Duration	Capability from 10 seconds to 600 seconds
Engine Starts	Multiple restart at sea level or altitude
Thrust Vector Control	Amplitude: ±7 deg; Rate: 30 deg/sec; Acceleration: 30 rad/sec^2
Control Capability	±3% accuracy in thrust and mixture ratio at nominal thrust. Excursions from extreme to extreme in thrust and mixture ratio within 5 seconds.
Propellant Conditions	LO_2: 16 ft NPSH from 1 atmosphere boiling temperature to 180°R LH_2: 60 ft NPSH from 1 atmosphere boiling temperature to 45°R
Environmental Conditions	Sea level to vacuum conditions Combined acceleration: 10 g axial with 2 g transverse, 6.5 g axial with 3 g transverse, 3 g axial with 6 g transverse
Engine Vehicle	The engine will receive no external power, with the exception of normal electrical power and 1590-psia helium from the vehicle

The general component arrangement of the demonstrator engine is shown in figure 1. A flow schematic is shown in figure 2. In the staged combustion cycle, the preburner produces hot fuel-rich gases that drive the turbines of the turbopumps, and these gases are burned in the main burner chamber with the balance of the oxygen to produce thrust. A two-position translating nozzle is used to decrease the overall stowed engine length. A full-scale mockup of the Demonstrator Engine was made as shown in figure 3, which shows the two-position nozzle extended. (For economy, the two-position nozzle used in this mockup was only a partial length nozzle, not the full length nozzle.)

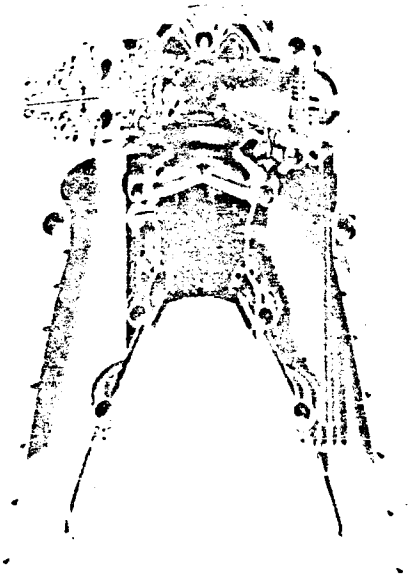

FIGURE 1. DEMONSTRATOR ENGINE ARRANGEMENT

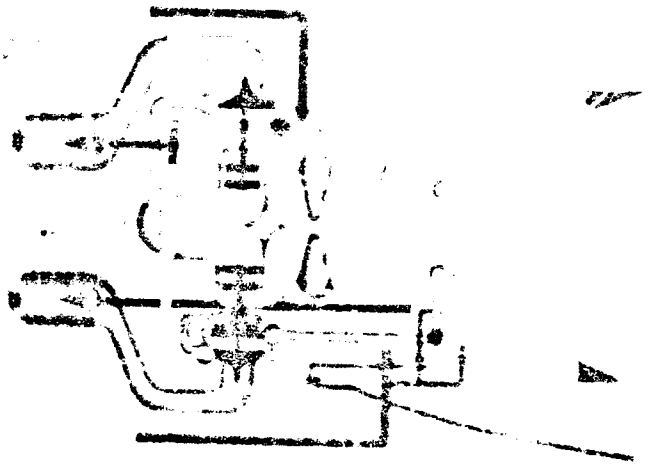

FIGURE 2. SCHEMATIC DIAGRAM OF FLOW

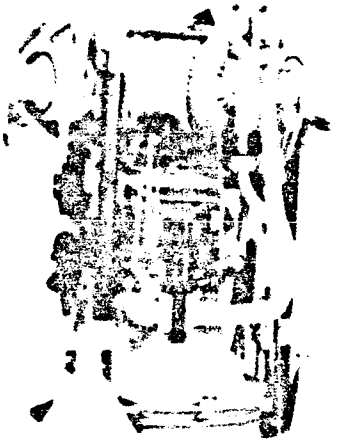

FIGURE 3. FULL-SCALE ENGINE MOCKUP

1. Component Test Results

a. Preburner Test Rig

A test rig consisting of the preburner oxidizer valve, the injector and igniter, the housing and cooled liners, and a main burner simulator was assembled as shown in figure 4 and tested. Objectives of these tests were to evaluate temperature profile, combustion stability, combustion efficiency, simulated engine starting and durability of the hardware. Twenty-two tests were conducted between August 1969 and April 1970, and a summary of the test results is presented in table II. These tests showed that the temperature profile on the last series of tests is suitable for continued testing with the fuel turbopump in the "powerhead" rig. Dynamic combustion stability was also demonstrated. Combustion efficiency was demonstrated to be quite high and approaching 100% in most cases. Engine starts were simulated and hardware durability for the basic components was shown to be satisfactory. Figure 5 is a plot of the preburner mixture ratio profile that was attained in a run at 75% thrust and at an equivalent engine mixture ratio of 7.0.

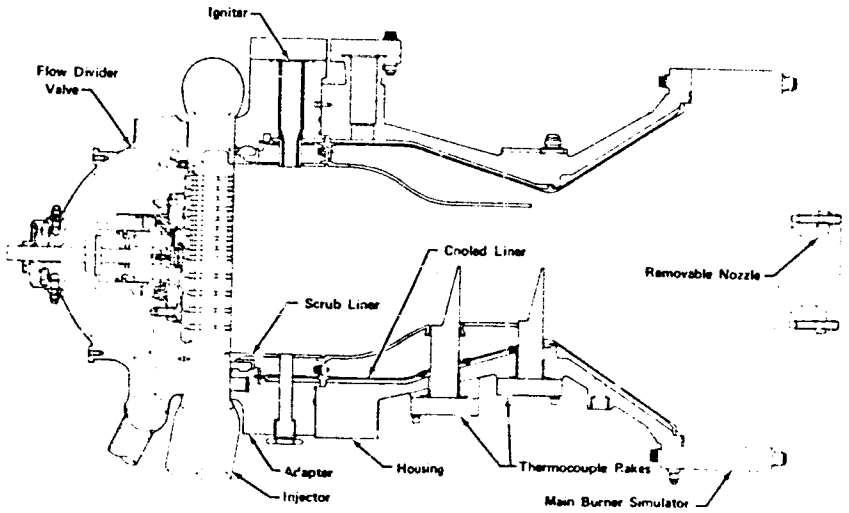

FIGURE 4. PREBURNER TEST RIG

TABLE II. SUMMARY OF PREBURNER TEST RESULTS

	Test No.	Date	Preburner Chamber Pressure (psia)	Percent Thrust (%)	Engine Mixture Ratio	Average Combustion Temperature (°R)	ΔT Profile at 15 in. (°R)	η_c at 15 in.
35131	1.01	27 Aug 1969	669	20	5	1,306	72	98.0
			672	20	6	1,722	98	97.8
			673	20	7	2,115	114	97.7
			1,247	35	5	1,263	121	97.7
	2.01	19 Sept 1969	693	20	5	1,302	215	97.1
			691	20	6	1,639	190	96.2
	3.01	20 Sept 1969	691	20	5	1,303	159	96.8
			700	20	6	1,702	234	96.0
			704	20	7	2,090	263	96.1
	6.01	19 Oct 1969	726	20	5	1,436	539	100.0
			741	20	6	1,827	621	100.1
			739	20	7	2,297	611	99.7
	7.01	31 Jan 1970	701	20	5	1,349	225	99.6
			2,020	50	5	1,402	190	97.5
	10.02	9 Feb 1970	694	20	5	1,349	196	102.0
	11.01	11 Feb 1970	2,032	50	5	1,415	119	98.0
			1,985	50	6	1,769	155	97.7
			1,964	50	7	2,106	173	98.1
	13.01	13 Feb 1970	3,283	75	5	1,692	150	98.7
			2,982	75	7	2,268	189	99.4
	14.01	14 Feb 1970	2,967	75	7	2,254	318	100.0
			4,276	100	6	2,050	259	100.0
35133	(15.01)	6 Apr 1970	724	20	5	1,344	280	99.3
			2,071	50	5	1,427	155	98.5
	(19.01)	10 Apr 1970	707	20	5	1,368	207	100.7
			708	20	6	1,765	258	99.6
			708	20	7	2,145	275	99.4
			2,042	50	5	1,429	203	98.6
			1,998	50	6	1,797	217	98.9
			1,964	50	7	2,136	267	99.2
	(21.01)	13 Apr 1970	2,957	75	7	2,190	252	98.6
	(22.01)	14 Apr 1970	2,964	75	7	2,203	258	99.4

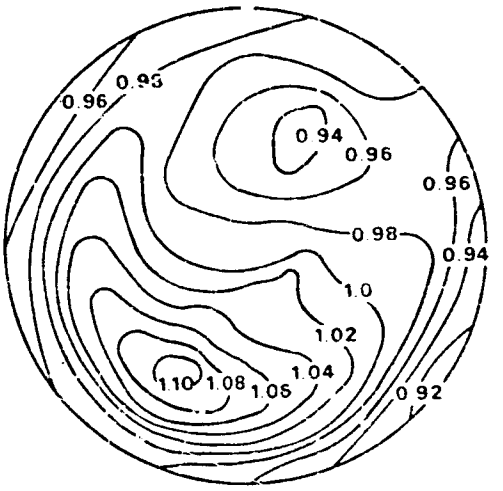

FIGURE 5. PREBURNER MIXTURE RATIO PROFILE

The XLR129-P-1 demonstrator engine program schedule is shown in figure 6. This 54-month program was divided into five basic phases. The first phase, which was completed early in 1968, generated test and analytical data to complete the technology necessary to design the engine and components. During the second phase, which ended in the latter portion of 1969, all the components were designed. The third phase which was the fabrication and testing of components was started, but was not completed because all test work on the contract was terminated. Some of the most significant components were fabricated and tested; these are described in the following sections. The fourth phase was to have been the integration of the components into the demonstrator engine and the testing of the demonstrator engine. The fifth phase was to have been the definition of a flight engine that could have resulted from a subsequent Engineering Development Program. These phases were not started.

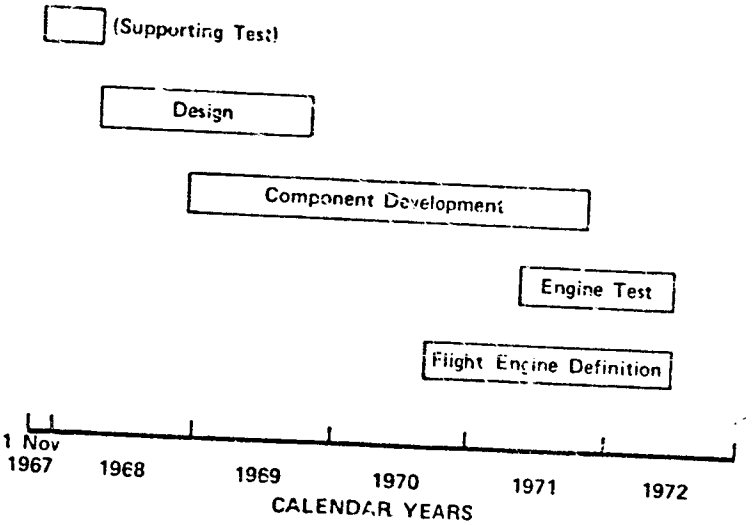

FIGURE 6. XLR129-P-1 DEMONSTRATOR ENGINE PROGRAM

b. Main Case

Procurement of raw material for the outer main case and fabrication of the case were started early in 1969. The coplanar intersecting sphere design was selected over the canted-components version after design studies and model testing had been conducted. This coplanar version was selected because it offered the best configuration considering the inner duct design, cooling, thrust load handling, and assembly and manufacturing. Figure 7 shows how the major components plug into the main case. Figure 8 shows an internal flow schematic of the main case with the fuel turbopump and the oxidizer turbopump turbine simulator installed. The intersecting sphere design was selected to minimize weight and maximize confidence in the predicted structural margins.

Following fabrication, the case was successfully proof pressure/thrust tested under conditions exceeding normal test levels. The case was tested under two internal pressure and thrust ratios; namely (1) Simulated preburner testing pressure-thrust ratio; 100% proof test load equal to 4500 psig and 69,000 pounds, and (2) simulated engine design pressure-thrust ratio; 100% proof test load equal to 4500 psig and 375,000 pounds. Figure 9 shows the case during testing, with stress coat to indicate areas of high stress. Figure 10 shows an internal view of the transition case with the internal centerbody installed.

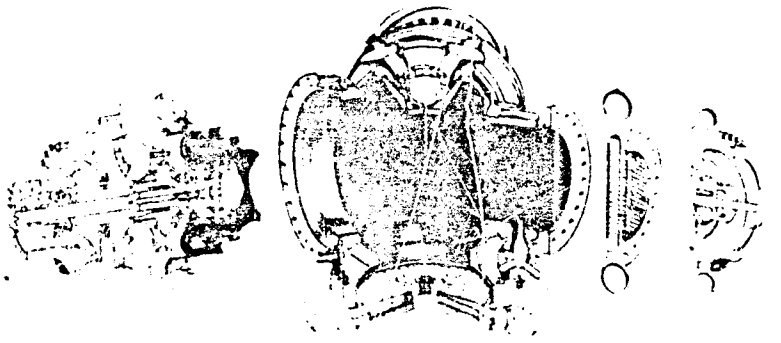

FIGURE 7. MAJOR COMPONENT PLUG-IN TO MAIN CASE

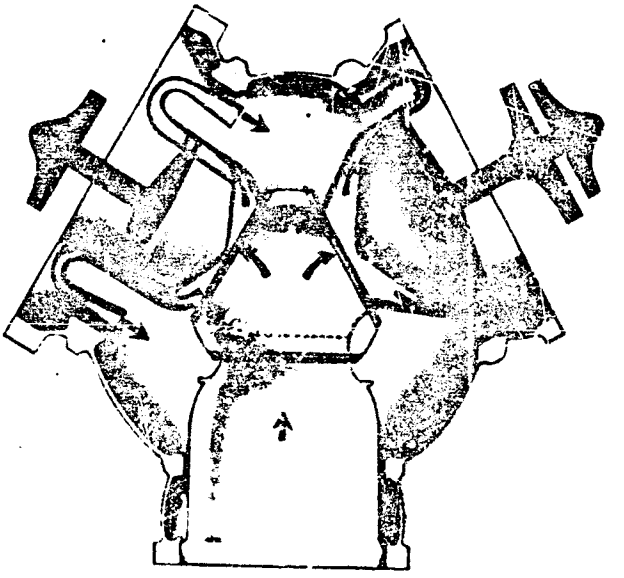

FIGURE 8. SCHEMATIC DIAGRAM OF INTERNAL FLOW

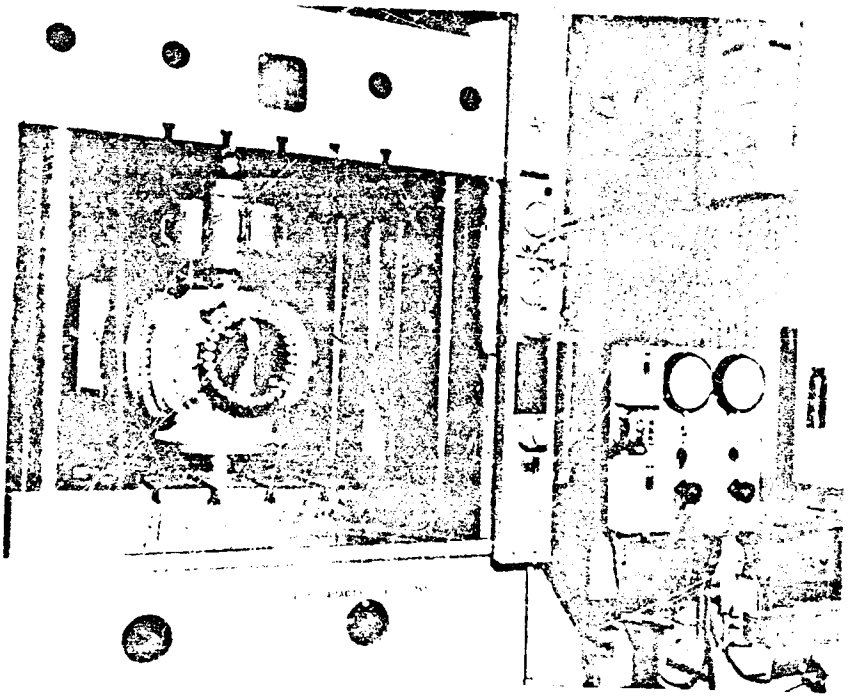

FIGURE 9. CASE DURING TESTING

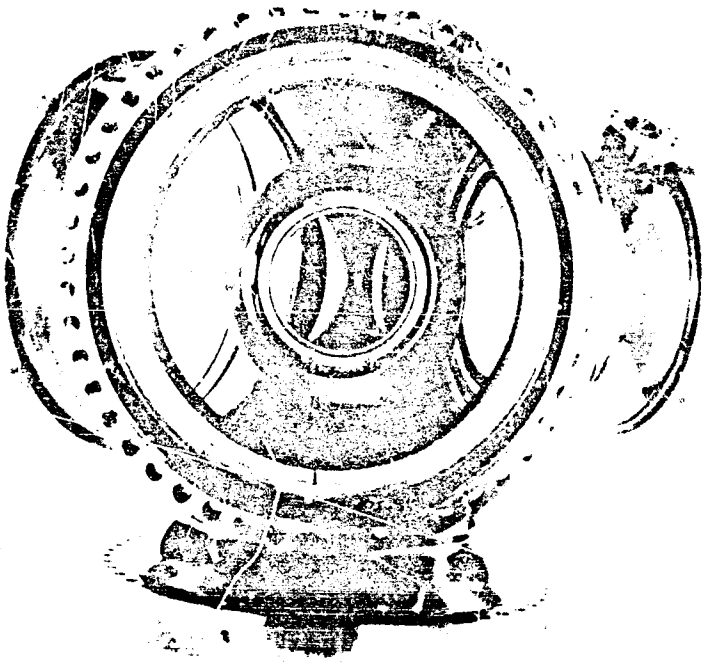

FIGURE 10. INTERNAL VIEW OF TRANSITION CASE

2. Fuel Turbopump Test Results

The fuel turbopump is a single shaft unit with two back-to-back centrifugal pump stages driven by a two-stage, pressure-compounded turbine. The turbopump shaft is located radially by two roller bearings and axially by a double-acting thrust balance piston. The fuel turbopump delivers liquid hydrogen at a flow rate of 91.3 lb/sec at a pressure of 5654 psia at the design point (mixture ratio of 5). The two-stage turbine delivers approximately 49,900 horsepower to the pump and operates at a minimum inlet temperature of 1980°R and a maximum inlet temperature of 2292°R at 100% thrust. One of the fuel turbopump assemblies that was tested is shown in figure 11.

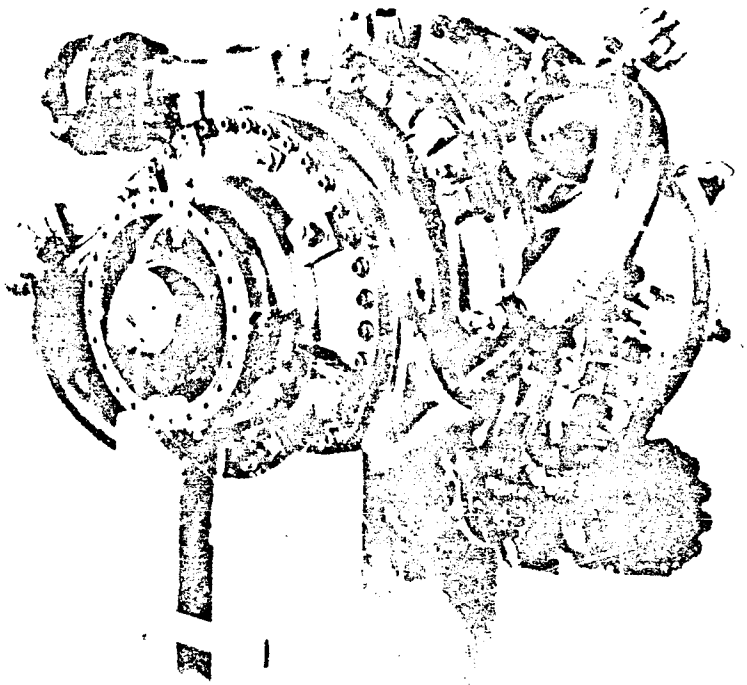

FIGURE 11. TESTED FUEL TURBOPUMP ASSEMBLY

Three fuel turbopump rigs were tested for a total of 488.7 seconds run duration and the results of these tests are summarized in table III. Objectives of these tests were to determine the pump performance, the thrust balance, and the suction performance. Flow excursions were conducted from 50% to 100% of pump speed. The pump performance was better than predicted, the thrust balance was satisfactory, and the suction performance was also better than predicted. Figure 12 shows numerous test points for overall pump efficiency compared to the predicted values. The test efficiencies were higher than the predicted efficiencies. Figure 13 presents two typical flow excursions, which show how the pump discharge pressure varied as the flow varied during two tests. Figure 14 is a plot of the fuel turbopump test data obtained at the conditions shown, which shows how closely the test values approach the predicted values.

TABLE III. XLR129 FUEL TURBOPUMP TEST SUMMARY

Rig	No. Test/Time, sec	Test Objectives	Remarks
35138-1	5/142.6	Pump Performance & Thrust Balance	Mapped pump at 50% and 83% speed. Lift-off seal failed during acceleration to 96% speed. Thrust balance satisfactory and performance better than predicted.
35138-2	6/262.7	Pump Performance, Thrust Balance and Suction Performance	Dummy lift-off seal and second impeller clearance reduced. Mapped pump at 50%, 67%, 83%, 88% speed. Vibration abort during flow excursion at 96%. Completed 4 suction performance tests. Thrust balance satisfactory. Pump performance and suction performance better than predicted.
35147-1	2/83.4	Pump Performance & Thrust Balance	Scalloped first impeller, recontoured second impeller housing and new lift-off seal. Mapped pump at 50%, 67%, 83%, 88% and 100% speed. Thrust balance satisfactory. Pump performance better than predicted. Lift-off seal operation satisfactory. Ready for hot turbine testing.
Total	13/488.7		

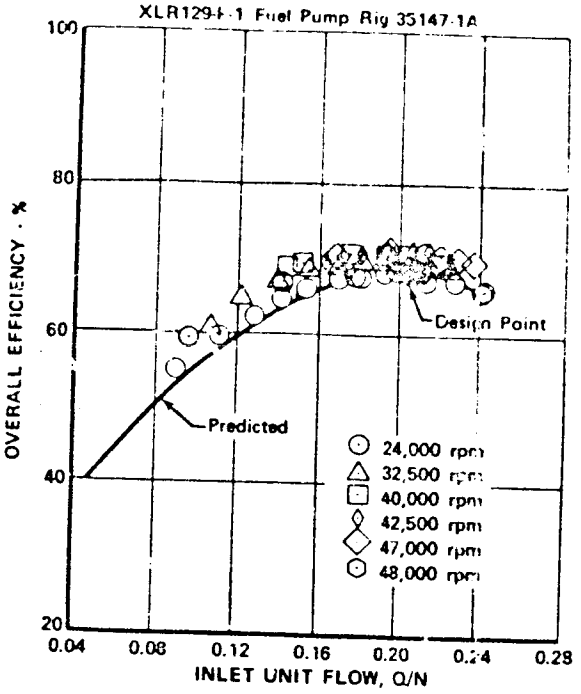

FIGURE 12. TEST POINTS FOR EFFICIENCY VS INLET AND FLOW

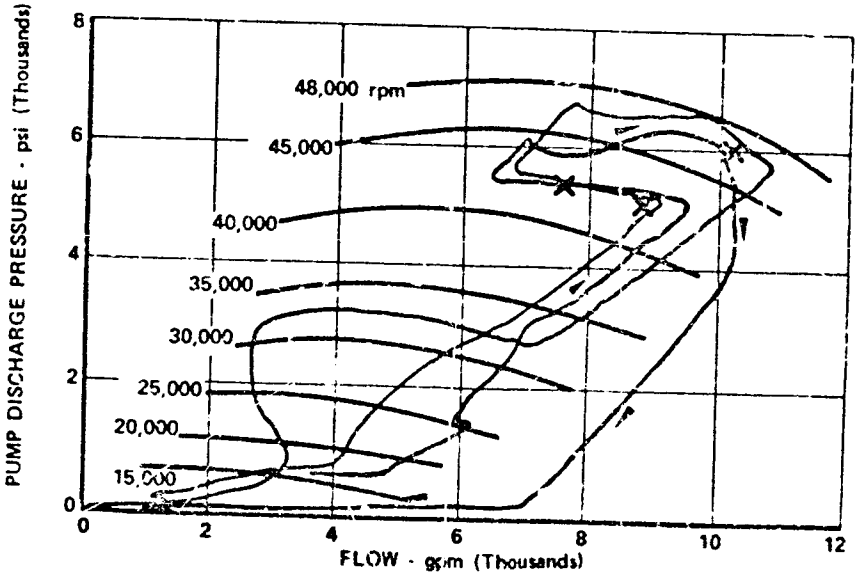

FIGURE 13. TYPICAL FLOW EXCURSIONS

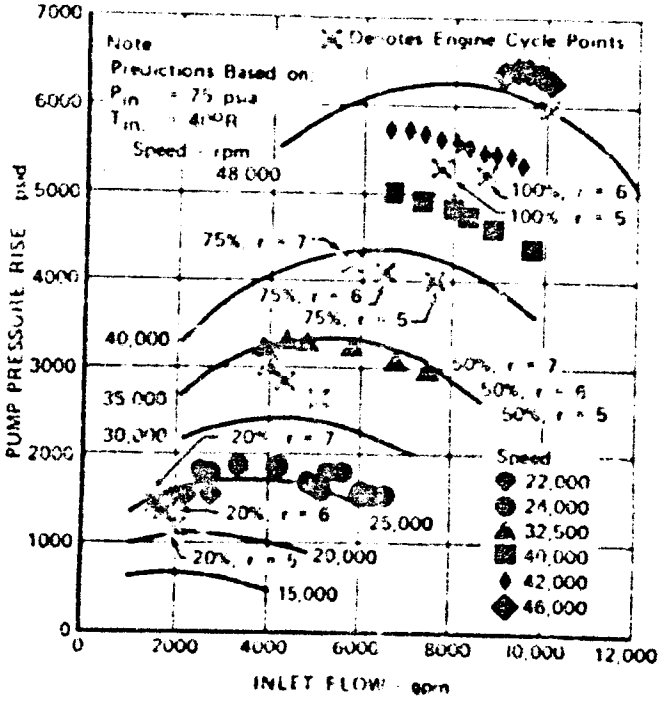

FIGURE 1-. TURBOPUMP TEST DATA PLOT

3. Powerhead Test Results

The hot gas system, was tested first during May and June of 1970 consisting of the preburner injector, preburner oxidizer valve, oxidizer pump simulator, fuel pump simulator and a nozzle back pressure plate mounted on the transition case. Figure 15 shows this hot gas system mounted on the test stand. Six combustion tests were conducted on this hot gas system which demonstrated the feasibility of all the hardware with hot gas that simulated engine conditions. The total test time was 42.8 seconds. Table IV presents a summary of the test data obtained.

Following the successful tests, the fuel turbopump was then substituted for the fuel pump simulator, and this powerhead or hot gas system rig assembly is shown in figure 16. One of the principal objectives of the second powerhead was to qualify the fuel turbopump turbine with hot gas for engine operation. Rig operation up to 75% of rated preburner conditions was attained. Table V summarizes the second series of powerhead tests. The hardware was in good condition following this series of tests. These tests demonstrated the feasibility of the integrated components, and particularly, the combination of the transition case and the fuel turbopump turbine under hot gas conditions. Figure 17 shows a flow schematic of the E-8 test stand that was used to test the hot gas system or powerhead.

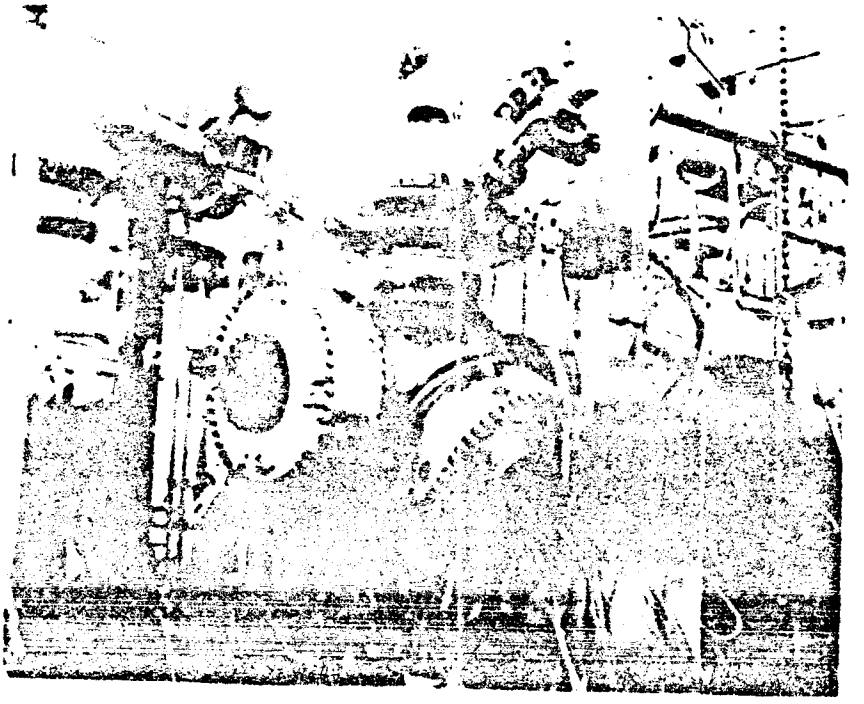

FIGURE 15. HOT GAS SYSTEM MOUNTED ON TEST STAND

TABLE IV. HOT GAS SYSTEM TEST SUMMARY RIG NO. 35139-1

Run No.	Preburner Chamber Press., psia	Main Case Press., psia	% Thrust/ Mixture Ratio	Avg Comb Temp, °R	$T_{max}-T_{avg}$	Comments
1.01	1335	1007	NA			False High Case Coolant Liner ΔP At 8.9 sec
3.01	2071	1555	50/5	1452	122	Full Duration Run, 13.7 sec
4.01	673	460	N/A			Hard Start; False High Case Liner ΔP at 6.7 sec
6.01	679	501	20/5	1330	221	Full Duration Run, 10.1 sec

FIGURE 16. HOT GAS SYSTEM RIG ASSEMBLY SCHEMATIC

TABLE V. HOT TURBINE TEST SUMMARY

Test No.	Thrust/ Mixture Ratio	Combustion Temperature °R	Combustion Pressure psia	Profile on Lox Turbine	Fuel Turbine Temperature (Calculated)	Pump Speed rpm	Pump Discharge Pressure psia
1.02	50/5	1450	1863	44	1534	29,360	2340
2.01	Instrumentation Advance						
3.01	75/5	1605	2970	26	1642	35,630	3610
4.01	75/5	1615	2965	28	1671	35,360	3560
	75/6	1985	2882	56	2012	34,610	3369
5.02	75/5	1610	3045	45	1649	36,085	3737
	100/6	2070	4086	94	2088	40,782	4981
	100/7	2395	3887	126	2410	39,498	4623
6.01	50/7	2118	1612	65	2143	30,000	2420
	100/5	1900	4200	65	1940	44,592	5512

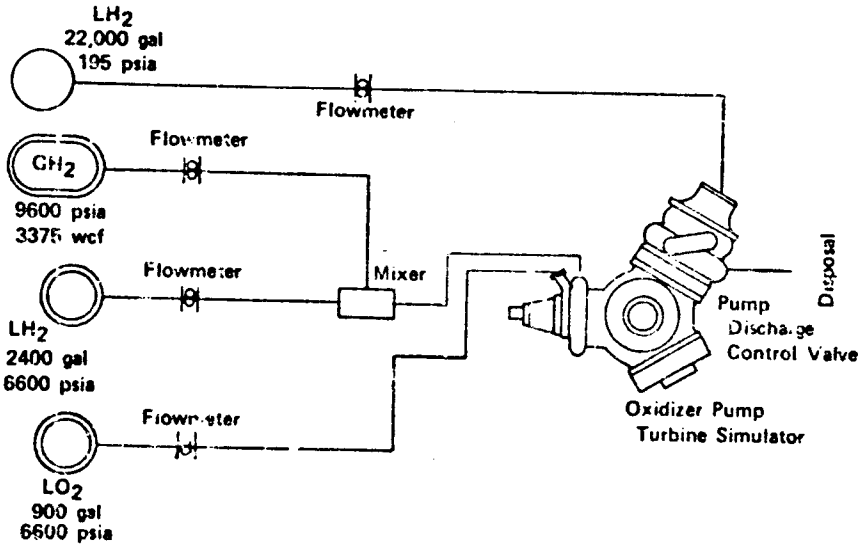

FIGURE 17. E-8 TEST STAND

4. Component Reusability

One of the specific life requirements of the XLR129-P-1 reusable rocket engine is a 10-hour Time Between Overhauls (TBO). Long engine life in either turbojet engines or rocket engines begins in the initial design of the components and engine and is achieved through endurance reliability and durability testing. At Pratt & Whitney Aircraft reliability and dependability are influential considerations from the start of design until the engine is retired from service. There are certain specific component life factors that have received close attention on the XLR129-P-1 reusable rocket engine. These component life factors are: wear, fatigue, low cycle fatigue and creep.

a. Wear

Wear of parts in rubbing contact becomes a dominant factor in the design of such parts as turbopump shaft-seals and shutoff valve seals. Pratt & Whitney Aircraft has conducted extensive valve seals tests under Air Force Contract to improve the life of these seals. For example, the main chamber oxidizer valve, which is a butterfly valve, incorporates a shutoff seal for the oxidizer flow to the main burner injector. To accommodate this shutoff feature a canted shaft with an integral disk was selected so that an uninterrupted disk sealing surface would be provided. Incorporation of the shutoff seal in this valve eliminates the need for a separate shutoff valve between the main chamber oxidizer valve and the main burner injector. A test rig was made for the purpose of environmental endurance tests on various designs of the main chamber oxidizer valves. The tests were conducted by submerging the valve in liquid nitrogen or liquid argon and pressurizing with nitrogen to internal pressure of 50 to 6000 psig.

The valves were cycled at these conditions, and valve seal leakages were measured periodically. For the latter tests, liquid argon was selected for the cryogenic bath to ensure that all of the nitrogen leakage vaporized at the valve external ambient pressure. This allowed satisfactory steady-state leakage measurement accuracy for all data points. The objective of the leakage tests was to obtain a seal design that would have less than 10 sccs leakage. A typical endurance test would consist of 10,000 shutoff cycles and 500 pressure cycles. A satisfactory hoop seal was developed with a configuration as shown in figure 18. This hoop seal was silver plated and had a 0.010 in. tight fit on the disk. Figure 19 shows a typical disassembly of the main chamber oxidizer valve seal rig. Figure 20 is a typical leakage curve versus shutoff cycles with the hoop shutoff seals. As a result of these tests a satisfactory seal was developed which showed that wear could be controlled to attain a 10-hour life, consisting of 10,000 shutoff cycles and 500 pressure cycles. This type of seal will be used on the main chamber oxidizer valve.

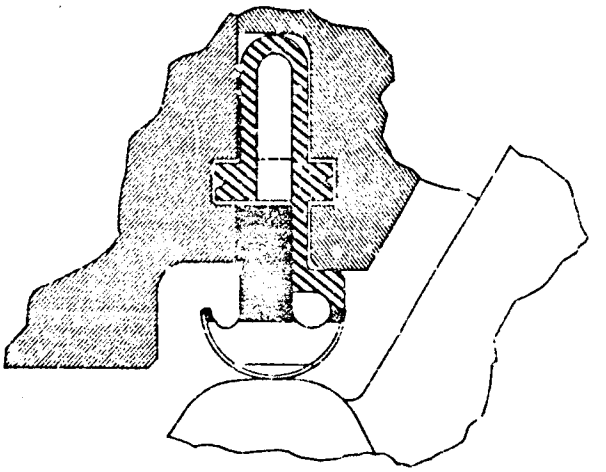

FIGURE 18. SATISFACTORY HOOP SEAL CONFIGURATION

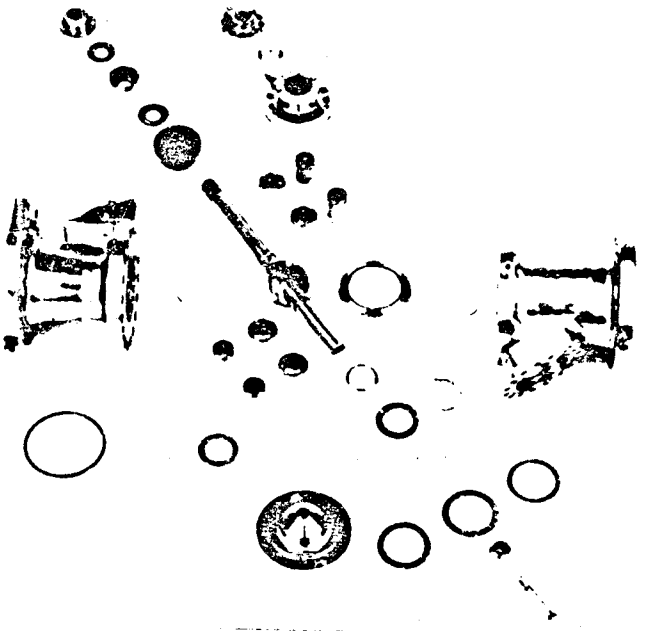

FIGURE 19. MAIN CHAMBER OXIDIZER VALVE SEAL RIG

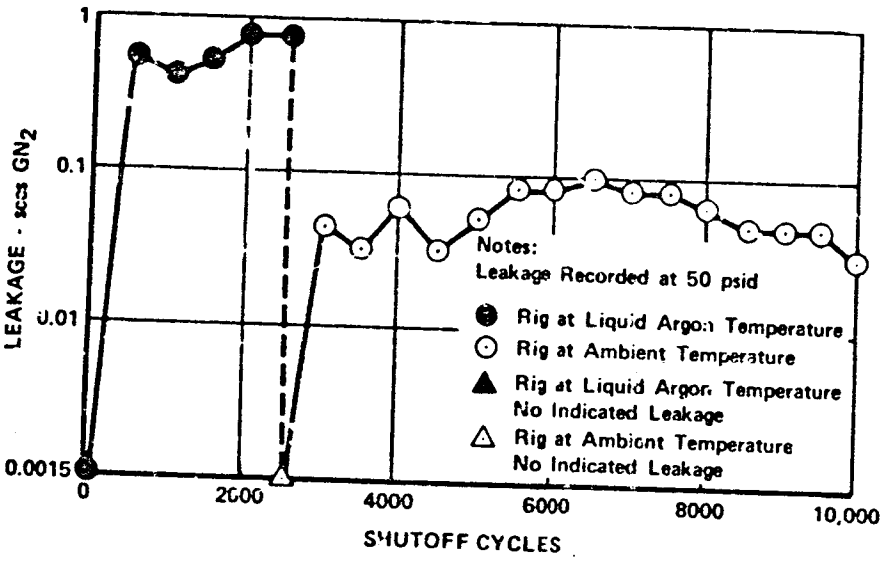

FIGURE 20. TYPICAL LEAKAGE CURVE VS SHUTOFF CYCLES

b. Fatigue

Fatigue, in which a part is subjected to a cyclic stress below the elastic limit for millions of cycles, becomes a dominant factor in the design of certain components such as propellant cooled bearings operating under high load where each time the ball or roller passes a point on a bearing race a stress is imposed on the race and removed after the bearing or roller has passed. At high rotational speed, with a large number of balls or rollers in the bearing, many millions of cycles can be accumulated in a short period of time. A roller bearing durability test program was conducted at Pratt & Whitney Aircraft, and 55 x 96.5 mm roller bearings were tested and evaluated for use in the XLR129-P-1 fuel turbopump. These fuel turbopump roller bearings operated at a maximum DN of about 2.65 million mm x rpm. The bearings operate in a liquid hydrogen environment that is provided by the propellant being pumped in the fuel turbopump. A test rig was made that has the capability of testing two bearings simultaneously at speeds up to 62,000 rpm with radial loads up to 2400 lb. Figure 21 shows a cutaway of the roller bearing test rig that was used. During Phase II of the advanced development program, a total of 85 hours of test time at 48,000 rpm was accumulated. These tests were conducted to evaluate the effects of roller length to diameter ratio, roller end to side rail clearance, internal clearance and roller crowning on roller end wear and bearing durability. During all these tests, a 1700-lb radial load was applied to the load bearing resulting in approximately 1445-lb radial load on the reaction bearing. Five bearing configurations were developed that passed the 10 hour goal test duration at the design operating conditions. Therefore, it can be concluded that fatigue on the race of the bearing can be controlled through proper design to attain the desired 10 hour life. Figure 22 shows a roller bearing after 15.3 hours of test. The most promising bearing configuration tested used stainless steel (AMS 5630) inner race and rollers; an outer race guided Armalon cage; a steel alloy (AMS 6265) outer race, single crown, L/D = 1.0 rollers with 0.020 in. roller end to inner race, side rail clearance and 0.0043 in. negative diametrical internal clearance. Bearings of this configuration will be used in the XLR129 fuel turbopump.

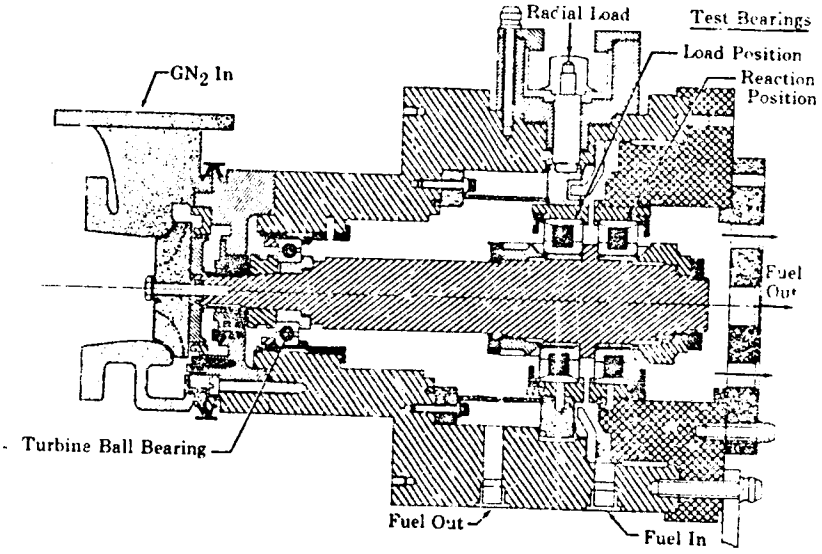

FIGURE 21. ROLLER BEARING TEST RIG

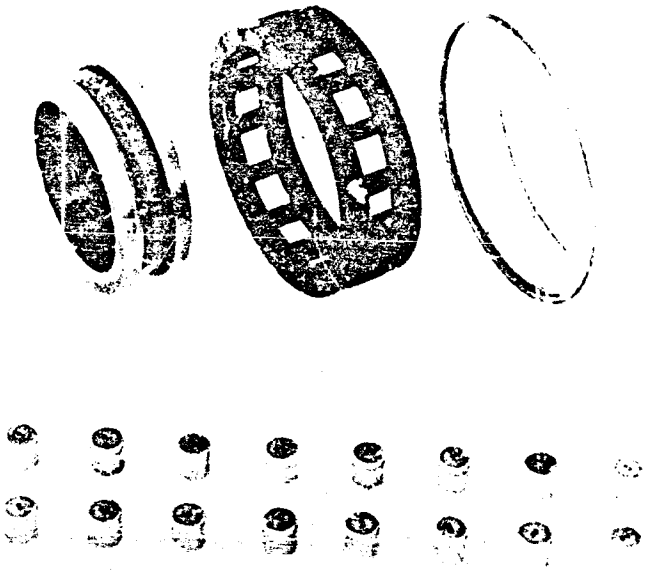

FIGURE 22. ROLLER BEARING AFTER TEST

c. Low-Cycle Fatigue

Low-cycle fatigue is also a major factor in the design of rocket engine components. Every time the engine starts and reaches full power, large thermal gradients are produced on the components. The component areas exposed to the high temperatures heat rapidly and expand rapidly. Those areas that are not exposed to the high temperatures do not heat as rapidly and, therefore, expand more slowly. These large temperature gradients result in high stresses. The thermal process reverses during the shutdown. Some of the components that heated rapidly during engine operation now cool rapidly, and many of the components that heated slowly now cool gradually. This results in stresses dropping to low levels. Some may even reverse producing compressive stresses. Therefore, with each ignition, acceleration to power, shutdown and cooldown, the engine is subjected to large stress variations consisting of both high tensile and compressive stresses. Low-cycle fatigue is characterized by loads imposed that strain the material beyond its elastic limit into the plastic region. This type of operation occurs, for example in the nozzle coolant tubes that have a large thermal gradient through the wall that cycles on and off each time the engine is started and stopped.

The primary nozzle of the XLR129-P-1 engine consists of two tubular heat exchangers. The material selected for the coolant tubes was Inconel 625 (AMS 5599). This material can be formed into tapered tubes and is easily brazed. The primary nozzle coolant tubes were sized by analytical considerations of temperatures and the fatigue cycle life requirements. The tubes had to be designed for a life of 300 operating cycles and a 10-hour total operating time. The 300-cycle requirement is actually more severe. This had to be defined from low-cycle fatigue tests, which were conducted by Pratt & Whitney Aircraft. Inconel 625 tubing with nominal 0.322 in. outside diameter and nominal 0.012 in. wall thickness was obtained, and 12 sample tubes were fabricated. Twelve Inconel 620 1-in. diameter bars were also fabricated, and the tubes were brazed to the stiffener blocks as shown in figure 23. The test equipment consisted of a copper induction heater coil, liquid nitrogen supply tank, plexiglas atmosphere container, helium supply bottles, radiation pyrometer, timer, cycle counter, thermocouples, potentiometer and pressure gage. Figure 24 shows the details of the test rig with a specimen supported in the liquid nitrogen trough and the method of induction heating. The twelve test specimens were pressurized internally with helium gas to the hoop stress requirements. The thermal strain was induced by placing the induction coil approximately 0.25 in. about the tube crown of the specimen and placing the stiffening block in liquid nitrogen. This method was the most representative of actual and engine conditions that the laboratory could accomplish. The crown of the tube was heated, and the temperature was determined by radiation pyrometers emissivity. Two thermocouples on each edge of the heated tube were used as a check. An optical pyrometer was used to verify the temperature readings of the radiation pyrometer at the 1880°R test points. Therefore, the temperatures recorded are fairly accurate. Each thermal cycle was controlled by an automatic timer and counter. The thermal cycle consisted of 60 seconds total time of which approximately 30 seconds were required to attain temperature, 15 seconds were at the test temperature, and 15 seconds to cool down to the liquid nitrogen temperature (159°R). The test data points are shown in figure 25. The number of cycles required for rupture of the tube samples at the stress level and temperature indicated are shown in parenthesis below each series of data points. From these data it can be concluded that at the engine design point of 29,300 psi tube stress level, the 300-cycle life can be attained if the maximum tube wall temperatures are maintained below 1300°F.

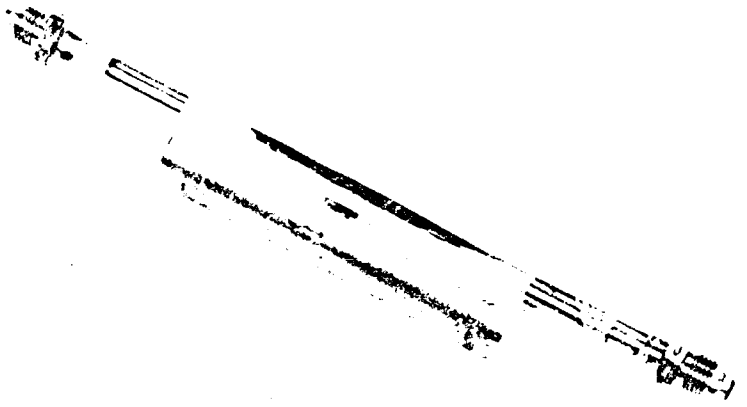

FIGURE 23. TUBES BRAZED TO STIFFENER BLOCKS

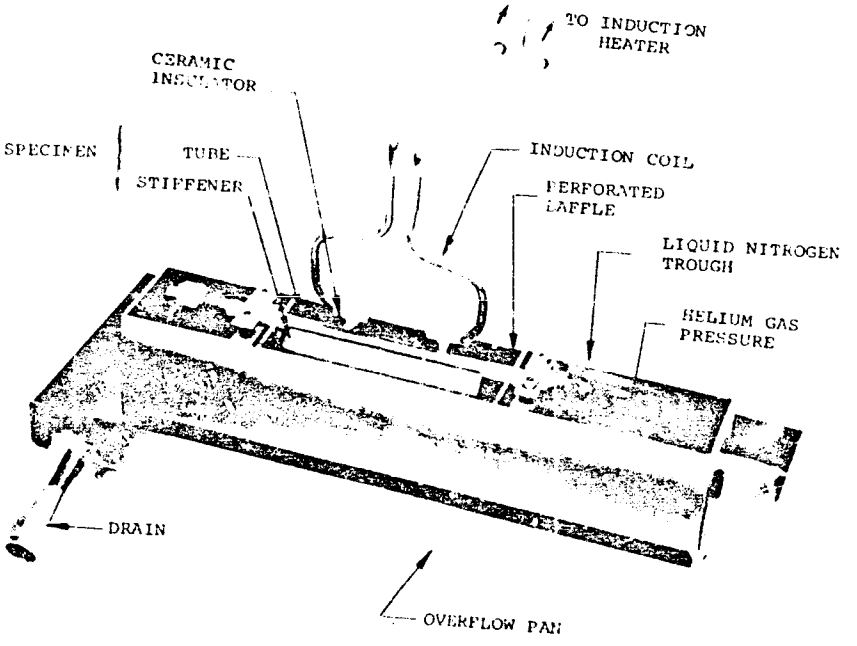

FIGURE 24. NOZZLE TUBE TEST RIG DETAILS

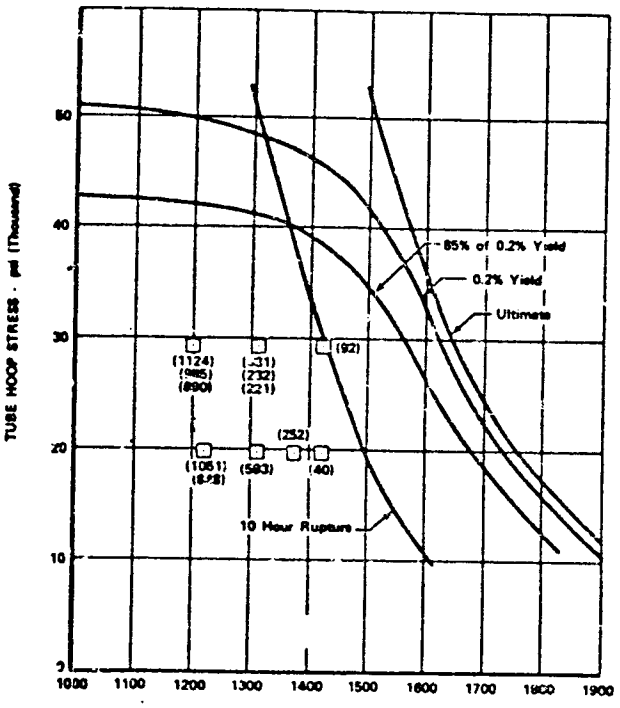

FIGURE 25. NOZZLE TUBE TEST DATA POINTS

Figure 26 shows a relationship between the stress and how long it takes this material to creep 1% at 1800°F. Similar data are available at other temperatures. Through proper design, and by maintaining the stress levels to attain a one-percent creep life, it is possible to attain extremely long life on the turbine blades and vanes in jet engines. This technology is directly applicable to the attainment of long life on the turbines and vanes of the reusable shuttle rocket engine.

d. Creep

Creep of components operating in a high temperature environment will occur, as it does in turbojet engines, particularly in turbine blades and vanes. Therefore, experience in turbojet blade and vane alloy development will be of direct benefit to the reusable shuttle rocket engine. For example, on advanced military jet engines, it has been demonstrated that it is feasible to attain a 3000-hour total life for cooled turbine blades with an average combustor temperature as high as 2400°F. One of the important developments that has contributed to this long life is the use of a directionally solidified high temperature alloy for the turbine blades. This particular alloy offers maximum strength and excellent fatigue and creep resistance at metal temperatures up to 2000°F.

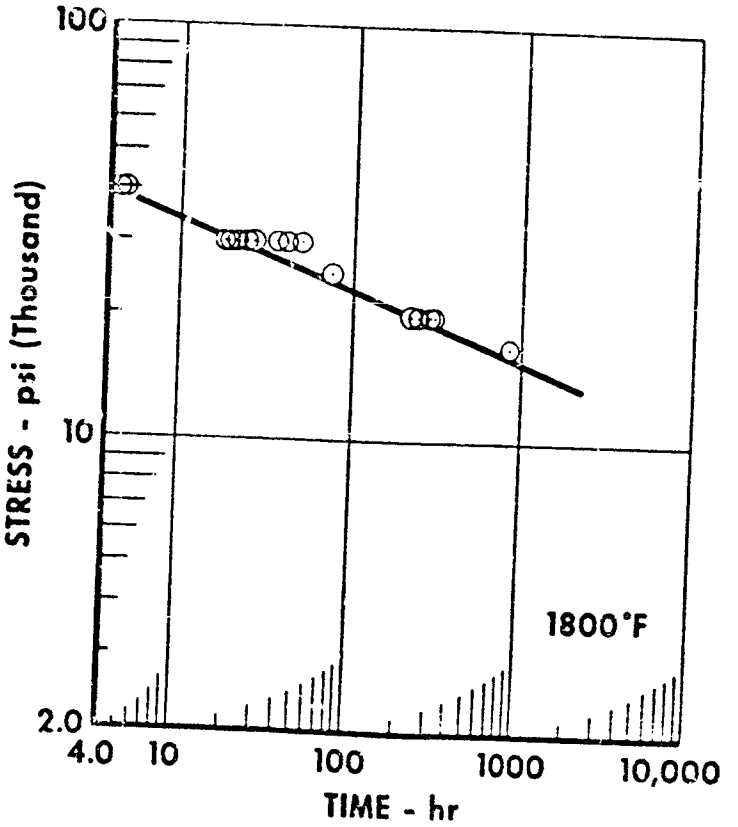

FIGURE 26. STRESS VS MATERIAL CREEP

"TWO-PHASE FLOW LH_2 PUMP INDUCERS"

J. A. KING

ROCKETDYNE

TECHNICAL MANAGER

C. D. MILLER

MARSHALL SPACE FLIGHT CENTER

TITLE: TWO-PHASE HYDROGEN PUMP INDUCERS

CONTRACT: NAS8-25069

PRESENTER: J. A. KING

COMPANY: ROCKETDYNE, DIV. OF NORTH AMERICAN ROCKWELL CORP.

NASA PROJECT MANAGER: CHARLES MILLER

Rocketdyne
North American Rockwell

INTRODUCTION

TWO-PHASE HYDROGEN IS A MIXTURE OF LIQUID AND GASEOUS HYDROGEN. A NEED EXISTS FOR THE DEVELOPMENT OF PUMPS THAT CAN HANDLE THESE MIXTURES BECAUSE FUTURE SPACE VEHICLE SYSTEMS HAVE PERFORMANCE REQUIREMENTS WITH UNPRESSURIZED TANKS, SATURATED PROPELLANTS AND MULTIPLE STARTS IN ZERO GRAVITY ENVIRONMENT. UNDER THESE CONDITIONS TWO-PHASE HYDROGEN MUST BE PUMPED.

HYDROGEN INDUCER AND PUMP

THE FOLLOWING PHOTOGRAPH SHOWS A LIQUID HYDROGEN INDUCER FOLLOWED BY A CENTRIFUGAL PUMP IMPELLER. AN INDUCER IS A HIGH-SOLIDITY ROTOR THAT IS CAREFULLY DESIGNED TO OPERATE AT LOW INLET PRESSURES AND PROVIDE SUFFICIENT HEAD TO PREVENT THE MAIN PUMP FROM CAVITATING.

329-995
3-71

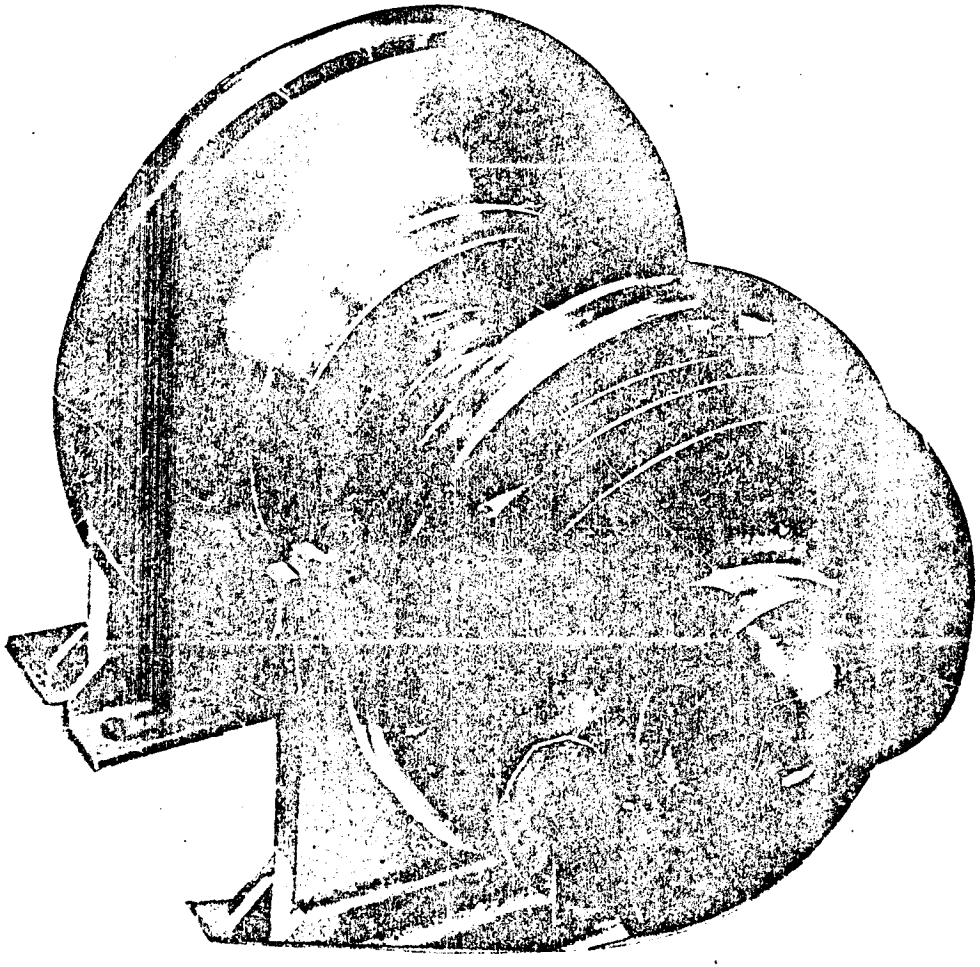

HYDROGEN INDUCER AND PUMP

Rocketdyne
North American Rockwell

PROGRAM OBJECTIVES

- TO DEVELOP A MATHEMATICAL FLOW MODEL FOR THE DESIGN AND EVALUATION OF INDUCERS THAT CAN PUMP TWO-PHASE HYDROGEN
- TO DESIGN AND FABRICATE AN INDUCER ACCORDING TO THIS MODEL
- TO TEST THE INDUCER IN TWO-PHASE HYDROGEN TO VERIFY THE THEORY.

ISENTROPIC EXPANSION FROM SATURATED LIQUID IN THE TANK TO EQUILIBRIUM CONDITIONS AT THE PUMP INLET RESULTS IN TWO-PHASE MIXTURES. AT CONSTANT MASS FLOW, AN INCREASE IN VAPOR PUMPING CAPACITY RESULTS IN A LOWER TANK PRESSURE. ALSO AN INCREASE IN THE INDUCER ANNULUS AREA, A, REDUCES W/A AND LOWERS THE TANK PRESSURE.

THE EXAMPLE SHOWN AT 280 LB PER SECOND PER SQ FT IS THAT OF THE J-2 IT SHOWS THAT IF THE VAPOR CAPACITY IS INCREASED FROM 12 PERCENT TO 43 PERCENT, THE TANK PRESSURE CAN BE REDUCED FROM 45 PSIA TO 20 PSIA.

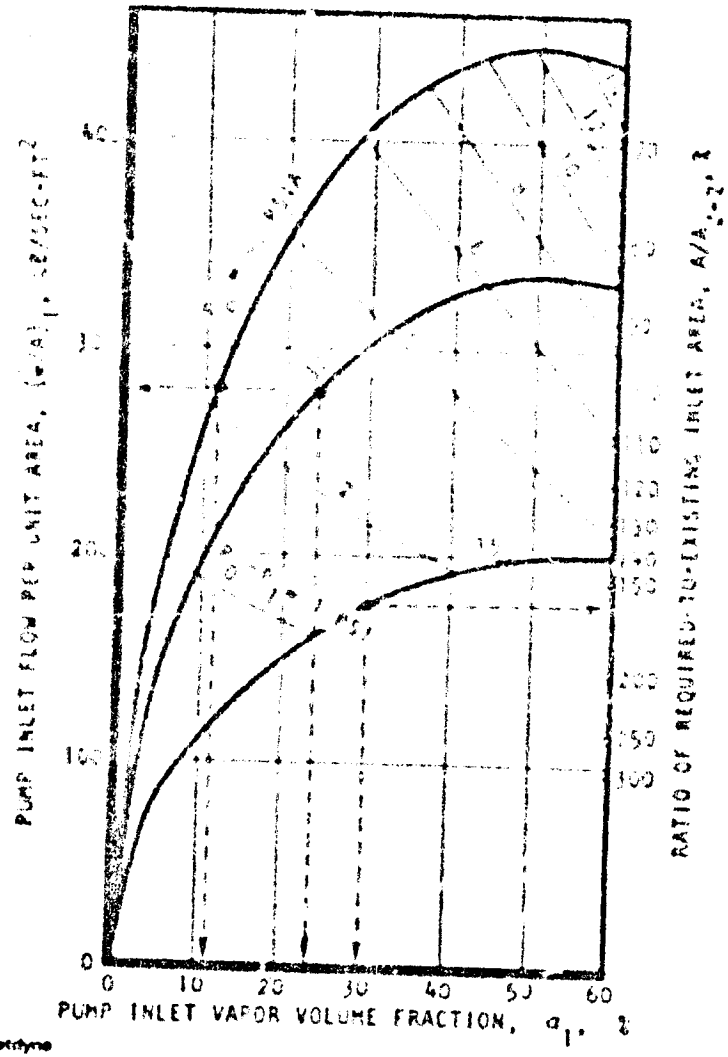

Rocketdyne
North American Rockwell

EQUILIBRIUM ISENTROPIC FLOW EXPANSION FROM SATURATED LIQUID HYDROGEN

- $\dot{W}$ ρAV
- LB/SEC (LB/FT^3) (FT^2) (FT/SEC)
- $\dot{W}/A$ ρV

THE ACOUSTIC VELOCITY FOR TWO-PHASE HYDROGEN IS MUCH LOWER THAN FOR EITHER PHASE ALONE. IN EQUILIBRIUM FLOW, THE VAPORIZATION AND CONDENSATION RATES ARE ASSUMED TO BE HIGH ENOUGH THAT THE VAPOR TEMPERATURE IS ALWAYS EQUAL TO THE LIQUID TEMPERATURE AND BOTH PHASES ARE ALWAYS AT SATURATION. A GIVEN PRESSURE DROP WILL CAUSE VAPORIZATION AS WELL AS EXPANSION OF THE EXISTING VAPOR. THIS WILL CAUSE A RELATIVELY LARGE DROP IN DENSITY AND, THEREFORE, A LOW ACOUSTIC VELOCITY BECAUSE THE VAPOR-TO-LIQUID DENSITY RATIO IS VERY SMALL (APPROXIMATELY 0.04 IN 30 PSIA HYDROGEN).

FOR CONSTANT-QUALITY FLOW, THE CONDENSATION AND VAPORIZATION RATES ARE ASSUMED TO BE SO LOW THAT NO SIGNIFICANT PHASE CHANGE TAKES PLACE. AN ISENTROPIC COMPRESSION, THEREFORE, WILL SUBCOOL THE LIQUID AND SUPERHEAT THE VAPOR. AS NO VAPORIZATION OCCURS, THE ACOUSTIC VELOCITY WILL BE HIGHER.

EQUATIONS FOR ACOUSTIC VELOCITY ARE GIVEN ON PAGE 710, JOURNAL OF SPACECRAFT AND ROCKETS, VOL 7, NO. 6, AIAA, JUNE 1970.

EFFECT OF FLOW PROCESS ON THE ACOUSTIC VELOCITY OF TWO-PHASE HYDROGEN

329-961
3-71

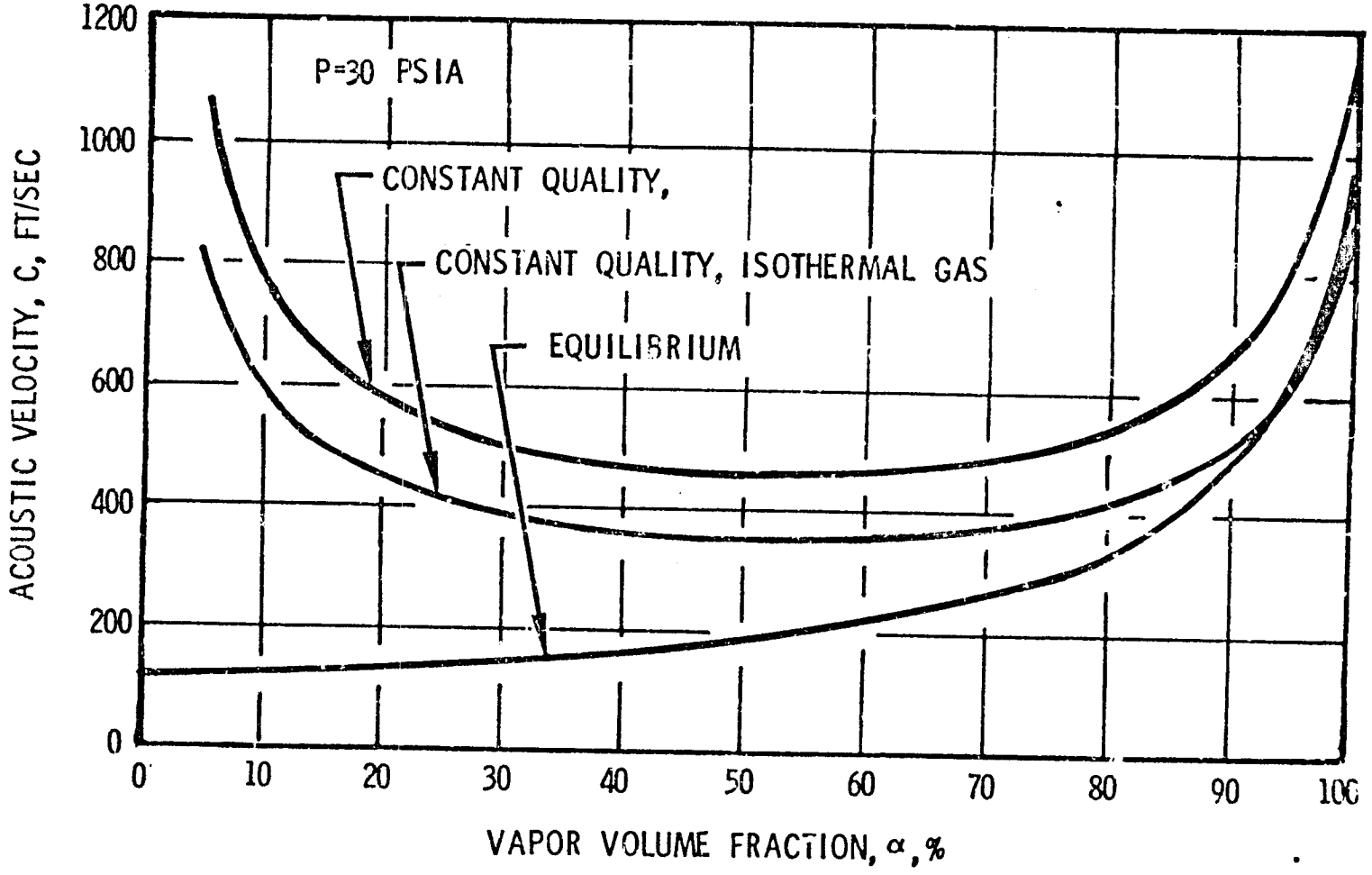

Rocketdyne
North American Rockwell

MATHEMATICAL MODEL

TWO-PHASE HYDROGEN FLOW IS ASSUMED TO BE A HOMOGENEOUS MIXTURE OF VAPOR AND LIQUID WITH ZERO SLIP BETWEEN THE TWO PHASES. IN THE INLET DUCT, THE FLOW HAS A RELATIVELY LARGE RESIDENCE TIME AT CONSTANT FLOW AREA AND, THEREFORE, SHOULD APPROACH EQUILIBRIUM. HOWEVER, RELATIVE TO MOVING INDUCER BLADES, THE RESIDENCE TIMES ARE SO SHORT AND THE AREA CHANGES ARE SO RAPID THAT THERE IS LITTLE TIME FOR VAPORIZATION OR CONDENSATION TO OCCUR; THEREFORE, THE FLOW PROCESS PROBABLY DOES NOT DEVIATE MUCH FROM CONSTANT QUALITY FLOW.

WHEN THE MASS FLOW IS CONSTANT, AN INCREASE IN VAPOR FRACTION CAUSES THE INDUCER BLADE FLOW PASSAGES PRESENTED TO THE FLOW TO CHANGE FROM A DIVERGING SECTION (A IN THE FOLLOWING FIGURE) TO A CONVERGING SECTION (B IN THE FOLLOWING FIGURE). THE DESIGN INCIDENCE-TO-BLADE ANGLE RATIO (i/β) IS A PERTINENT CRITERION.

EFFECT OF FLOW COEFFICIENT ON FLOW GEOMETRY AT INDUCER INLET

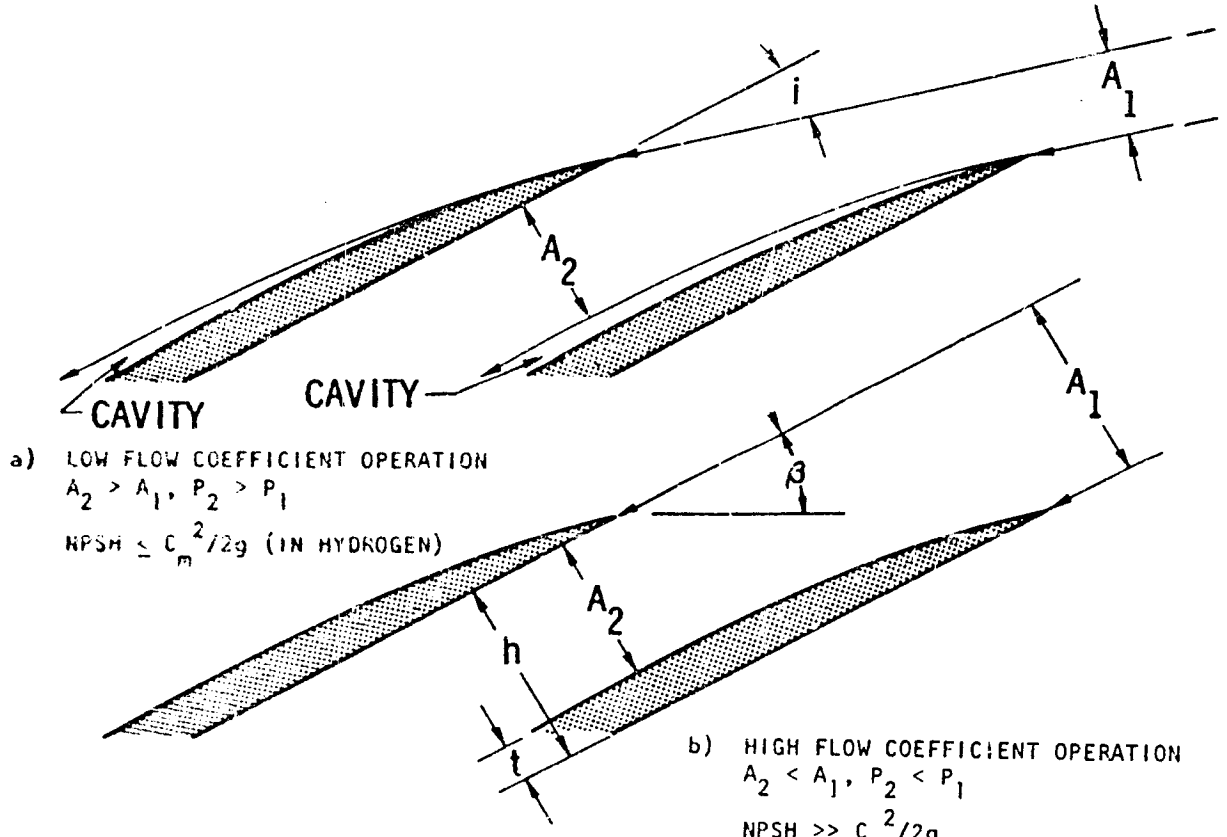

a) LOW FLOW COEFFICIENT OPERATION
$A_2 > A_1$, $P_2 > P_1$
NPSH $\leq C_m^2/2g$ (IN HYDROGEN)

b) HIGH FLOW COEFFICIENT OPERATION
$A_2 < A_1$, $P_2 < P_1$
NPSH $>> C_m^2/2g$

THE VAPOR FRACTION OF AN INDUCER CAN BE APPROXIMATED BY

$$\alpha_i = 1 - \frac{\left[1 - (i/\beta)_L\right]}{1 - B}$$

WHERE $B = \frac{n\,t}{\pi\,D\,\sin\beta}$:

t IS THE BLADE PLUS BOUNDARY LAYER THICKNESS

n, THE NUMBER OF BLADES

D, THE INDUCER DIAMETER AT THE RMS

β, THE BLADE ANGLE AT THE RMS

$(i/\beta)_L$, THE INCIDENCE-TO-BLADE ANGLE RATIO OF LIQUID AT THE RMS WHERE THE AXIAL VELOCITY IS CALCULATED FROM THE EQUATION $\dot{w} = \rho_L A C_m$

DERIVATION OF THE EQUATION IS BASED ON AREA RATIOS

THE FOLLOWING FIGURE IS A PLOT OF THIS RELATIONSHIP. IT SHOWS THAT THE VAPOR PUMPING CAPACITY MAY BE INCREASED BY DECREASING BLADE BLOCKAGE OR BY INCREASING i/β . AVAILABLE DATA SHOWED GOOD AGREEMENT FOR THE MK 15, THE MK 25 AND THE MK 29 PUMPS WHICH ARE SPOTTED ON THE CURVE. THE PREDICTION FOR THE TWO-PHASE INDUCER WAS LATER VERIFIED.

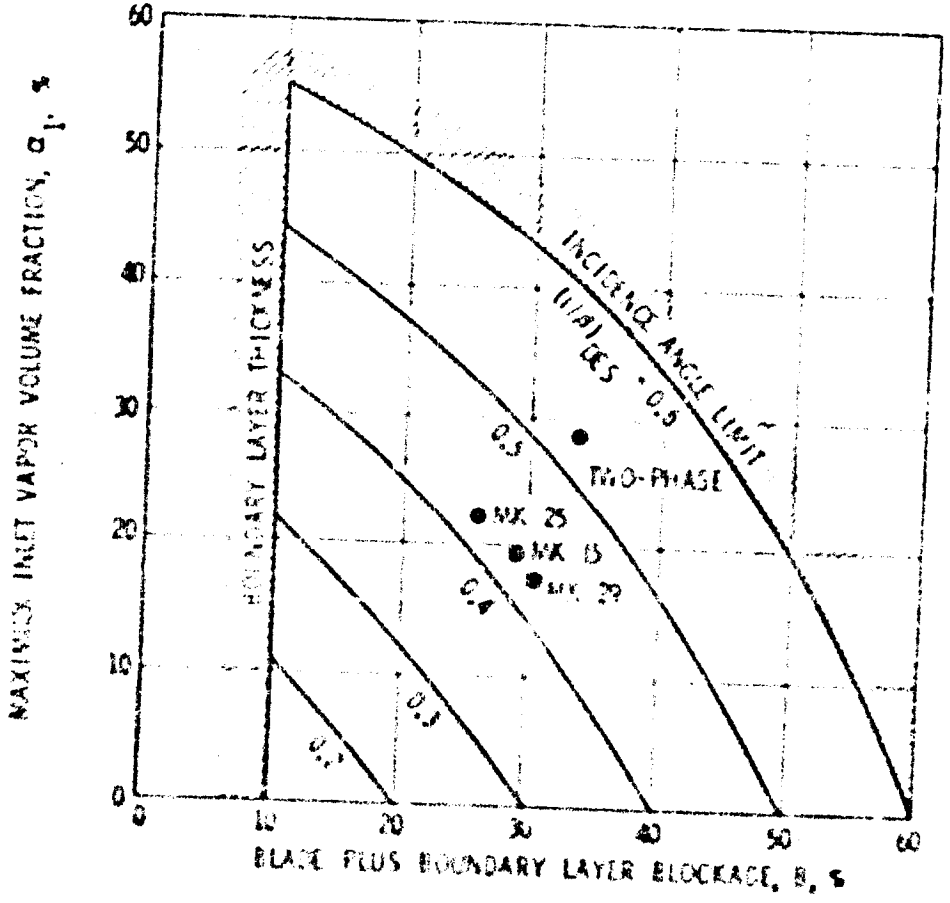

INDUCER VAPOR PUMPING CAPABILITIES DURING DESIGN POINT OPERATION

THE FOLLOWING TABLE LISTS THE VARIOUS MODELS THAT WERE PROGRAMMED ON THE COMPUTER. ALL REPRESENT A CONSTANT QUALITY FLOW PROCESS BECAUSE THE INDUCER ENTRY TIME IS PROBABLY INSUFFICIENT FOR THE TWO PHASES TO REACH EQUILIBRIUM. THE FIRST FOUR MODELS (FOR ISOTHERMAL GAS IN WHICH THE DENSITY WAS PROPORTIONAL TO THE PRESSURE) WERE ELIMINATED BECAUSE OF POOR AGREEMENT WITH AVAILABLE DATA. THE LAST 7 MODELS ARE SHOWN PLOTTED ON THE FIGURE FOLLOWING THE TABLE.

FLOW MODELS INVESTIGATED

MODEL	GASEOUS PHASE	OBLIQUE SHOCK WAVE TYPE (NORMAL IF MI < MI_{MIN})	ASSUMED NORMAL SHOCKS	FLOW CONDITION AFTER NORMAL SHOCK	VAPOR CAVITY
MOD-1T	ISOTHERMAL	WEAK	NONE	TWO-PHASE	NONE
MOD-2T	↓	STRONG	NONE	↓	↓
MOD-3T		WEAK	DISCHARGE PRESSURE SURFACE		
MOD-4T		NONE	INLET SUCTION SURFACE		
MOD-1PG	PERFECT	WEAK	NONE		
MOD-2PG	↓	STRONG	↓		
MOD-5PG		STRONG			IF $A_t > A_1$
MOD-6PG		WEAK		LIQUID	IF $A_t > A_1$
MOD-7PG		WEAK		LIQUID IF $A_t > A_1$	IF $A_t > A_1$

PERFECT GAS FLOW MODEL PREDICTIONS

THE CHARACTERISTICS OF THE FLOW MODELS IN WHICH THE GASEOUS PHASE IS A PERFECT GAS (SEE PRECEEDING TABLE) ARE ILLUSTRATED IN THIS FIGURE. OBSERVATION OF TWO-PHASE HYDROGEN TEST DATA (MK 15-F AND MK-25 PUMPS) INDICATES THAT THE INDUCER STATIC PRESSURES DO NOT FALL SIGNIFICANTLY UNTIL THE VAPOR PUMPING LIMIT IS REACHED AND THAT THE CURVES DO NOT HAVE A SUDDEN RISE JUST BEFORE REACHING THE LIMIT. THE ONLY PERFECT GASEOUS PHASE MODEL THAT HAS THESE GENERAL CHARACTERISTICS IS MOD-7PG. THE ISOTHERMAL GASEOUS PHASE MODELS ALL PREDICTED A LARGE DROP IN PRESSURE AND A HIGH VAPOR FRACTION AT THE VAPOR PUMPING LIMIT.

FLOW MODEL COMPARISON--PERFECT GAS

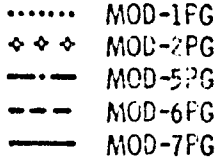

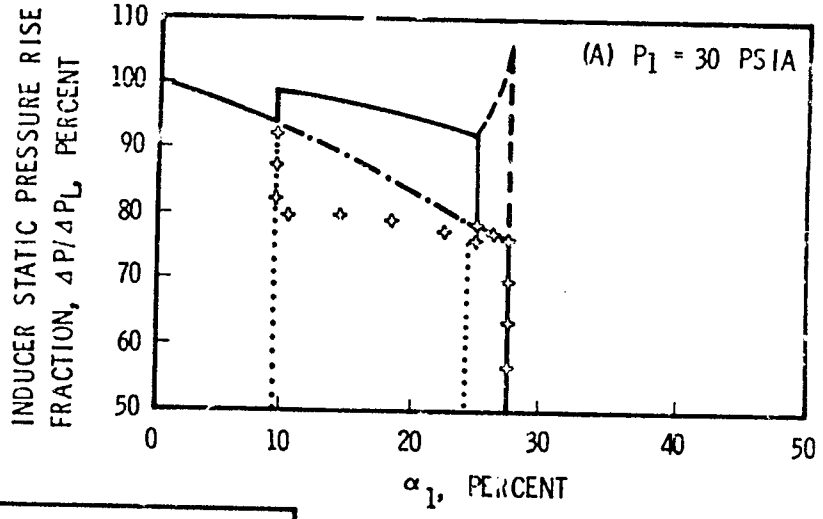

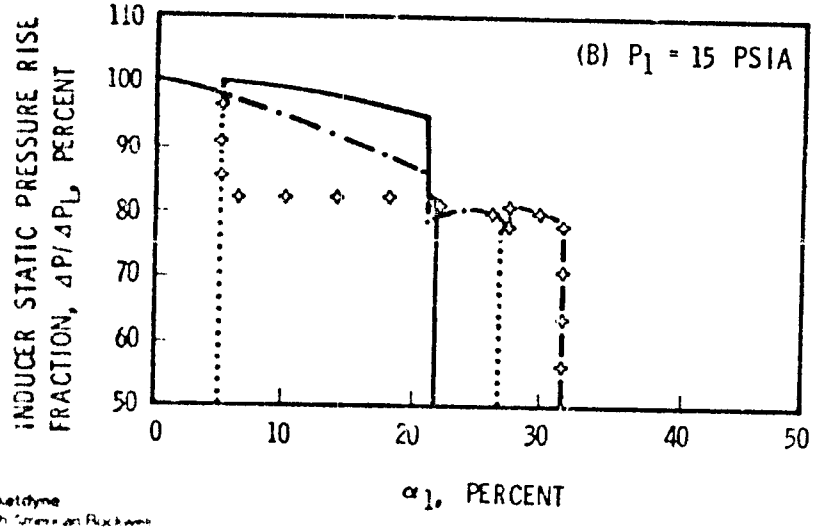

TYPICAL FLAT PLATE INDUCER
- $\beta_1 = \beta_2$
- Um = 800 FT/SEC
- BLADE BLOCKAGE = 25%
- ϕ_{LM} = 0.10

TWO-PHASE HYDROGEN INDUCER CONTOUR

THE FOLLOWING FIGURE IS A LAYOUT SHOWING THE CONTOUR OF THE TWO-PHASE HYDROGEN INDUCER. THE MAXIMUM DIAMETER AT THE INDUCER ENTRANCE IS 8.6 INCHES, BUT BECAUSE OF THE SWEEPBACK OF THE BLADE, THE MAXIMUM INDUCER DIAMETER IS 8.33 INCHES; THIS RESULTS IN A DESIGN INCIDENCE ANGLE OF 3.65 DEGREES AND AN INCIDENCE-TO-BLADE ANGLE RATIO OF 0.531.

NOTE THAT THE HOLE IN THE SPINNER, THROUGH WHICH RETURN FLOW FROM THE REAR BEARING NORMALLY OCCURS, WAS BLANKED OFF, AND THE RETURN FLOW WAS VENTED OVERBOARD TO AVOID ANY EXTRA VAPOR AT THE INLET.

NOMINAL CONDITIONS FOR THE INDUCER-PUMP COMBINATION WERE:

N = 28,000 RPM Q = 8648 GPM ΔH = 41,800 FT

INDUCER CONTOUR

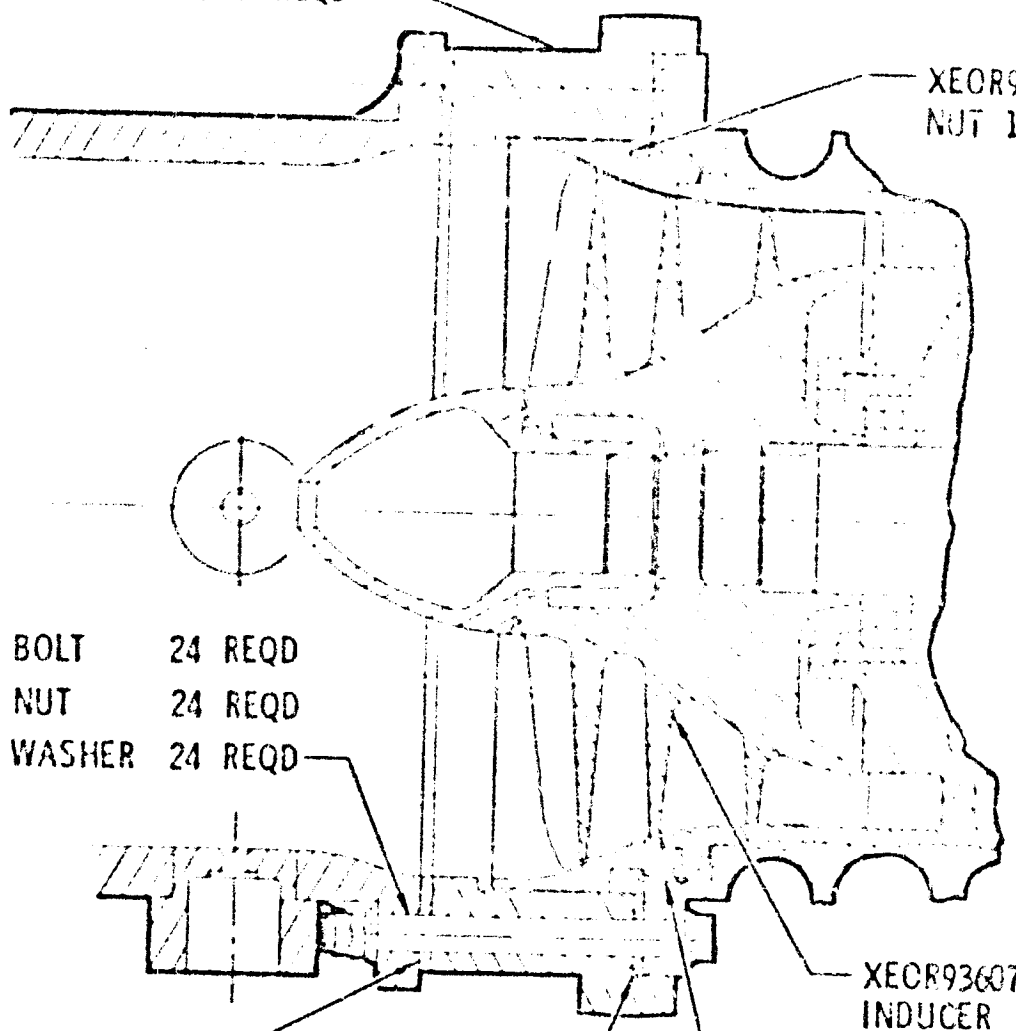

Rocketdyne
North American Rockwell

TWO-PHASE INDUCER

THE FOLLOWING FIGURE IS A PHOTOGRAPH OF THE TWO-PHASE HYDROGEN INDUCER

TWO-PHASE INDUCER

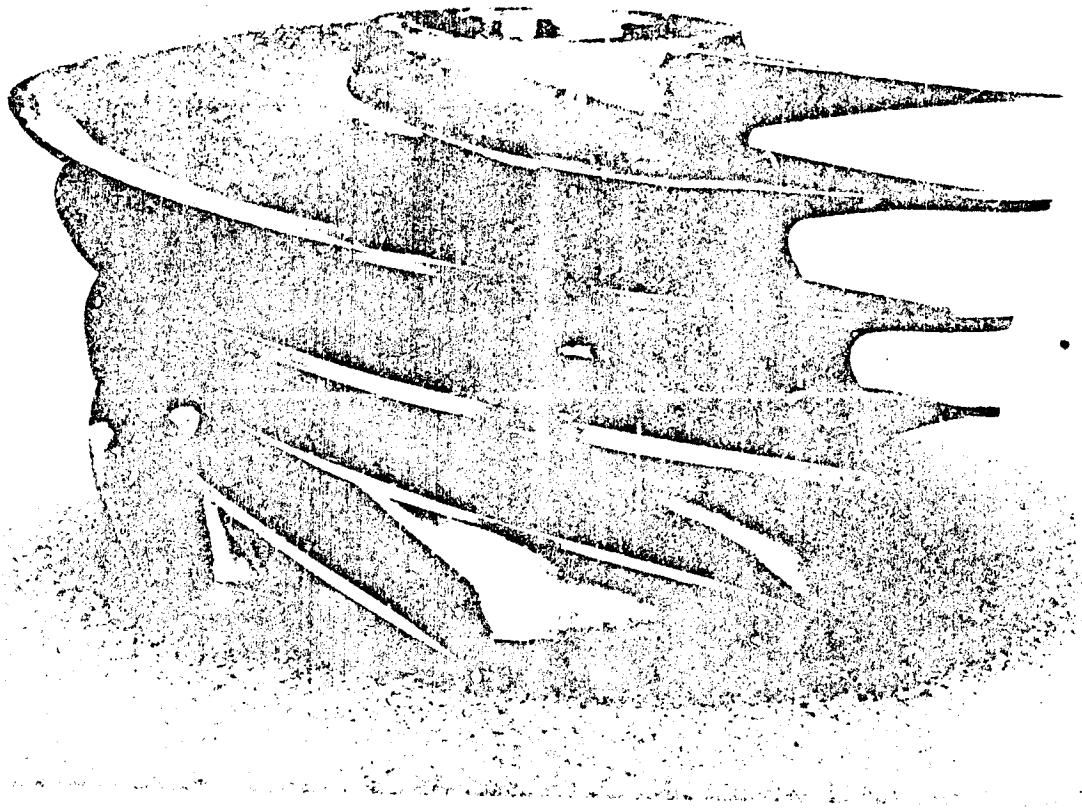

Rocketdyne
North American Rockwell

TEST SETUP

THE FOLLOWING SKETCH SHOWS DETAILS OF THE HORIZONTAL PORTION OF THE INLET DUCT. THE THROTTLING SECTION IN THIS DUCT CONSISTED OF A 40-MESH SCREEN (33 PERCENT THROUGH AREA) BACKED BY A FRANTZ-TYPE SCREEN (APPROXIMATELY 5/32-INCH TRIANGULAR OPENINGS). THIS COMBINATION RESULTED IN APPROXIMATELY A 5 PSI DROP AT 28,000 RPM FLOWRATES. REDUNDANT PRESSURE AND TEMPERATURE MEASUREMENTS WERE MADE ON BOTH SIDES OF THE SCREEN.

THE VAPOR FRACTION CALCULATION AT THE INDUCER INLET WAS BASED ON A CONSTANT-ENTHALPY THROTTLING PROCESS ACROSS THE SCREEN. WHEN TWO-PHASE FLOW EXISTED AFTER THE SCREEN, THE TEMPERATURE AT THIS STATION DROPPED AND WAS CONSIDERED TO BE INACCURATE BECAUSE OF VAPORIZATION ON THE TEMPERATURE PROBE.

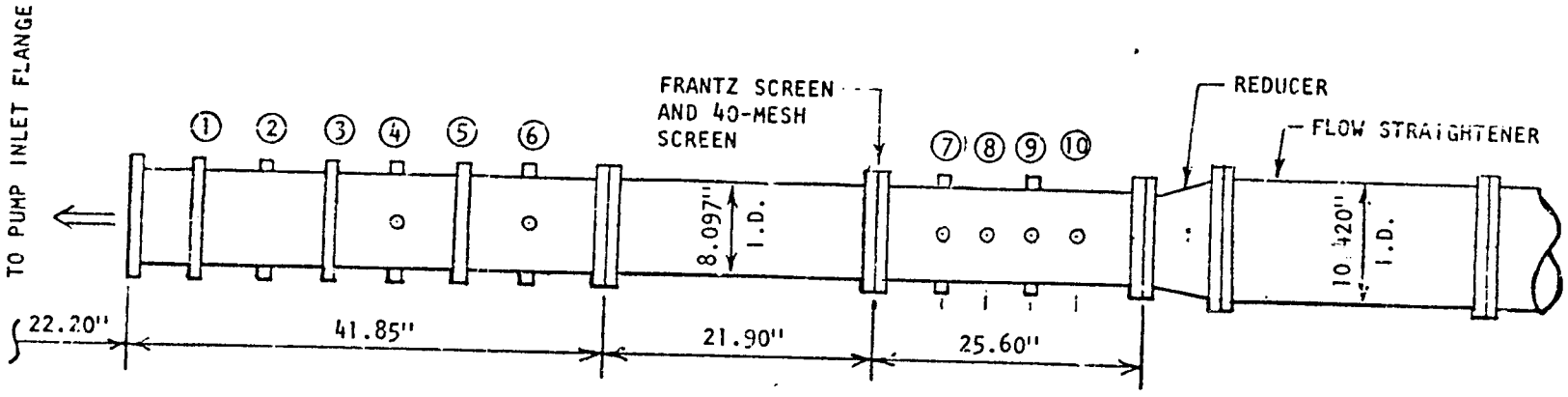

STATION	PARAMETER
1	STATIC PR #1
2	TOTAL PR
3	STATIC PR #2
4	TEMP #1
5	STATIC PR #3
6	TEMP #2
7	STATIC PR #4
8	TEMP #3 (RMS)
"	TEMP #4 (CENTERLINE)
9	STATIC PR #5
10	TEMP #5 (RMS)
"	TEMP #6 (CENTERLINE)

INSTALLED PUMP

THE PHOTOGRAPH SHOWS THE INSTALLED PUMP WITH THE VERTICAL HEATER IN THE FOREFRONT. THE PUMP WAS DRIVEN BY AN ELECTRIC MOTOR AND GEARBOX ON THE OTHER SIDE OF THE WALL. THE PUMP DISCHARGED THROUGH THE VERTICAL PIPE NEAR THE REAR WALL. ALL INSTRUMENTATION READINGS WERE REMOTE.

PUMP INLET LINE

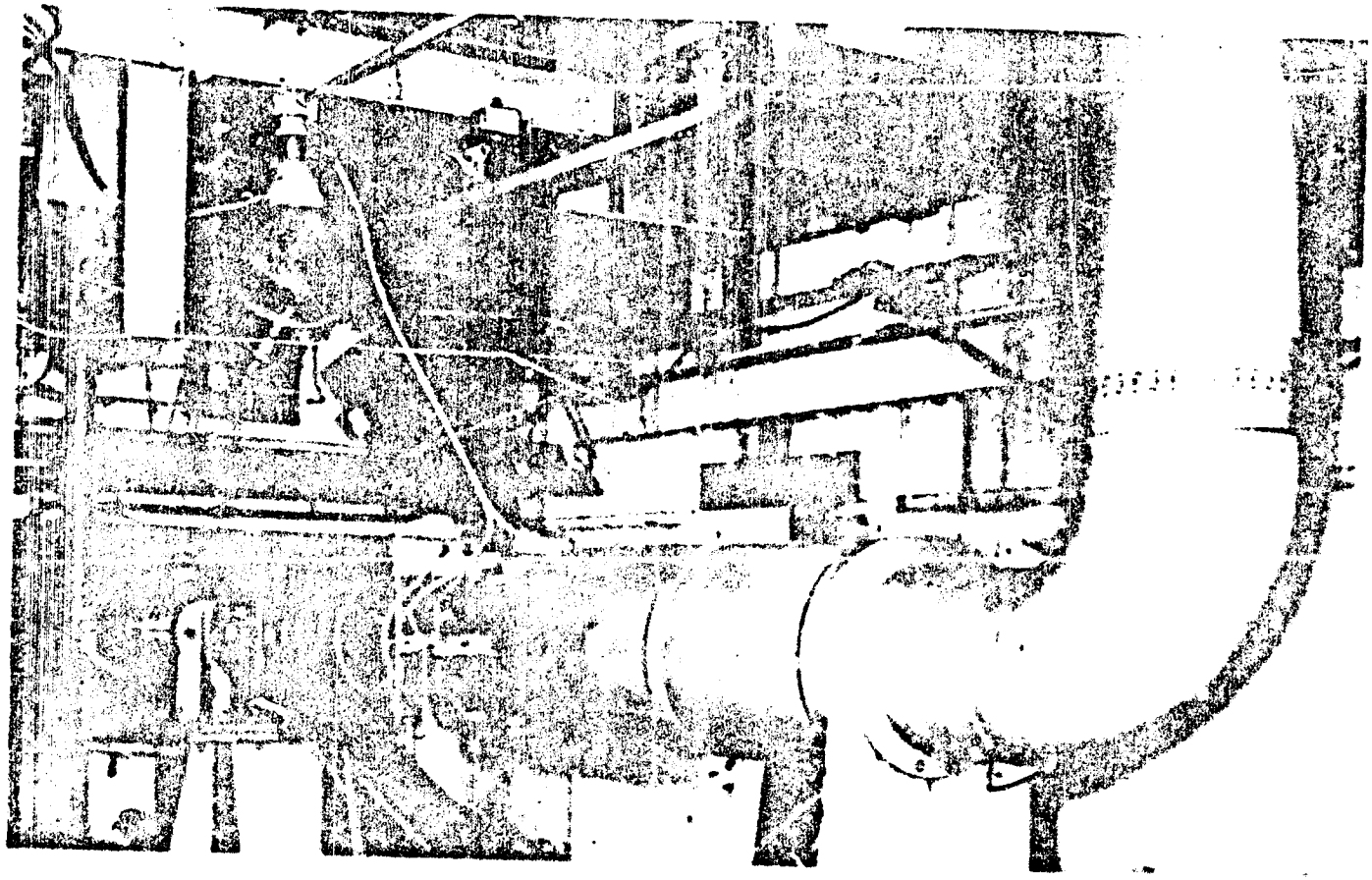

Rocketdyne
North American Rockwell

TEST RESULTS OF TWO-PHASE HYDROGEN INDUCER

TWO CAVITATION CURVES BASED ON OVERALL PUMP HEAD RISE ARE SHOWN AT THE DESIGN SPEED OF 28,000 RPM. THE FIRST IS AT A LOW FLOW COEFFICIENT; THE SECOND IS AT NOMINAL FLOW. THE Q/N VALUE SHOWN IN EACH CURVE TITLE IS A NOMINAL VALUE REPRESENTING TEST CONDITIONS AT THE START OF THE VENT-DOWN. THE CRITICAL VALUES CORRESPOND TO CONDITIONS AT 2-PERCENT HEAD LOSS. THE SUBSCRIPT L DENOTES THE LIQUID STATE AND REFERS TO THE EQUIVALENT VOLUMETRIC FLOW OBTAINED BY USING THE SATURATED LIQUID DENSITY CORRESPONDING TO THE TEMPERATURE AND PRESSURE. THE ABSENCE OF THE SUBSCRIPT L DENOTES ACTUAL CONDITIONS, I.E., A TWO-PHASE CONDITION.

THE CURVES ARE WELL DEFINED AND SMOOTH EXCEPT FOR A 2- TO 3-PERCENT DIP AND RAPID RECOVERY THAT WAS PRESENT ONLY FOR THE 28,000 RPM TESTS AT 37R AS SATURATION CONDITIONS WERE APPROACHED. THE PHENOMENON OCCURRED OVER THE ENTIRE RANGE OF Q/N VALUES.

TEST RESULTS--TWO-PHASE FLOW INDUCER (P/N XEOR 936071)

$Q/N = 0.295$, $(i/\beta)_L = 0.552$, N=28000 RPM

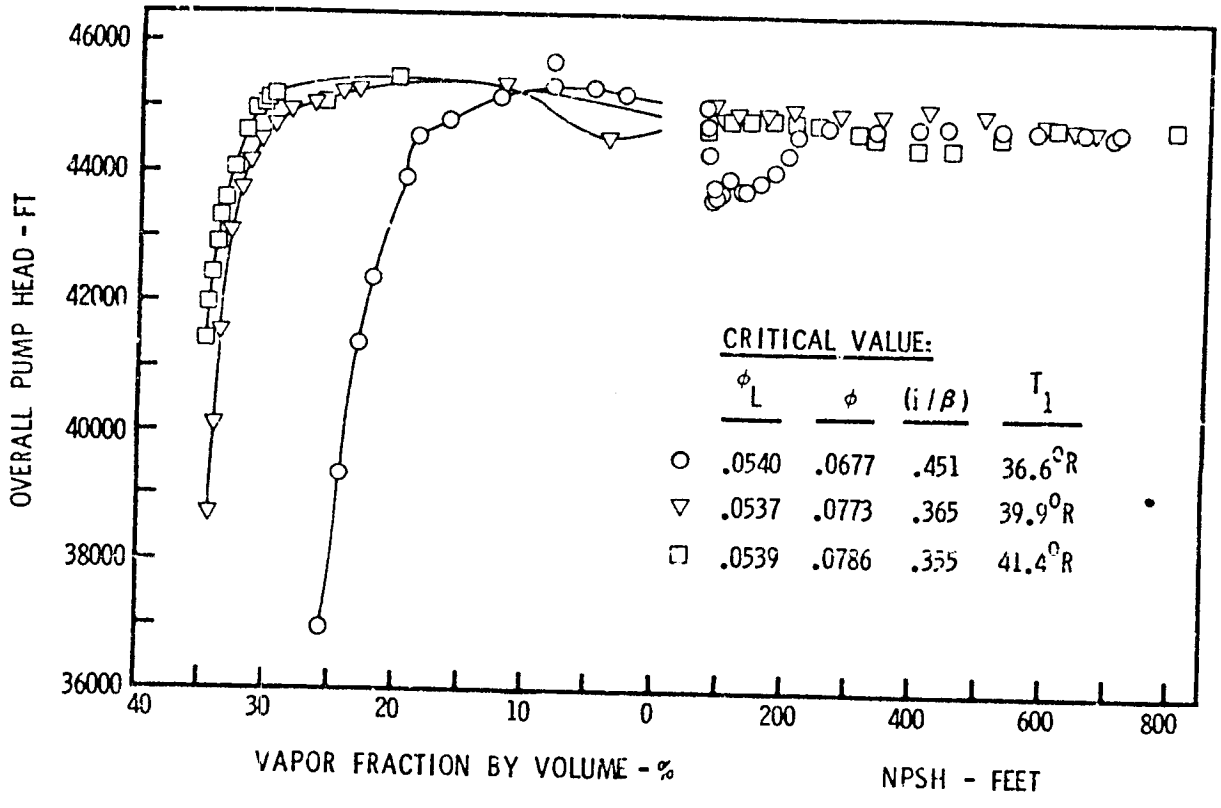

Rocketdyne
North American Rockwell

TEST RESULTS--TWO-PHASE FLOW INDUCER (P/N XEOR 936071)

$Q/N=0.318$, $(i/\beta)_1=0.515$, N=28,000 RPM

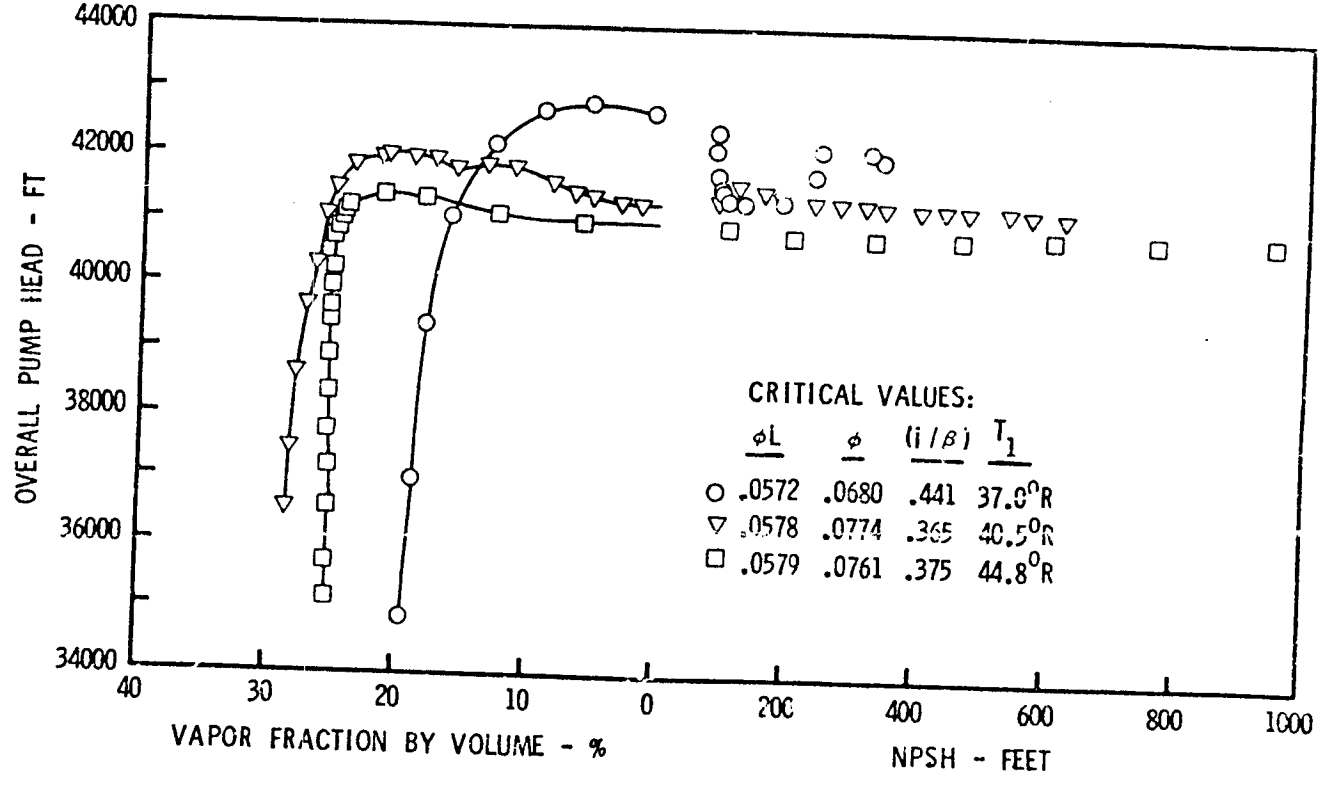

Rocketdyne
North American Rockwell

PERFORMANCE SUMMARY

ALL TWO-PHASE PERFORMANCE DATA AT 28,000 RPM OBTAINED ON THE TWO-PHASE HYDROGEN INDUCER ARE SUMMARIZED IN THE NEXT FIGURE. THE DATA ARE PLOTTED IN TERMS OF CRITICAL INCIDENCE-TO-BLADE ANGLE RATIO FOR THE TWO-PHASE VALUE AS A FUNCTION OF HYDROGEN TEMPERATURE. ALL RESULTS ARE AT 2-PERCENT LOSS IN PUMP HEAD. THE AREA BELOW THE TOP CURVE REPRESENTS A REGION OF LARGE HEAD LOSS. WHEN THE PUMP OPERATES AT VALUES ABOVE THE CURVE IT CAN HANDLE TWO-PHASE HYDROGEN WITH NO APPRECIABLE LOSS IN HEAD. THERE WOULD, HOWEVER, BE AN UPPER LIMIT BECAUSE PUMPS OPERATING AT TOO HIGH AN INDUCER INCIDENCE ANGLE CAN BECOME UNSTABLE, THE INDUCER MIGHT EVEN STALL.

IT IS PROBABLE THAT THE CURVE BECOMES VERTICAL AT SOME LOWER HYDROGEN TEMPERATURE BECAUSE OF CHOKING IN THE INLET LINE. THE CURVE APPEARS TO REACH A MINIMUM AT 43R BUT THIS OBSERVATION IS TENTATIVE BECAUSE THE DECLINE IN THE CRITICAL VALUE OF α IS BASED ON ONLY ONE DATA POINT AT 44.8R. THE MATHEMATICAL MODEL, HOWEVER, ALSO INDICATES A SLIGHT DECLINE IN VAPOR VOLUME AT THESE HIGHER TEMPERATURES.

PERFORMANCE SUMMARY OF TWO-PHASE FLOW INDUCER (P/N XEOR 936071) N=28,000 RPM

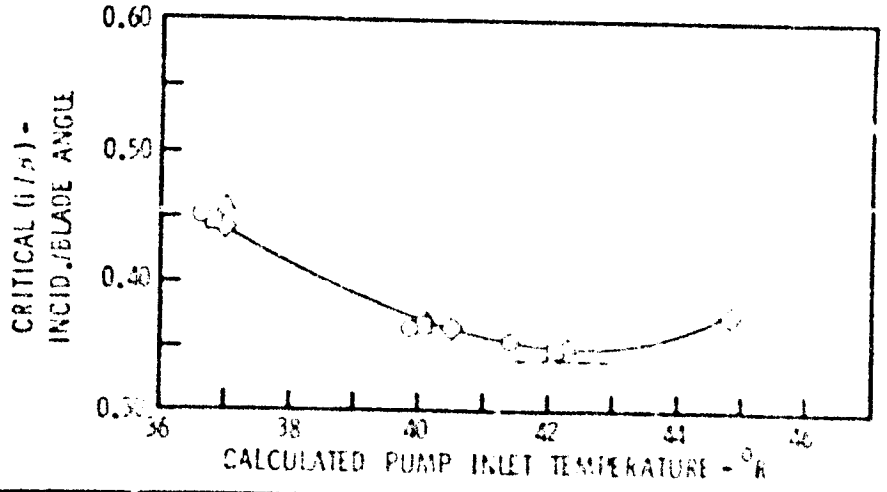

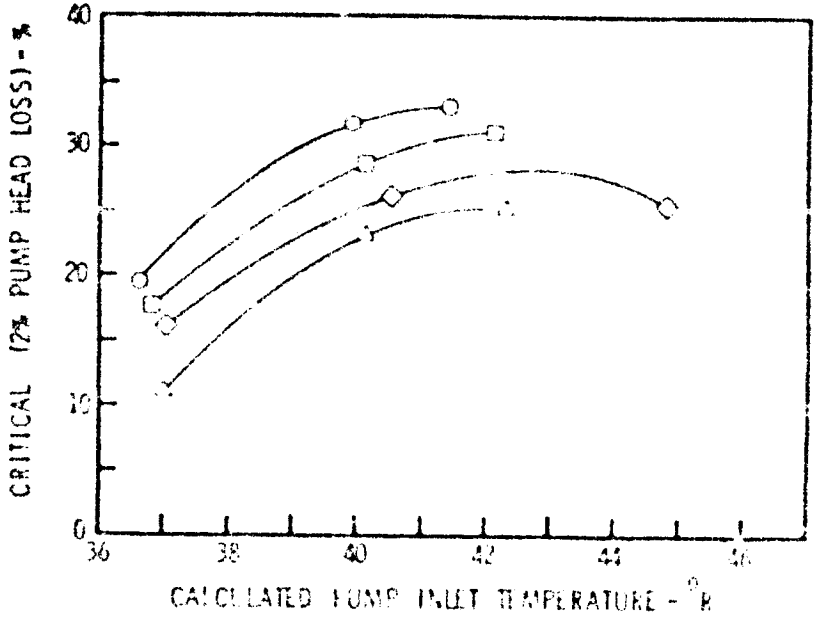

Φ_L	% Q/N
.0539	93.0
.0558	96.5
.0576	100.0
.0600	103.5

THE SUMMARIZED DATA AT THE LOWER SPEED OF 22,000 RPM ARE SHOWN NEXT. BECAUSE OF THE LOWER FLOWS THE CURVE WOULD BECOME VERTICAL AT A HIGHER TEMPERATURE AND IS, THUS, SIMILAR TO THE PREVIOUS CURVE BUT SHIFTED TO THE LEFT.

PERFORMANCE SUMMARY OF TWO-PHASE FLOW INDUCER (P/N XEOR 936071) N=22,000 RPM

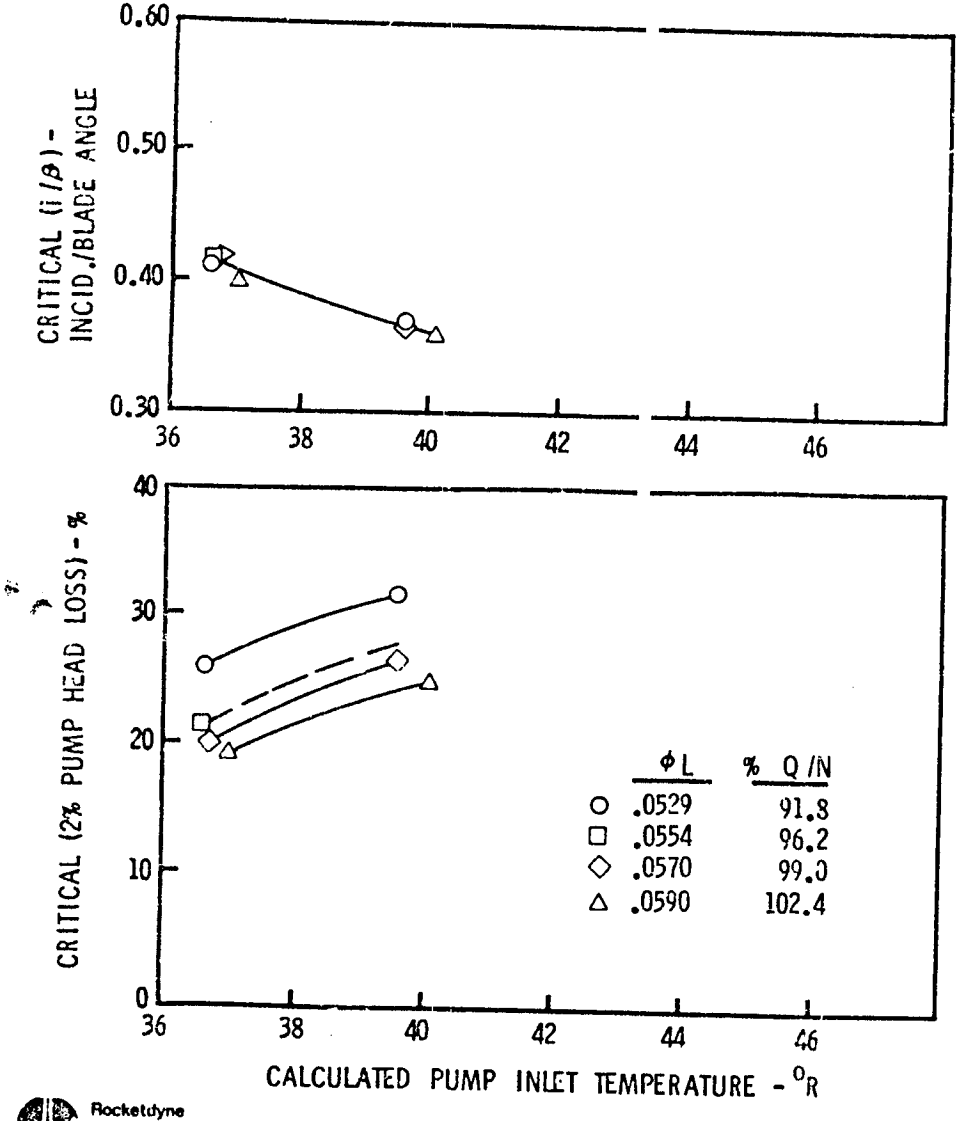

Rocketdyne
North American Rockwell

COMPARISON OF INDUCERS

THE PERFORMANCE OF THE TWO-PHASE INDUCER AT 20-PERCENT LOSS IN STATIC PRESSURE RISE IS COMPARED WITH THAT OF THE J-2 MARK 15 INDUCER IN THE NEXT FIGURE. BOTH INDUCERS WERE TESTED ON THE MARK 15 HYDROGEN PUMP AT THE SAME FACILITY. AT 41 R, THE TWO-PHASE INDUCER WAS ABLE TO ACCEPT MORE THAN THREE TIMES AS MUCH VAPOR ($\alpha_{cr} \cong 30$ PERCENT) AS THE MARK 15 INDUCER ($\alpha_{cr} \cong 10$ PERCENT). AT 37R, THE TWO-PHASE INDUCER WAS ABLE TO ACCEPT 20 PERCENT VAPOR, WHEREAS THE MARK 15 WAS UNABLE TO ACCEPT ANY VAPOR BELOW 39R.

COMPARISON OF INDUCER TWO-PHASE FLOW PERFORMANCES WITH HYDROGEN

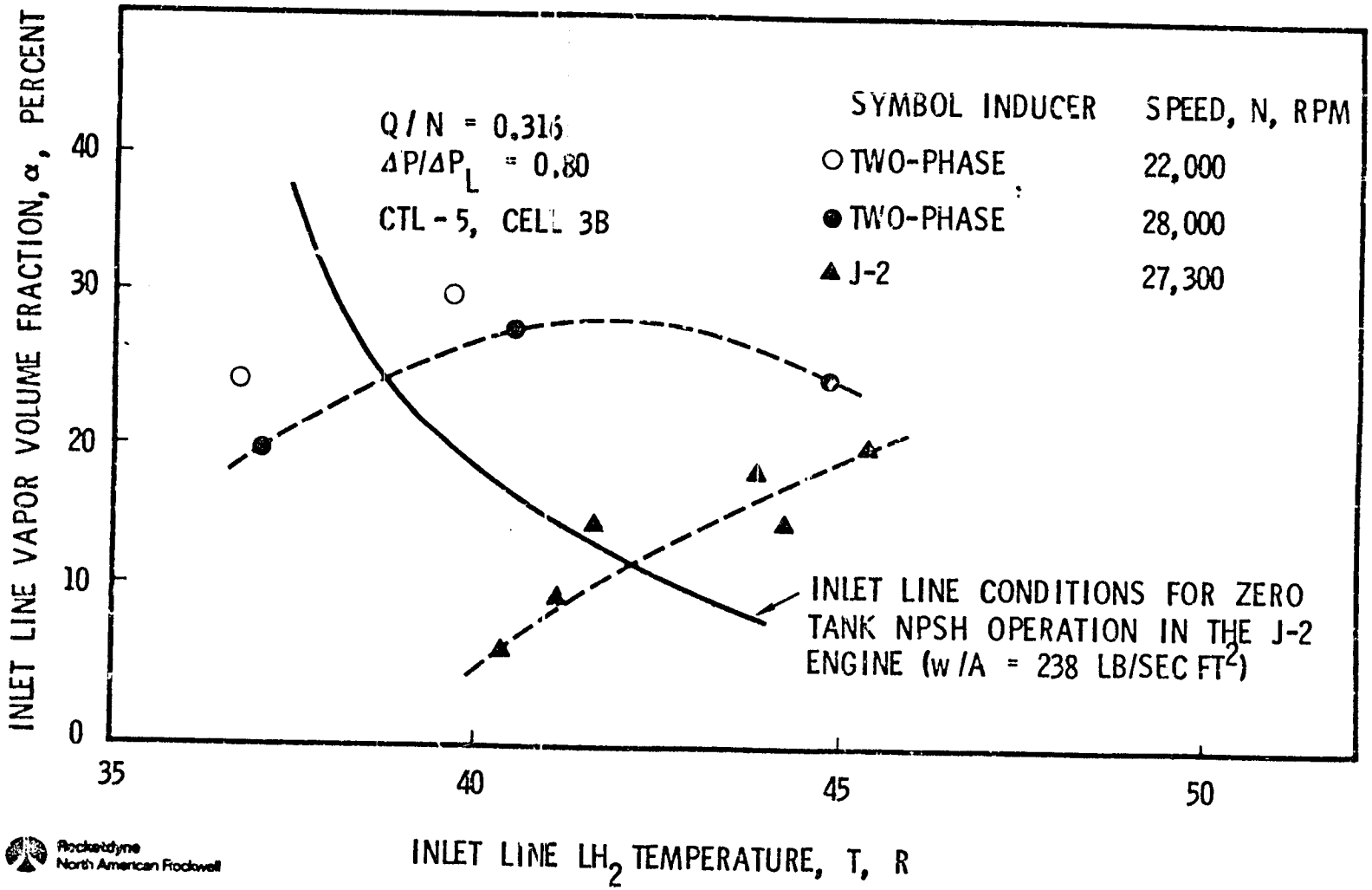

Rocketdyne
North American Rockwell

COMPARISON OF TEST DATA WITH MODEL PREDICTIONS

THE PREDICTED STATIC PRESSURE RISES ACROSS THE TWO-PHASE INDUCER ARE COMPARED WITH THE RESULTS OF THREE TEST RUNS IN THE FOLLOWING FIGURE. THE COMPARISON SHOWS THAT THE MODEL PREDICTS THE TEST DATA TRENDS OVER A RANGE OF INLET PRESSURES FROM 16 TO 47 PSIA. FOR EXAMPLE, THE SUDDEN JUMP AT THE TRANSITION FROM SUBSONIC TO SUPERSONIC INLET FLOW SEEMS TO COINCIDE WITH THE RISE IN THE TEST DATA.

THE LOW INLET PRESSURE CURVE PREDICTS A VERTICAL DROP AT HIGH VAPOR VOLUME FLOWS BECAUSE OF CHOKING IN THE INLET ANNULUS RATHER THAN IN THE BLADES. HOWEVER, THE DATA SHOWS A "DROOPIER" TREND THAT STARTS WHEN THE BLADE RELATIVE MACH NUMBER IS 1.0.

COMPARISON OF TWO-PHASE INDUCER FLOW MODEL PERFORMANCE WITH TWO-PHASE HYDROGEN INDUCER TEST PERFORMANCE AT 28,000 RPM

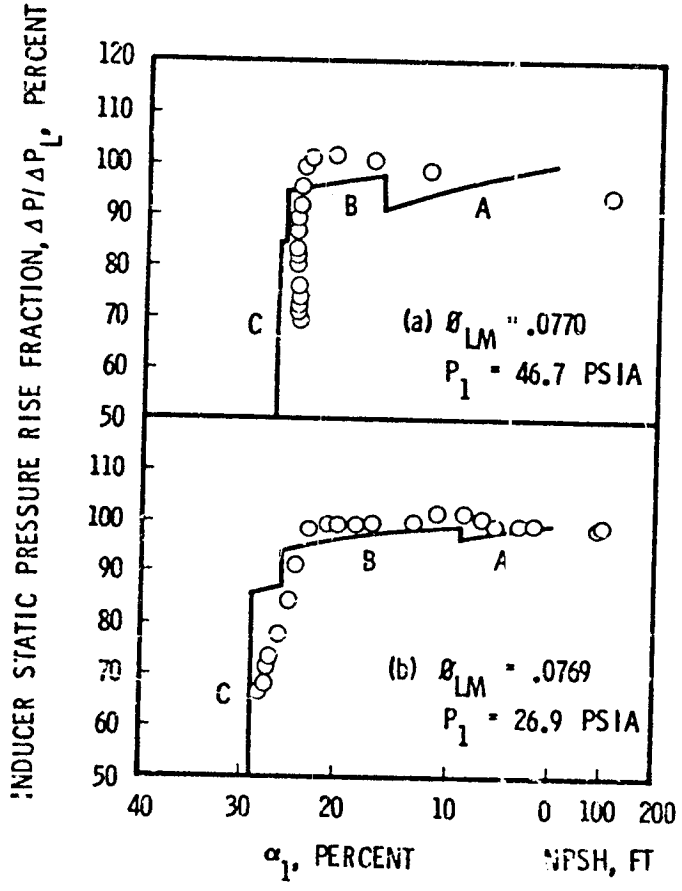

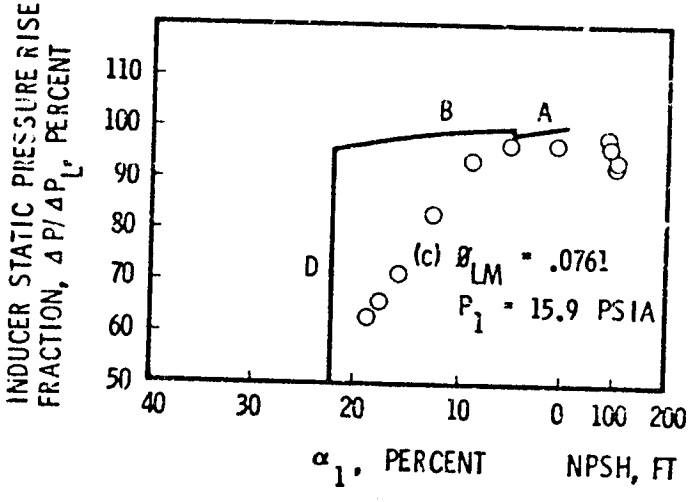

A SUBSONIC FLOW AT INLET

B SUPERSONIC FLOW AT INLET

C BLADE CHOKING LIMIT

D INLET ANNULUS CHOKING LIMIT

Rocketdyne
North American Rockwell

THE INDUCER VAPOR PUMPING LIMITS FOR ALL TEST RUNS AT 28,000 RPM ARE SHOWN NEXT. AGREEMENT WITH MATHEMATICAL MODEL PREDICTIONS IS GOOD OVER THE ENTIRE TEST RANGE OF INLET PRESSURE AND TEMPERATURE. AT LOW INLET PRESSURES, THE VAPOR PUMPING LIMIT IS CHOKING IN THE INLET ANNULUS; AT SLIGHTLY HIGHER INLET PRESSURES, THE LIMIT APPEARS TO BE SUPERSONIC FLOW DOWNSTREAM OF A WEAK OBLIQUE SHOCK WAVE AT BLADE OVERLAP; AT INTERMEDIATE TO HIGH INLET PRESSURES, THE LIMIT IS BLADE CHOKING.

COMPARISON OF FLOW MODEL VAPOR FRACTION LIMITS WITH TEST LIMITS AT 28,000 RPM

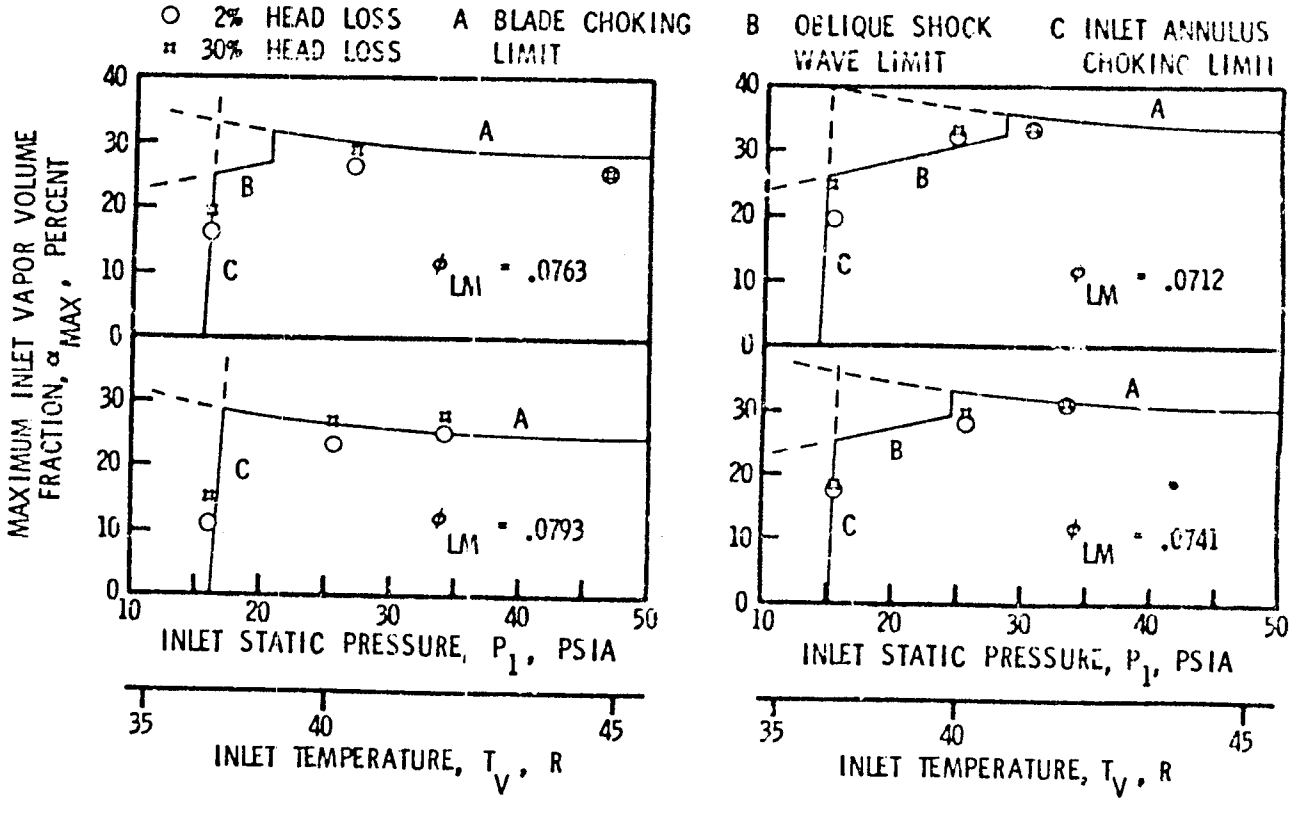

Rocketdyne
North American Rockwell

CONCLUSIONS

- THE ANALYTICAL PREDICTIONS OF MAXIMUM VAPOR VOLUME FRACTION FOR THE TWO-PHASE INDUCER, BASED ON THE MINIMUM VALUE OF THE FOLLOWING LIMITS, (A) BLADE BLOCKAGE CHOKING; (B) FLOW ACCELERATION AND PRESSURE DROP DUE TO SUPERSONIC FLOW; AND (C) INLET ANNULUS CHOKING, WERE FOUND TO AGREE VERY WELL WITH EXPERIMENTAL RESULTS FOR HYDROGEN TEMPERATURES BETWEEN 37 AND 45R.

- THE TWO-PHASE INDUCER, DESIGNED WITH AN INCIDENCE-TO-BLADE ANGLE RATIO OF 0.531, WAS FOUND TO ACCEPT THREE TIMES MORE VAPOR (α_{CR} = 30 PERCENT) THAN THE MARK 15 INDUCER (α_{CR} = 10 PERCENT) AT A HYDROGEN TEMPERATURE OF 41R.

- THE TWO-PHASE INDUCER WAS FOUND TO ACCEPT AT LEAST 20 PERCENT VAPOR VOLUME FRACTION DOWN TO 37R WHEREAS THE MARK 15 INDUCER HAD ZERO VAPOR CAPACITY AT 39R

- THE TWO-PHASE INDUCER IS CAPABLE OF OPERATING AT ZERO-TANK NPSH AT A LOWER TANK PRESSURE (P_{TANK} = 23.2 PSIA, T = 39.5R) THAN THE MARK 15 INDUCER (P_{TANK} = 34.6 PSIA, T = 42.4R)

"SATURATED LH_2 TURBOPUMP OPERATION"

H. P. STINSON

MARSHALL SPACE FLIGHT CENTER

INTRODUCTION

THE SATURATED LH_2 TURBOPUMP - LOX/LH_2 ENGINE OPERATION PROGRAM WAS CONDUCTED AT THE MARSHALL SPACE FLIGHT CENTER TO DEMONSTRATE THE FEASIBILITY OF "ZERO-TANK NPSH" USING J-2 ENGINE AND S-IVB STAGE HARDWARE. THE FIRST PHASE OF THE PROGRAM WAS J-2 HYDROGEN PUMP TESTING, AND THE SECOND PHASE J-2 ENGINE TESTING.

THE DEFINITION OF "ZERO-TANK NPSH", THE DESIRABILITY OF THIS OPERATIONAL MODE, AND THE TEST PROGRAM TO DEMONSTRATE ITS FEASIBILITY IS PRESENTED.

MARSHALL SPACE FLIGHT CENTER SCIENCE & ENGINEERING	INTRODUCTION	LAB: S&E-ASTN-PPA NAME: H. P. Stinson DATE: April 6, 1971

- IN-HOUSE TEST PROGRAM
  - J-2 TURBOPUMP FACILITY
  - J-2 ENGINE TEST FACILITY (S-IVB BATTLESHIP)
- OBJECTIVE
  - DEMONSTRATE THE FEASIBILITY OF "ZERO-TANK NPSH" OPERATION USING J-2 HARDWARE

MSFC - Form 3149 (Rev June 1970)

CHART No. _____

ZERO-TANK NPSH

WHAT IS "ZERO-TANK NPSH", AND WHAT OPERATING REQUIREMENTS ARE PLACED ON THE PUMP? NET POSITIVE SUCTION HEAD (NPSH) IS BY DEFINITION THE TOTAL PRESSURE ABOVE VAPOR PRESSURE. SINCE VELOCITY PRESSURE IN A PROPELLANT TANK IS ESSENTIALLY ZERO, THE TANK IS SAID TO HAVE "ZERO-NPSH" WHEN THE TANK STATIC PRESSURE EQUALS THE VAPOR PRESSURE. LOOKING AT A TEMPERATURE-ENTROPY DIAGRAM THE "ZERO-TANK NPSH" CONDITION IS REPRESENTED BY A POINT ON THE SATURATED LIQUID LINE. WITH THE PROPELLANT IN THE TANK AT THIS CONDITION (SATURATED LIQUID IN THE TANK) ANY PRESSURE REDUCTION DUE TO VELOCITY OR LINE LOSSES WILL RESULT IN TWO-PHASE FLUID AT PUMP INLET. THEREFORE, TO OPERATE AT "ZERO-TANK NPSH" THE PUMP MUST BE CAPABLE OF OPERATING WITH TWO-PHASE PROPELLANT AT ITS INLET.

MARSHALL SPACE FLIGHT CENTER SCIENCE & ENGINEERING	SATURATED LH_2 TURBOPUMP OPERATION	LAB: S&E-ASTN-PPA NAME: H. P. Stinson DATE: April 6, 1971

ZERO-TANK NPSH

● - TANK
▲ - PUMP INLET

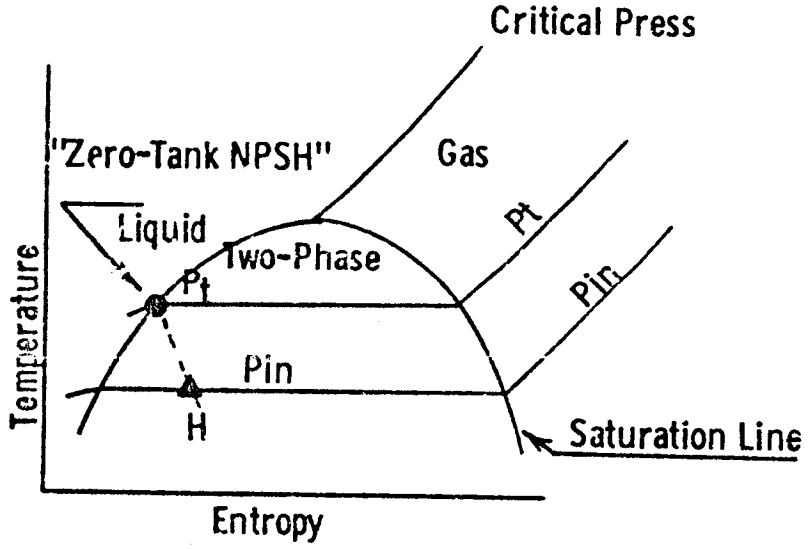

MSFC - Form 3369 (Rev June 1970)

CHART No. _____

ADVANTAGES OF "ZERO-TANK NPSH"

WHY IS "ZERO-TANK NPSH" A DESIRABLE MODE OF OPERATION? THIS CAN BEST BE EXPLAINED BY EXAMINING THE RESTART REQUIREMENTS OF THE S-IVB STAGE OF THE SATURN V. FOLLOWING THE FIRST BURN, THE PROPELLANT TANK IS CONTINUOUSLY VENTED TO A LOWER PRESSURE TO MAINTAIN COLD PROPELLANTS DURING ORBITAL COAST. PRIOR TO ENGINE RESTART THE TANKS MUST BE REPRESSURIZED TO PROVIDE PROPELLANTS MEETING START REQUIREMENTS. THIS IN TURN NECESSITATES A SPECIAL ONBOARD REPRESSURIZATION SYSTEM.

IF, ON THE OTHER HAND, "ZERO-TANK NPSH" WERE EMPLOYED, THE PROPELLANT WOULD HEAT UP DURING ORBITAL COAST, REACH SATURATION AT MAXIMUM ALLOWABLE TANK PRESSURE, AND REMAIN AT THIS CONDITION UNTIL ENGINE RESTART. SINCE THE ENGINE CAN START WITH THE PROPELLANT IN THE TANK AT SATURATION, A REPRESSURIZATION SYSTEM CAN BE ELIMINATED, AND TANK VENTING MINIMIZED.

MARSHALL SPACE FLIGHT CENTER SCIENCE & ENGINEERING	SATURATED LH_2 TURBOPUMP OPERATION	LAB: S&E-ASTN-PPA NAME: H. P. Stinson DATE: April 6, 1971

ADVANTAGES OF "ZERO-TANK NPSH"

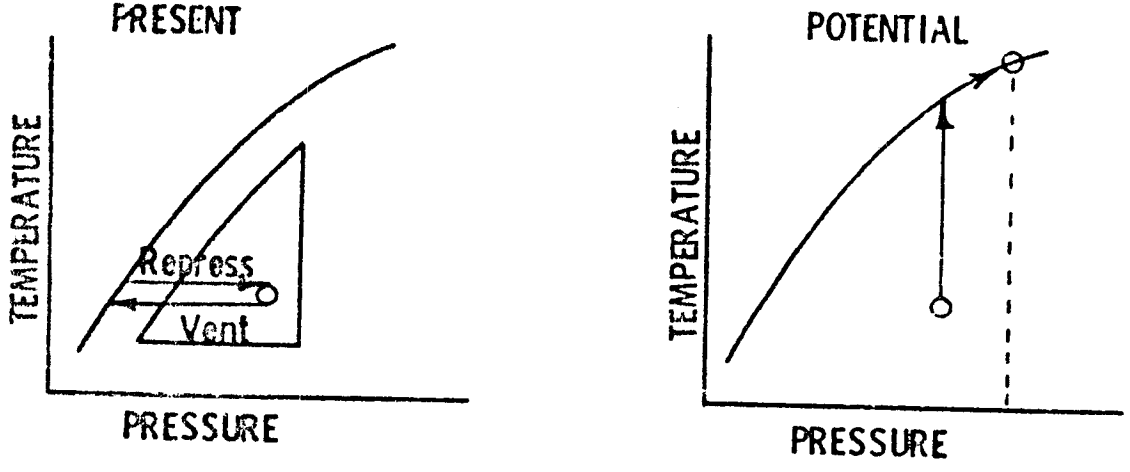

- ELIMINATES ONBOARD REPRESSURIZATION SYSTEM
- MINIMIZES TANK VENTING

MCFC - Form 3369 (Rev June 1970)

CHART No. _____

PUMP TESTS

(FACILITY AND PROCEDURES)

The pump test program was run at the J-2 turbopump test facility at MSFC. This facility includes a 36,00 gallon tank, a 14" sump, a 10" sump adapter and the S-IVB fuel feed system. The tank, sump, sump adapter, and the S-IVB suction line are vacuum jacketed; however, the sump prevalve, sump dead end, and the S-IVB prevalve are not vacuum jacketed. A pressure-fed J-2 engine gas generator powered the turbopump, a valve in the pump discharge duct controlled the flow and pump speed was controlled by throttling the gas generator. Pressure and temperature measurements, critical to establishing propellant properties, and pump performance were taken at the tank bottom, pump inlet (scissors bellows inlet), and the pump discharge. The scissors bellows inlet (22" upstream of inducer inlet) was used for the measurement because it is the measurement reference on the engine. Decreased until a cavitation cutoff was obtained (10% head loss). For the start tests the propellant in the tank was maintained at saturation for the entire test. The normal pump The normal pump chilldown procedure of allowing flow through the pump prior to initiation of the test was employed.

Cavitation tests were conducted at hydrogen bulk temperature of 39, 41, 43, and 45°R at three different flows and speeds. Start tests were conducted at hydrogen bulk temperatures of 43, 44, and 45°R. The desired hydrogen bulk temperature was obtained by bubbling ambient hydrogen gas into the bulk liquid.

MARSHALL SPACE FLIGHT CENTER

SCIENCE & ENGINEERING

SATURATED LH_2 TURBOPUMP OPERATION

LAB: S&E-ASTN-PPA

NAME: H. P. STINSON

DATE: April 6, 1971

FACILITY

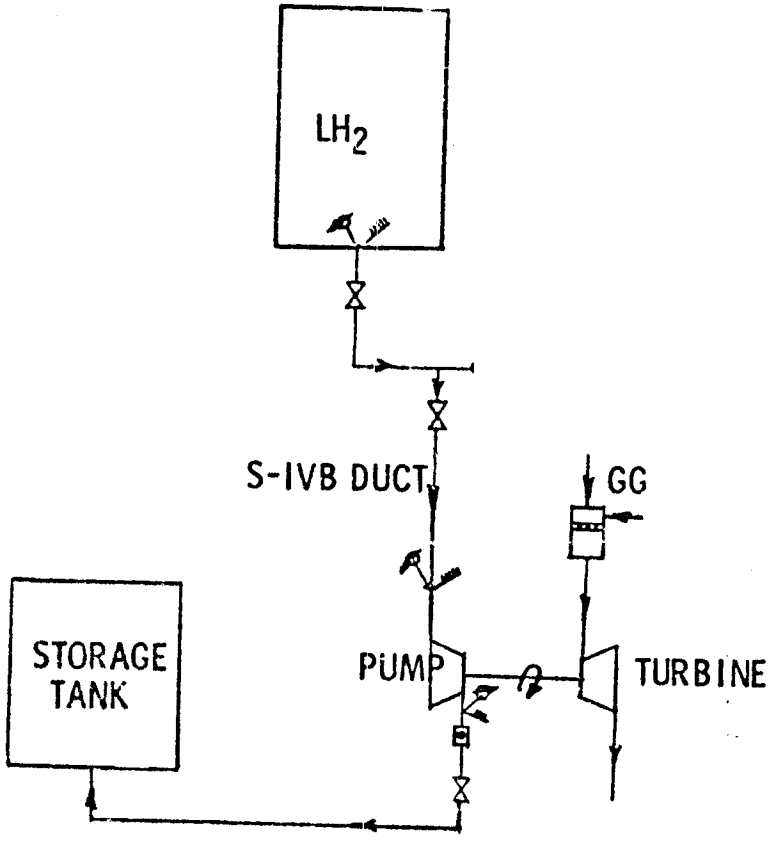

PROCEDURE

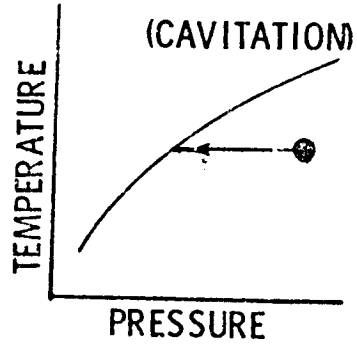

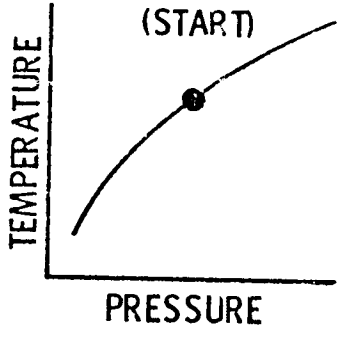

MSFC - Form 3361 (Rev June 1970)

CHART No. _____

CAVITATION TESTS

(TANK CONDITIONS)

TANK CONDITIONS FOR FOUR OF THE CAVITATION TESTS ARE PRESENTED; THESE TESTS WERE RUN AT FLOWS AND SPEEDS EQUIVALENT TO THE J-2 ENGINE OPERATION AT A 4.5 MIXTURE RATIO. EACH TEST WAS INITIATED AT THE HIGHEST PRESSURE SHOWN. THE PRESSURE WAS THEN LOWERED UNTIL THE TEST WAS TERMINATED AT 10 PERCENT HEAD LOSS. THE LAST DATA POINT PRESENTED FOR EACH TEST IS THE TANK CONDITION AT TEST TERMINATION. THESE DATA SHOW THAT USING THE J-2 HYDROGEN PUMP AND S-IVB FEED SYSTEM, IT IS POSSIBLE TO OPERATE WITH "ZERO-TANK NPSH" (TANK PRESSURE EQUAL TO THE VAPOR PRESSURE) AT HYDROGEN BULK TEMPERATURES ABOVE $42^{\circ}R$.

MARSHALL SPACE FLIGHT CENTER

SCIENCE & ENGINEERING

SATURATED LH_2 TURBOPUMP OPERATION

LAB: S&E-ASTN-PPA

NAME: H. Stinson

DATE: April 6, 1971

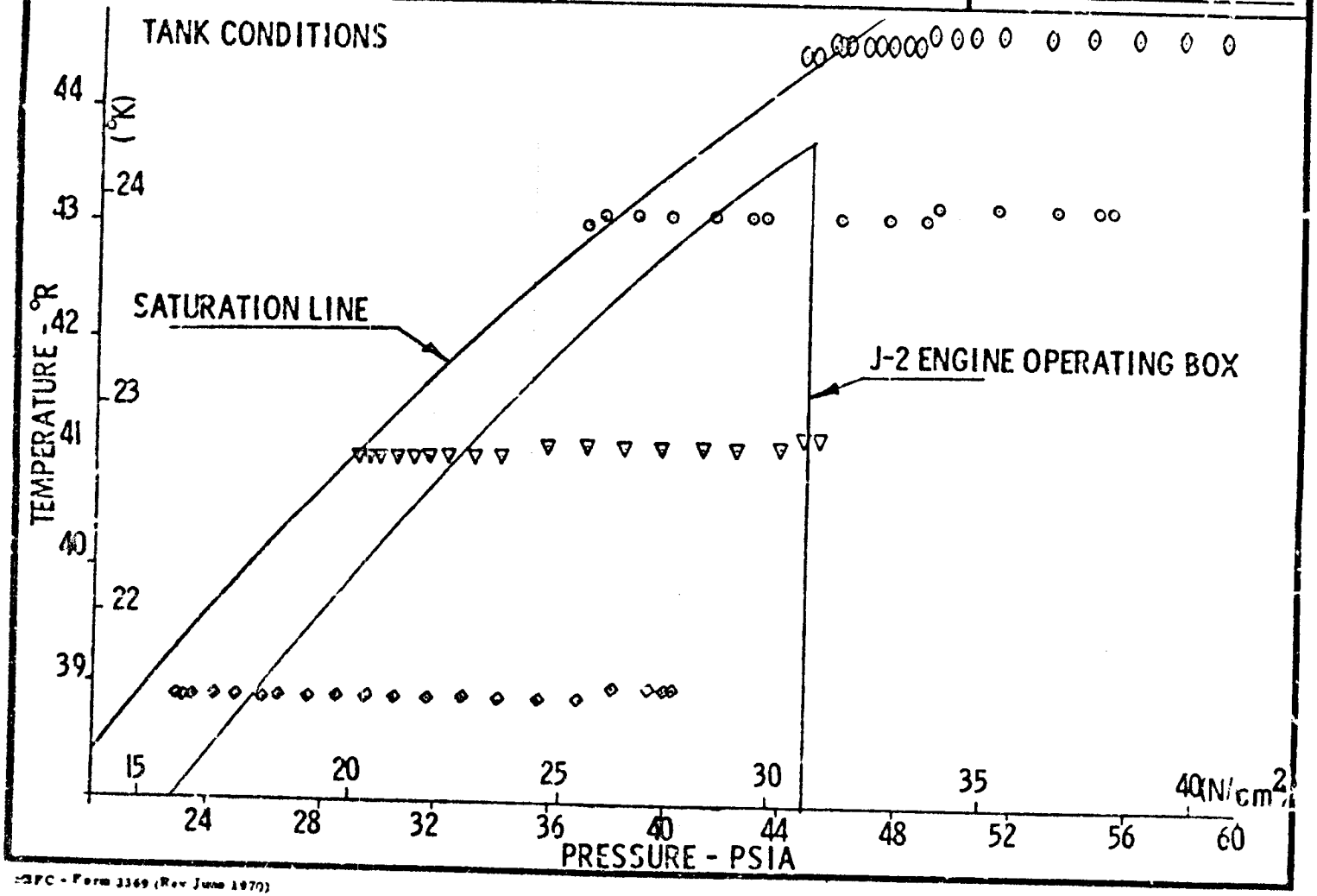

NASA - Form 3369 (Rev June 1970)

CHART No. _____

DATA REDUCTION

To evaluate the pump's performance during these cavitation tests, the quality of the propellant at the inlet to the pump had to be determined. The measured tank temperature and pressure was used to determine the enthalpy in the tank, and a constant enthalpy flow process to the pump inlet was assumed. Based on the constant enthalpy assumption the measured pump inlet pressure and the tank enthalpy served for finding the vapor fraction at the pump inlet. This method of calculating the vapor fraction is reasonable until the "zero-tank NPSH" condition is reached. At this point the temperature and pressure will no longer define the fluid state. Two methods of calculating the vapor fraction at the pump inlet were used after the "zero-tank NPSH" condition was reached.

One method assumes that after the tank saturation condition has been reached, and the tank pressure continues to decrease, the propellant remains all liquid. The inlet vapor fraction is then calculated from the enthalpy of saturated liquid as determined from the measured tank temperature and pressure. Looking at the temperature-entropy diagram, point A represents the initial "zero-tank NPSH" condition, then point A' represents the state in the tank at some lower pressure assuming the propellant remains all liquid. Point B' represents the inlet condition based on this assumption.

The second method assumes a constant enthalpy process within the tank. For this assumption the tank enthalpy is held constant after the "zero-tank NPSH" condition is reached. The tank and inlet conditions at some lower pressure after attaining "zero-tank NPSH" are represented by point A" and B" on the temperature-entropy diagram. From the temperature-entropy diagram, it is ovbious that this method results in a much larger inlet vapor fraction than does the first method.

It should be noted that after the "zero-tank NPSH" condition is reached, the vapor fraction values calculated using these two methods represent a best estimate of the range in which the actual vapor fraction exist.

MARSHALL SPACE FLIGHT CENTER SCIENCE & ENGINEERING	SATURATED LH_2 TURBOPUMP OPERATION	LAB: S&E-ASTN-PPA NAME: H. P. Stinson DATE: April 6, 1971

H - ENTHALPY
X - QUALITY
P - PRESSURE

DATA REDUCTION

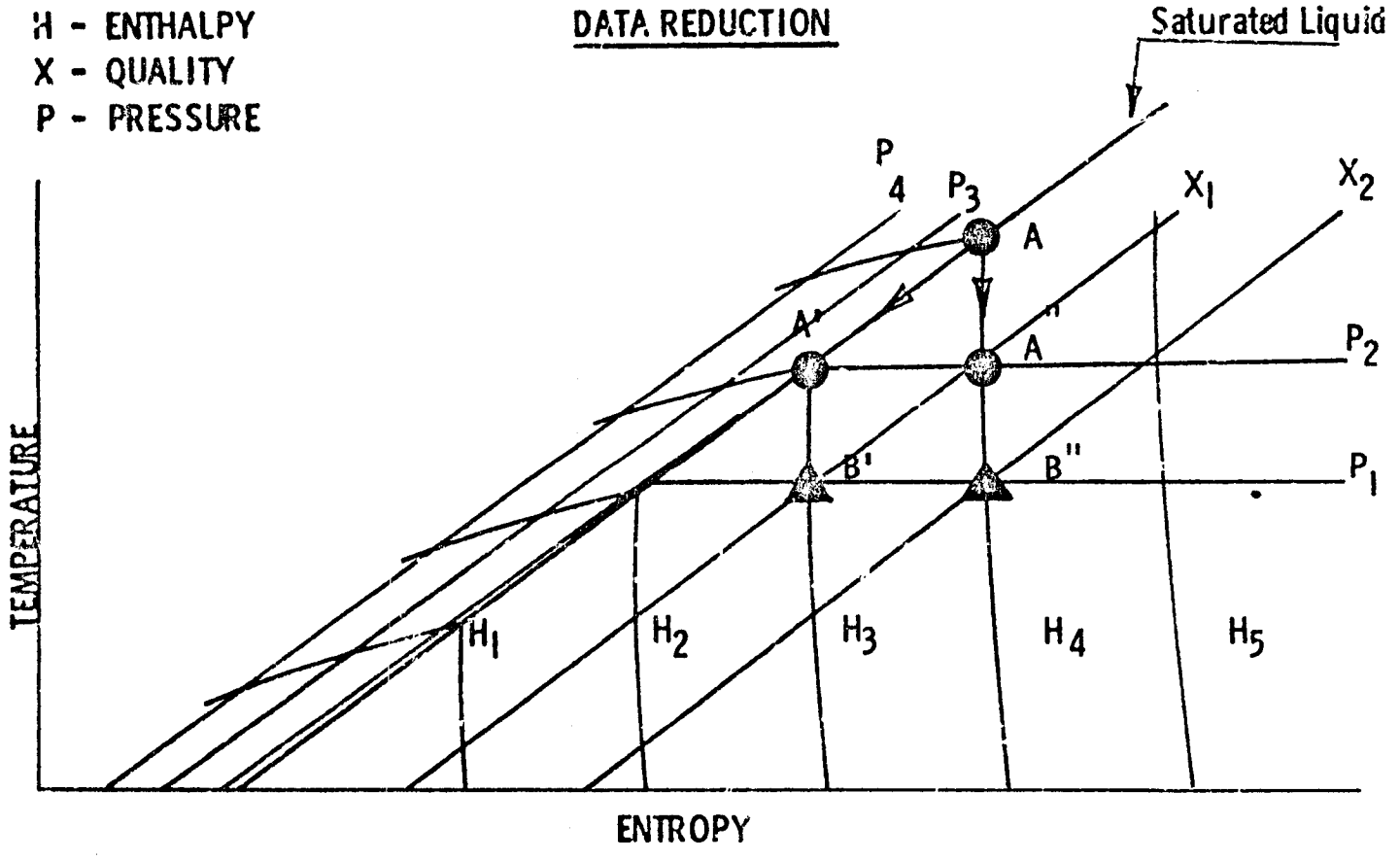

MSFC - Form 3369 (Rev June 1970)

CHART No. _____

CAVITATION TESTS

(PUMP PERFORMANCE)

A TYPICAL SET OF PUMP PERFORMANCE DATA IS PRESENTED. THE PUMP DEVELOPED HEAD, AS A PERCENTAGE OF NOMINAL, IS SHOWN AS A FUNCTION OF THE VAPOR VOLUME FRACTION AT PUMP INLET FOR FOUR HYDROGEN BULK TEMPERATURES INVESTIGATED. THE MARKED INCREASE IN THE PUMP'S VAPOR HANDLING CAPABILITY WITH INCREASING HYDROGEN BULK TEMPERATURE IS OBVIOUS FROM THE TEST DATA.

THE DASHED LINES REPRESENT THE PUMP PERFORMANCE AFTER "ZERO-TANK NPSH" IS REACHED. NOTE THAT AFTER THIS POINT, TWO PUMP PERFORMANCE CURVES ARE SHOWN. THESE CORRESPOND TO THE TWO METHODS OF CALCULATING THE VAPOR FRACTION DISCUSSED EARLIER, AND ARE INTENDED TO ESTIMATE THE ACTUAL VAPOR FRACTION. THE MAXIMUM VAPOR HANDLING CAPABILITY EXISTS AT A HYDROGEN BULK TEMPERATURE OF $45^{\circ}R$ AND IS ESTIMATED TO BE BETWEEN 20 AND 30 PERCENT VAPOR BY VOLUME AT THE PUMP BELLOWS INLET.

MARSHALL SPACE FLIGHT CENTER

SCIENCE & ENGINEERING

SATURATED LH_2 TURBOPUMP OPERATION

LAB: S&E-ASTN-PPA

NAME: H. P. Stinson

DATE: April 6, 1971

CAVITATION TESTS

(PUMP PERFORMANCE)

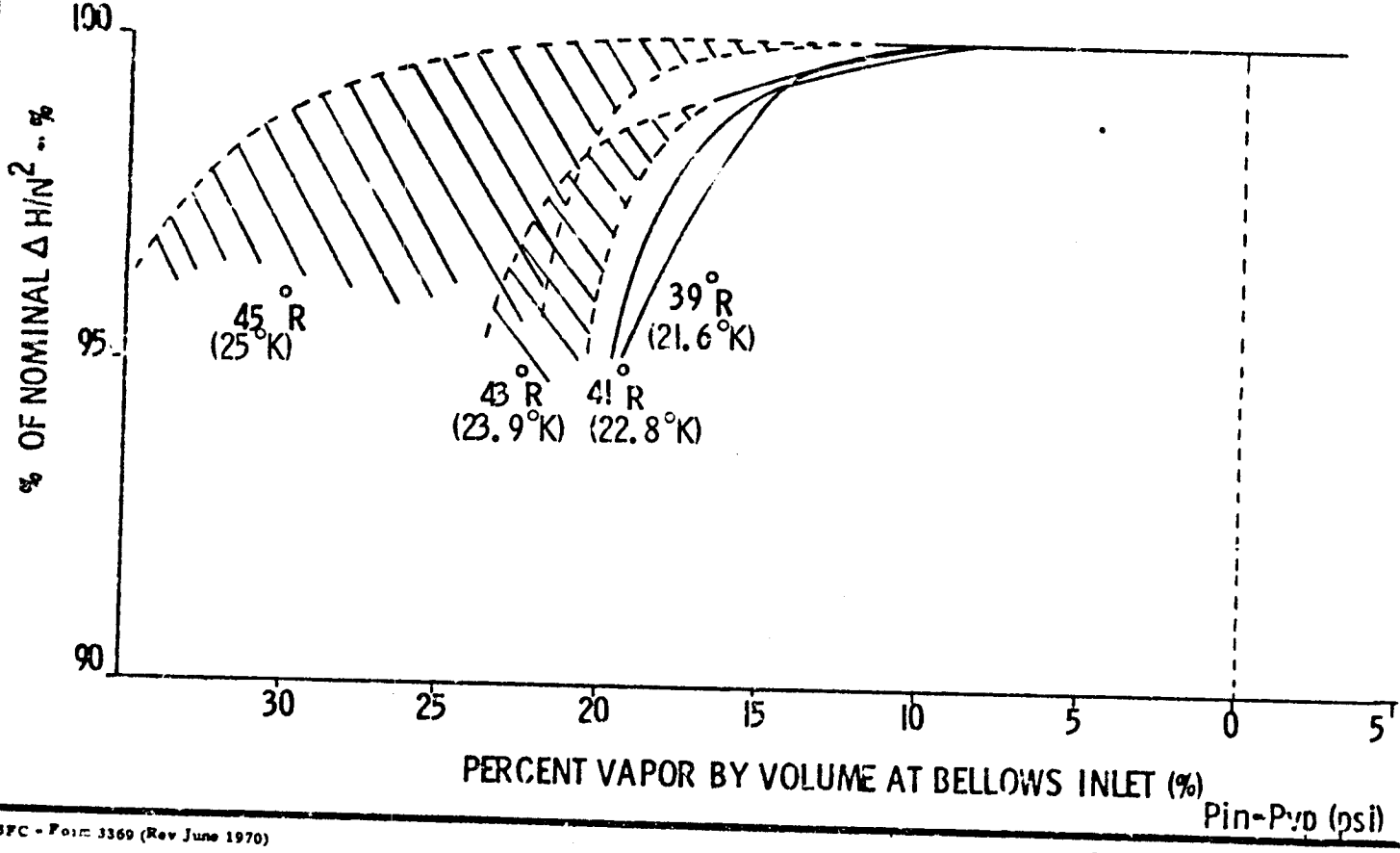

MSFC - Form 3369 (Rev June 1970)

CHART No. _____

START TESTS

TEN TESTS WERE CONDUCTED DURING THIS PHASE OF THE PUMP TEST PROGRAM. EIGHT OF THE TEN STARTED SATISFACTORILY. PUMP SPEED AND FLOW DATA FOR TWO OF THESE TESTS ARE COMPARED TO A NORMAL PUMP START WITH HIGH NPSH, AND A NORMAL J-2 ENGINE START. THE TWO "ZERO-TANK NPSH" STARTS ARE FOR THE BEST AND WORST CASES OBTAINED DURING THE SERIES.

THE FIRST TEST IN THIS SERIES (SEE OPEN CIRCLES) WAS TERMINATED BY THE PUMP OVER-SPEED CUTOFF PRIOR TO ATTAINING MAINSTAGE OPERATION. SUBSEQUENT INVESTIGATION INDICATED A LARGE BUBBLE BEING INTRODUCED INTO THE SYSTEM DURING THE TRANSIENT. TO MINIMIZE THIS BUBBLE FORMATION, THE MOST PROBABLE SOURCE OF A BUBBLE (THE 14" SUMP DEADEND) WAS INSULATED PRIOR TO THE NEXT TEST. ALSO, THE GAS GENERATOR START SEQUENCE WAS MODIFIED TO OBTAIN A SLOWER PUMP START. AFTER THESE CHANGES, EIGHT SUCCESSFUL PUMP STARTS WERE OBTAINED; HOWEVER, ALL INDICATED THAT A BUBBLE WAS BEING INTRODUCED INTO THE PUMP DURING TRANSITION. THE START TRANSIENT REMAINED FASTER THAN THE J-2 ENGINE. IT IS SIGNIFICANT THAT IN SPITE OF THESE TWO MAJOR HANDICAPS, THE PUMP WAS CAPABLE OF STARTING WITH "ZERO-TANK NPSH".

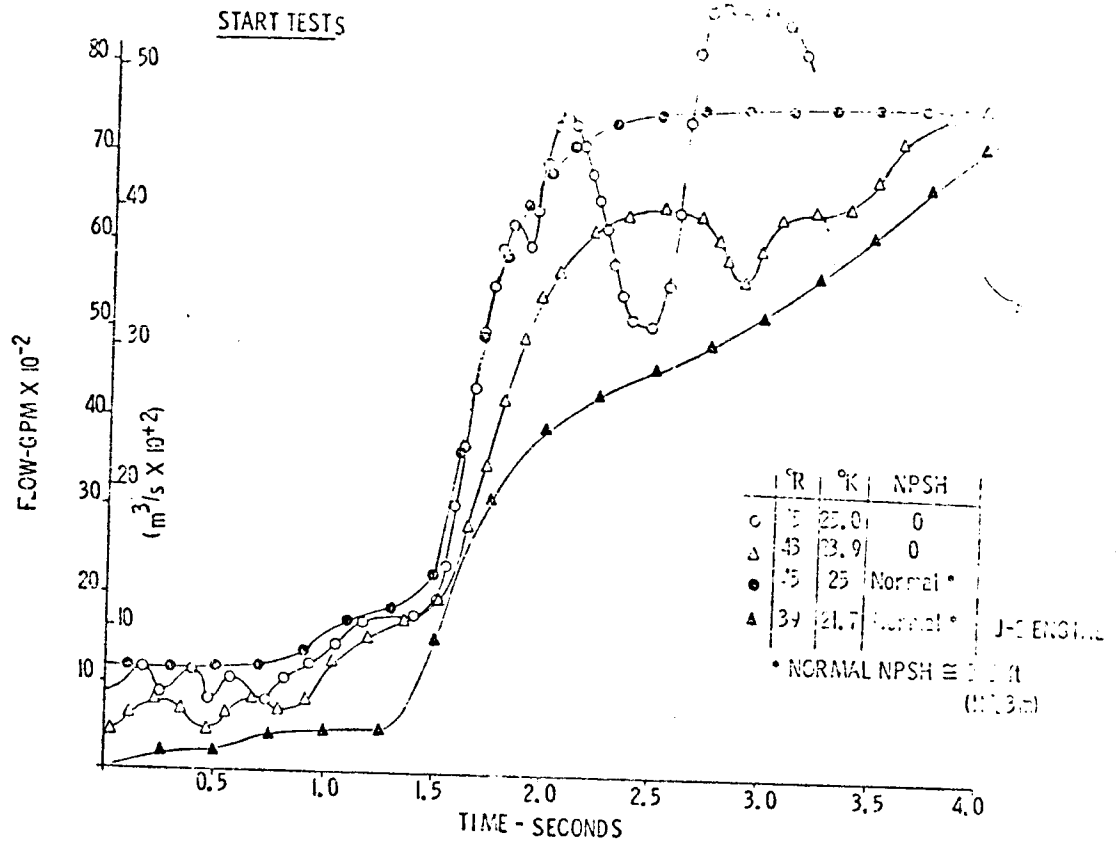
START TESTS
FLOW-GPM X 10⁻²
(m³/s X 10⁺²)
TIME - SECONDS
°R
°K
NPSH
Normal*
J-2 ENGINE
* NORMAL NPSH ≅

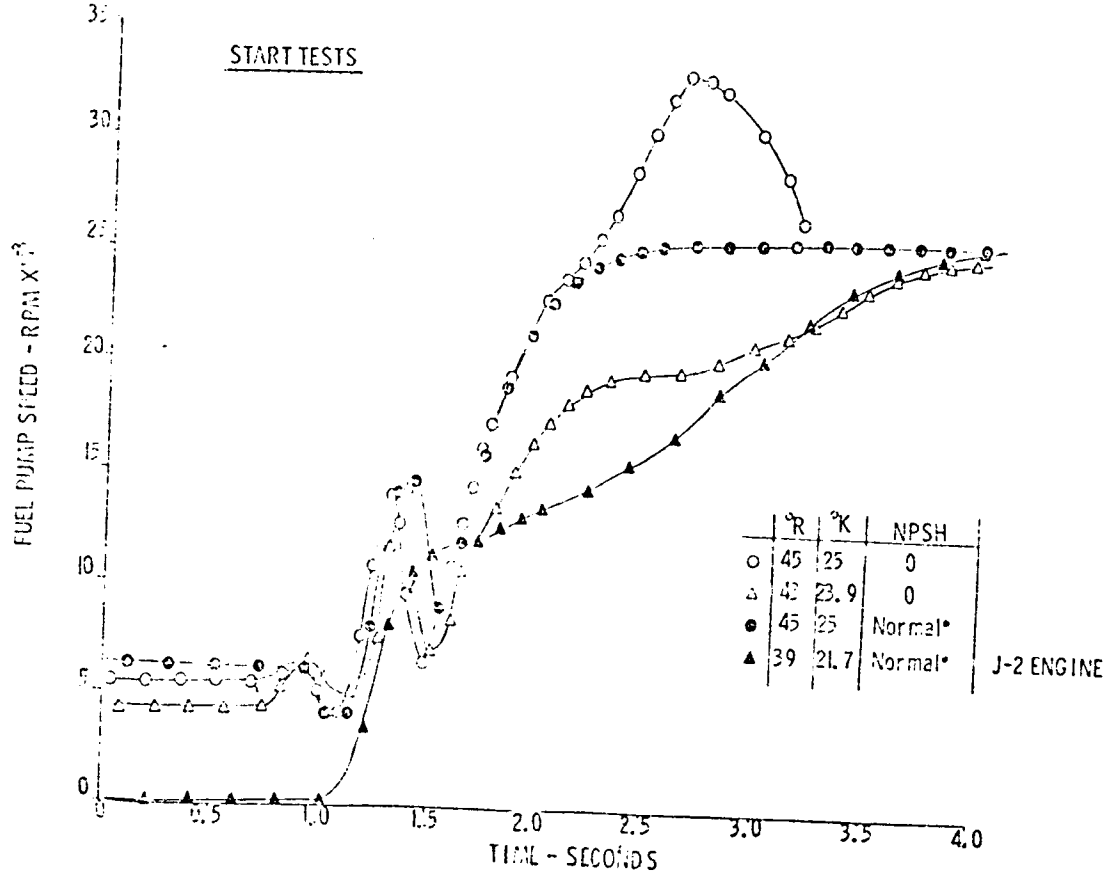
START TESTS
FUEL PUMP SPEED - RPM X
TIME - SECONDS
°R
°K
NPSH
Normal*
J-2 ENGINE

ENGINE TESTS

(FACILITY AND PROCEDURE)

THE J-2 ENGINE PROGRAM WAS ALSO CONDUCTED AS A TWO PART PROGRAM; STEADY-STATE OPERATION AT "ZERO-TANK NPSH", AND START TESTS WITH "ZERO-TANK NPSH. THE STEADY-STATE TESTS WERE INITIATED WITH TANK PRESSURE 10 PSI ABOVE THE VAPOR PRESSURE. AFTER ATTAINING MAINSTAGE OPERATION TANK PRESSURE WAS DECREASED UNTIL "ZERO-TANK NPSH" WAS REACHED. THE PRESSURE WAS THEN HELD CONSTANT AND THE ENGINE RUN FOR 20 SECONDS AT THIS CONDITION. TESTS WERE CONDUCTED AT 4.5 MIXTURE RATIO WITH HYDROGEN BULK TEMPERATURES OF 42, 43, AND 45°R, AND AT 5.0 MIXTURE RATIO WITH HYDROGEN BULK TEMPERATURES OF 43 AND 45°R.

THE START TRANSIENT TESTS WERE INITIATED WITH THE HYDROGEN IN THE TANK AT THE "ZERO-TANK NPSH" CONDITION. THE STAGE RECIRCULATION SYSTEM WAS USED TO CONDITION THE PUMP PRIOR TO ENGINE IGNITION. PROPELLANT WAS ALLOWED TO FLOW, UNDER TANK HEAD PRESSURE, FROM THE TANK THROUGH THE PUMP AND OVERBOARD. THIS FLOW WAS CONTINUED UNTIL ENGINE IGNITION, AT WHICH TIME THE BLEED VALVE WAS CLOSED. START TRANSIENT TESTS WERE CONDUCTED WITH HYDROGEN BULK TEMPERATURES OF 43, 44 AND 45°R.

MARSHALL SPACE FLIGHT CENTER

SCIENCE & ENGINEERING

SATURATED LOX/LH_2 ENGINE OPERATION

LAB: S&E-ASTN-PPA

NAME: H. P. STINSON

DATE: APRIL 6, 1971

FACILITY

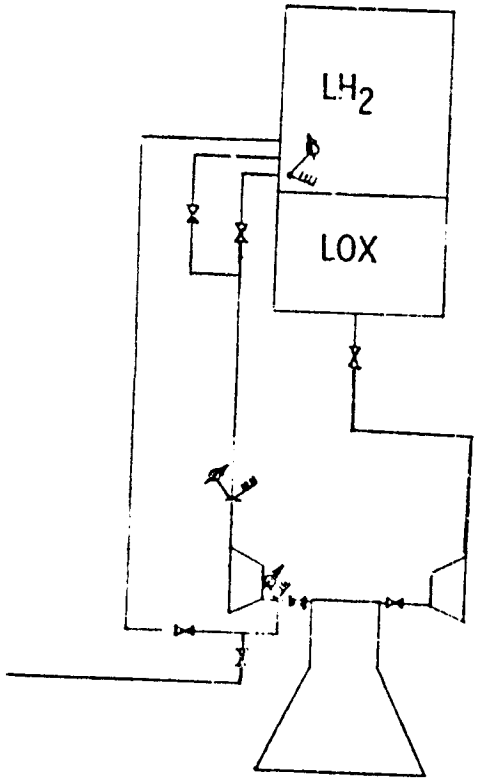

PROCEDURE

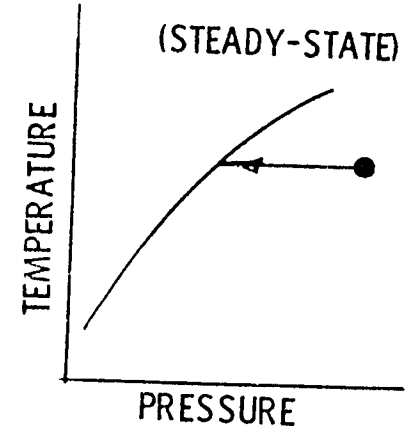

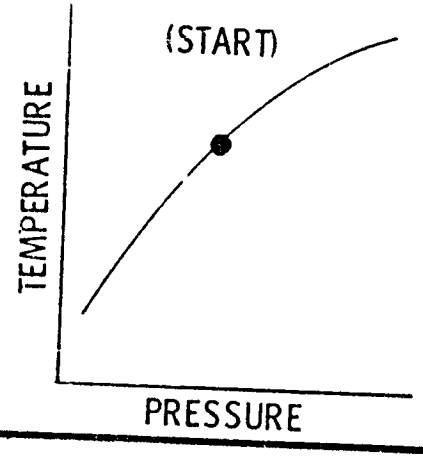

MSFC - Form 3369 (Rev June 1970)

CHART No. _____

STEADY STATE TESTS RESULTS

DATA FROM TWO OF THE STEADY-STATE RUNS ARE PRESENTED. TANK CONDITIONS FOR THESE TWO TESTS GIVEN ON A TEMPERATURE-PRESSURE PLOT SHOW THAT "ZERO-TANK NPSH" WAS OBTAINED. PUMP PERFORMANCE DATA ARE PRESENTED AS DEVELOPED HEAD DIVIDED BY SPEED SQUARED, VERSUS THE VAPOR VOLUME AT THE PUMP INLET. FROM THESE PUMP DATA IT CAN BE SEEN THAT THE PUMP WAS OPERATING AT THREE PERCENT HEAD LOSS AT THE TIME THE "ZERO-TANK NPSH" CONDITION WAS REACHED DURING THE 43°R TEST. FOR THE 45°R TEST NO APPRECIABLE PUMP PERFORMANCE LOSS WAS EXPERIENCED AT THE TIME THE "ZERO-TANK NPSH" CONDITION WAS REACHED. THESE PUMP PERFORMANCE EFFECTS ARE ALSO REFLECTED IN THE ENGINE'S PERFORMANCE. THE 43°R TEST SHOWS A LOSS IN COMBUSTION CHAMBER PRESSURE CORRESPONDING TO THE LOSS IN PUMP PERFORMANCE. NO APPRECIABLE CHANGE IN THE CHAMBER PRESSURE OCCURRED ON THE 45°R TEST.

THESE TESTS SHOW THE J-2 ENGINE CAN OPERATE WITH "ZERO-HYDROGEN TANK NPSH". THE MAXIMUM ENGINE PERFORMANCE LOSS OCCURRED AT THE LOWEST HYDROGEN BULK TEMPERATURE TESTED.

SATURATED PROPELLANT TESTING
ZERO TANK NPSH
J-2 ENGINE TESTING @ S-IVB BATTLESHIP

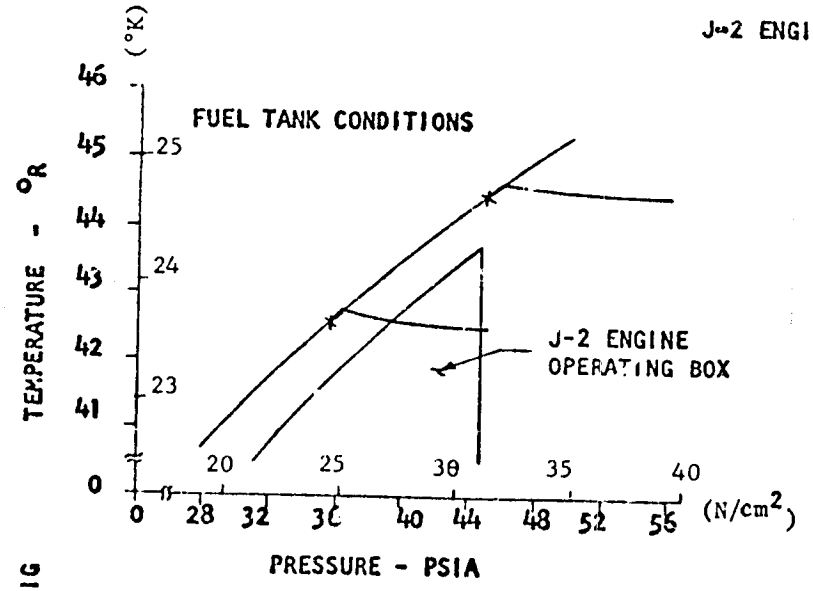

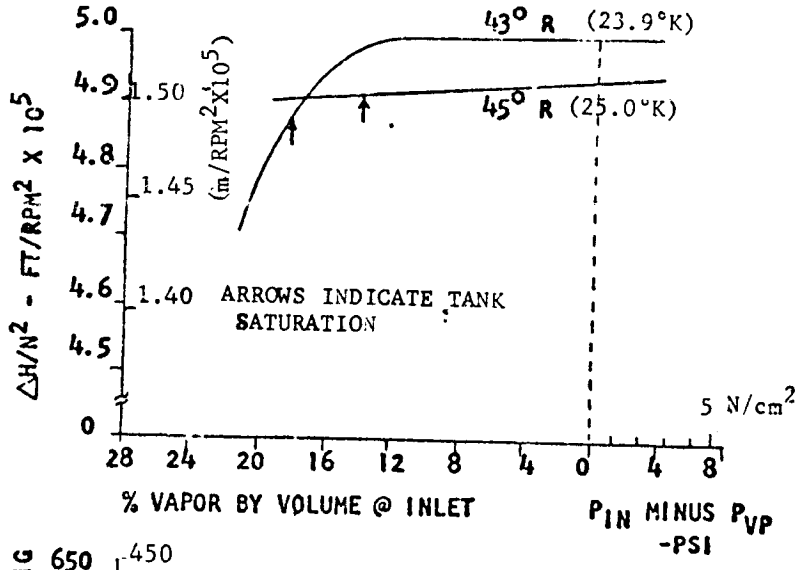

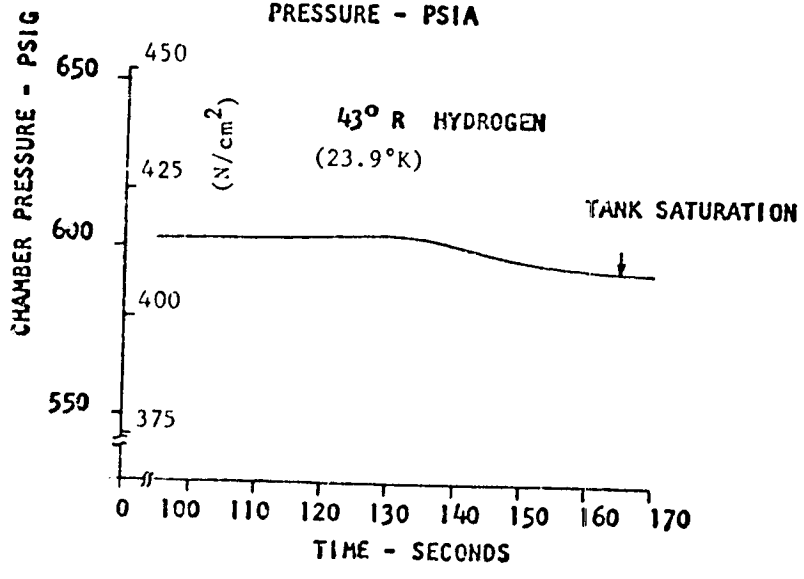

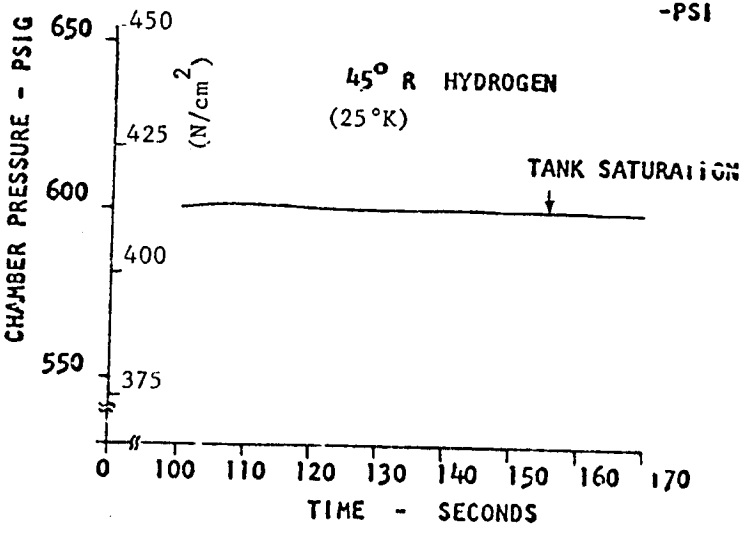

START TESTS RESULTS

COMBUSTION CHAMBER PRESSURE, FUEL PUMP DISCHARGE PRESSURE AND FUEL PUMP SPEED FOR A "ZERO-TANK NPSH" START, WITH 45 ^{o}R HYDROGEN ARE COMPARED TO A NORMAL ENGINE START. NO SIGNIFICANT CHANGES IN THE ENGINE'S START CHARACTERISTICS CAN BE OBSERVED ON THE "ZERO-TANK NPSH" START. TESTS WERE ALSO CONDUCTED AT HYDROGEN BULK TEMPERATURES OF 44 AND 43^{o}R. A SLIGHT INCREASE IN GAS GENERATOR CHAMBER TEMPERATURE OCCURRED DURING TRANSITION ON THESE TESTS. HOWEVER, THE MAXIMUM TEMPERATURES OBSERVED WERE WELL BELOW THE TEMPERATURE LIMIT.

THESE TESTS DEMONSTRATE THE ABILITY TO START AND OPERATE THE ENGINE WITH "ZERO-TANK NPSH".

MARSHALL SPACE FLIGHT CENTER SCIENCE & ENGINEERING	SATURATED LOX/LH_2 ENGINE OPERATION	LAB: S&E-ASTN-PPA NAME: H. Stinson DATE: April 6, 1971

START TESTS RESULTS

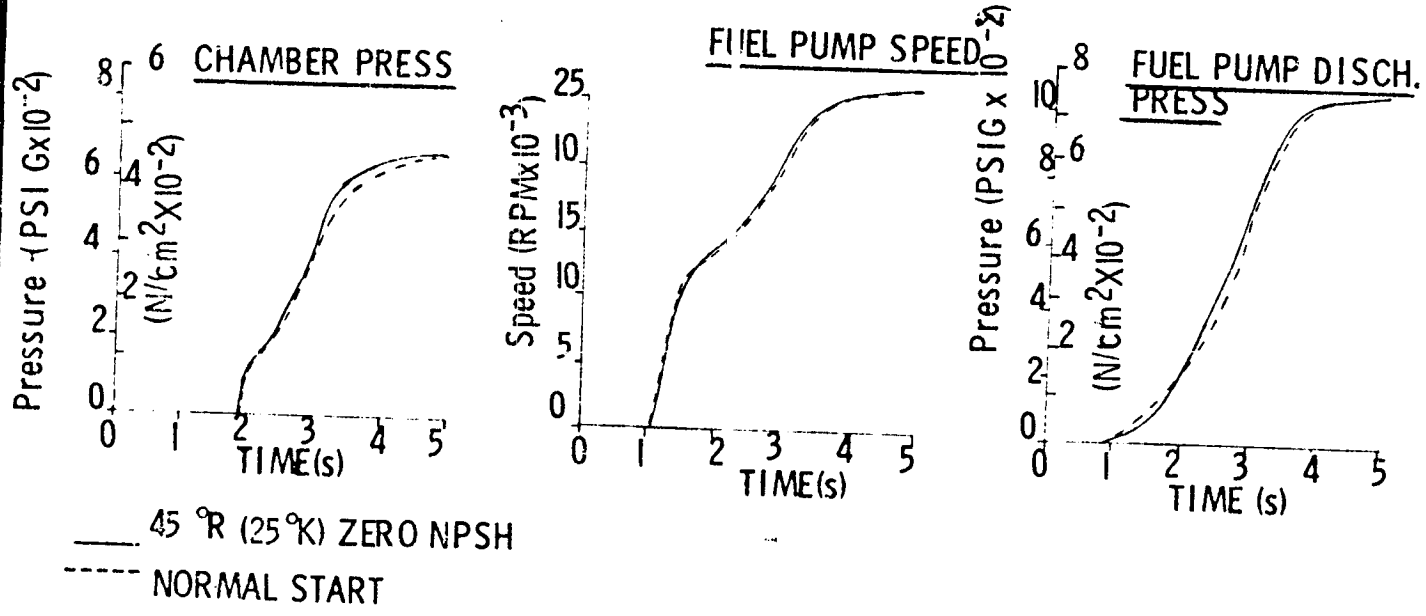

MSFC - Form 3369 (Rev June 1970)

CHART No. _____

CONCLUSION

$J\text{-}2/LH_2$ PUMP AND J-2 ENGINE TESTS PROVE "ZERO-TANK NPSH" OPERATION IS REALISTIC WITH HYDROGEN, AND SHOULD BE GIVEN CONSIDERATION FOR FUTURE APPLICATIONS. "ZERO-TANK NPSH" OPERATION COULD BE PARTICULARLY ATTRACTIVE FOR THE SPACE SHUTTLE AUXILIARY PROPULSION SYSTEM.

MARSHALL SPACE FLIGHT CENTER SCIENCE & ENGINEERING	SATURATED LOX/LH_2 ENGINE OPERATION	LAB: S&E-ASTN-PPA NAME: H. P. Stinson DATE: April 6, 1971

CONCLUSION

- "ZERO-TANK NPSH" OPERATION IS REALISTIC WITH HYDROGEN, AND SHOULD BE GIVEN CONSIDERATION FOR FUTURE APPLICATIONS.

MSFC - Form 3369 (Rev June 1970)

CHART No. _____

"CHARACTERISTICS OF FEED SYSTEM INSTABILITIES"

R. D. VAAGE

MARTIN MARIETTA CORPORATION

TECHNICAL MANAGER

R. SPINK

MARSHALL SPACE FLIGHT CENTER

INVESTIGATION OF CHARACTERISTICS OF FEED SYSTEM INSTABILITIES

Contract NAS 8 20266

Robert D. Vaaje

Martin Marietta Corporation
Denver Division

Study Reasons and Objectives

In the investigation of structure-propulsion system coupled longitudinal oscillations (POGO), the relationship between the structural and feed system natural frequencies is of major importance. The structural frequencies can be adequately defined by existing analytical techniques. The feed system frequencies are usually very dependent upon the compressibility (compliance) of cavitation bubbles that exist to some extent in all operating turbopumps. The amount of cavitation that occurs is a function of the turbopump design, operating conditions, and propellant properties. Test data have shown an order of magnitude variation in cavitation compliance between vehicle stages that have experienced POGO problems. There are currently no accurate means of analytically predicting the amount of cavitation compliance in a new turbopump application. In the past, this has delayed the completion of POGO stability analysis until after the turbopump has been built and tested. This has been one of the factors that has usually led to the design and installation of POGO suppression devices after the vehicle has been built, flown, and experienced POGO instabilities. This approach sometimes endangers a mission, is usually restricted to the incorporation of non-optimum designs, and is always inefficient.

The objective of this study is to develop an analytical model which will predict the amount of cavitation compliance that will occur in a new turbopump. In order that the results be credible, analytical predictions must show reasonable agreement with test results for existing turbopump configurations.

STUDY REASONS AND OBJECTIVES

MARTIN MARIETTA
DENVER DIVISION

- REASONS FOR STUDY
  - Turbopump Cavitation Important Parameter in POGO Analysis.
  - Currently Must Be Determined From Test Program.
  - Final POGO Analysis After Hardware Fabrication.
- OBJECTIVES OF STUDY
  - Analytically Determine Turbopump Cavitation Compliance.
  - Verify Results With Test Data.

Study Approach

The approach taken to meet the study objectives is: develop a model, analyze available test data, and compare results. Development of the analytical model was initiated during an Air Force Study Contract*, but had to be abandoned at that time because of higher priority study objectives and funding limitations. The math model uses the compressible flow equations in finite difference form and solves them iteratively. Isentropic conditions of thermodynamic equilibritum between the vapor (cavitation) and liquid phases are assumed. The solution yields the amount of vapor at several grid points throughout the cavitation region of a turbopump. This approach will be compared with other analytical methods of calculating the amount of cavitation.

Test data analysis consists of assembling and comparing all available test data and related analysis; analytically reconstructing most of the tests in an attempt to resolve differences and derive a cavitation compliance value, or at least the range of values; and evaluating the test results in an attempt to determine a strictly empirical correlation between cavitation compliance and turbopump and propellant parameters.

Verification of the turbopump model consists of comparing the results of the analytical model with test data, determining sensitivity of results to turbopump and propellant parameters (which may account for scatter in the test data), and an assessment of the effect of analytical modeling assumptions.

*"A Study of System-Coupled Instability Analysis Techniques," AFRPL-TR-66-143, Air Force Rocket Propulsion Laboratory, Edwards Air Force Base, June 1966.

STUDY APPROACH

MARTIN MARIETTA
DENVER DIVISION

- TURBOPUMP FLOW MODEL
  - Numerical Solution of Compressible Flow Equations Assuming Therodynamic Equilibrium.
  - Yields Vapor Fraction in Each Fluid Element.
  - Review Other Methods.
- TEST DATA ANALYSIS
  - Assemble and Compare All Data and Analysis.
  - Derive Range of Cavitation Compliance.
  - Perform Empirical Evaluation of Results.
- MODEL VERIFICATION
  - Compare Model and Test Results.
  - Assess Model Assumptions.

Turbopump Flow Model

For an element of fluid within the turbopump two equations are used. The momentum around an element is equated to zero which is the condition for irrotational flow. The energy of each element is equated to the inlet energy plus the energy supplied by the rotating turbopump blades. The energy of each element is made up of kinetic energy and thermodynamic energy (enthalpy). The equations are solved to determine enthalpy. Then assuming an isentropic process, which is in equilibrium, the quality of the fluid element (vapor-liquid ratio) can be determined from standard propellant thermodynamic tables.

A computerized solution of the equations requires that the r, θ, z coordinates of the blade be transformed into the E, F coordinates of a streamsheet. Analysis of several streamsheets makes the solution quasi-three dimensional. A gridwork is established in the E, F plane and the flow equations are converted to a finite difference form. The solution then starts at a known boundary condition and progresses grid point by grid point using error minimization techniques. The program iterates on a final solution which balances the stream function at all the grid intersections and satisfies the boundary conditions to within some specified tolerance.

TURBOPUMP FLOW MODEL

MARTIN MARIETTA
DENVER DIVISION

- FLOW ELEMENT EQUATIONS
  - Momentum and Energy Equation For Compressible Flow.
  - Thermodynamic Equilibrium Yields Density.
- COMPUTERIZED SOLUTION
  - Transform Blade Coordinates To Streamsheet Coordinates.

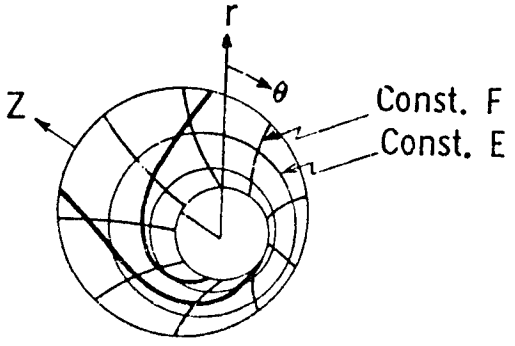

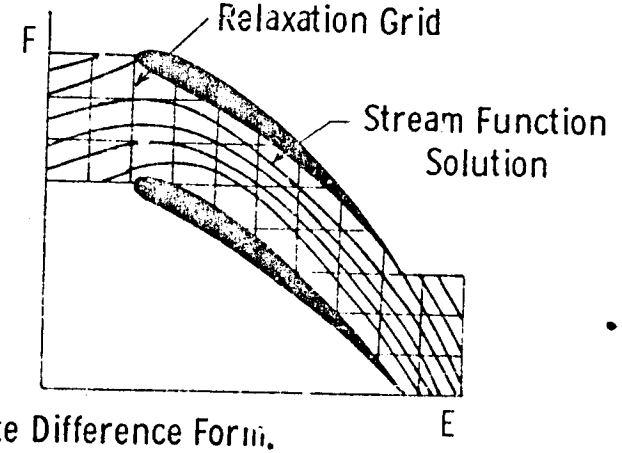

  - Program Equations In Finite Difference Form.
  - Perform Iterative Relaxation Solution (Satisfy Grid Intersection and Boundary Conditions).

Turbopump Model Assumptions

The assumptions made in the development of the turbopump flow model are listed in the accompanying chart. The model was designed to compute turbopump blade cavitation and does not account for blade tip clearance flow cavitation. Tip cavitation could have a significant effect when considering unshrouded blades. The assumption of subsonic flow should be adequate for determination of cavitation compliance over the normal operating range of a turbopump. Sonic velocities are generally believed to occur at cavitation breakdown and turbopumps usually operate well above the condition. The importance of viscous effects are unknown, but at most should be significant only in the vicinity of the blades. Boundary layer equations, accounting for viscosity, could be included as an extension to the current model. Some data exists which indicates that cavitation is not an instantaneous process. This was determined by producing large inlet pressure oscillations in a turbopump operating near the cavitation breakdown point. Extrapolation of this data to small inlet pressure oscillations, and to the phase changes in a fluid element as it passes over the turbopump blades, is not possible; however, the trend will be noted when attempting to match analytical and empirical results. The assumption that adjacent turbopump blades are identical is a bookkeeping convenience which could be changed after the validity of the model is determined.

TURBOPUMP MODEL ASSUMPTIONS

MARTIN MARIETTA
DENVER DIVISION

- CAVITATION ONLY OCCURS ON THE BLADE SURFACES
- FLOW RELATIVE TO THE BLADE IS SUBSONIC
- VISCOUS EFFECTS ARE NEGLIGIBLE
- PHASE CHANGES ARE INSTANTANEOUS AND IN THERODYNAMIC EQUILIBRIUM
- ADJACENT BLADES ARE IDENTICAL

Turbopump Model Results

Checkout of the turbopump model has recently been completed for the case of incompressible flow. This required the solution of several problems associated with the stability and convergence of the numerical iteration scheme. Streamlines for incompressible flow through typical turbopump blades are shown in the accompanying figure. Checkout of the compressible flow case is progressing. Solution of the compressible flow case will yield a cavitation vapor volume for a given set of inlet conditions. Relating a change in cavitation vapor volume to a change in inlet pressure results in an analytical prediction of cavitation compliance.

TURBOPUMP MODEL RESULTS

MARTIN MARIETTA
DENVER DIVISION

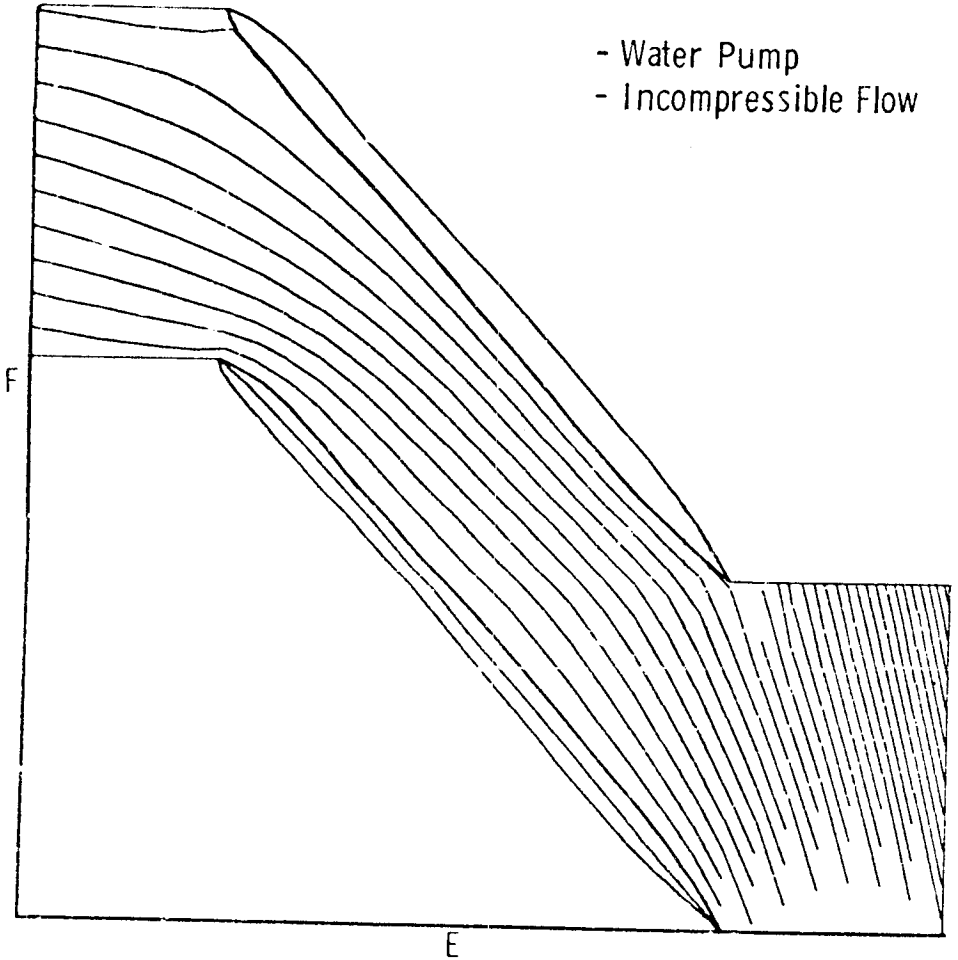

COORDINATES IN E, F PLANE

- Water Pump
- Incompressible Flow

- Model Working For Incompressible Flow
- Cavitation Compliance

$= \rho \frac{\Delta V_{Vap.}}{\Delta P_{Inlet}}$ From Compressiole Flow Solution.

Related Analysis Methods

Two other methods have been presented which yield an analytical solution for cavitation compliance. They are referred to as the separation cavity model and the cavitation breakdown model.

The separation cavity model* employs a separation type cavity on the suction side of the blade. The shape of the cavity can be defined up to the point of maximum height. At this point some assumption regarding the reclosing of the cavity downstream on the blade must be made. An application of this technique** is similar to the approach developed in this study except for the treatment of the cavitation region.

The cavitation breakdown model*** is a semi-empirical method of relating cavitation compliance to a calculated cavitation compliance at cavitation breakdown. This method is unique in that the theory includes the effect of blade tip clearance back flow in the cavitation model.

---

* Stripling, L.B. and Acosta, A. J. "Cavitation in Turbopumps" Parts I and II"; transactions of the ASME, Journal of Basic Engineering, September 1962.

** Davis, R. E.; Coons, L. L.; and Scheer, D. D. "Internal Streamline Flow Analysis for Turbopump Inducers Under Cavitating and Noncavitating Flow Conditions"; AIAA paper No. 70-623.

*** Ghahremani, F. "Turbopump Cavitation Compliance", Report TOR-0059 (6531-01)-2, The Aerospace Corporation, El Segundo, California, September 1970 (Contract F04701-70-C-0059).

RELATED ANALYSIS METHODS

- SEPARATION CAVITY MODEL (L.B. STRIPLING & A.J. ACOSTA)
  - Assumes Complete Separation of Liquid & Vapor Phases
  - Cavity Closure Condition Must Be Assumed
- CAVITATION BREAKDOWN MODEL (F. GHAHREMANI)
  - Derives Cavitation at Breakdown Assuming Sonic Flow
  - Relates Normal Cavitation to Breakdown Cavitation
  - Requires Empirical Data
  - Includes Blade Tip Flow Cavitation

Test Data Reduction

Several sources of test data are available for most of the existing vehicles that have experienced POGO problems. The best combination of tests for accurate determination of cavitation compliance are: flow and non-flow feed system pulse tests for determining feed system and turbopump response, feed line component tests for analytic verification of the non-flow system response, and flight data for verification of the flow system response.

Cavitation compliance is determined by assuming a model for feed system frequency in terms of the system parameters. If the frequency and all the parameters, except cavitation compliance, are given by test or analysis the desired result can be calculated.

Several conditions which often result in large variations in test derived cavitation compliance are listed in the accompanying chart.

TEST DATA REDUCTION

MARTIN MARIETTA
DENVER DIVISION

- SOURCES OF TEST DATA
  - System Tests (Flow and Non-Flow)
  - Feedline Component Tests
  - Flight Data
- DERIVE CAVITATION COMPLIANCE (C_b) FROM FEED SYSTEM FREQ. (w)

  $w = f(C_b, C, M)$ Where C = Line + Fluid Compliance
  M = Fluid Mass
- SOURCES OF CAVITATION COMPLIANCE UNCERTAINTY
  - Disagreement Between Test Results
  - Dispersions In Test Results
  - Unknown Feedline Compliance
  - Test Data Will Not Fit Physical Model
  - Frequency Insensitive To Cavitation Compliance

F-1 LOX Turbopump Cavitation Compliance

The accompanying figure shows typical cavitation compliance derived from different sources of test data. The variation in test results is sometimes larger than the average value. When equally valid conflicting results are derived the mean value is used for comparison with both analytical results and test results for other configurations.

F-1 LOX TURBOPUMP CAVITATION COMPLIANCE

MARTIN MARIETTA
DENVER DIVISION

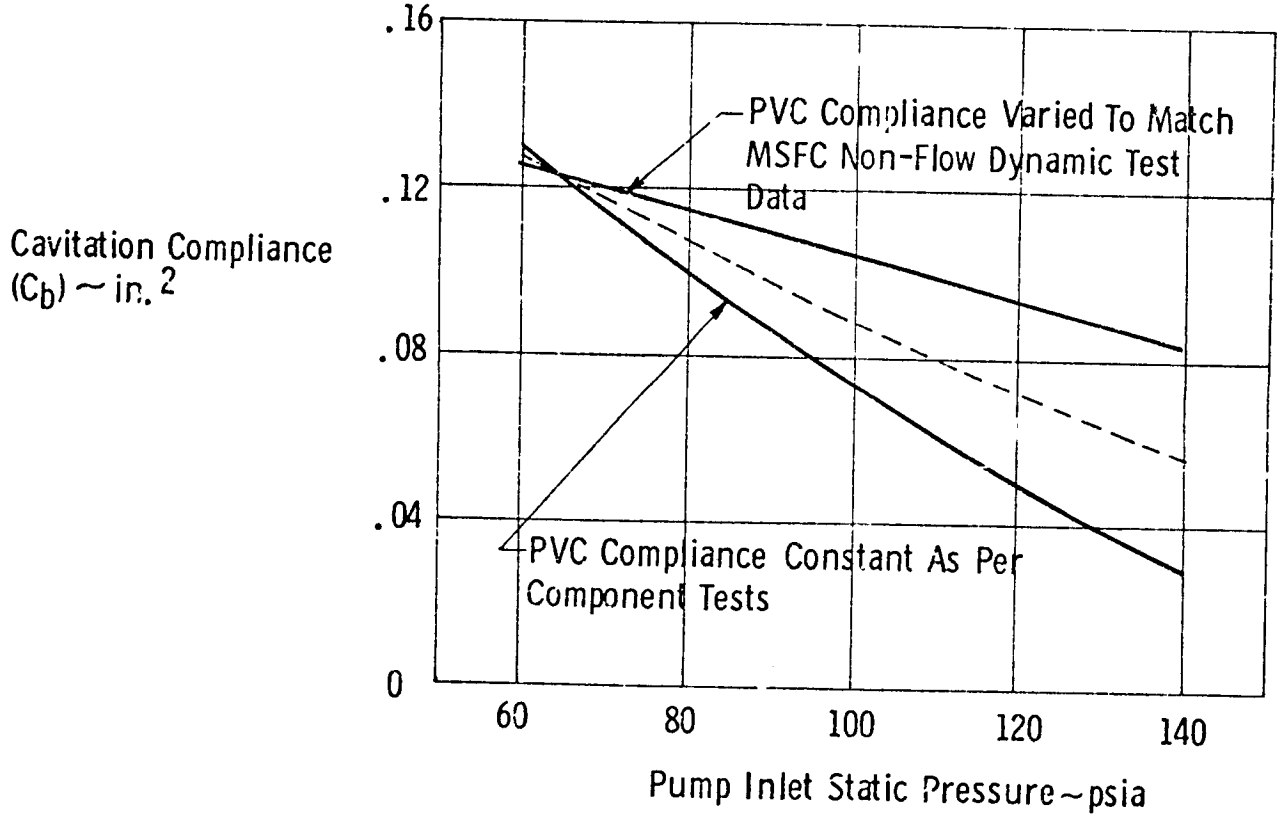

Empirical Evaluation of Test Results

Several propellant properties, turbopump configuration, and operating parameters affect the amount of cavitation that occurs. Unfortunately, however, past test programs have only been run at normal operating conditions (usually only inlet pressure is varied) which does not give the empirical dependence of cavitation compliance on such parameters as: blade tip clearance, turbopump speed, head rise, flow rate, propellant temperature, disolved gases, etc. These parameters do vary for different turbopump configurations, but the effects cannot be separated from the configuration effects. Thus, only a qualitative empirical evaluation of the results can be performed. This is accomplished by comparing non-dimensional cavitation compliance against non-dimensional turbopump and propellant parameters.

EMPIRICAL EVALUATION OF TEST RESULTS

MARTIN MARIETTA
DENVER DIVISION

- PROBABLE INFLUENTIAL PARAMETERS
  - Turbopump Configuration and Size
  - Turbopump Speed and Head Rise
  - Propellant Properties
  - Inlet Pressure and Flow Rate
- AVAILABLE RESULTS
  - Different Turbopump Configurations
  - Nominal Operating Conditions Only
- NON-DIMENSIONAL CAVITATION VERSUS NON-DIMENSIONAL PERFORMANCE PARAMETERS

Test Derived Cavitation Compliance

Non-dimensional cavitation compliance, as a function of cavitation index, is shown in the accompanying figure for several turbopump configurations. The non-dimensionalizing parameters used for this case are nD^2, where n is the no. of inducer blades and D is the inducer diameter. All "good" test derived cavitation compliance implies that log C_b varies linearily with inlet pressure. This relationship is within the test data uncertainty for all configurations. Non-dimensionalizing C_b in the manner shown only reduces the overall dispersion 25 per cent indicating that the influential parameters are not properly accounted for. Other pump performance parameters have been investigated without significantly decreasing the variation between configurations. A better empirical correlation between configurations may be possible after the analytical model produces a better understanding of the sensitivity of cavitation compliance to system parameters.

TEST DERIVED CAVITATION COMPLIANCE

MARTIN MARIETTA
DENVER DIVISION

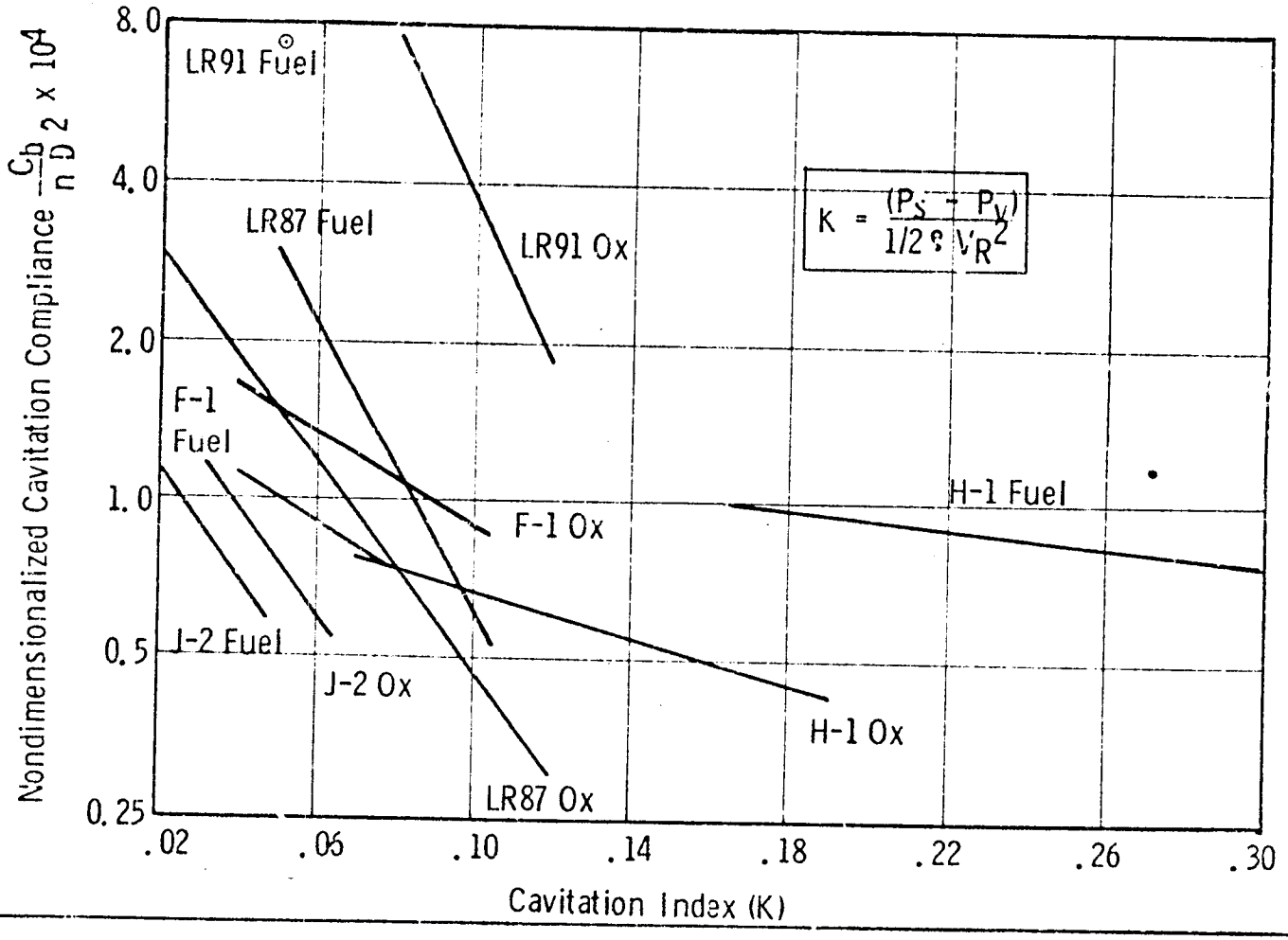

Additional Application of Turbopump Model

In addition to cavitation compliance, the turbopump model is capable of generating other information which is of interest in the analysis of turbopump response and the design of turbopump blades. Turbopump discharge dynamic pressure gain can be determined as a function of inlet pressure (pump gain, $\partial Pd/\partial Ps$), exit flow (pump resistance, $\partial Pd/\partial \dot{w}d$), and blade speed (speed gain, $\partial Pd/\partial N$). These parameters are also important in POGO stability analysis. Unlike cavitation compliance, there are currently methods available for estimating these parameters; however, the use of a cavitating turbopump model may result in a significant improvement.

This model can also be used for design analysis of turbopump blades. This could include blade pressure loading, and the influence of blade shape on cavitation, seperation, etc.

ADDITIONAL APPLICATIONS OF TRUBOPUMP MODEL

MARTIN MARIETTA
DENVER DIVISION

- PRESSURE, FLOW, AND SPEED GAINS
- BLADE PRESSURE LOADING
- BLADE SHAPE DESIGN FOR MINIMUM CAVITATION

"COMBUSTION OSCILLATIONS DAMPING DEVICES"

G. GARRISON

PRATT & WHITNEY AIRCRAFT

TECHNICAL MANAGER

R. COUNTS

MARSHALL SPACE FLIGHT CENTER

Combustion Oscillations Damping Devices Investigation

Pratt & Whitney Aircraft, Florida
Research and Development Center

Gary Garrison

Contract NAS8-21310

SOLUTIONS FOR HIGH FREQUENCY COMBUSTION INSTABILITY PROBLEMS

High frequency combustion instability can be eliminated in rocket thrust chambers by reducing the coupling between the oscillations and the driving combustion process and/or by increasing the damping in the combustion chamber. Injector modifications and face-mounted baffles effect the coupling process; acoustic devices are used to increase the chamber damping.

Stabilizing combustion by modifying the injector is a cut-and-try process, furthermore, the necessary modifications are often made at the expense of performance. To be effective, baffles must extend well into the propellant mixing and combustion zone, which not only presents a difficult cooling problem, but can also cause performance degradation. Acoustic damping devices are excellent for stabilizing combustion because

1. They are reliable and effective; only a small amount of damping will stabilize most systems.
2. They can be provided in a wide variety of configurations such as resonator arrays, individual resonators, quarter-wave tubes, slots and cavities.
3. They are located in the combustion chamber surfaces outside the mixing zones; thus, they do not cause performance penalties and when incorporated in the original chamber design they present no unusually difficult cooling problems.

SOLUTIONS FOR HIGH FREQUENCY COMBUSTION INSTABILITY PROBLEMS

- Modification of Injector
- Use of Injector Face Baffles
- Use of Acoustic Damping Devices

ABSORBING LINERS

The most effective type of damping device, arrays of resonators called absorbing liners, has been used for many years to eliminate high frequency combustion instability or "screech" in airbreathing engine afterburners. The liners are designed to damp pressure disturbances in the chamber thereby preventing their amplification by the combustion process. Although the mechanisms causing "screech" in afterburners are not completely understood, the use of absorbing liners has solved the problem. A properly designed liner will cause combustion to be stable over the entire range of engine operating conditions, which include extremely wide variation in mixture ratio and chamber pressure.

When combustion instability in rockets became a problem of significance, the airbreathing engine liner success suggested a similar approach. In 1963 work devoted to the development of theory and to the determination of practical methods for the application of absorbing liners to suppress rocket engine combustion instability was started at Pratt & Whitney Aircraft sponsored by the NASA Marshall Space Flight Center. The development of absorber arrays has now been accomplished; effort at Pratt & Whitney Aircraft on mechanical damping devices for combustion instability suppression is currently devoted to the development of other types of acoustic devices including single resonators, slots and quarter-wave tubes. A review of work performed at Pratt & Whitney Aircraft on acoustic absorbing devices follows.

SOLUTION FOR HIGH-FREQUENCY COMBUSTION INSTABILITY IN AFTERBURNERS

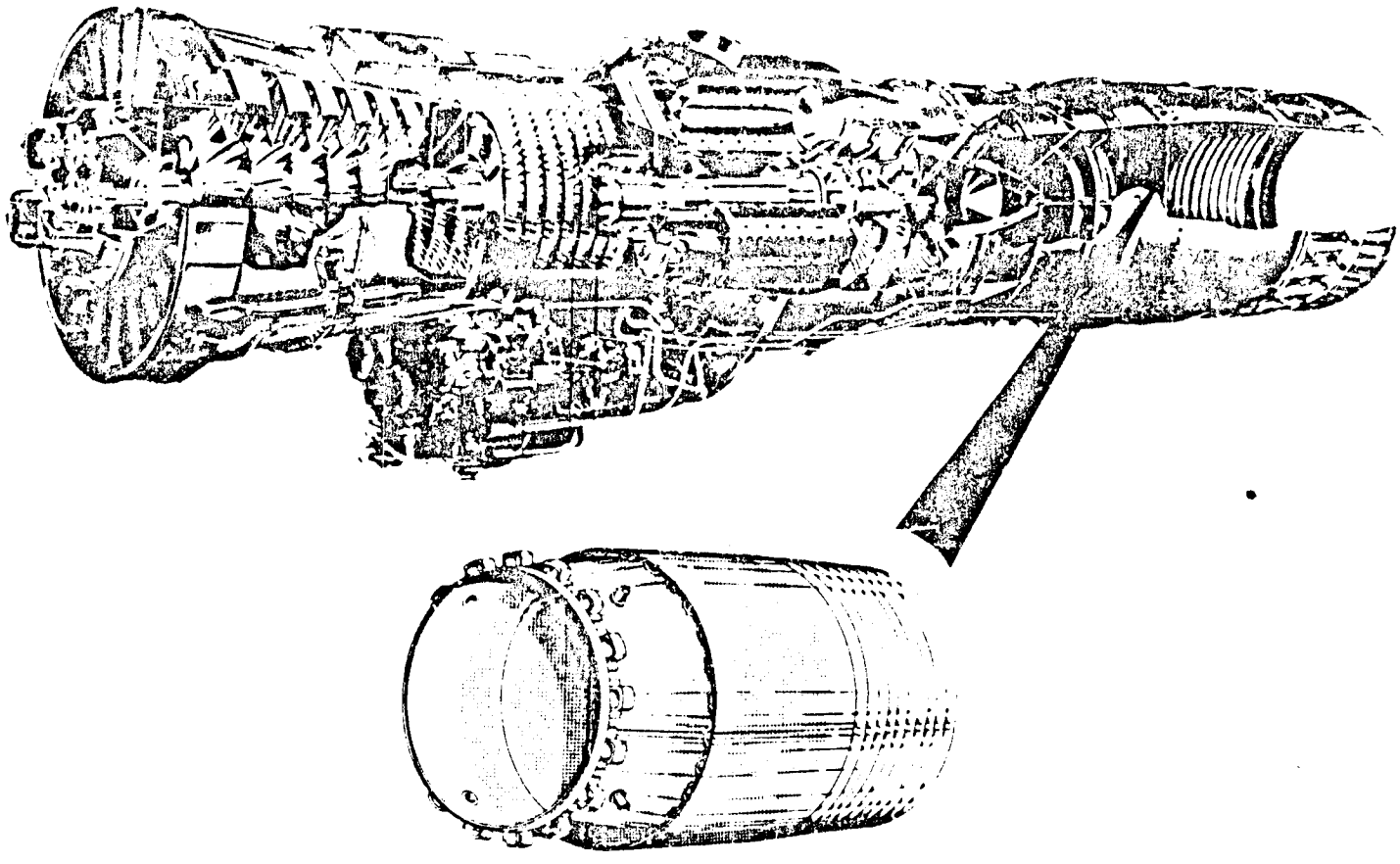

Absorbing Liner

ABSORBING LINER PRINCIPLES

An absorbing liner consists of a perforated wall (liner) separated by a volume of gas from a solid wall - usually the chamber pressure vessel. The mass of gas in the liner apertures and the volume of gas in the cavity behind the liner form an oscillatory system that is analogous to a spring mass system and has the typical frequency response of a damped oscillator. An effective liner may be designed with no detailed knowledge of the mechanism of combustion instability because the only properties of an unstable combustion process that affect the acoustic performance of the liner are the frequency and amplitude of the oscillations. The acoustic performance is expressed by the absorption coefficient, defined as the fraction of incident energy dissipated by the liner. The energy loss in the system results from turbulence and the friction on the side walls of the apertures. At low incident wave amplitudes, energy dissipation is predominately caused by viscous losses from the oscillation of the gas in the aperture. At high incident wave amplitudes, turbulence and circulation due to high oscillatory velocities control the absorbing characteristics. For design purposes the absorption coefficient is described for a given medium by specifying the two components, resistance and reactance of the acoustic wall impedance. The components are functions of the liner geometry, the properties of the gas in the liner apertures and the frequency and amplitude of the pressure oscillations. To obtain good absorption characteristics, liners are designed so that the resonant frequency of the system is near the frequency of the potential combustion instability in the thrust chamber.

ABSORBING LINER PRINCIPLES

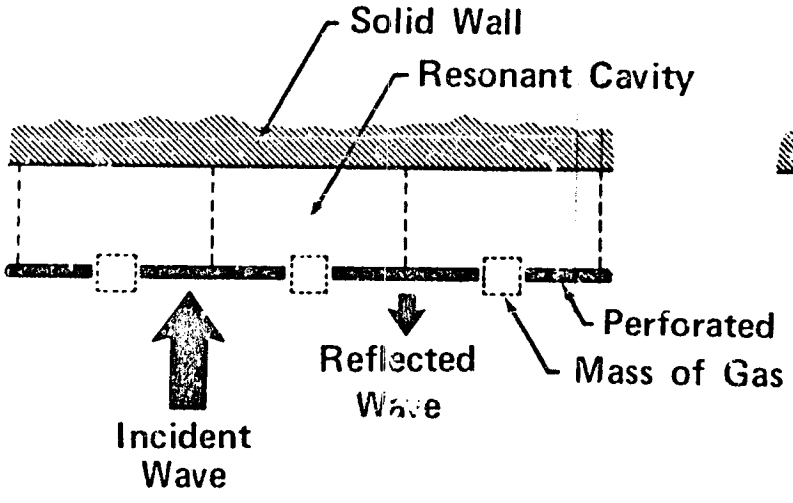

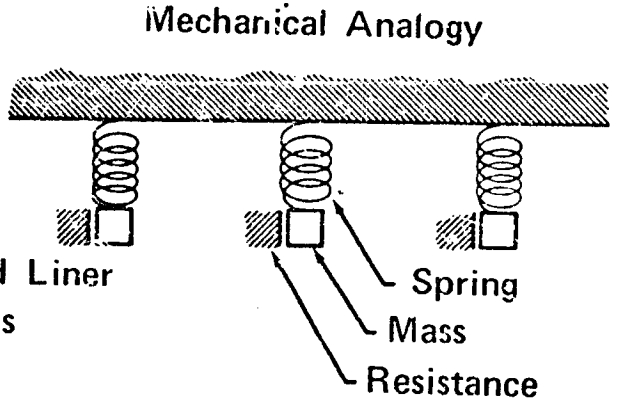

$$a, \text{ Absorption Coefficient} = \frac{\text{Energy Absorbed}}{\text{Incident Wave Energy}}$$

$a = a$ (Wall Impedance)

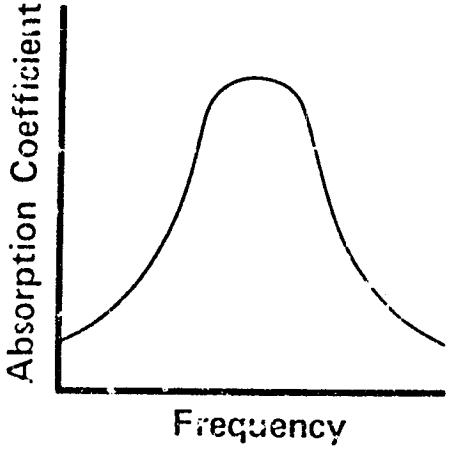

AMOUNT OF ABSORPTION REQUIRED

If the amount of absorption required to eliminate instability in a particular rocket combustion chamber could be predicted from theoretical considerations alone, the design of absorbing liners would be relatively simple. Unfortunately, this is not the case; hence, considerable experimental research has been devoted to the problem. In experiments conducted at Pratt & Whitney Aircraft, full chamber length liners with absorption coefficients of up to 85 percent were used in tests with LO_2/LH_2 propellants at a chamber pressure of 300 psia and with space storable propellants at chamber pressures of 100 and 200 psia. All of the liners with absorption coefficients of 17 percent or greater suppressed the spontaneous instability of the test motors so that the resulting peak-to-peak pressure oscillations were less than 10 percent of the mean chamber pressure.

Although the history indicates that only a small amount of absorption is required to stabilize most motors, the stability characteristics of every injector-chamber configuration are different; hence, these results do not imply that liners with low absorption coefficients will provide sufficient damping in all cases. It is suggested that liners for new systems be designed for the highest possible absorption over the anticipated frequency range of the potential instability.

AMOUNT OF ABSORPTION REQUIRED TO SUPPRESS COMBUSTION INSTABILITY IN ROCKET THRUST CHAMBERS

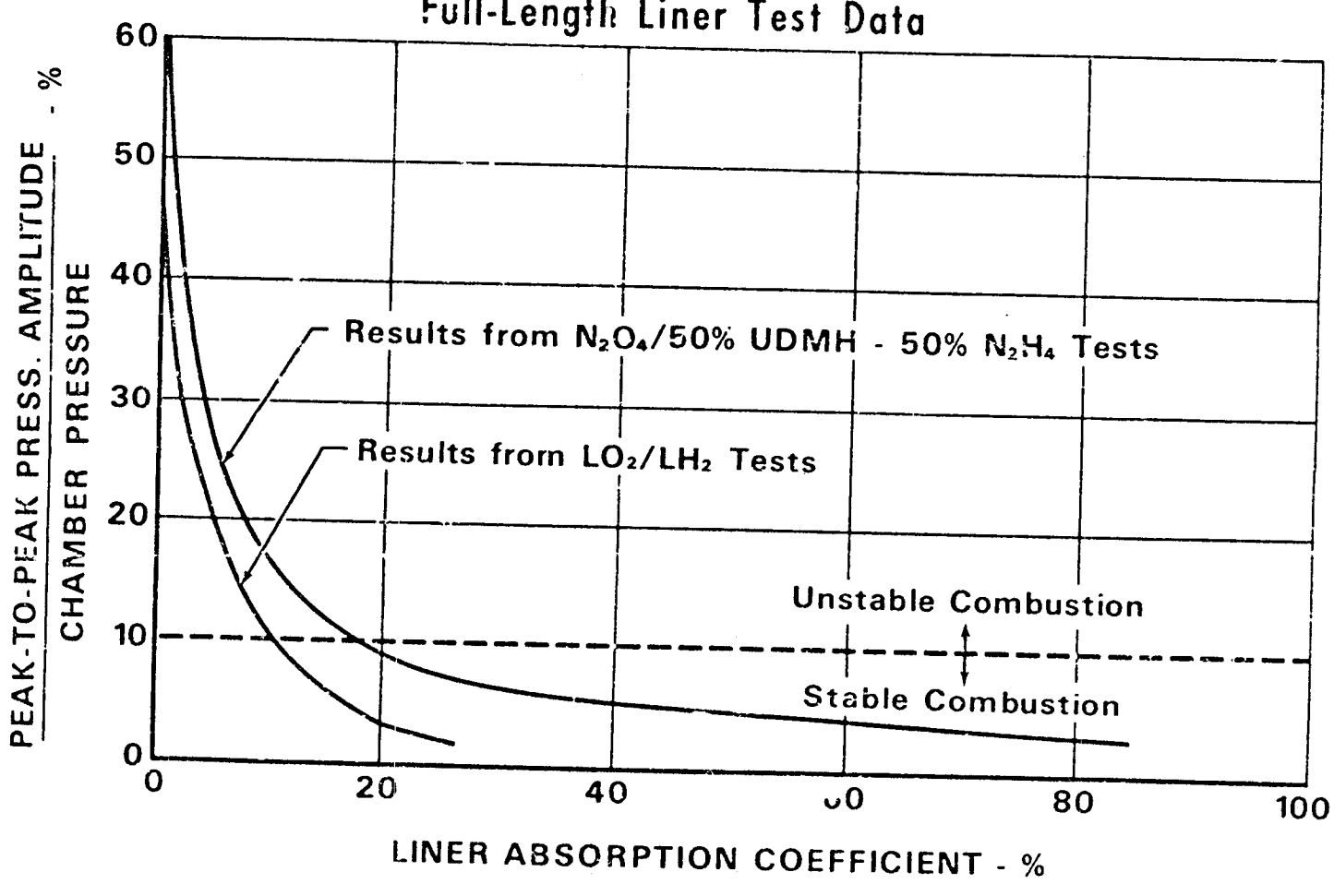

EFFECT OF LINER LOCATION AND LENGTH

An absorbing liner installed on the chamber wall near the injector face should be more effective than an identical one installed further downstream. The upstream liner is in a position closest to the most critical combustion zone and, therefore, can damp or absorb the pressure waves that would otherwise be reflected directly back to the source of the instability. The first test of this concept used a liner consisting of an array of resonators with a common cavity volume that had provided stable combustion in full-length liner tests. The liner was cut into quarter-length sections; each section was individually tested in its respective axial position to determine the most effective absorber location for preventing unstable combustion. The remainder of the chamber was made up of solid liner sections. Combustion was stable with the liner installed in the first two positions. Intermittent instability was encountered with the liner in the third position, and continuous instability was encountered with the liner in the fourth position.

A second series of tests was conducted with storable propellants to determine the effects of the liner length on suppression characteristics. Successive tests were conducted with liners of full, 1/2, 1/4, and 1/8 chamber length located next to the injector face; each liner section was a common-cavity array with an open area ratio of 5.7 percent (absorption coefficient of 23 percent). The remainder of the chamber was made up of solid liners. The tests were conducted at a nominal chamber pressure of 100 psia with a mixture ratio of 2. A decrease in the liner length from full to 1/4 chamber length did not change the stability characteristics of the motor; however, a decrease in length from 1/4 to 1/8 chamber length resulted in pressure amplitudes greater than 10 percent of chamber pressure, an unstable condition.

EFFECT OF LINER LOCATION ON COMBUSTION INSTABILITY

Quarter Length 50% Absorption Liner

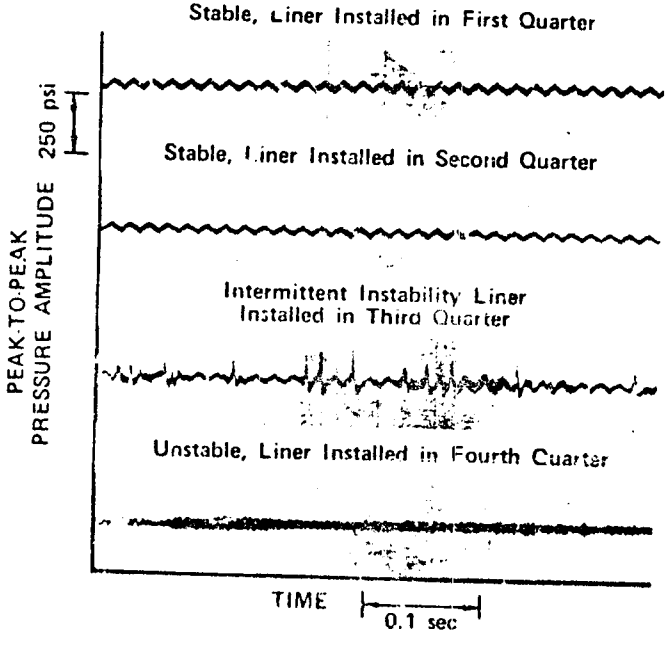

EFFECT OF LINER LENGTH ON COMBUSTION INSTABILITY

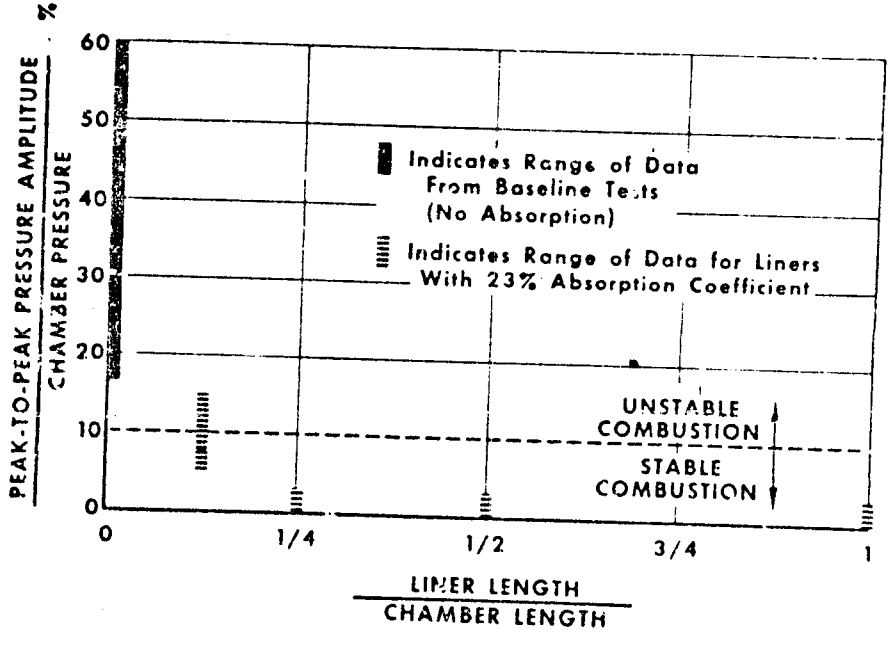

RESEARCH CONDUCTED FOR THE DEVELOPMENT OF ROCKET ABSORBING LINERS

The design of resonator arrays for usual acoustical applications is a simple and straightforward process; however, many complex factors affect the application of the theory to the design of rocket chamber absorbers. The high gas temperatures, complex flow situations, high pressure amplitudes, and other related effects impose serious limitations and uncertainties on the design techniques. In the NASA-sponsored program, a systematic approach to the solution of these problems has been taken. The effects of each of the above factors on absorption has been quantitatively described and corroborated through cold flow experiments using ambient air and gaseous helium and nitrogen as test media. However, extrapolation of the liner design theory, based on the results of cold-flow experiments to hot firing conditions, also introduces significant uncertainties, primarily because the rocket chamber environment can only be simulated in cold-flow experiments. In the past, it has been necessary to assume that the results from the cold-flow experiments would be applicable, because no reliable experimental techniques for making similar measurements during firings were known. Therefore, a new impedance measuring technique was developed for use during actual rocket firings. Carefully controlled hot-firing experiments were conducted to provide data for final verification of the improved theory.

SUMMARY OF NASA SPONSORED RESEARCH CONDUCTED FOR THE DEVELOPMENT OF ROCKET ABSORBING LINERS

Problem	Cooling Requirements
Effort	Analysis Supplemented with Hot-Firing Thermal Data
Conclusions	No problem if small apertures (≈ .150 in dia) and partitioned cavities are used; several different practical cooling schemes recommended.

Problem	Effects of High Oscillation Amplitudes on Absorption
Effort	Cold Flow Acoustic Experiments
Results	Extended existing acoustic theory; developed empirical correlations for use in design theory; found aperture discharge coefficient was significant independent variable.

SUMMARY OF NASA SPONSORED RESEARCH CONDUCTED FOR THE DEVELOPMENT OF ROCKET ABSORBING LINERS (cont.)

Problem	Effects of Chamber Gas Flows on Liner Performance
Effort	Analysis Supplemented with Data from Cold Flow Acoustic Experiments
Results	Development liner design theory applicable with any type of flow situation (past and/or through apertures).

Problem	Improvement of Liner Abosrbing Bandwidth Characteristics
Effort	Analysis Supplemented with data from Ambient Impedance experiments
Conclusions	Effective wideband absorbing characteristics can be obtained with complex resonator assemblies.

SUMMARY OF NASA SPONSORED RESEARCH CONDUCTED FOR THE DEVELOPMENT OF ROCKET ABSORBING LINERS (cont.)

Problem	Final Verification of Improved Liner Design Theory
Effort	Developed necessary instrumentation and calibration techniques and measured liner impedance during hot firings of actual rocket thrust chamber.
Results	Average deviation between theoretical and experimental absorption was 11%.
Conclusions	Improved theory is satisfactory for use in designing absorbing liners for rocket combustion chambers.

POROUS ABSORBING LINERS

Porous liners are another type of damping device that has been evaluated at Pratt & Whitney Aircraft. The liner shown was fabricated from a rolled and welded sheet of stainless steel Rigimesh. It was found to be effective for suppressing combustion instability in a LO_2/LH_2 thrust chamber that was spontaneously unstable when fired with a solid liner at 340 psia chamber pressure, mixture ratio of 5.

Theoretically, excellent wide band absorbing capability can be obtained with porous materials; inherently they do not exhibit the resonant absorbing characteristics of conventional acoustical devices. Porous liners are especially worthy of consideration for application in engines with high heat fluxes, such as the Space Shuttle, because often adequate cooling can be obtained with low transpiration flows at no sacrifice in absorption. Unfortunately, the absorbing characteristics of porous materials in general cannot be predicated from theory alone; a model for the specific material, based on cold flow impedance data, is required.

POROUS ABSORBING LINER

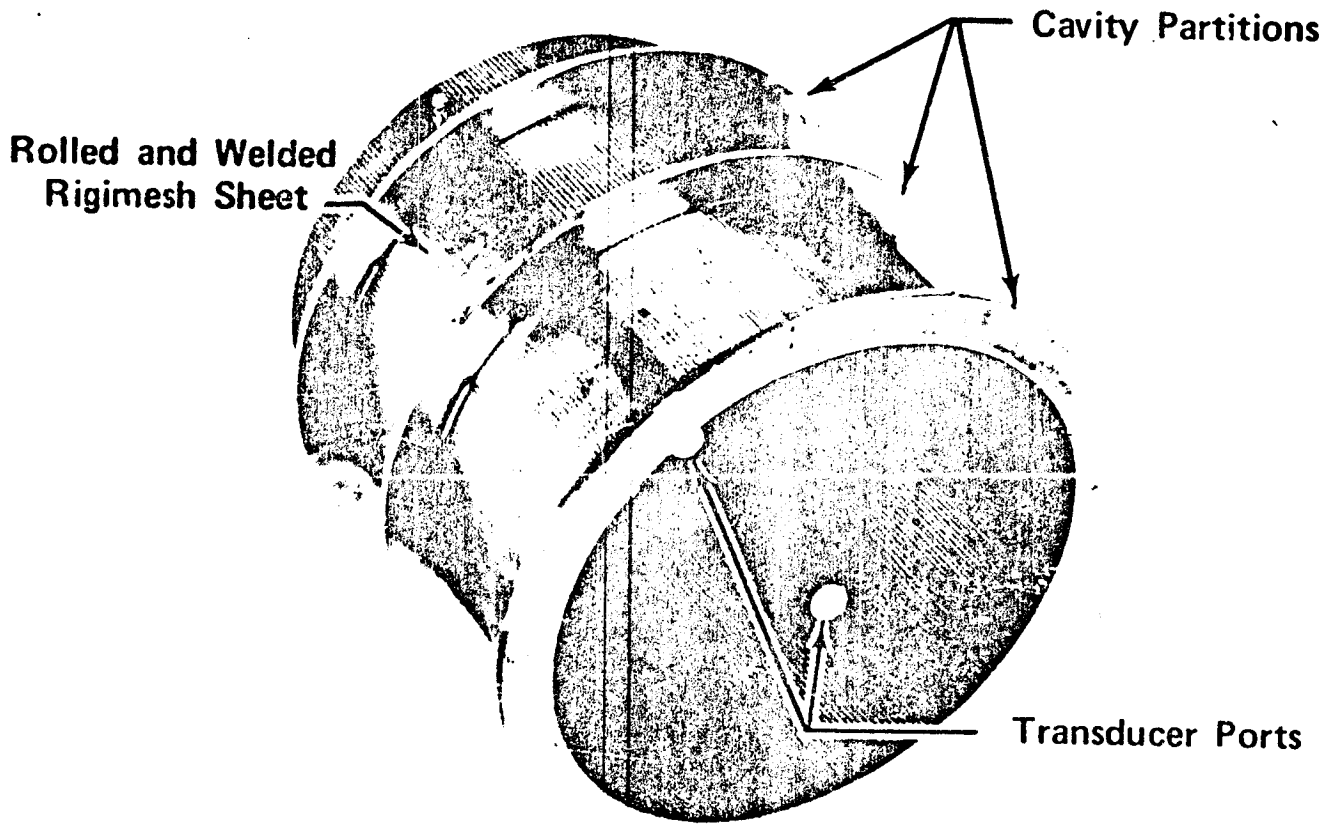

OTHER TYPES OF DAMPING DEVICES

Other types of devices that can be used to suppress combustion instability are individual resonators and acoustical cavities, i.e., quarter wave tubes or slots. These devices are particularly good for application to engines with limited chamber surface areas. Furthermore, they can usually be incorporated with existing chamber designs or hardware more easily than resonator arrays can be. However, their damping characteristics are quite sensitive to their resonant frequency; thus, they must be carefully tuned to obtain maximum damping at the frequency of the potential instability. They can be located in injector faces, at the intersection between injector and chamber or in the chamber walls. Highest damping is obtained when the aperture is located at the antinode of the potential instability, therefore, the best location in a particular chamber will depend on the mode of the instability to be damped.

ACOUSTIC CAVITIES AND INDIVIDUAL RESONATORS USED AS DAMPING DEVICES-EXAMPLE CONFIGURATIONS AND LOCATIONS FOR ROCKET CHAMBER INSTALLATIONS

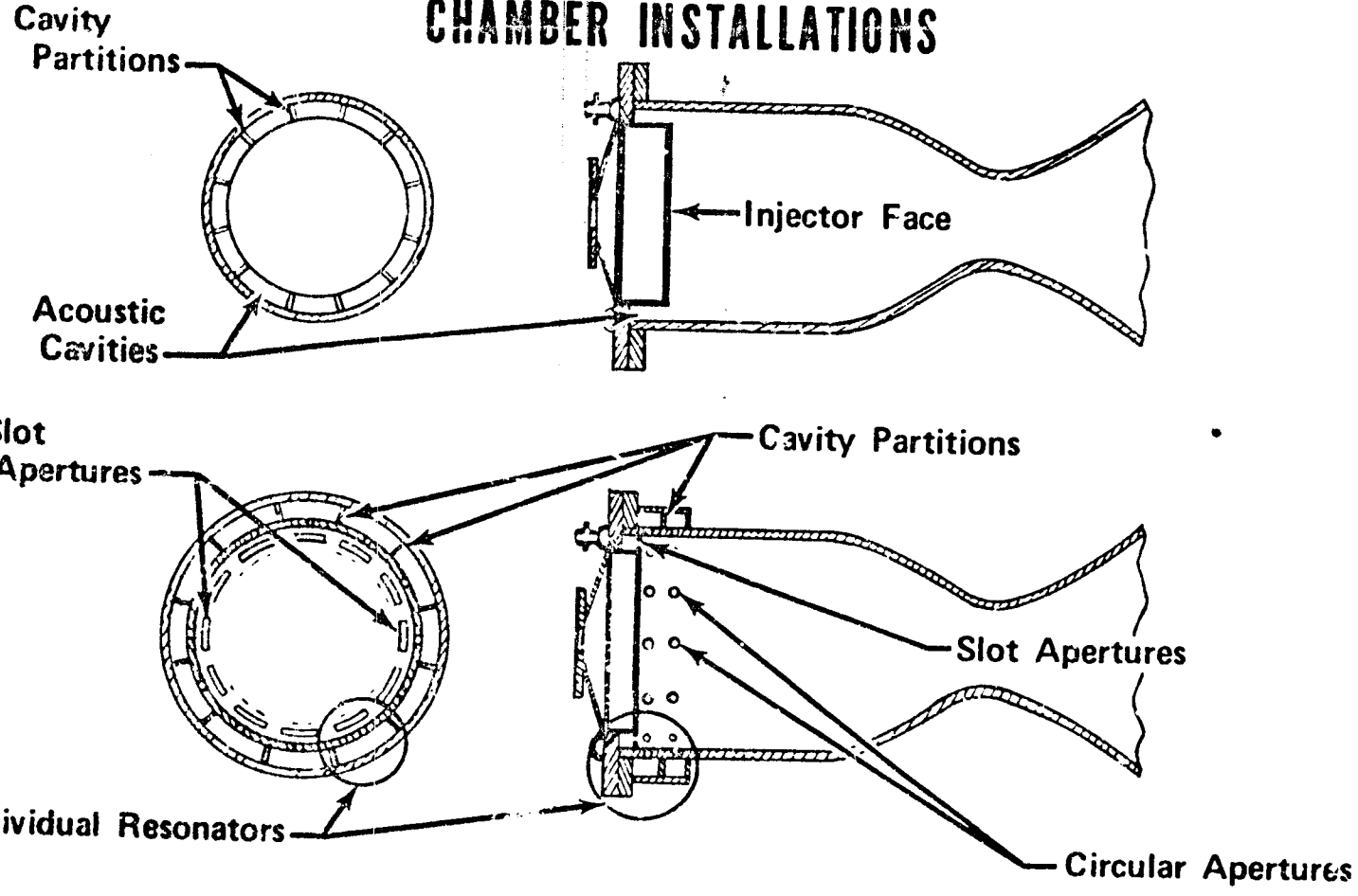

CURRENT DAMPING DEVICE PROGRAM

Acoustic liners consisting of arrays of resonators are good combustion instability suppressors because they can absorb a large percentage of the pressure wave energy acting on the surface of the liner. Thus, an array covering a significant portion of the combustion chamber surface is desirable to ensure stable combustion. However, in many instances, such as the SSME, surface areas are limited because of cooling and structural requirements and only a few damping devices can be installed. Under this circumstance the resonator array theory is not valid; in fact, both the absorption coefficient and the open area ratio used in the present theory can only be arbitrarily defined.

For acoustic energy absorbers other than arrays of resonators, a design analysis based on total energy absorption is a valid approach; however, no theory is known for use in the nonlinear acoustic regime where rocket chamber acoustic devices must operate. Hence, the objective of the efforts under our current program is the development and verification, using cold-flow acoustic devices, of a design theory for nonarray absorbing devices. Additionally, two other cold-flow acoustic experiments are being conducted: an investigation of the dimensional limitations of acoustic suppression devices, including resonators, slots, and quarter-wave tubes; and the determination of the effects of wide band background noise, which is always present in combustion chambers, on liner impedance.

DAMPING DEVICE INVESTIGATION NOW UNDERWAY AT PRATT & WHITNEY AIRCRAFT

Objective	Development and Verification of Design Theory for Acoustic Energy Absorbers Other Than Arrays of Resonators
Sponsor	NASA Marshall Space Flight Center
Technical Monitor	R. H. Counts
Contract No.	NAS8-21310

NONARRAY DAMPING DEVICE THEORY

A theory that can be used for the design of nonarray acoustic devices has recently been formulated at FRDC. The dependent variable we are using, the resonator coefficient, is similar to the absorption coefficient of the array theory. The resonator coefficient, which varies between zero and unity, is both a measure of the energy absorbing characteristics and the efficiency of the device. Values near zero mean that essentially all the acoustic energy is being reflected or reradiated; values of unity mean that the particular device is absorbing as much acoustic energy as possible at that frequency. Values of the coefficient less than unity indicate that, at least theoretically, it is possible to select a different configuration that will absorb more energy under the same conditions, i.e., pressure amplitude and frequency.

The theory, applied to an individual resonator, shows excellent agreement with experimental data, particularly in the vicinity of resonance. Although slight modification of the theory was required, similar agreement with quarter-wave tube data was found, indicating that the theory is more general than first believed. Application to other types of acoustic cavities will be attempted in the near future.

COMPARISON OF EXPERIMENTAL RESULTS WITH NONARRAY DESIGN THEORIES

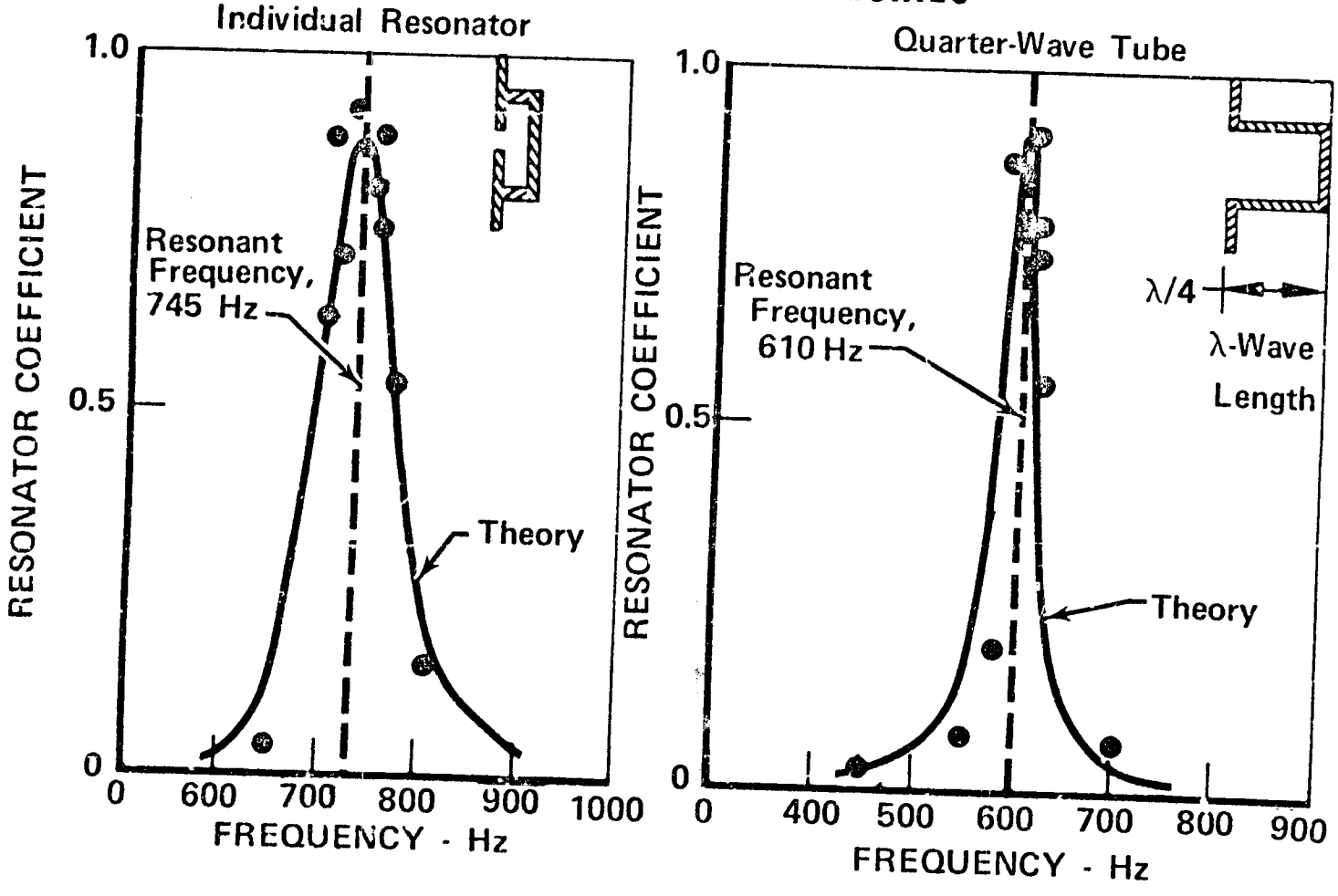

"MINIMUM PRESSURE LOSS IN HIGH VELOCITY FLOW DUCT SYSTEMS"

C. R. GERLOCK

SOUTHWEST RESEARCH INSTITUTE

TECHNICAL MANAGER

R. VEITCH

MARSHALL SPACE FLIGHT CENTER

MINIMUM PRESSURE LOSS IN HIGH VELOCITY FLOW DUCT SYSTEMS

SOUTHWEST RESEARCH INSTITUTE
C. R. GERLACH

CONTRACT NAS8 - 21133

INTRODUCTION

Objectives

As initially defined in the contract, the objectives of this study were to perform a theoretical and experimental investigation of ducting and ducting components to minimize pressure drop, surge pressures and vibration levels and, thus, to generally improve flow conditions of gases and liquids in space vehicle feed systems.

Scope of Work

Project efforts have been concentrated in three areas which are:

(a) Study of bellows pressure losses for liquid and gas flows, with and without liners

(b) The study of duct elbow losses, and the definition and verification of a new "Los Loss" shaping concept, and

(c) The study of bellows flow-induced vibrations for gaseous and liquid (including cryogenic) flows.

Because of certain fatigue failure problems with flex hoses and bellows on early Saturn flights, emphasis for the project was early placed on the study of bellows flow excitation. This discussion will dwell totally on bellows vibrations, however, the interested reader may find details of the bellows and elbow pressure loss work in the report: "Study of Minimum Pressure Loss in High Velocity Duct Systems," by C. R. Gerlach and E. C. Schroeder, Interim Technical Report No. 1, Contract No. NAS8-21133, Southwest Research Institute, July 1969.

Illus. 1

- OBJECTIVE
  - Perform theoretical and experimental investigations of ducting components to minimize pressure losses and vibrations for gaseous and liquid flows

- SCOPE OF WORK
  - Study of bellows pressure losses for liquid and gas flows, with and without liners
  - Study of duct elbow flow losses and definition "low loss" shaping concept
  - Study of bellows and flex hose flow-induced vibrations for gaseous and liquid media, including cryogenic liquids

OUTLINE OF BELLOWS FLOW-INDUCED VIBRATION INVESTIGATION

The investigation of bellows flow excitation has developed, over the project period, into a number of distinct investigation areas. First was identification of the flow excitation mechanism. Here a mutual dynamic coupling between a vortex formation and shedding process and the bellows longitudinal vibration modes was verified as the responsible mechanism. Other investigators have chosen to call the excitation mechanism a boundary layer instability, however, both concepts may be regarded as identical. As in any nonsteady fluid mechanics problem, the generation of nonsteady circulation or vorticity must occur in order that nonsteady dynamic fluid forces can be exerted on the bellows convolutes. If, then, the term boundary layer instability is used to imply the occurence of this necessary nonsteady circulation or eddying, then the concepts may be argued as being the same, and there is no inconsistency in the usage of the terms "vortex excitation" and "boundary layer instability."

The second general area of investigation involved the correlation of flow and bellows variables for conditions where excitation is possible. The definition of a Strouhal number $f\sigma/V$, where f is the vibration frequency, σ the convolute tip width and V the fluid velocity, has been found entirely satisfactory for making this correlation. Use of a simple mass-spring permits easy prediction of velocity conditions for which a given bellows might be excited.

The third area of investigation involved formulation of a coupled bellows-fluid force mathematical model. From this model, prediction of flow-induced vibration levels for a given situation is possible. Supplementing this analysis, the fourth area of study involved tests of numerous sizes and geometries of bellows to verify the force model for typical stage hardware configurations employing water, liquid nitrogen and gas flows.

The final area of study has been the identification and investigation of an acoustic resonance phenomena which occurs when a gas is the media flowing through a bellows or flex hose.

• OUTLINE OF BELLOWS FLOW-INDUCED VIBRATION INVESTIGATION

- Identification of flow excitation mechanism
- Correlation of flow and bellows variables for conditions where excitation is possible
- Formulation of coupled bellows-flow force mathematical model
- Correlation of model with test results for water, liquid nitrogen and gas flows
- Identification and investigation of acoustic resonance phenomena

GENERAL ILLUSTRATION OF BELLOWS FLOW EXCITED BEHAVIOR

The general behavior of a bellows excited by flow is illustrated in this figure. As the flow increases, excitation of successive longitudinal modes occurs. Each mode is excited over some velocity range called a lock-in range. Lock-in occurs when the conditions for coupling of the vortex phenomena and a particular bellows mode are correct. The lower frequency longitudinal modes are excited only in a free bellows. For a flex hose, only the highest frequency mode, that is the "out of phase" mode, may occur. This "out of phase" mode also occurs in a free bellows and is the most severe of the possible free bellows modes since conditions for the vortex shedding is most favorable.

In general, not all of the longitudinal modes for a given bellows are excited. Some structural vibration modes, while possible, may not be excited for one of several reasons. First, the flow forces may be too small to permit dynamic coupling with the structure. Second, some modes may not be excited because of poor coupling with the vortex phenomena. Third, some of the higher order longitudinal modes are never observed since the out of phase mode, which is much more severe, couples with the fluid instead, and does not permit these other modes to be excited.

With gas flows an acoustic resonance phenomena occurs at very high velocities, and may produce excitation of higher order convolute bending modes whose frequencies are above that of the highest longitudinal mode.

- General Illustration of Bellows Flow Excited Behavior

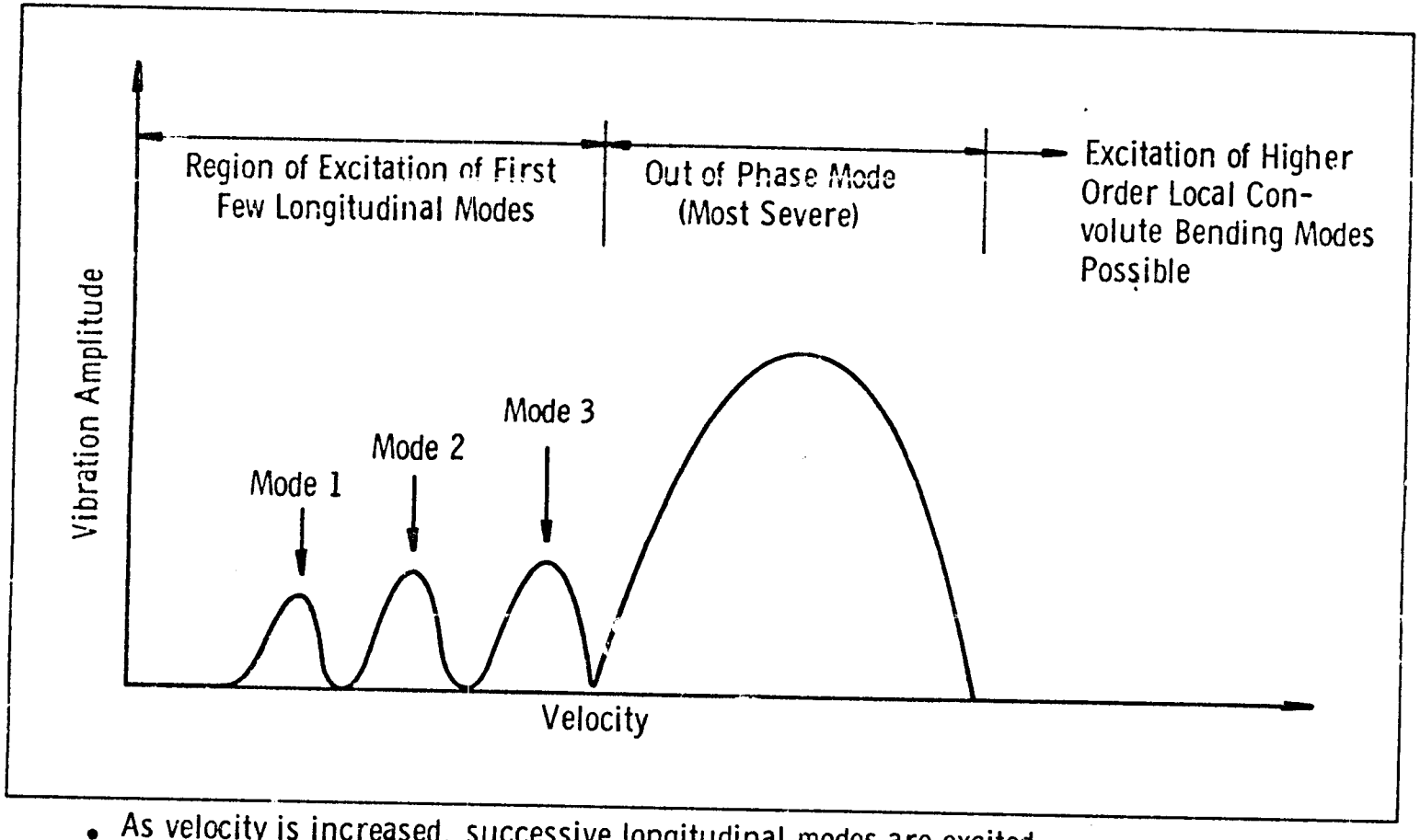

- As velocity is increased, successive longitudinal modes are excited
- The most favorable mode for excitation is the highest longitudinal or "out of phase" mode
- At very high velocities, local convolute bending modes may be excited

SEQUENCE OF COUPLED FLUID-CONVOLUTION EVENTS OBSERVED WITH TWO-DIMENSIONAL BELLOWS FLOW VISUALIZATION MODEL

This figure illustrates a sequence of vortex formation and shedding events which were actually observed from an experimental flow visualization model. This model consisted of a number of bellows convolutes mounted in a special two-dimensional plexiglass test section. Flow patterns within this model were conveniently observed by injecting ink immediately upstream of the first convolution. Detailed studies of motion pictures taken of the visualized fluid and convolute motions resulted in a definition of the events indicated. This sequence clearly illustrates the formation and shedding of vortices in the vicinity of the convolutes. As may be noted, formation of a vortex on the downstream side of a convolution occurs as adjacent convolutions move apart. This vortex is subsequently forced from between the convolutes as they move together. It may also be noted, as indicated, that movement of a vortex shed in the downstream direction can result in its aiding or reinforcing the formation of the vortex on the downstream convolute. The convolute motions indicated in this figure correspond to the highest longitudinal or the "out-of-phase" bellows mode. This mode is also that which occurs for a flex hose.

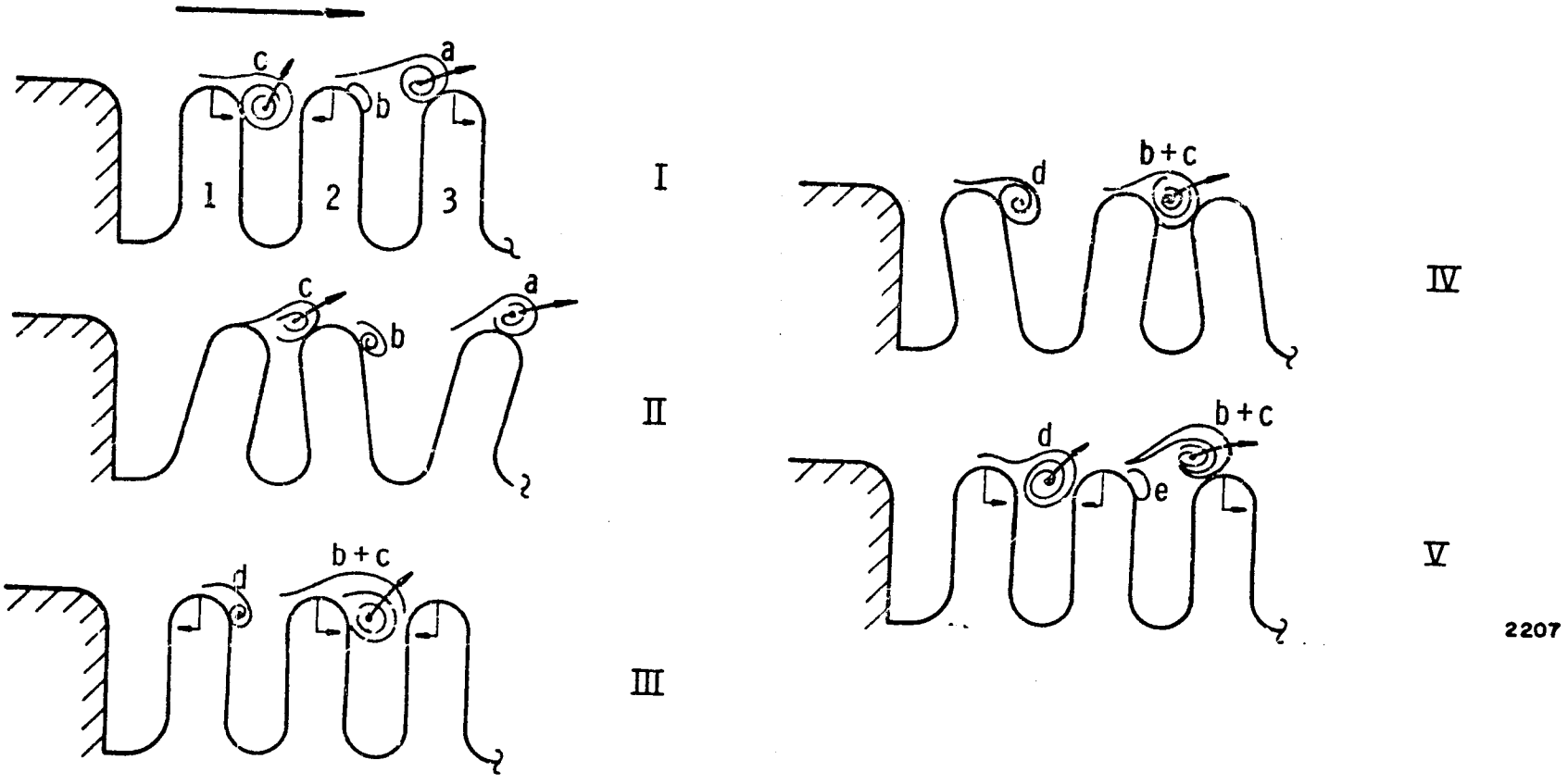

2207

Sequence Of Coupled Fluid - Convolution Events Observed
With Two-Dimensional Bellows Flow Visualization Model

CONCEPT OF VORTEX FORCE ON BELLOWS VIBRATING IN THE FIRST LONGITUDINAL MODE

This figure illustrates the vortex to structural coupling for the first longitudinal mode. As may be noted, the vortex formation and shedding is dependent on the relative convolute motion. The vortex is formed on the trailing side of a convolute during its opening motion. Conversely, the formed vortex is shed or pinched out from between adjacent convolutes as they move together. The forces resulting on the convolute are a result of non-steady pressures produced by the generation and movement of these vortices. As shown for the first longitudinal mode, the pressure forces act in such a way that a net force is exerted only on the center convolute. A mechanical spring-mass model may be conveniently employed for analytically predicting the effect of this net vortex force on a given bellows.

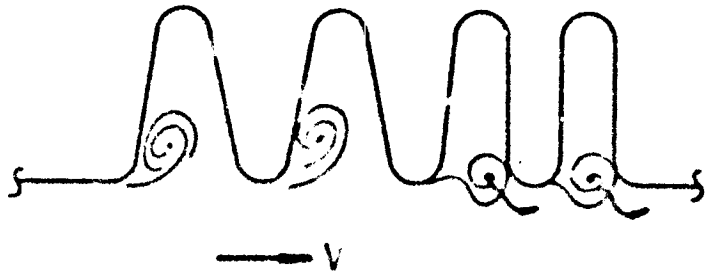

Vortex Activity On Bellows Vibrating In 1st Mode

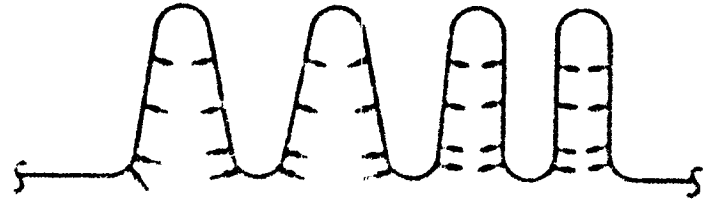

Resultant Pressure Forces On Convolutions

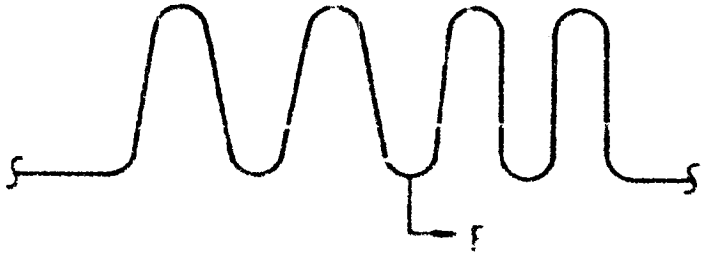

Net Effective Force On Convolutions

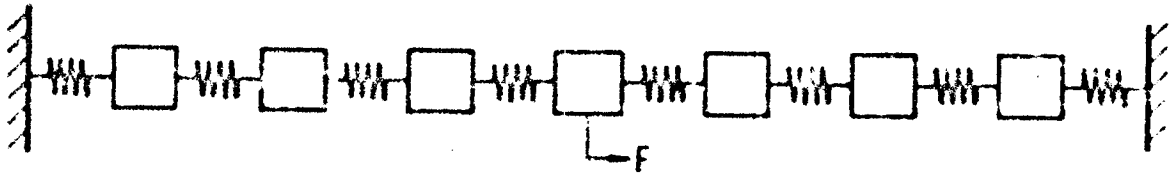

Equivalent Mechanical Model

Concept of Vortex Force on Bellows Vibrating In The First Longitudinal Mode

ILLUSTRATION OF BELLOWS FLOW INDUCED STRESS MODEL

A mathematical representation for convolution flow induced stresses is given in this illustration. As shown in this figure, which represents excitation of the "out-of-phase" mode, the vortex activity produces opposing or out of phase forces on adjacent convolutes. This force may be represented in the form:

$$F = C_F C_L A_p (1/2 \rho V^2)$$

where C_F is a dimensionless vortex force coefficient, A_p is the projected convolute area, and the quantity $(1/2 \rho V^2)$ is the dynamic fluid pressure. The vortex force F produces a corresponding convolute displacement x, where x and F are related by the equation

$$x = \frac{C_m F Q}{k_A}$$

Here the quantity Q is the conventional dynamic amplification factor. k_A is the overall bellows spring rate, and the quantity C_m is a vibration mode factor which depends on the number of bellows convolutes and the vibration mode. Finally, stress is related to convolution displacement, x by the expression

$$\text{Stress} = \frac{C_s E t x}{h^2}$$

where C_s is a bellows geometry factor, E is Young's modulus, t is bellows ply thickness, and h is convolute height. The interested reader should consult the earlier referenced report for details of this model.

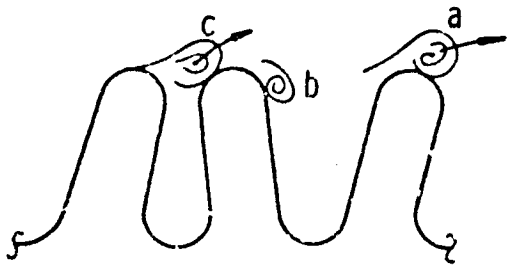

Vortex Shedding From Convolutions

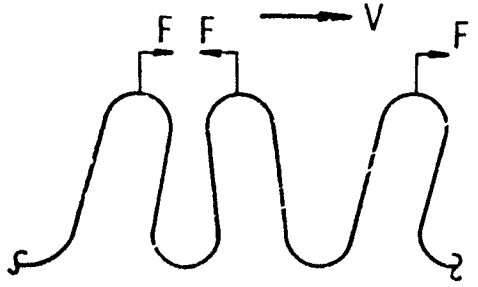

Vortex Force

$$F = C_F C_E A_p \left(\frac{1}{2} \rho V^2 \right)$$

In these equations
- C_F = vortex force coefficient
- C_E = elbow factor
- C_m = vibration mode factor
- Q = dynamic amplification (damping)
- C_S = geometric stress factor

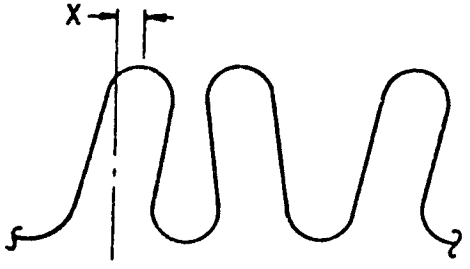

Convolution Displacement

$$x = \frac{C_m F Q}{k_A}$$

The resultant stress is

$$\text{Stress} = \frac{C_S E t x}{h^2}$$

Illustration of Bellows Flow-Induced Stress Model

LABORATORY BELLOWS DYNAMIC STRAIN INSTRUMENTATION

This figure illustrates the data gathering scheme employed in all tests of bellows flow excitation. An early study of various monitoring methods, including convolute strain, flange or duct acceleration, acoustic emission and internal dynamic pressure fluctuations showed that the only reliable method was the use of strain gages. Therefore, the basic output variable is dynamic strain measured at the external tip of one or more convolutes. Use of careful gage and lead wire installation practices has allowed strain measurements under conditions of very high frequencies and strain levels, plus measurements at cryogenic temperatures with much success.

To bypass frequency limitation problems a D. C. excitation is employed with the strain gage bridge. Output of the bridge is capacitively coupled into an amplifier having the required frequency range. The output of this amplifier is used to drive the vertical axis of an X-Y plotter, and the horizontal axis is driven proportional to the fluid test velocity. In this manner, direct plots of convolute strain versus fluid velocity are conveniently generated in the laboratory. As a supplement to the strain--velocity plots, a spectral analyzer is also employed to allow generation of strain-frequency plots.

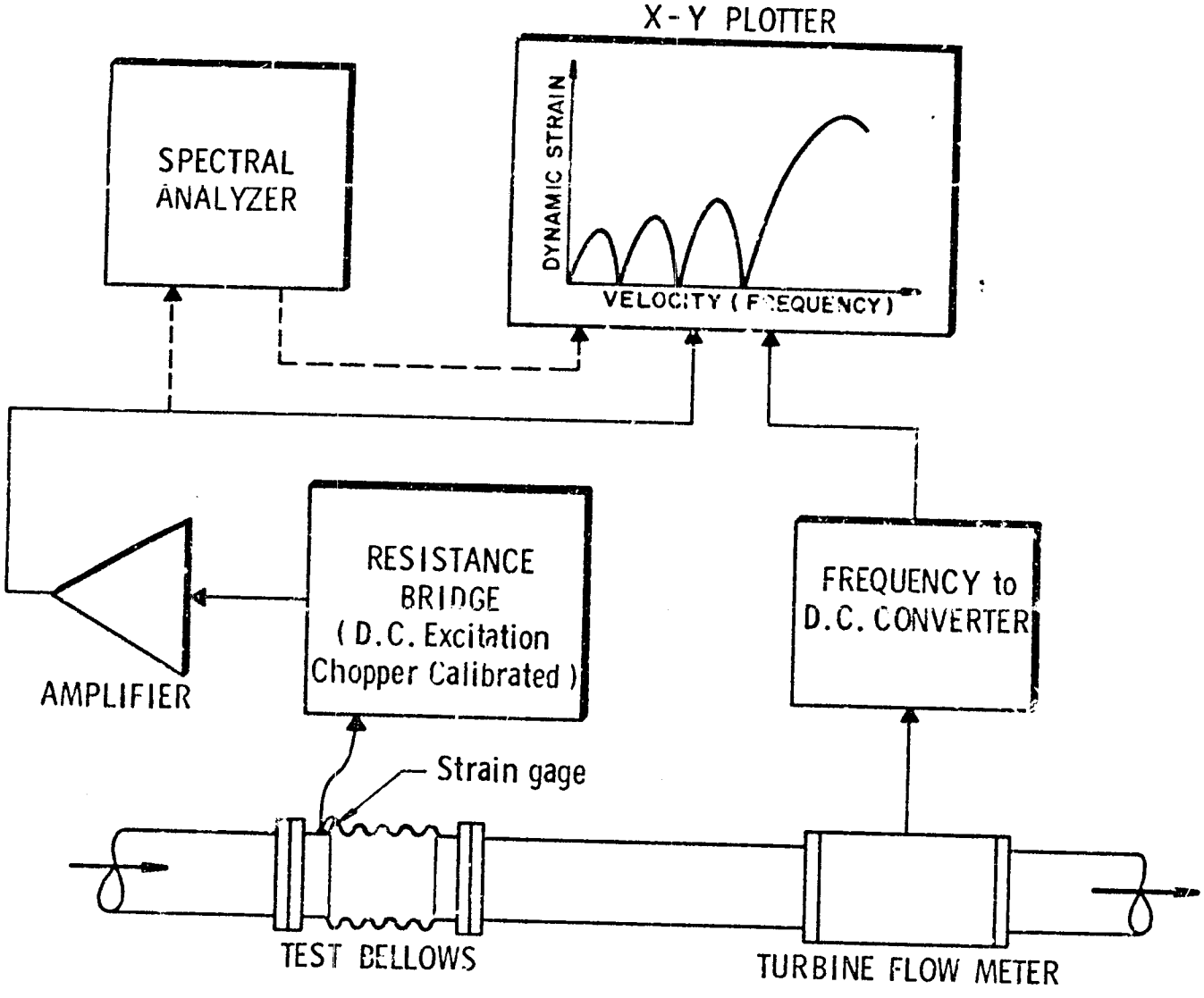

Schematic Illustration of Laboratory Bellows Dynamic Strain Instrumentation

TYPICAL FLOW INDUCED STRAIN AND FORCE COEFFICIENT RESULTS

From the strain-velocity plots generated in the laboratory, a data reduction process is employed to obtain experimental vortex force coefficient values. This data reduction process involves "working backward" through the model analysis procedure to finally arrive at the experimental C_F value. This plot illustrates some typical results for one bellows which was incrementally stretched and compressed to vary the pitch dimension. Note how the force coefficient changes with pitch.

From data of this type, a generally valid set of curves for C_F has been generated. Tests to date with various size bellows and bellows having a wide range of geometry show good agreement with this analytical flow-induced stress model.

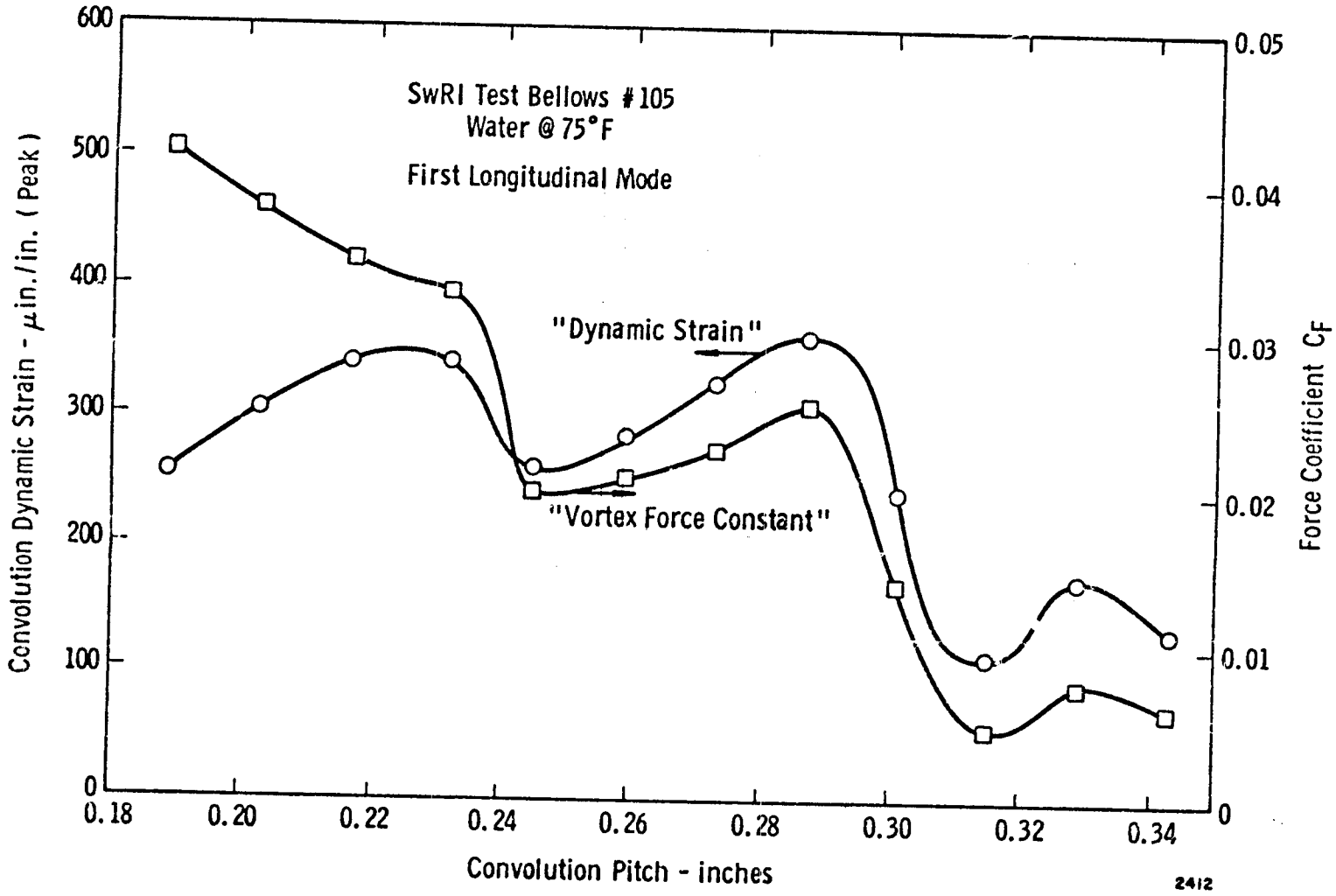

Typical Flow Induced Strain and Corresponding Vortex Force Coefficient Results for Test Bellows

BELLOWS DYNAMIC AMPLIFICATION VALUES

A very important aspect in the determination of bellows flow induced stress is use of an appropriate dynamic amplification factor Q. Laboratory tests have shown that the value of Q is strongly dependent on several factors. First, Q is highly dependent on the vibratory stress level. Second, Q is dependent on the number of bellows plies, and on the flow media. Finally, it is dependent on the stiffness. From a number of laboratory tests involving mechanical excitation of bellows, with various internal media, Q values have been determined for different applications. This figure illustrates the result of this investigation of bellows damping. The different curves shown correspond to various bellows and internal media situations. This data is set up in a form to be of easy use for a designer. As shown, Q values are given in terms of a bellows operational parameter which reflects the stress level at a given operating condition. Use of damping data of this type is mandatory for satisfactory prediction of bellows stress levels.

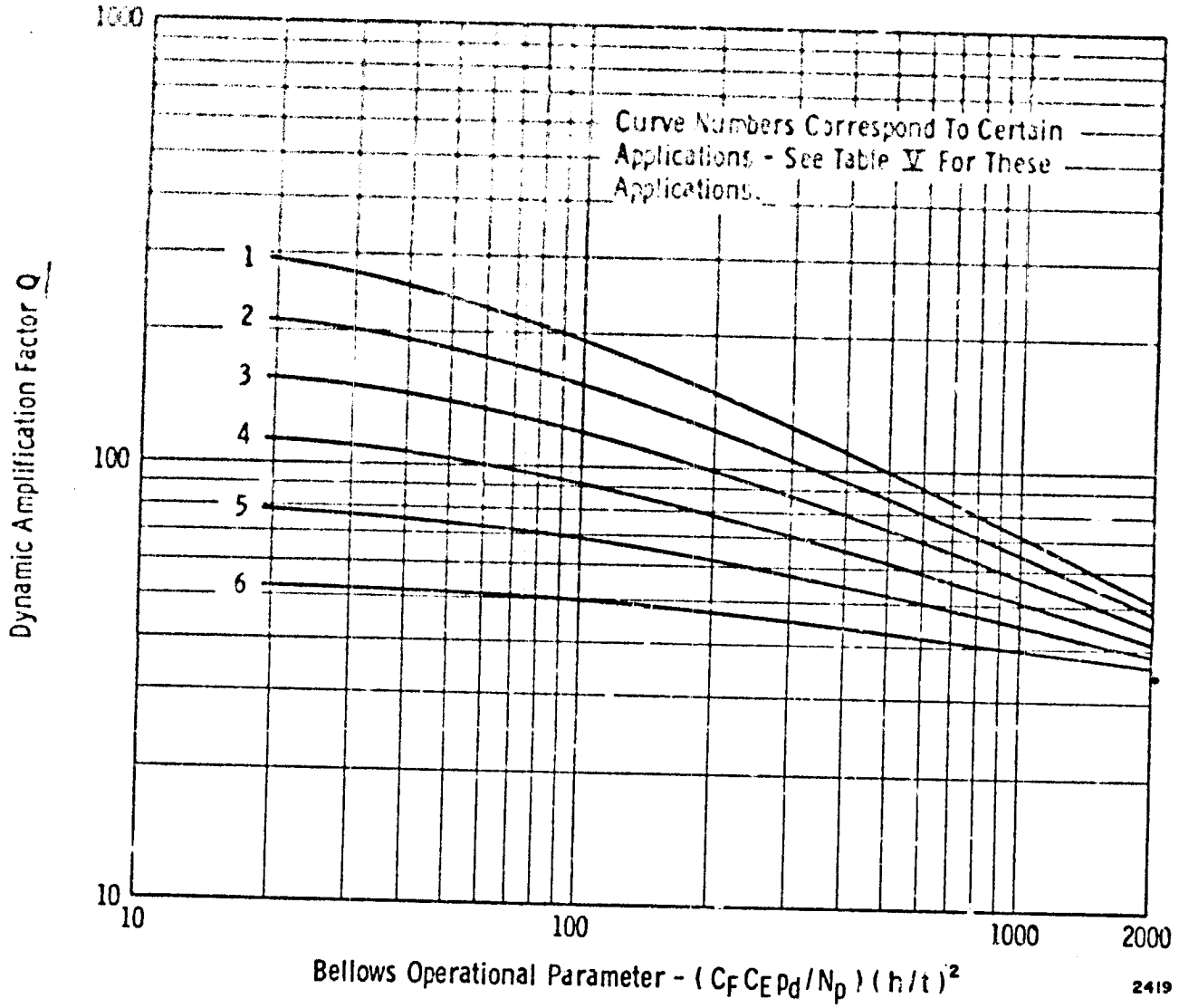

Dynamic Amplification Factors for Various Bellows Applications

STRESS INDICATOR - FATIGUE LIFE CORRELATION FOR BELLOWS

A simplified version of the bellows flow-induced stress model has been developed. This simple model has been formulated as a "Stress Indicator" parameter which is proportional to flow-induced stress, and is therefore of value for judging the relative severity of various situations. The "Stress Indicator" is given by

$$S.I. = \frac{C_F C_E Q p_d}{N_P} \left(\frac{h}{t}\right)^2$$

which consists of readily obtained or calculated parameters or numbers.

Complementing this simplified approach, a correlation between the S.I. value and observed cycles-to failure for a number of failure cases has been prepared. This illustration shows the resultant correlation. With this type of information, the bellows designer may easily determine the potential integrity of a proposed application.

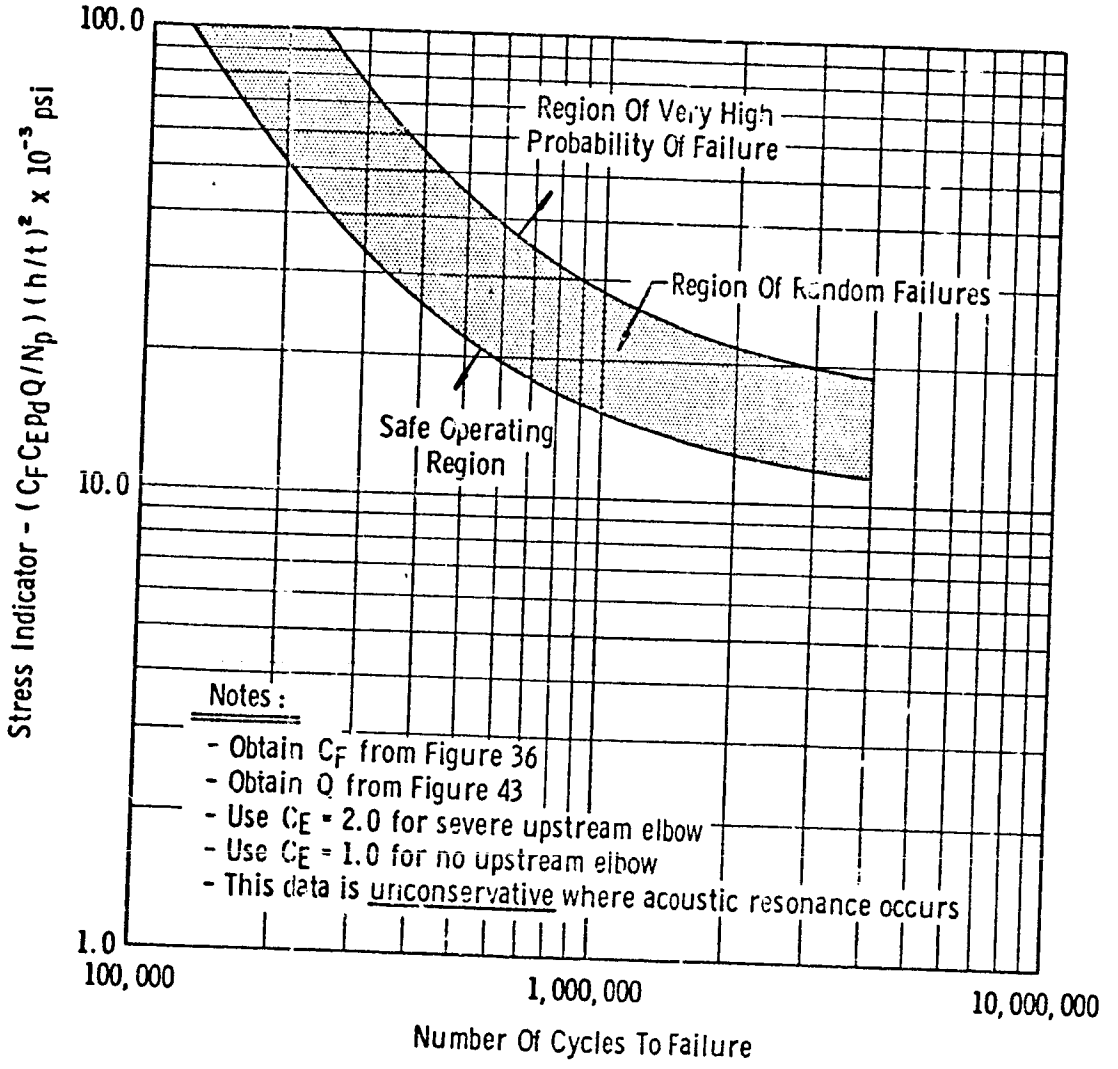

Stress Indicator - Fatigue Life Correlation for Bellows

ILLUSTRATION OF BELLOWS ACOUSTIC RESONANCE PHENOMENA

For the case of gas flows in free bellows or flex hose, an acoustic resonance phenomena produces a serious force amplification effect not observed with internal liquid flows. This resonance occurs when the vortex frequencies become high enough to excite a radial acoustic mode within the bellows. With this resonance, strain levels are observed to increase manyfold over strain levels which occur in the absence of the acoustic phenomena. Thus, flow of one gas at a given velocity may produce drastically different dynamic strains than flow of another gas at the same velocity assuming resonance occurs in one case but not in the other. For example, acoustic resonance may occur with gaseous nitrogen flows at about 1/3 the velocity for which it occurs with helium flow. Thus, we can expect much higher flow induced stress levels with nitrogen at a lower velocity than for helium flows at the same velocity, even with similar density conditions. The acoustic resonance phenomena generally precludes the use of a substitute gas for test purposes except where a similarity of speed of sound and density may be produced.

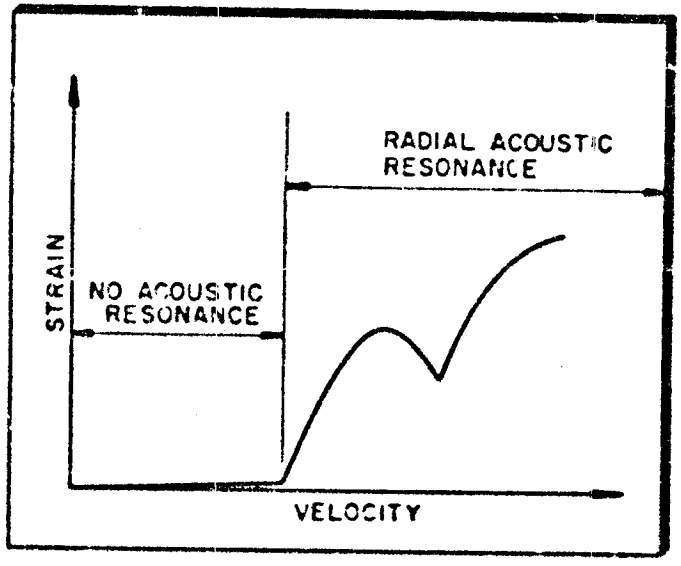

WITH GAS FLOW IN BELLOWS, ACOUSTIC RESONANCES EXCITED BY VORTEX ACTIVITY CAN PRODUCE VERY HIGH STRESSES IN CERTAIN VELOCITY RANGES

223

AT HIGH GAS VELOCITIES RADIAL ACOUSTIC RESONANCE COUPLES WITH VORTEX ACTIVITY AND AMPLIFIES DYNAMIC FORCES

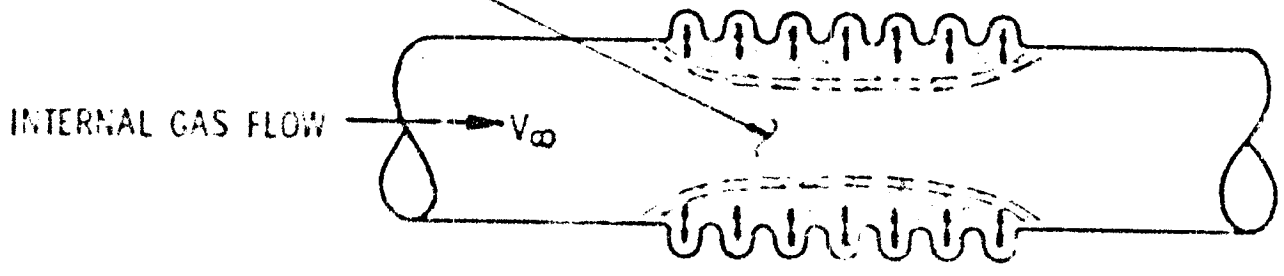

3245

Illustration of Bellows Acoustic Resonance Phenomena

- EFFECT OF HEATING INPUT TO BELLOWS

  - With cryogenic flows in bellows, heating can suppress vibrations
  - Suppression generally caused by reduction of vortex forces because of local cavitation and boiling
  - Frost, slush and ice buildup on exterior can also produce vibration suppression
  - Use of water as a substitute test fluid for LOX or LN_2 will produce satisfactory results, since non-suppressed vibrations are produced.

CONCLUSIONS

- Bellows flow excitation is a result of dynamic coupling between the bellows structure and a vortex generation and shedding process.
- The potential occurence of flow excitation may be predicted by means of a Strouhal number correlation relating fluid velocity, bellows mode frequencies and bellows geometry.
- Flow-induced stress levels may be predicted by means of a mathematical model. A simplified form of this model, called the "Stress Indicator" approach is convenient for comparing relative stress levels for various situations, and for predicting fatigue life.
- Heating inputs for the case of cryogenic fluid flows may cause local boiling or cavitation which serves to reduce the severity of the vortex process. Thus excitation amplitudes are reduced.
- With gas flows, an acoustic resonance phenomena can occur, producing severe amplification of the excitation forces relative to the conditions where no acoustic resonance occurs.
- Substitution of test fluids must be carefully considered in view of heating effects for cryogens, and possible acoustic resonance with gases.

- CONCLUSIONS

  - Bellows flow excitation is caused by structure-vortex coupling potential
  - Excitation conditions are predictable by Strouhal number
  - Stress levels are predictable by use of a mathematical model
  - Simplified form of model or "Stress Indicator" has been correlated with failure cases to allow fatigue prediction
  - Heat input with cryogenic flows can suppress bellows flow excitation
  - Acoustic resonance with gas flows can produce serious force amplification
  - Test fluid substitutions must be considered with care.

"ENGINE ONBOARD CHECKOUT SYSTEM STUDY"

R. W. VANDEKOPPEL

MARTIN MARIETTA CORPORATION

TECHNICAL MANAGER

W. VOSS

MARSHALL SPACE FLIGHT CENTER

SPACE SHUTTLE PROPULSION SYSTEMS ON-BOARD CHECKOUT AND MONITORING SYSTEM DEVELOPMENT STUDY

Contract NAS 8-25619

Richard W. VandeKoppel
Martin Marietta Corporation
Denver Division

The Space Shuttle program objective of providing an economical space transportation system requires maximum reuse of components as well as minimal time, labor and equipment for servicing and checkout between flights. A requirement for high mission success probability also is inherent in this objective. Recent technology has demonstrated the feasibility of meeting these requirements by incorporating on-board checkout and performance monitoring capability. The propulsion systems (particularly the main engines) are pacing items in the Space Shuttle program; therefore, the checkout and performance monitoring techniques, data management requirements, and sensor requirements must be defined for incorporation in the basic propulsion system designs. This study has been conducted to define an approach and establish procedures, methods and design requirements for implementation of the Space Shuttle propulsion systems on-board checkout and monitoring function.

BACKGROUND

MARTIN MARIETTA
DENVER DIVISION

- SPACE SHUTTLE PROGRAM OBJECTIVES

  Minimal Turnaround Time (10 Working Days)

  Minimum Cost For Maintenance

  Minimum Cost For Preflight Activities (Ground Equipment, Labor)

  Maximum Reuse Of Components

  Maximum Mission Success & Flight Safety

- DEFINE PROPULSION SYSTEMS ONBOARD CHECKOUT, INFLIGHT MONITORING, EMERGENCY DETECTION, POSTFLIGHT EVALUATION FUNCTIONS, AND ESTABLISH APPROACH FOR IMPLEMENTATION.

The intent of the program was to develop analytical techniques and apply them in defining an approach for accomplishing the checkout and performance monitoring functions of the Space Shuttle propulsion systems. Program guidelines used to ensure applicability of the results to the Space Shuttle program included the following:

Pertinent Space Shuttle Phase B program definitions and requirements were to be incorporated.

The study was directed specifically at the operational Space Shuttle program, rather than the development test phase.

Inflight maintenance of the Space Shuttle vehicle was excluded; all maintenance was to be performed in ground operations, with a total time allowed for turnaround between flights of 14 calendar days (10 working days).

A telemetry data link (for checkout and monitoring) between the Space Shuttle vehicle and ground stations or a space station was excluded.

The study was to be conducted on a selected vehicle configuration (including the booster and orbiter propulsion system configurations) and a defined mission.

In-flight fault isolation to the line replaceable unit (LRU) level was a requirement, where an LRU is a propulsion element that can be removed, replaced and verified during maintenance without deleteriously impacting the Space Shuttle turnaround time.

SCOPE & GUIDELINES

MARTIN MARIETTA
DENVER DIVISION

- SCOPE

  Develop Methods and Analytical Techniques, and Apply Them In Defining an Approach For The Checkout and Monitoring Functions.

- GUIDELINES

  Operational Space Shuttle Program

  Booster and Orbiter Main, Auxiliary and Air Breathing Propulsion Systems

  No Telemetry Data Link

  No In-Flight Maintenance

  10 Working Day Turnaround

Chart 3

Chart 4

The study developed and applied methods and criteria for the propulsion system checkout and monitoring functions. The study has shown that the checkout and monitoring requirements of the operational Space Shuttle propulsion systems can be implemented as on-board functions. To ensure an optimum implementation of the function, a substantial degree of coordination must be conducted between the propulsion and avionics disciplines. The development of the propulsion systems' checkout and monitoring criteria (measurement requirements, sampling rates, sequences of functional operations, etc.) and the design of the data management system to accomodate the propulsion functions requires an integrated systems approach.

The basic design of the propulsion system must incorporate the checkout and monitoring functional requirements. Component configuration designs must enable readiness assessment, fault detection and performance monitoring, and must incorporate the requisite sensor elements. Subsystem designs must allow redundancy assessment and fault isolation, and must enable usage of the onboard system for post-maintenance verification testing.

The design and implementation of the onboard checkout and monitoring function must be in accordance with a requirements standard, i.e., a general specification, to ensure that the necessary approach and methodology are utilized and so that the requisite degree of propulsion and electronics systems integration is accomplished.

GENERAL CONCLUSIONS

MARTIN MARIETTA
DENVER DIVISION

Propulsion Systems Onboard Checkout and Monitoring Function is Feasible for Incorporation

Requires Substantial Degree of Integration Between Propulsion and Electronics

Provisions Must Be Implemented in Basic Design of Propulsion and Electronics Systems

Systems Definitions Must Be In Accordance With Specifications

Chart 4

Chart 5

The approach used in developing the requirements for the propulsion checkout and monitoring is illustrated. A baseline vehicle configuration, propulsion systems and mission was used in the study. However, the applicability of the results are not limited to this baseline, since the intent of the study was to establish the feasibility of on board checkout and monitoring and to develop an approach, rather than to define solutions for specific checkout problems. The baseline booster and orbiter both had integrated main, auxiliary and airbreathing propulsion systems. These propulsion systems were defined to the components level. The baseline space station resupply mission was defined by activity timelines for each phase of the ferry, ground, and flight operations. The propulsion systems were then related to the mission requirements by defining the propulsion performance and functional requirements for each mission phase; this included definition of operational interfaces with ground systems.

A key element of the propulsion evaluations was a failure modes and effects analysis conducted to the components level. This analysis provided visibility to hazard warning functions and candidate measurements and sensors, as well as identifying single point failures and excessive redundancy.

Line replaceable units (propulsion elements which could be fault-isolated in flight and replaced in maintenance operations) were identified.

The sequences and logic involved in such propulsion control functions as start, modulation, and shutdown were defined.

Leakage sources and consequences were determined, and techniques were defined for detecting leaks and monitoring for hazardous concentration levels of hydrogen gas.

The propulsion evaluation culminated in a comprehensive analysis of the checkout and monitoring requirements. By sequential mission phase, each checkout and monitoring step was identified, including expected values for each measurement.

APPROACH

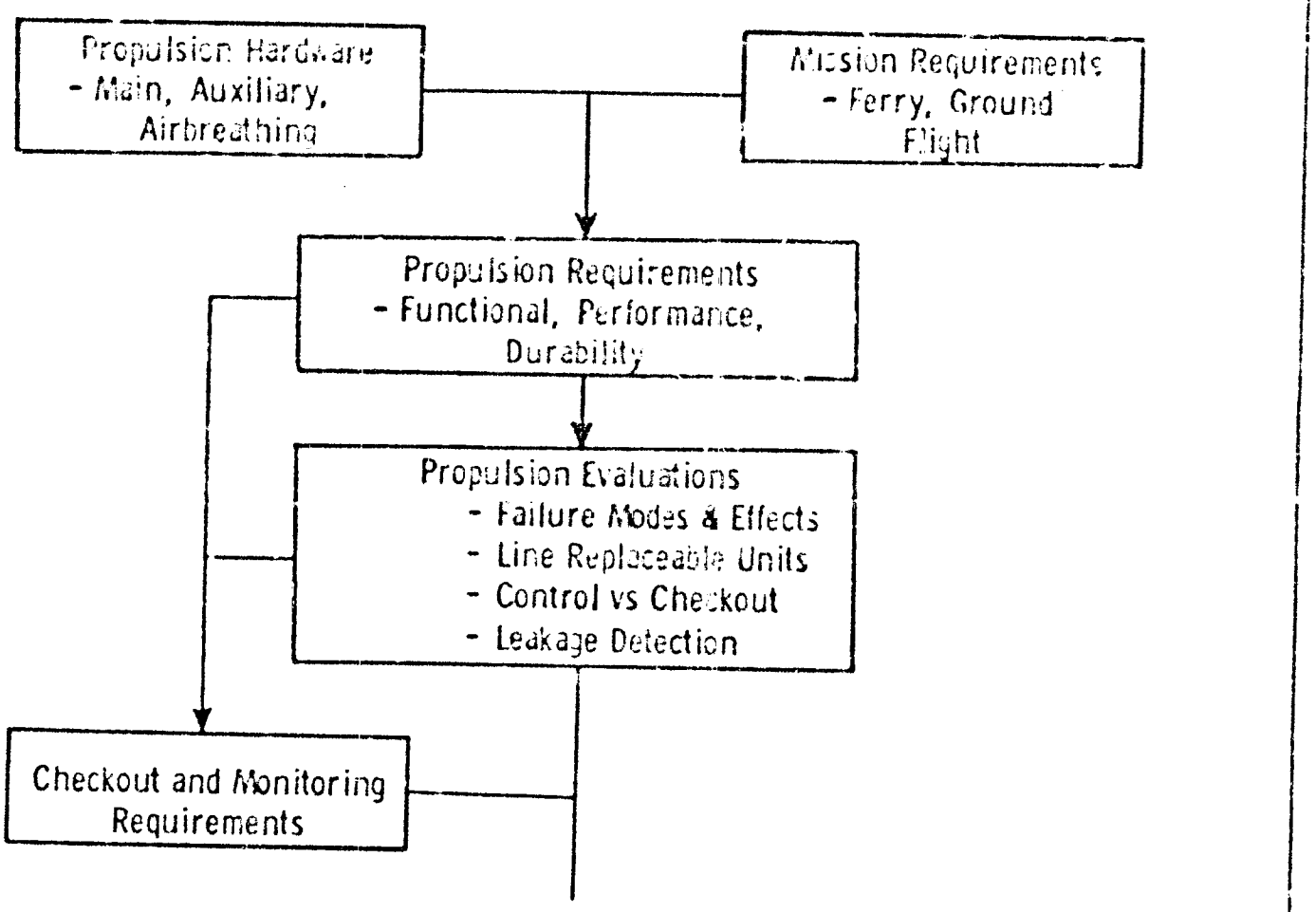

Chart 5

Chart 6

The analysis of the propulsion checkout and monitoring requirements to define the onboard concept and design criteria is shown. A sensor vendor survey was conducted and an evaluation of new sensor technology was made. These data were utilized in refining the candidate propulsion parameters into a definition of required measurements and corresponding sensors. Required sampling rates were also established.

The vehicle data bus traffic and the processing loads on the central computer complex were defined, and the compatibility of the vehicle baseline data management system configuration with respect to the propulsion checkout and monitoring requirements was established.

The study was completed by defining the propulsion systems onboard checkout and monitoring concept. The definition was in terms of criteria for functional capability and usage for preflight checkout and monitoring, inflight monitoring, post flight evaluation, maintenance retest, and integration of control and checkout.

APPROACH (Concl.)

MARTIN MARIETTA
DENVER DIVISION

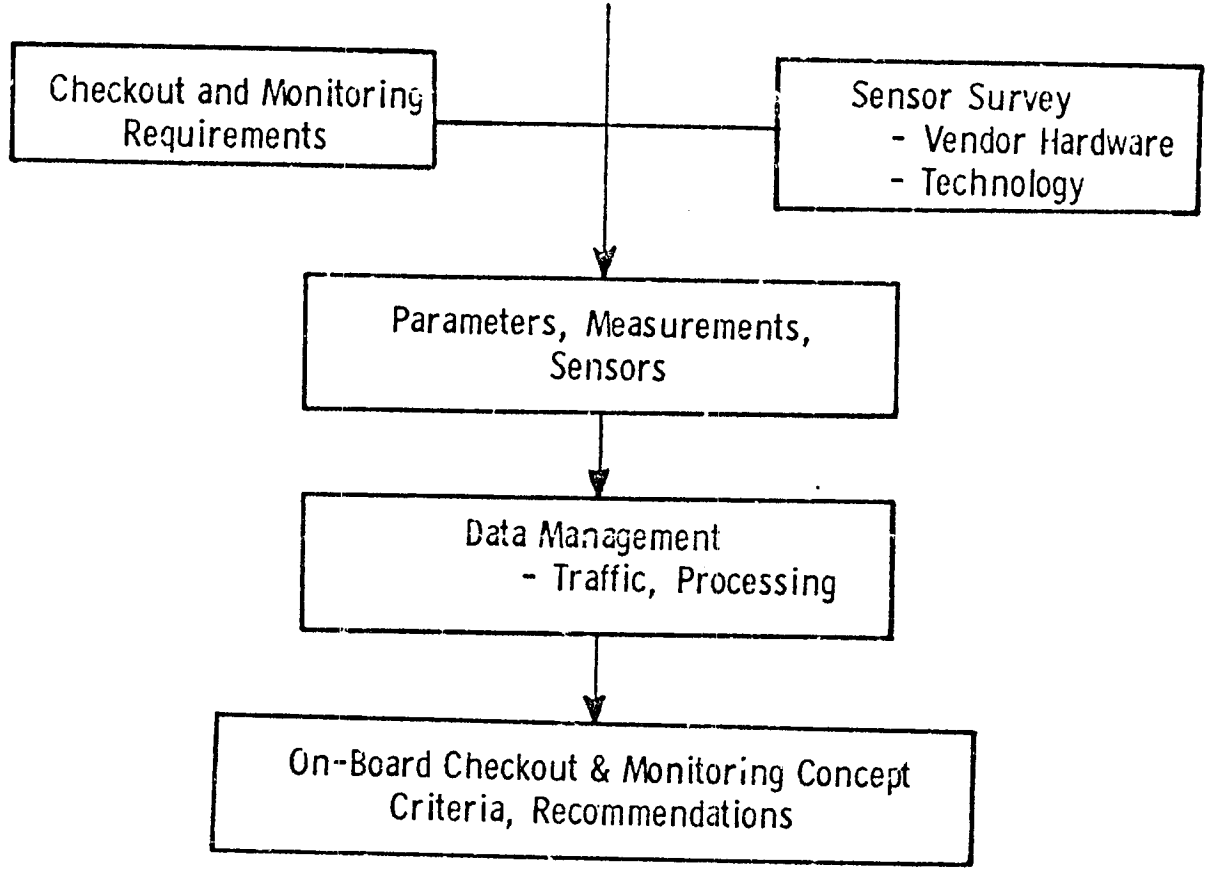

Chart 6

Chart 7

A baseline configuration was used in the study. Both the booster and the orbiter had main, auxiliary, and airbreathing propulsion systems. These systems were defined in functional schematics, and all components were identified. The main and auxiliary engines were defined and analyzed by the Aerojet Liquid Rocket Company as a major subcontractor in the study. Both General Electric and Pratt & Whitney assisted in the definition of the turbofan engines. The other propulsion components were identified by selecting from the Saturn V propulsion systems. The chart illustrates the quantities of components involved in the study.

The chart also shows the number of line replaceable units (LRU's) which were identified. The LRU's are those elements that could be fault-isolated in flight, and could be removed, replaced and verified during a normal maintenance period. (Top level LRU's are those which contain other LRU's, i.e., the main engines). Where possible the propulsion sensors will be LRU's, but are not included in these quantities.

PROPULSION ELEMENTS

BOOSTER

	Main	APS	A/B	Total
Subsystems	3	6	3	12
Components	664	404	235	1303
LRUs (Top Level)	110	138	32	280
LRUs (Total)	582	192	155	929

ORBITER

	Main	APS	A/B	Total
Subsystems	5	4	2	11
Components	177	324	124	625
LRUs (Top Level)	40	102	24	166
LRUs (Total)	125	118	79	322

Chart 7

Chart 8

A failure modes and effects analysis (FMEA) was conducted as a key part of the study. The failure modes for each component were established, effects on the propulsion system, vehicle, crew and mission identified, and candidate methods for detecting the failures were determined. The FMEA results were used to define candidate parameters, measurements and sensors; to define hazard warning functions; and to identify areas of excessive or inadequate redundancy. The chart illustrates candidate detection methods derived from the FMEA's.

The FMEA's showed that leakage was a major failure mode. Therefore, special emphasis was placed on identifying potential leakage sources and effects. This resulted in the definition of a recommended approach to leakage detection and monitoring that primarily utilized ultrasonic detectors for leakage detection, and a mass spectrometer/sampling probe system to monitor for hazardous concentration levels of hydrogen gas.

FMEA PARAMETERS

MARTIN MARIETTA
DENVER DIVISION

	BOOSTER	ORBITER
Pressure	219	126
Pressure Differential	7	3
Temperature	164	66
Vibration	21	15
Speed	30	15
Position	626	292
Current	61	49
Voltage	77	58
Flow Rate	9	3
Ignition Detectors	7	3
Liquid Level	32	21

Chart 8

A comprehensive analysis was made of the checkout and monitoring requirements to identify each checkout and monitoring step for sequential mission phases. This analysis, together with the FMEA's, were evaluated to identify the candidate parameters for propulsion systems' checkout and monitoring, as well as to identify techniques for implementing the checkout and monitoring functions. To assist in defining measurements and sensors, this program included a survey of sensor vendors. Information was acquired on the availability, characteristics and applications of sensors to match the potential requirements. Additionally, a sensor technology study was made by literature reviews and contacts with appropriate government agencies and industry to identify new work with potential applications.

The candidate propulsion system parameters were refined into a definition of required measurements and corresponding sensors. Criteria were prepared for many of the sensors to illustrate the approach necessary for adequate sensor definition.

The chart shows the resultant measurements for the booster and the orbiter.

MEASUREMENT SUMMARY

MARTIN MARIETTA
DENVER DIVISION

	BOOSTER					ORBITER				
	Main Eng	A/B Eng	Leak Det'n	All Other	Total	Main Eng	A/B Eng	Leak Det'n	All Other	Total
Pressure	434	63		182	679	62	27		121	210
Temperature	168	63	32	110	373	24	27	6	53	110
Discr. Posit'n	266	21	64	374	725	52	9	12	263	336
Analog. Posit'n	140				140	22				22
Quan. Gaging	14	7		33	54	2	3		24	29
Flow Rate	56	7		2	65	8	3			11
Ignition Det'n	42	14			56	6	6			12
Vibration	56	28	252	15	351	8	12	126	18	164
Current	42	14		47	103	6	6		43	55
Speed	56	21		18	95	8	9		15	32
Voltage		49		408	457		21		292	319
Gas Anal.			32		32			48		48
Totals	1274	287	380	1189	3130	198	123	192	835	1348

(Redundancy Not Included)

Chart 10

A baseline vehicle data management system was used in the study. As illustrated, the major elements include a central computer complex for centralized data management and vehicle control, dedicated peripheral computers, a data bus, displays and controls, and recorders. All data flow is between digital interface units and the central computer complex. (The quadrupal redundancy of the data management system is not shown on the chart). The technique for communications between the central computer complex and the digital interface units was selected to provide significant system flexibility by allowing any device on the data bus to be contacted by the central computer at any time. This flexibility was achieved at the expense of relatively high traffic load on the data bus and a high processing load in the central computer. Analyses were made to establish propulsion traffic loads on the vehicle data bus and processing loads in the central computer during peak periods. Each main engine controller required an engine-to-vehicle data bus traffic load (excluding commands and system overhead) of 10,584 bits/second during start and 5,848 bits/second during steady state. During the period of booster main engine start, the total propulsion traffic on the vehicle data bus peaked at 430,000 bits/second, and about 75% of the central computer processing capacity of 500,000 instructions/second utilized. The propulsion traffic on the data bus has decreased to about 380,000 bits/second by the time that the start sequence is completed, and the processing load has decreased to about 60% of capacity.

DATA MANAGEMENT SYSTEM

MARTIN MARIETTA
DENVER DIVISION

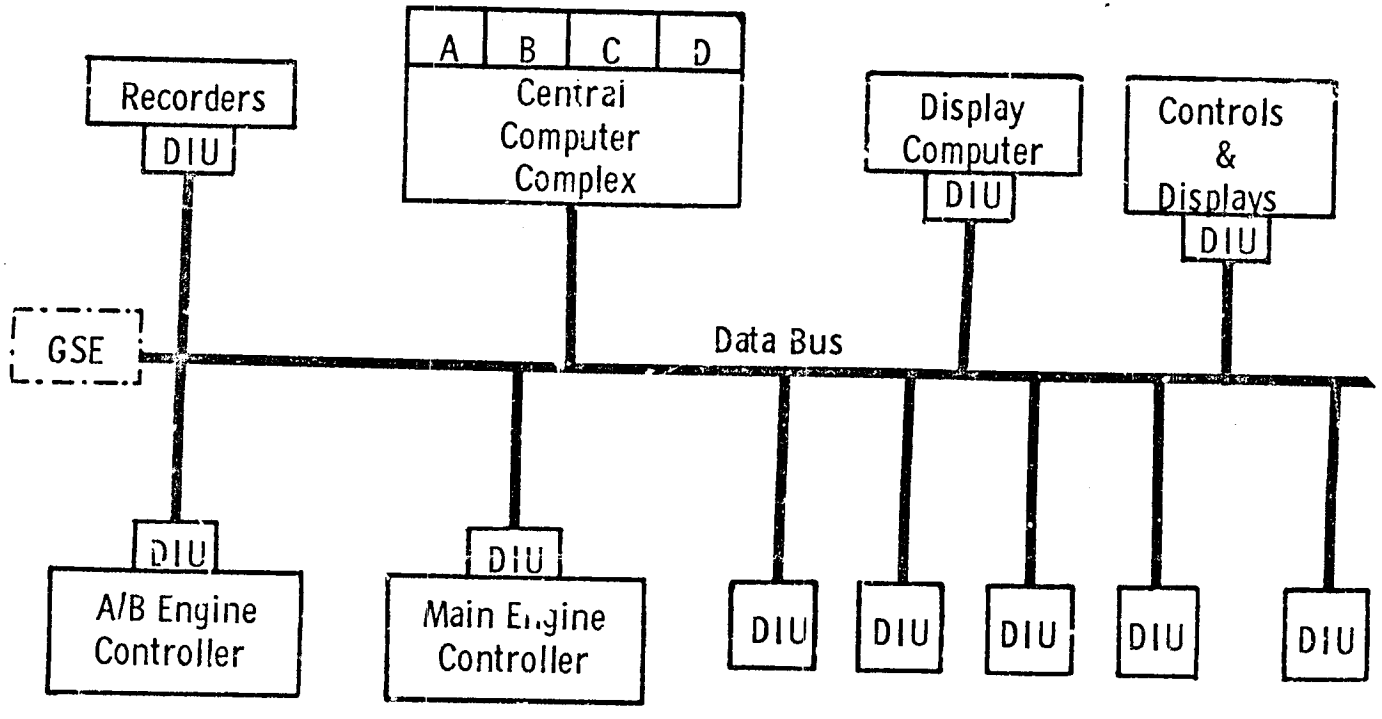

Chart 10

Criteria for functional capability and usage were developed to establish the degree of on-board checkout, monitoring, and evaluation functions. The chart indicates the functions to be accomplished by the on-board equipment.

The propulsion elements will be monitored and evaluated by the on-board equipment during ground operations. Preflight checkout of mechanical elements will be limited to verification of correct initial conditions for start. Complete preflight self-checks of the electronics, including sensor elements, will be performed.

The in-flight functions are indicated on the chart. Correct initial conditions will be verified prior to in-flight start of propulsion subsystems. In-flight emergency detection provisions will be redundant, as will the caution and warning display capability for loss of major functions, flight safety parameters exceeding safe limits, loss of redundancy, and hazardous leakage. Inflight detection of failures will be accomplished, and data acquired to enable fault isolation to the line replaceable unit level. Real time trend analysis will be performed for those identified failure modes where a progression to a more critical failure could be averted.

Operating history data will be maintained for those propulsion elements that have a correlation of maintenance requirements with parameters such as cumulative cycles, discrete stress levels, etc. Also, flight performance data will be recorded to enable postflight evaluations. The inflight type monitoring and evaluation will continue until postflight shutdown. The flight programs will then be replaced in the on-board computers by servicing programs. This will allow the on-board computer complex to evaluate the flight data for maintenance requirements, trends, and performance data.

Finally, maintenance retest for verification of the replaced line replaceable units will utilize the on-board checkout equipment.

ON-BOARD CHECKOUT AND MONITORING CRITERIA

GE AER DIVISION

PREFLIGHT CHECKOUT AND MONITORING

- Fault Detection and Isolation, and Operating History Recording During Ground Operations.
- Mechanical Elements Ready-To-Start Verification.
- Electronic Elements and Subsystems Preflight Self-Checks.

INFLIGHT

- Ready-To-Start
- Emergency Detection
- Fault Detection and Isolation
- Real Time Trend Analysis
- Operating Histories
- Performance Data

POST FLIGHT

MAINTENANCE RETEST

Chart 12

The majority of the measurement requirements identified for the propulsion on-board checkout and monitoring function can be accommodated through use of conventional sensor concepts. However, it is recommended that additional technology work be conducted in the following categories.

Acoustic/Ultrasonic Techniques appear to hold the most promise for resolving many fault detection/isolation/prediction requirements not amenable to conventional sensing techniques. Work by Boeing has shown acoustic emission to be a good indicator of bearing incipient failures. Deflection measurement is a possible alternative or supplementary technique. Further work should be done to establish the feasibility of applying both acoustic emission and deflection measurement approaches in application to Space Shuttle propulsion system rotating machinery, and to establish feasibility of applying acoustic emission sensor approaches to ignition detection and igniter spark location discrimination.

Ultrasonic Leak Detection for both internal and external leaks has been shown to be feasible, using combinations of ultrasonic contact probes and ultrasonic microphones. There is insufficient data, however, to show that existing devices will work satisfactorily and maintain integrity with cryogenic temperature cycling and at Space Shuttle vibration and acoustic environment levels.

Accurate Measurement of Small Differential Pressures in high pressure systems cannot be accomplished with today's technology except in the laboratory. A study to identify and assess approaches for measurement of small differential pressures in high system pressure is recommended. A primary application would be for derivation of flow rate, as an alternate to use of a flow meter.

SENSOR TECHNOLOGY

MARTIN MARIETTA
DENVER DIVISION

BEARING INCIPIENT FAILURE DETECTION -

Establish Feasibility Of Acoustic Emission And Deflection Measurement Approaches.

ONBOARD LEAK DETECTION -

Evaluate Ultrasonic Detectors In Cryogenic And Vibration Environment.

FLOW MEASUREMENT -

Identify And Assess Approaches To Provide Accurate Measure Of Small Pressure Differential With High System Pressure.

Chart 12

A substantial degree of coordination between the propulsion and avionics disciplines is necessary to ensure an optimum implementation of the propulsion systems onboard checkout and performance monitoring function. Both the development of the propulsion systems' checkout and monitoring criteria (measurement requirements and sampling rates, sequences of functional operations, etc.) and the design of the data management system to accommodate the propulsion functions require an integrated systems approach.

The basic design of the propulsion system must incorporate the checkout and monitoring functional requirements. Component configuration designs must enable readiness assessment, fault detection and performance monitoring, and incorporate the requisite sensing elements. Subsystem designs must allow redundancy assessment and fault isolation, and must enable usage of the on-board system for post-maintenance (LRU replacement) verification testing.

Emphasis must be placed on minimizing the number of measurements and the complexity of the sensors. The measurements required for propulsion control functions should also be used for checkout and monitoring functions; alternative measurement and sensor techniques (including application of new technology) must be investigated for each candidate parameter; and the sensor criteria (accuracy, sample rate, response, etc.) should be determined by analyzing the requirements of each individual measurement with emphasis on imposing the least stringent criteria.

The propulsion control functions must be completely integrated with the on-board checkout function. Since the checkout function must be cognizant of responses to control commands, and the control function must provide data management for cataloging and utilizing redundant hardware, a minimization of total data management complexity can result from combining these two functions.

Incorporation of the on-board checkout and monitoring function for the Space Shuttle propulsion systems is feasible. The function should be implemented as a step towards meeting the operational Space Shuttle program objectives of low operating cost, rapid turnaround, and high probability of mission success.

RECOMMENDATIONS

MARTIN MARIETTA
DENVER DIVISION

Integrated Approach Between Propulsion and Electronics Must Be Followed.

Provisions Must Be Incorporated In Basic Design.

Emphasis Must Be Placed On Minimizing Quantity and Complexity of Sensors.

Propulsion Control Functions Must Be Integrated With The Checkout and Monitoring Functions.

Propulsion Systems On-Board Checkout and Monitoring Function Is Feasible and Should Be Implemented.

"LOW FREQUENCY ANALYSIS OF ROCKET ENGINES USING COMPRESSIBLE PROPELLANTS"

J. M. McBRIDE

AEROJET

TECHNICAL MANAGER

R. RICHMOND

MARSHALL SPACE FLIGHT CENTER

LOW FREQUENCY ANALYSIS OF ROCKET ENGINES USING COMPRESSIBLE PROPELLANTS

by

J. M. McBride

AEROJET LIQUID ROCKET COMPANY

ABSTRACT

A low frequency stability model has been developed to represent the case where one or more of the propellants used in a rocket engine is a compressible fluid. Results for two oxygen - hydrogen rocket combustors are discussed. Also included is a discussion of the predicted effects of mixture ratio and propellant temperature.

INTRODUCTION

The motivation for developing a model which treats the particular case of compressible reactants was an inability to predict the trends noted in stability of a gaseous hydrogen - oxygen rocket engine using the conventional low frequency models such as the type discussed in Reference 1, which were specifically developed for liquid propellant systems. Experimental data such as shown in Figures 1 and 2 indicated that increasing the fuel injector pressure drop reduced the stability of gaseous propellant rockets. The trend toward reduced stability margin with increased injector stiffness is just the opposite to predicted trends of current models.

Previous treatments of the problem of low frequency instability generally postulate a model based on the conservation of mass and assumed that all significant energy release is coincident with conversion of liquid reactants to gaseous products. It was also assumed that the dense liquid propellants occupied a negligible volume on entering the chamber, making it possible to ignore their effect on chamber pressure the instant they enter the chamber. It was not until the reactants were gasified and reacted that their presence was felt, and these two events were assumed to occur simultaneously.

The analysis presented here takes a somewhat different approach in that the conservation of energy law is invoked as a means of determining the stability of a system. By so doing, it is possible to separate the effect gaseous reactants have on chamber pressure the instant they enter the chamber and their effect when they are converted to products.

TECHNICAL DISCUSSION

GENERAL -- Consideration of the low frequency feed system coupled stability characteristics of a rocket engine using gaseous propellants introduces some analytical complexity beyond that of an equivalent liquid system. However, of more importance are the questions concerning the stability of such a system as compared to a liquid propellant system. The questions are prompted by the fact that the gaseous system generally requires larger injector orifices, which improves acoustic coupling between the feed system and the combustion chamber. The injection velocities are higher with consideration being given to velocities approaching the speed of sound of the injected gases. It is also interesting to note that the tuned gas cavities, such as resonators and quarter-wave tubes, have been used to stabilize an engine. If such were the case with a gaseous feed system, this would imply that it would be desirable to maintain good coupling between the feed system and the combustion chamber-- an approach just the opposite to that taken for liquid systems.

The basic difficulty in developing a stability model for gas - gas or gas - liquid combustors is the problem of separating the effect of gases as they enter the combustion chamber, and their effect when they combust. The propellants could react at the instant they enter the chamber or after they have been in the chamber for sufficient time to mix, diffuse, or reach a critical temperature. In order to overcome this difficulty, it was necessary to use both the conservation mass and energy equations to develop a characteristic equation for determining the stability of a system. This approach allows for an accounting of the energy added by the gases as they enter the chamber separately from the release of chemical energy when they react. The gases, as they enter the chamber, are considered to be isentropic perfect gases, possessing both internal and flow energy. The enthalpy of the gases includes only the internal and pressure, or potential, energy of the fluids and not the chemical energy associated with each propellant in going from reactants to products.

The chemical energy released by the reactants is simulated by a heat source located in the chamber. The quantity of energy released per lb_m of reactants is the difference between the energy levels of the fluids entering and leaving the chamber. In this way, it is possible to avoid a detailed description of the intermediate processes.

In addition to the unsteady energy release associated with the perturbed flow, a second source of energy is included which is developed using a linearized Arrenhius rate function to describe this source of energy. The inclusion of this source turn was prompted primarily based on trends observed in experimental data from gas - gas rocket testing. A block diagram of the entire model is shown in Figure 3.

UNSTEADY FLOW EFFECTS -- Starting first with the fluid entering the chamber, there are three sources of unsteady energy flow into the chamber associated with each of the reactants. The first is that energy convected in with the perturbed flow which is given by

$$E'_{x_1} = W'_x \bar{e}_x \tag{1}$$

The energy per unit mass of the fluid, $\bar{e}_x$, is given by

$$\bar{e}_x = \bar{h} + \frac{\bar{V}_x^2}{2y} \tag{2}$$

The perturbed flow can be described by a feed system admittance, Y_x, and the chamber pressure, P'_c, where Y_x is defined as

$$Y_x = \frac{W'_x}{P'_c} \tag{3}$$

The feed system admittance, Y_x, is, in general, complex and a function of the physical properties of the propellant, the pressure drops in feed system, and the dynamic characteristics of the feed lines upstream of the injector.

In order to make the analysis as general as possible and yet not so complex, as to make interpretation of the results impractical, two types of feed systems are considered. The first feed system considered is one which is terminated upstream of the injector by an "open line" -- the open line being representative of a feed line which terminates in a propellant tank having a diameter several times larger than the feed line. The second type of termination considered is a closed line, which is indicative of a feed line with a sonic flow control nozzle or a high pressure drop point upstream of the injector.

The starting point in both cases is the acoustic wave equation and the momentum equation. For the case of no mean flow effects and no distributed line pressure drops, the wave equation is

$$\nabla^2 p = \frac{1}{C^2} \frac{\partial^2 p}{\partial t^2}$$

and the momentum equation is

$$\nabla P = \bar{\rho} \frac{du}{dt}$$

Transferring the above equations to the Laplace domain, it can be shown that the admittance for a constant area duct is given by

$$\frac{V'_{xy}}{P_{xy}} = -\frac{1}{g \bar{\rho}_{xy} \bar{C}_{xy}} \left[\frac{\bar{g} \bar{\rho}_{xy} \bar{C}_{xy} G_{xo} + i \operatorname{Tan} \frac{\omega}{\bar{C}_{xy}} L_{xy}}{1 - i\, g \bar{\rho}_{xy} \bar{C}_{xy} G_{xo} \operatorname{Tan} \frac{\omega}{\bar{C}_{xy}} L_{xy}} \right] \qquad (4)$$

where G_{xo} is the admittance at $L_x = 0$.

In order to make the feed line representative of an actual rocket engine feed system, the system is assumed to be as shown in Figure 4, with the restriction in the line representing an injector orifice. The assumption of an "open" ($G_{xo} \to \infty$) and a "closed" feed line ($G_{xo} = 0$) represents the two possible extremes encountered in a rocket engine. Only one of these cases, the "closed" feed line will be discussed.

CLOSED FEED LINE TERMINATION -- The closed feed line termination, in the acoustic sense, is one where the velocity perturbations are zero or very nearly so. Under this condition, from the definition of admittance

$$G_{ox} = \frac{u'}{p'}$$

it can be seen that $G_{ox} = 0$ and $Z_{ox} = \infty$. Flow conditions which approach a closed end or solid wall would be the position just downstream of a sonic plane, a high pressure drop orifice, or a normal shock. All of these conditions can exist in a gaseous propellant feed system.

From Equation (4), it can be seen that, for $G_{ox} = 0$.

$$\frac{V'_{xy}}{P'_{xy}} = - \frac{i}{g \bar{\rho}_{xy} \bar{a}_{xy}} \operatorname{Tan} \frac{\omega}{a_{xy}} L_{xy} \qquad (5)$$

In going from the feed line to the injector orifice inlet, there is usually a large pressure drop. Using the orifice flow equation (Ref 2).

$$P_{1x} - P_{2x} = \frac{W_{2x} V_{2x}}{2 A_{2x} g} (1 + K_c) - \frac{W_{1x} V_{1x}}{2 A_{1x} g} \qquad (6)$$

Expanding this equation in terms of its steady-state and perturbation quantities and incorporating Equation 5 gives

$$\frac{P'_{2x}}{W'_{2x}} = \frac{-1}{g\left[1 - \frac{1+K_c}{2} M^2_{2x}\right]} \left[\frac{K_c+1}{A_{2x}} \bar{V}_{2x} - \frac{\bar{V}_{1x}}{2 A_{1x}} - \frac{\bar{a}^2_{1x} \{g + \frac{\bar{W}_{1x}}{2 A_{1x}} (G_{1x})\}}{(g \bar{V}_{1x} + \bar{\rho}_{1x} \bar{a}^2_{1x} G_{1x}) A_{1x}} \right] \tag{7}$$

Writing the equation of motion for the orifice gives

$$(P_{2x} - P_{3x}) A_{2x} = \frac{d}{dt} \left(\frac{\rho \ell A u}{g}\right) = \frac{d}{dt} \left(\frac{W_{2x}}{g}\right) \tag{8}$$

which, when linearized and only the perturbed quantities considered, gives when is transferred to the Laplacian domain

$$\frac{P'_{3x}}{W'_{2x}} = - \frac{S \ell}{g A_{2x}} + \frac{P'_{2x}}{W'_{2x}} \tag{9}$$

If it is assumed in Equation (7) that over the distance, ℓ

$$\frac{\partial \rho'}{\partial t} \approx 0$$

then

$$W'_{2x} = W'_{3x} \tag{10}$$

which gives, from Equations (7) and (9), for S = $i\omega$

$$\frac{P'_{3x}}{W'_{3x}} = \frac{-1}{g\left[1 + \frac{1+K_c}{2} M_{2x}^2\right]} \left[\frac{K_c+1}{A_{2x}} \bar{V}_{2x} - \frac{\bar{V}_{1x}}{2 A_{1x}} \right.$$

$$\left. - \frac{\bar{a}_{1x}^2 \left\{g + \frac{\bar{W}_{1x}}{2 A_{1x}} (g_{1x})\right\}}{(g \bar{V}_{1x} + \bar{\rho}_{1x} \bar{a}_{1x}^2 G_{1x}) A_{1x}} \right] - \frac{i \omega \ell}{g A_{2x}} \tag{11}$$

Letting

$$\frac{P'_{3x}}{W'_{3x}} = \frac{1}{Y_x} \tag{12}$$

The flow energy convected in with the perturbed flow becomes, from Equation (1)

$$E'_{x1} = \bar{e}_x Y_x P'_{3x} \tag{13}$$

A second source of perturbed energy entering the chamber with the reactants is that convected in with the mean flow and is given by

$$E'_{x2} = \bar{W}_x e'_x \tag{14}$$

The perturbed energy per lb_m of propellant is given by perturbing the energy eqaution and assuming constant heat capacities

$$\bar{e}_x + e'_x = C_{vx} (\bar{T}_x + T'_x) + \frac{\bar{P}_x + P'_x}{\bar{\rho}_x + \rho'_x} + \frac{(\bar{V}_x + V'_x)^2}{2g} \tag{15}$$

and assuming the gas is isentropic and applying the small perturbation restrictions gives for the perturbed energy e'_x

$$e'_x = \frac{\gamma-1}{\gamma} \bar{h}_x \frac{P'_c}{\bar{P}_c} + \frac{\bar{V}_x V'_x}{g} \tag{16}$$

Noting V'_x is the perturbed velocity at the injector orifice exit, a relationship for V'_x can be derived

$$W' = (\bar{\rho}_x V'_x + \bar{V}_x \rho'_x) A_o \tag{17}$$

the perturbation velocity, V'_{xy}, is given by

$$V'_x = \frac{1}{\bar{\rho}_x A_x} [Y_x - \frac{\bar{V}_x A_x g}{a_x^2}] P'_{xy} \tag{18}$$

Substitution of Equation (18) into Equation (16) gives

$$e'_x = [\frac{\gamma_x-1}{\gamma_x} \bar{h}_x + \frac{\bar{V}_x \bar{P}_c}{\bar{\rho}_x g A_x} (Y_x - \frac{\bar{V}_x A_x g}{a_x^2})] \frac{P'_c}{\bar{P}_c} \tag{19}$$

and finally substitution of Equation (19) into (14) gives

$$E'_{x2} = \bar{W}_x [\frac{\gamma_x-1}{\gamma_x} \bar{h}_x + \frac{\bar{V}_x \bar{P}_c}{\bar{\rho}_x A_x g} (Y_x - \frac{\bar{V}_x A_x g}{a_x^2})] \frac{P'_c}{\bar{P}_c} \tag{20}$$

The third and most important, in terms of the amount of energy added by the incoming reactants, is that energy released when the reactants are converted to products. Previous analysis of this type (Ref 1) have assumed that the energy released by the reactants can occur at times other than when the

reactants enter the chamber. This time delay, which is generally referred to as the total time lag, is intended to physically represent the time required to complete the precombustion processes such as evaporization in the case of liquid reactants, gas phase mixing, heat-up periods, or any of the many precombustion processes associated with reactants which are not premixed. This synthesis is devised to avoid the complexities of mechanistic representation of processes, which are, in general, difficult to determine in a rocket engine. This assumption is retained in this analysis. This analysis deviates from the approaches of Reference 1 in that the perturbed reactants flowing into the chamber are assumed to combust independently of each other. This assumption was made for two reasons: the first being that it would seem physically more representative of what could occur rather than assuming the two perturbed flows concurrently arrived at the right time and under the right conditions to react with each other. The second reason was that the previous approach did not show sufficient gain in the system to sustain a low frequency instability in a number of rocket engine systems where low frequency instability had been observed.

Using the above assumptions, the following representation is developed for the energy released by each of the reactants:

$$E'_{x3} = G_x W'_x \bar{e}_c \tag{21}$$

where G is an amplification factor resulting from the fact that the perturbed reactant flow reacts in its steady-state counterpart and the net perturbed gas generation rate is the sum of the perturbed flow plus the amount of its counterpart with which it reacts, which is assumed to be available from the steady flow. The degree to which each perturbed reactant is assumed to interact with the steady state reactants is dependent on where the steady state mixture ratio is relative to the stoichiometric mixture (SR). If the steady combustion is fuel rich, all the perturbed oxidizer is assumed to react at the

stoichiometric mixture ratio, SR, and only a portion of the perturbed fuel for which oxidizer is available. It is assumed the amount available is $W'_{of} = W'_f R$ which gives

$$G_o = \frac{(SR + 1)}{SR}$$

and

$$G_f = \frac{R}{SR} (SR + 1)$$

If the steady state mixture ratio results in oxidizer rich combustion

$$G_o = \frac{(SR + 1)}{R}$$

and

$$G_f = SR + 1$$

The energy release associated with each of the reactants is that associated with the energy release at the Stoichiometric mixture ratio ΔH_c giving

$$E'_{x3} = G_x W'_x \Delta H_c \tag{22}$$

Referring to Equation (12), W'_x is given by

$$W'_x (t - \tau_x) = Y_x \frac{P'_c (t - \tau_x)}{\bar{P}_c} \tag{23}$$

where τ_x is the time delay between injection and combustion of particular element of propellant. Substitution of Equation (23) into Equation (22) gives

$$E'_x = G_x Y_x \Delta H_c \frac{P'_c (t - \tau_x)}{\bar{P}_c} \tag{24}$$

TEMPERATURE SENSITIVE COMBUSTION -- Result of analytical work indicate (Reference 3) there is a dependence of engine stability on mixture ratio. Attempts to show this type of trend using only the representation for the energy added by combustion just discussed were unsuccessful. For this reason, a second source of energy of combustion is included based on reaction kinetics. This particular mechanism was selected primarily because it is physically plausible with gaseous propellants, and the experimental and analytical work indicated that deviation from stoichiometric mixture ratio tends to degrade the stability of a gaseous rocket engine.

The approach used in developing an unsteady energy release rate is to start with an Arrenhium rate function based on an assumed first-order reaction given by

$$\frac{dc_1}{dt} = \prod_{j=1}^{N} C_j \, K \tag{25}$$

where K is given by

$$K = B \, e^{E_a/RT} \tag{26}$$

B, the frequency factor from the kinetic theory of gases, has been shown to be a function of the reactants involved and is also proportional to the temperature of the reactants; thus, for a given reaction

$$A = B \, T^{\alpha}$$

where α, in general, varies between 0 and 1 and is commonly assumed to be equal to 1/2 and B is a constant and a function of the reactants.

If it is assumed that the mass fraction, Y_i, of each constituent is constant within the chamber and noting that the concentration C_i is given by

$$C_1 = \frac{Y_1 \rho_c}{MW_1} \tag{27}$$

then substitution of Equation (26) and (27) into (25) gives

$$\frac{Y_1}{MW_1} \frac{d\rho_c}{dt} = \prod_{j=1}^{N} \frac{Y_j}{MW_j} \rho_c^{N_F} T^{1/2} e^{-E_a/RT_c}$$

or for a two species reaction

$$\frac{d\rho_c}{dt} = \frac{\bar{\rho}_c^{\,2}}{MW_c} B T^{1/2} e^{E_a/RT_c} \tag{28}$$

Defining Q_c' as the energy release rate and using small perturbation assumptions to expand Equation (28) gives

$$Q_c' = \bar{Q} \left[\frac{2\rho'}{\bar{\rho}} + \left(\frac{E_a}{R\bar{T}_c} + \frac{1}{2} \right) \frac{T'}{\bar{T}_c} \right] \tag{29}$$

where $\bar{Q}$ is given by

$$\bar{Q} = \bar{W}_T [\Delta H_c]$$

Using the isentropic relationships, Equation (29) becomes

$$Q_c' = \bar{W}_T \left[\frac{3+\gamma}{2\gamma} + \frac{\gamma-1}{\gamma} \frac{E_a}{R\bar{T}_c} \right] [\Delta H_c] \frac{P_c'}{\bar{P}_c} \tag{30}$$

What has been developed thus far are analytical expressions for the flow and internal energies of the reactants entering the chamber and the unsteady energy

released when the reactants are converted to products, all of which are expressed as a function of the perturbed chamber pressure. What remains to be determined is the unsteady energy being stored in the chamber and the unsteady energy leaving the chamber via the sonic exhaust nozzle.

Considering first the energy leaving the chamber, E'_N

$$E'_N = W'_T \bar{e}_N + \bar{W}_T e'_N \tag{31}$$

From Equation (16)

$$e'_N = \frac{\gamma-1}{\gamma} \bar{h}^* \frac{P^{*'}}{\bar{P}^*} + \frac{\bar{V}^* V^{*'}}{g} \tag{32}$$

where the $(^*)$ is used to designate conditions at the sonic plane of the chamber.

From the isentropic flow relationships and for small Mach numbers in the combustion chamber it can be shown that

$$W'_T = \bar{W}_t \left(\frac{\gamma+1}{2\gamma}\right) \frac{P'_c}{\bar{P}_c} \tag{33}$$

Noting that

$$W'_T = (\bar{\rho}^* V^{*'} + \bar{V}^* \rho^{*'}) A_t \tag{34}$$

The following relationship can be developed for E'_N

$$E'_N = \bar{W}_T \frac{3\gamma_c - 1}{2\gamma_c} \left[\bar{h}^* + \frac{\bar{V}^*}{2g}\right] \frac{P'_c}{\bar{P}_c} \tag{35}$$

Considering next the rate of energy stored in the chamber

$$\frac{d E_c}{dt} = \frac{d}{dt}\left[\bar{M}_c\, e'_c + M'_c\, \bar{e}_c\right] \tag{36}$$

$$\frac{d E_c}{dt} = \frac{d}{dt}\left(\bar{\rho}\, V_c\, \frac{\gamma-1}{\gamma}\, h_c + \frac{\bar{\rho}}{\gamma}\, V_c\, h_c\right) \frac{P'_c}{\bar{P}_c} \tag{37}$$

From the conservation of energy

$$E'_{o1} + E'_{o2} + E'_{o3} + E'_{f1} + E'_{f2} + E'_{f3} - E'_N + Q_c = \frac{d E_c}{dt} \tag{38}$$

Expressing Equation (38) in the Laplace domain gives

$$E'_{o1}(S) + E'_{o2}(S) + E'_{o3}(S) + E'_{f1}(S) + E'_{f3}(S) + Q_c - E'_N(S) = S\, E_c(S) \tag{39}$$

where $E_c(S)$ is the initial perturbation energy in the chamber.

From the above equations, the characteristic polynomial, K G H (S), can be determined, and the Nyquist criterion used to determine system stability. In conventional control loop notation, the various components of the system are shown in Figure 3. It should be noted that the system, as treated in this analysis is a positive feedback system with a characteristic polynomial ratio in the form

$$\frac{C}{R}(S) = \frac{K\, G\, (S)}{1 - K\, G\, H\, (S)} \tag{40}$$

Thus, the Nyquist instability criterion is that the gain must be greater than one and the phase equal to zero degrees.

RESULTS

COMPARISON WITH EXPERIMENTAL RESULTS -- Table I is a list of the experimental and predicted results for two rocket engine combustors using oxygen - hydrogen propellants. One of the combustors which was the power source of a turbopump operates at a mixture ratio in the range of 0.80 at chamber pressures in excess of 2000 psia.

The agreement is quite good in terms of the resulting stability characteristics and the predicted frequency of instability. At each of the frequencies listed the Nyquist criteria of zero phase was satisfied. The frequency at which the gain is greater than 1.0 would be the observed frequency of instability.

The second group of test results were obtained from a oxygen - hydrogen engine which operated at nominal chamber pressure of 500 psia over the mixture ratio range of 3.7 to 9.8. The agreement between experimental and analytical results are also quite good in this case.

The actual system pressure drops and propellant temperatures were used as input to the model in making the predictions listed.

In all cases evaluated the time lag between the oxidizer injection and combustion was assumed to be 0.001 seconds. For the fuel the time lag was assumed to be zero.

It was also necessary to assume an effective activation energy. A review of the literature indicated a value in the order of 25000°R was reasonable. This value was used for all cases analyzed.

PARAMETRIC STUDY -- In evaluating the results from the analysis two versions of the model were evaluated. This first included all energy terms with the exception of the energy addition due to a non-unsteady rate of reaction given by Equation (30). The second version included all terms. Several parametric studies were made in each case.

For the version without the rate equation included, effects of mixture ratio and propellant inlet temperature were evaluated. Typical of the results obtained for a rocket engine having the design characteristics, and using the propellants indicated in Table II are shown in Figures 5 and 6. From these results, three significant trends were noted. The first, which is indicated by the results shown in Figure 4, is that low frequency stability improves with a decrease in mixture ratio. Improved stability is also obtained by increasing propellant temperature while maintaining a constant injector pressure drop, the improvement being most noticeable at low mixture ratios where the propellant enthalpy is significant relative to that added by combustion.

The parametric studies of the same rocket engine with the rate function included were identical to the previous results with the exception that the trend with mixture ratio was reversed in that stability decreased with decreasing mixture ratio (Figure 8) and the effect of propellant inlet is not as pronounced as can be seen from Figure 8. As with the case with no combustion, the effect of propellant temperature is more pronounced at low mixture ratios. During all the above parametric studies injector pressure drops were held constant which would be representative of a design study of a fixed pressure drop system.

A parametric study was also made for the case where the injector design was fixed and the propellant inlet temperature was allowed to vary. For this case the increase in propellant temperature resulted in increased system pressure drop. Two conditions were considered, one where the fuel and oxidizer time lags were equal, and the other where the fuel time lag was zero. The results are shown in Figures 9a and b respectively along with the constant Δp cases. Figure 9b is representative of the experimental results discussed previously in that system stability was decreased with increasing fuel injector pressure drop.

1. [illegible] propellant temperature and, in particular, hydrogen temperature are most significant at low mixture ratios.

2. [illegible] mixture ratio is destabilizing in gaseous rockets.

3. The trends predicted by the model, which include the temperature sensitive combustion, gave the best results in that the model predicted the trends indicated by the experimental data.

4. The results of the model are in general agreement with experimental results.

5. Low frequency stability trends with propellant temperature will be dependent on injector design characteristics which effects propellant time lags (see Figures 7a and b).

REFERENCES

1. Summerfield, M., "A Theory of Unstable Combustion in Liquid Propellant Rocket Systems," Journal of the ARS, September 1951, pp 108-114.

2. Rohsenow, W. M., Choi, H., Heat, Mass, and Momentum Transfer, Prentice-Hall Inc., Englewood Cliffs, New Jersey, 1961, pp 67-70.

3. Culick, F. E., Stability of High Frequency Pressure Oscillations in Gas and Liquid Rocket Combustion Chambers, MIT Report 480, dated June 1961.

NOMENCLATURE

a	Speed of sound, in./sec
A	Orifice area, $in.^2$
B	Kinetic theory frequency factor
C_p	Constant pressure specific heat capacity, $in.-lb_f/lb_m-°R$
C_v	Constant volume specific heat capacity, $in.-lb_f/lb_m-°R$
C	Concentration
e	Specific energy, $in.-lb_f/lb_m$
E	Energy flow rate, $in.-lb_f/sec$
g	Gravitational constant, lb_m-ft/lb_f-sec^2
G	See Equation 16
h	Enthalpy, $in.-lb_f/lb_m$
i	Imaginary
k	Orifice flow constant
K	Rate constant
ℓ	Orifice length, in.
L	Feed line length, in.
N	Integer
P	Pressure, $lb_f/in.^2$
Q	Rate of heat added due to reaction, $in.-lb_f/sec$
R	Mixture ratio
S	Laplacian operator
T	Temperature, °R
t	Time, sec
V	Velocity, in./sec

NOMENCLATURE (cont.)

$\dot{W}$	Mass flow rate, lb_m/sec
Y	Feed system admittance, $lb_m\text{-}in.^2/lb_f\text{-}sec$
y	Mass fraction
ΔP	Pressure drop, $lb_f/in.^2$
ρ	Density, $lb_m/in.^3$
γ	Specific heat
τ	Time lag, sec
α	Rate equation constant
ω	Angular frequency, rad/sec

Superscripts

-	Steady state quantity
'	Unsteady quantity
*	Sonic plane value

Subscripts

a	Activation energy
c	Chamber
v	Constant volume specific heat
p	Constant pressure specific heat
o	Oxidizer
f	Fuel
T	Total flow rate
N	Nozzle

TABLE I

PREDICTED VERSUS EXPERIMENT RESULTS

Turbopump Combustor

Stable Tests Predicted	
Freq	Gain
935	1.0
935	1.0
750	0.78
780	0.86
760	0.78
770	0.76
730	0.79
740	0.87
720	0.63

Unstable Tests		
Predicted		Observed
Freq	Gain	Freq
1470	1.95	1500
840	1.27	875
810	1.34	770
850	1.40	1250
950	1.02	950
950	1.02	950
940	1.03	750
850	1.24	800

500 psia Engine

Stable Tests Predicted	
Freq	Gain
850	0.57
800	0.49
740	0.80
780	0.78
770	0.77
760	0.81
750	0.88
760	0.73
750	0.80
730	0.86
750	0.84
760	0.82
760	0.87
750	0.91
780	0.76
760	0.95
770	0.81
790	0.74

Unstable Tests		
Predicted		Observed
Freq	Gain	Freq
750	1.0	800
750	0.98	800
760	0.98	800
640	1.13	740
720	0.93	800

TABLE II

CHARACTERISTICS OF PARAMETRIC STUDY ENGINE

Effect of Mixture Ratio	
Injector Oxid, ΔP_o	45
Injector Fuel, ΔP_f	70
Chamber Pressure	500
Throat Area	5.6
Oxid Orifice Area	Variable*
Fuel Orifice Area	Variable
Fuel Temp	500°R
Oxid Temp	500°R
Propellants (Fuel/Oxid)	Hydrogen/Oxygen
Effect of Propellant Temp	
Same as Above Except	
Mixture Ratio	5.0 and 1.0
Fuel Temp	500°R to 1000°R
Oxid Temp	500°R to 1000°R

*Varied to keep ΔP_o and ΔP_f constant

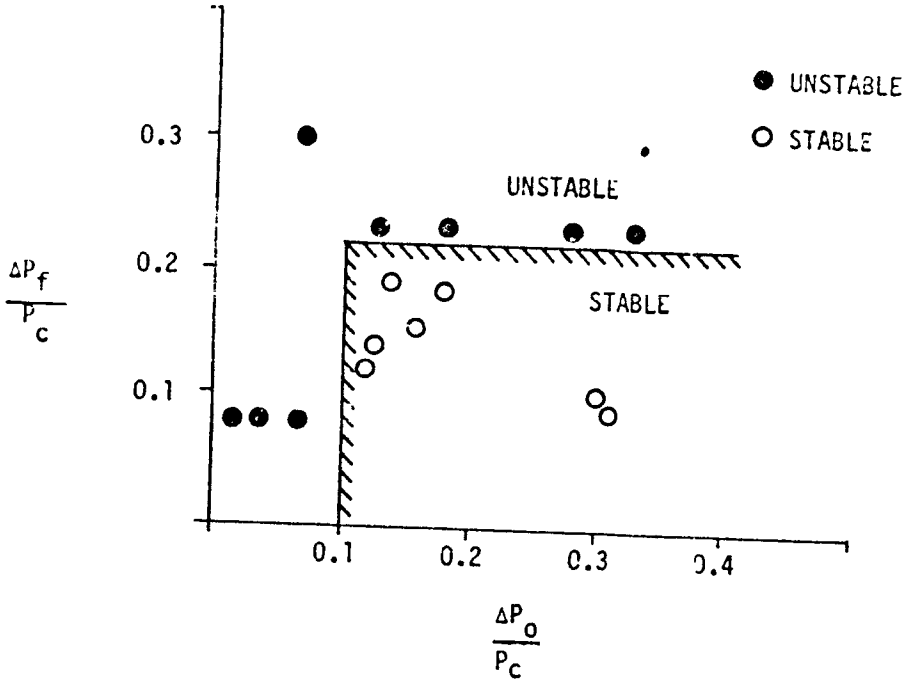

Figure 1. Turbopump Combustor

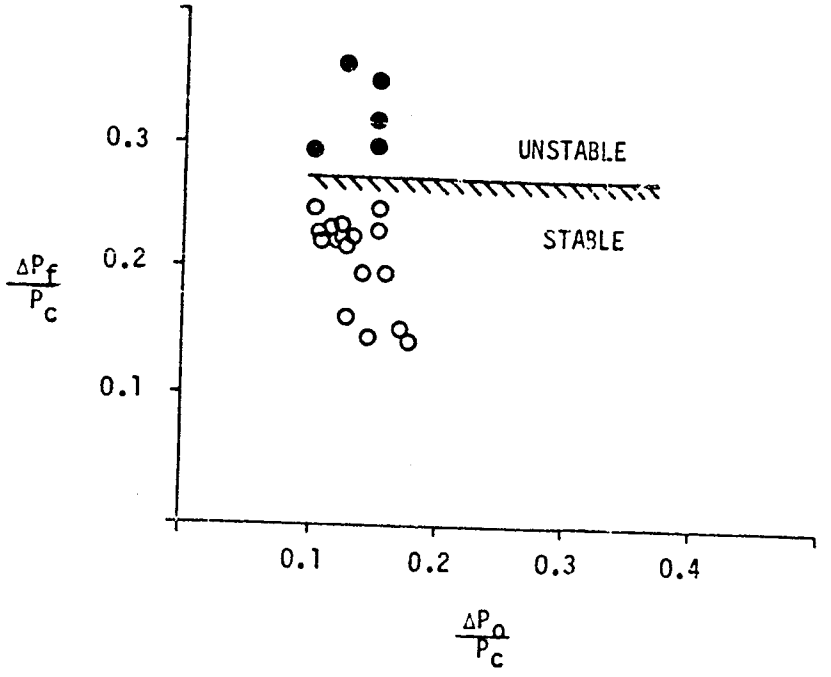

Figure 2. 500 psia Combustor

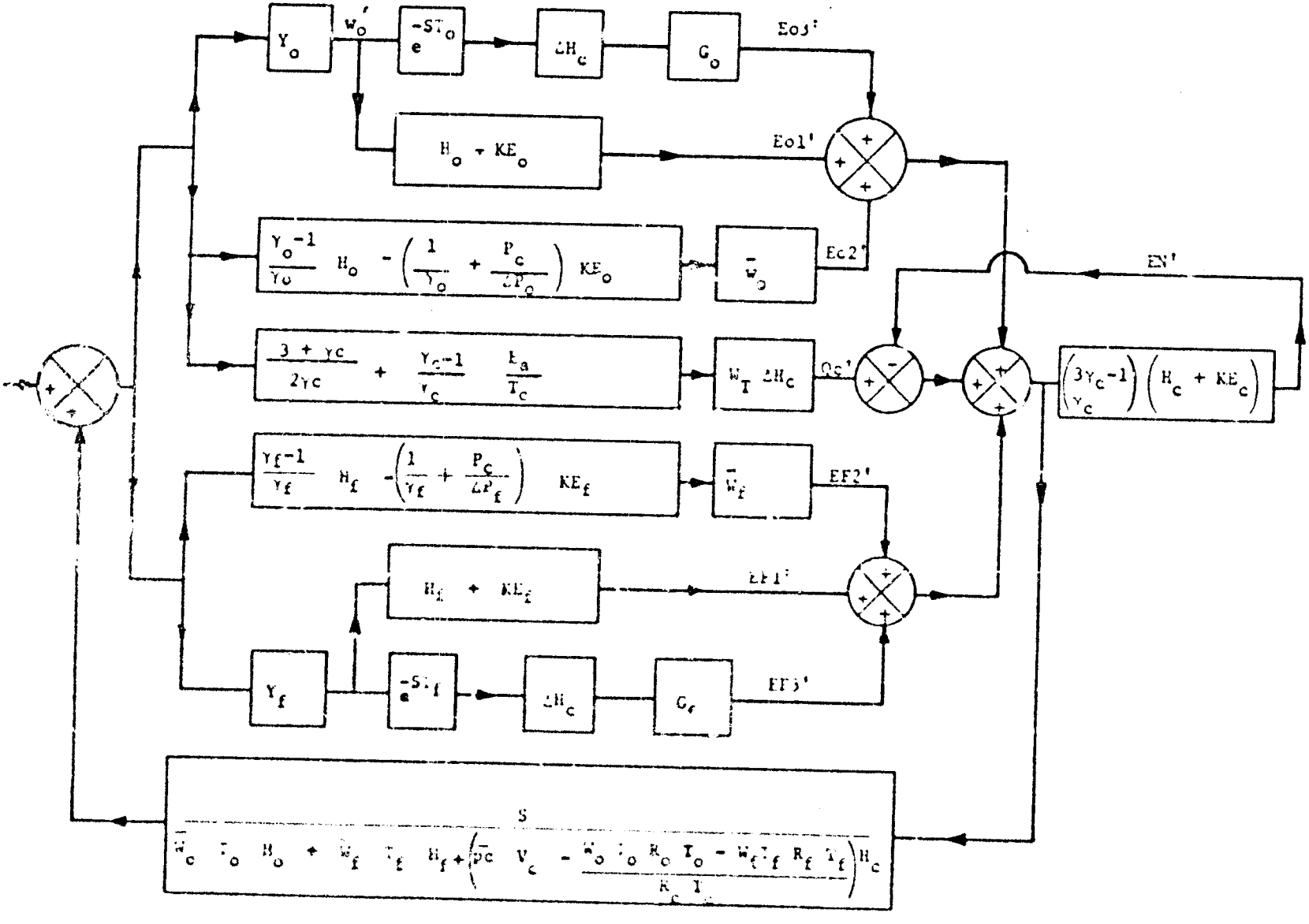

Figure 3. Model Block Diagram

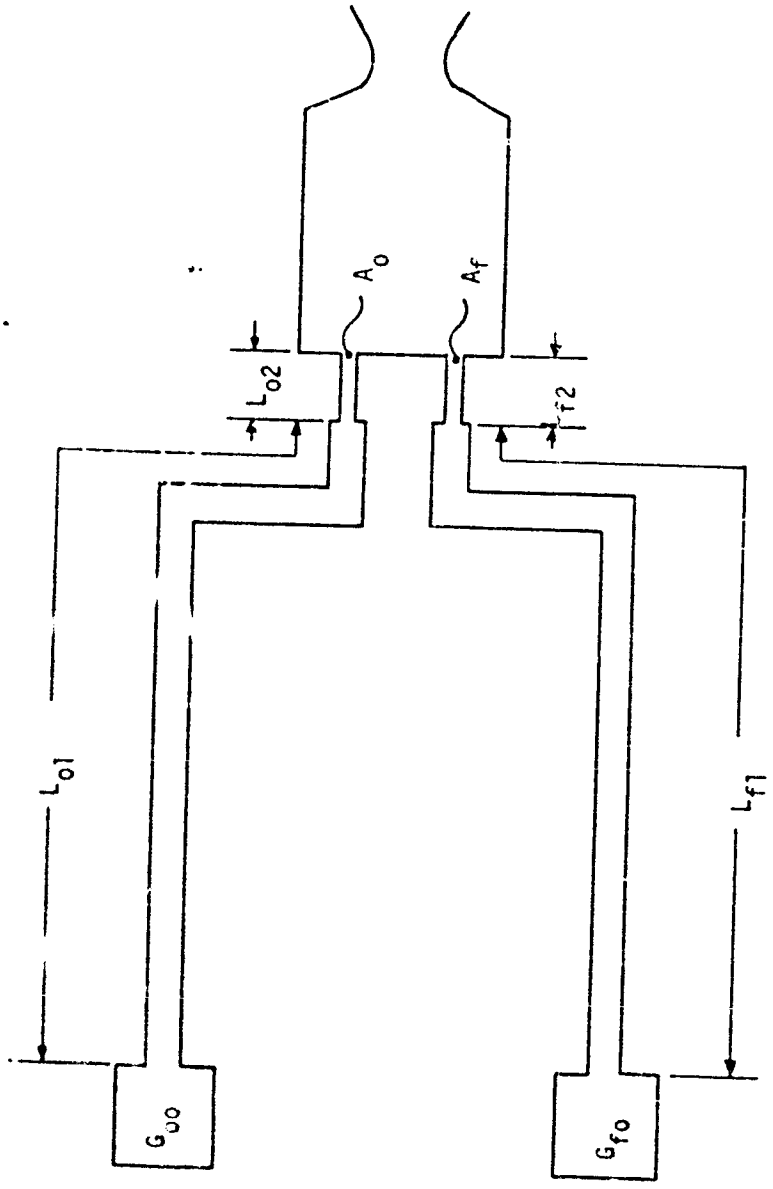

Figure 4. Feed System Schematic

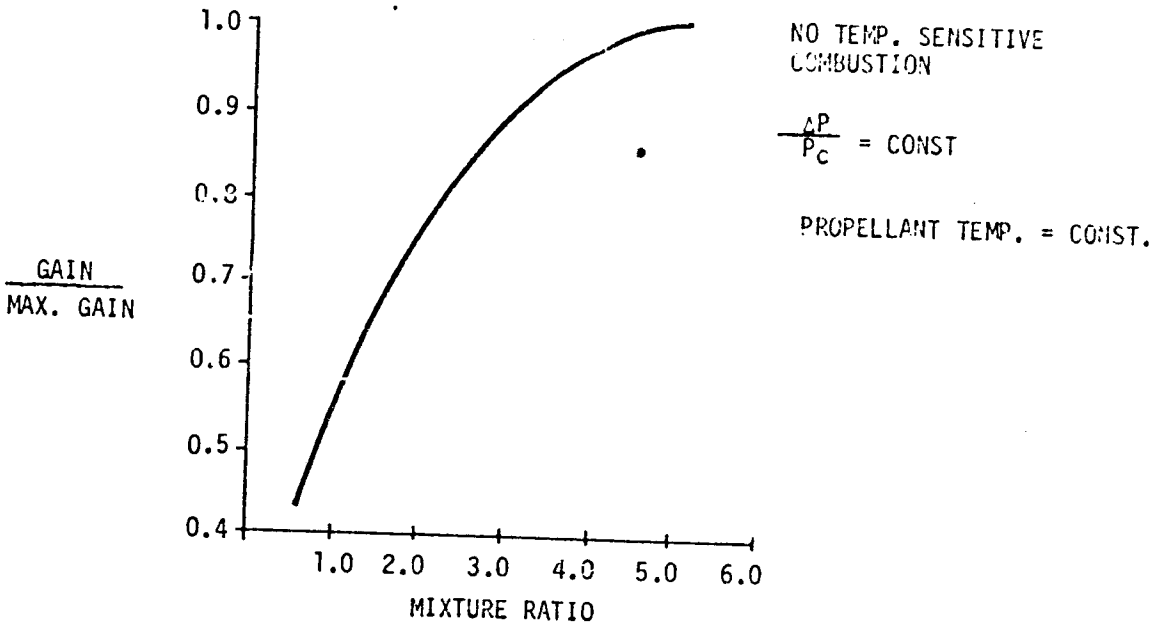

Figure 5. Effect of Mixture Ratio

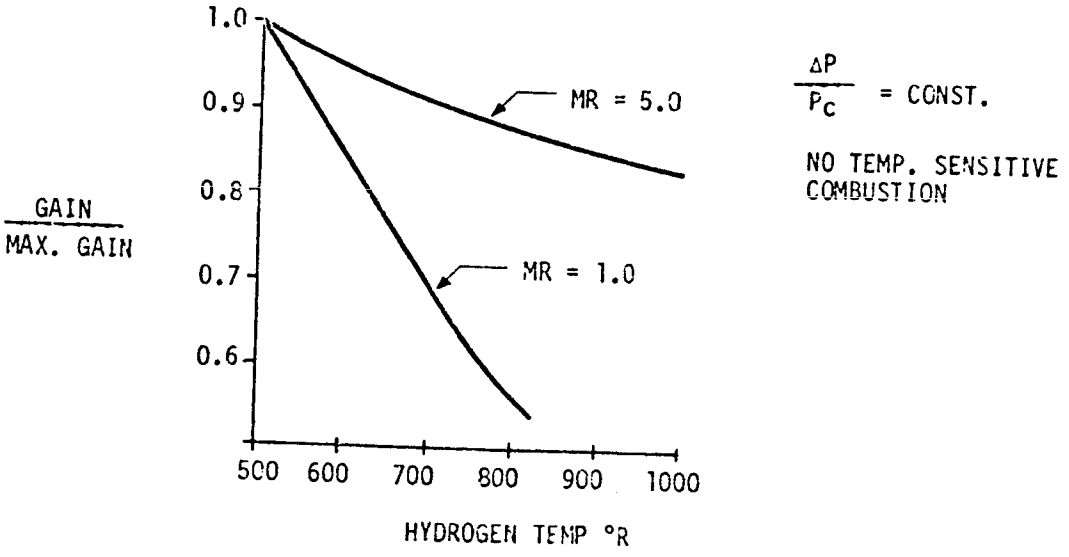

Figure 6. Effect of Hydrogen Temperature

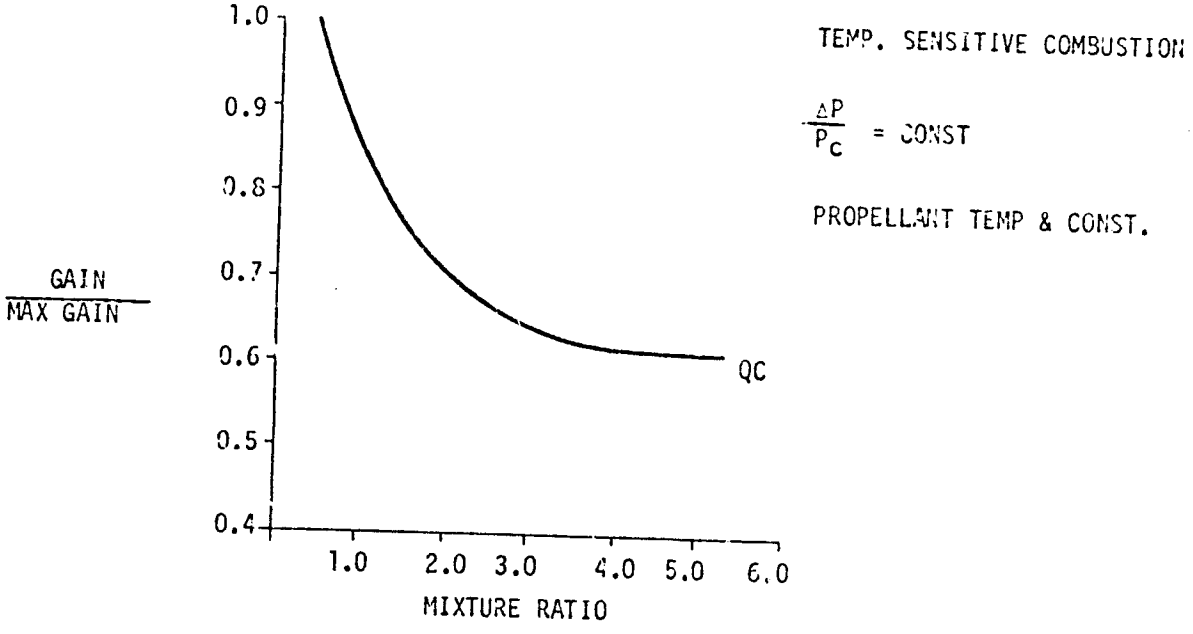

Figure 7. Effect of Mixture Ratio

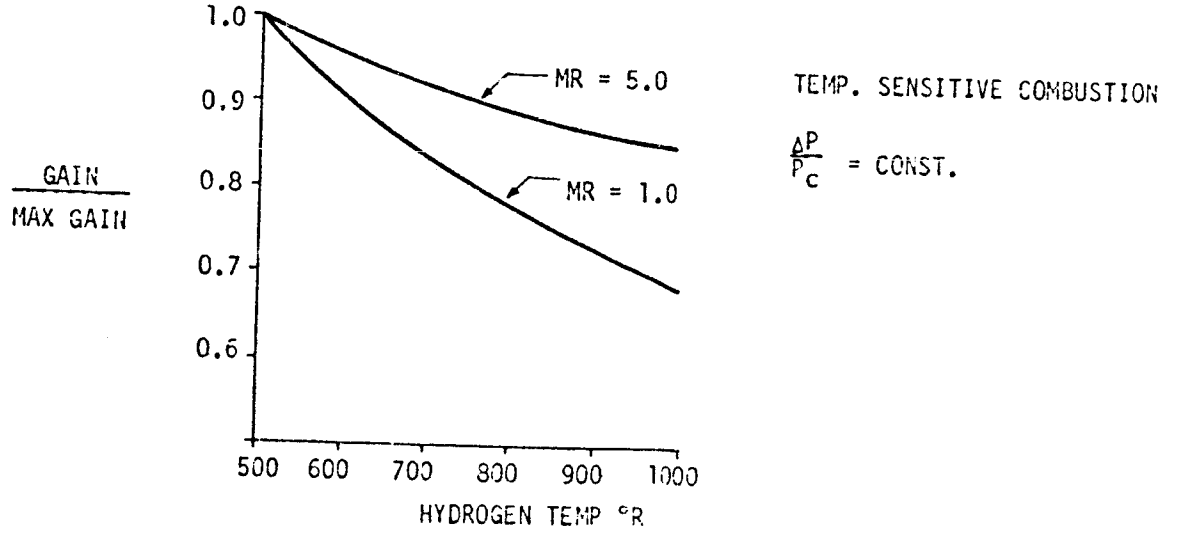

Figure 8. Effect of Hydrogen Temperature

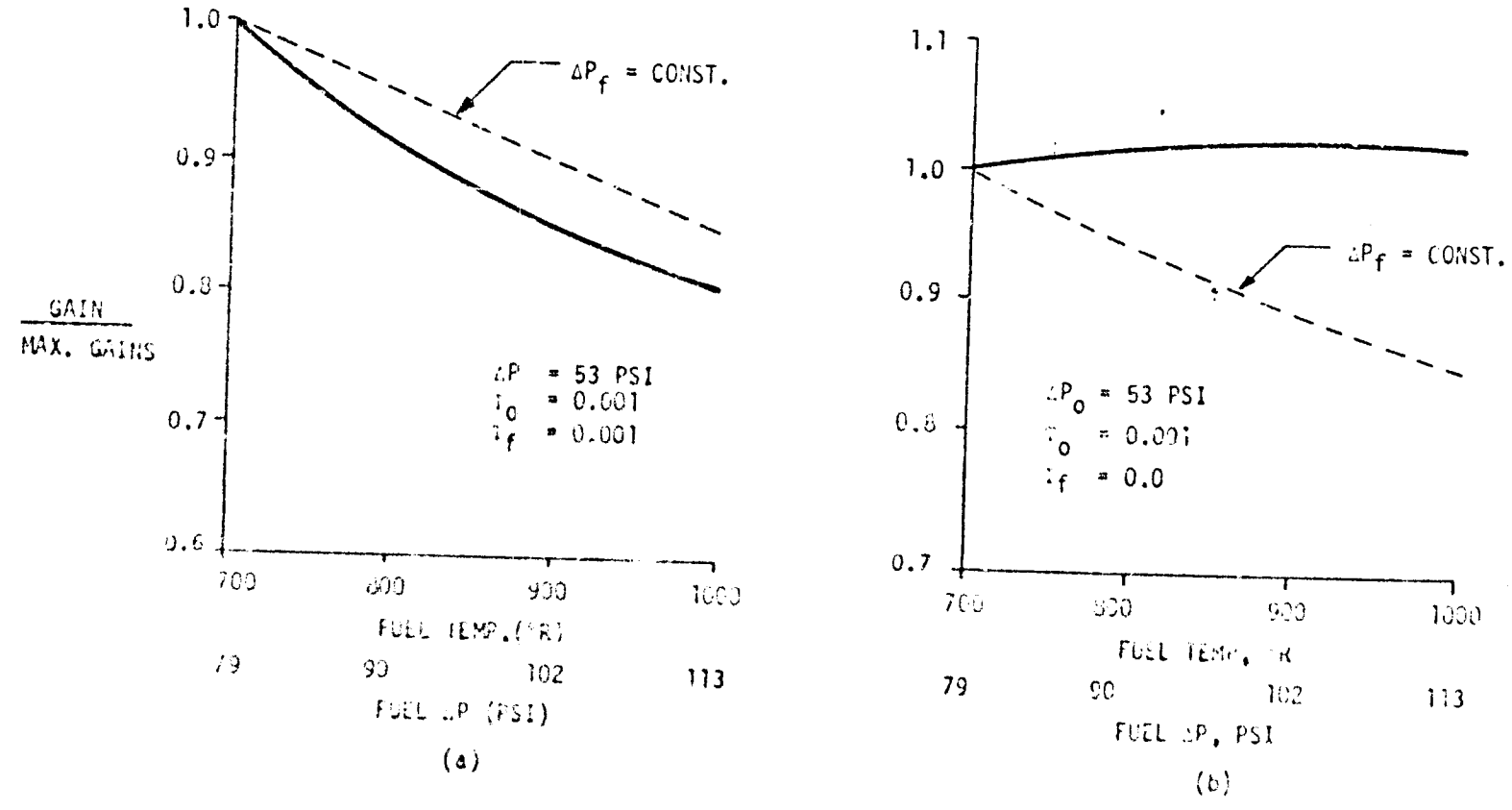

Figure 9. Effect of Propellant Temperature and Time Lag

N71-29585

"TITANIUM PUMP IMPELLER FABRICATION AND TESTING"

J. F. WOLF

ROCKETDYNE

TECHNICAL MANAGER

C. MILLER

MARSHALL SPACE FLIGHT CENTER

TITLE TITANIUM PUMP IMPELLER FABRICATION AND TESTING

CONTRACTS NAS8-20761
NAS8-25860

PRESENTER J. E. WOLF

COMPANY ROCKETDYNE DIVISION OF NORTH AMERICAN ROCKWELL CORP.

NASA PROJECT MANAGER CHARLES MILLER

Rocketdyne
North American Rockwell

INTRODUCTION

Recent oxygen/hydrogen engine development programs have emphasized the need for developing high speed centrifugal impellers for high pressure liquid hydrogen pumps. High speed, unshrouded impellers are easily machined; however, sensitivity of hydrodynamic performance and axial thrust to impeller clearance can be a problem. Shrouded impellers do not have this problem and thus have high hydrodynamic performance and stability in addition to good thermal characteristics for minimum chilldown.

Current machining practices can impose some undesirable hydrodynamic limitations on impeller design such as shape, depth and curvature of the passages as well as minimum blade discharge angle. For this reason a program was undertaken, under the sponsorship of Marshall Space Flight Center, NASA, to a) develop shrouded impeller fabrication techniques not limited by current machining practices, b) design and fabricate two test impellers using these techniques, and c) test the impellers to evaluate the hydrodynamic performance and determine the structural characteristics. To obtain high operating speeds, a high strength-to-density ratio, forged titanium alloy 5al-2.5 S was selected as the material for the impellers.

SUMMARY

The "Titanium Pump Impeller Fabrication and Testing" program was accomplished in two main phases. During Phase I, fabrication and bonding techniques were investigated to determine the most promising method of producing satisfactory joints between components of complex shapes. The diffusion bonding technique was selected and two sample impellers were designed, fabricated and bonded to develop procedures and verify the feasibility of the approach. A shrouded impeller was then designed. The head (46,100 ft), flow (9754 gpm), and speed (29,800 rpm) selected for the design point is the same as for the Mark 29 fuel impeller for the J-2S engine so that stress and performance comparisons could be made with a conventionally machined impeller.

The blade discharge angle was set at 37° (Mark 29 is 60° because of machining limitations) and in order to develop the same head at the same rpm the impeller OD was increased from 11.5 in. (MK 29) to 12 inches. Components of two impellers were fabricated, tooling was constructed, the impellers were diffusion bonded, finish machined and balanced and spun in a spin pit to 31,000 rpm for 2 minutes. This phase of the program demonstrated the feasibility of the diffusion bonding technique for fabricating shrouded impellers.

In Phase II one impeller was stress coated and spin tested to determine the magnitude and distribution of centrifugal stresses, then burst tested to determine the bonded joint efficiency. The second impeller was installed in a Mark 29F (J-2S) pump assembly and run under actual pump operating conditions in LH_2 to determine its hydrodynamic performance. The ceramic stress coat test indicated a significant reduction in centrifugal stresses relative to the geometrically similar, but conventional two piece Mark 29F (J2-S) machined shrouded impeller. The room temperature burst test resulted in partial failure of the diffusion bond at 49,000 rpm. The vane tip speed at failure (2560 ft/sec) was higher than that of the Mark 29F (J2-S) impeller which failed at a vane tip speed of 2510 ft/sec. The failure speed ratioed to minimum material properties at the -370°F operating temperature is 52,400 rpm (vane tip speed of 2740 ft/sec).

Three H-Q (head-flow) pump tests, to map impeller performance, were successfully conducted at constant speeds of 12,000, 24,000, and 28,000 rpm. The tests were run at flows ranging from 30% to 135% nominal at 12,000 rpm and 80% to 120% nominal at 24,000 and 28,000 rpm.

PHASE I

Fabrication Investigation of Technique Selection

Two methods of fabrication were investigated - diffusion bonding and electron beam welding. The problem areas involved and the advantages and disadvantages of both methods were studied and based on this investigation it was concluded that with sufficient development either process could be employed; however, it appeared that the diffusion bonded process offered a lower per-part production cost and somewhat more simple design and pre-bond fabrication requirements. For this reason the diffusion bonding process was selected as the method to develop.

It was felt that the most expeditious approach toward achieving a diffusion bonded impeller was to fabricate a simulated simplified impeller using existing material, processing and tool concepts. Modifications to these concepts could then be predicated on results obtained in these trials.

A titanium alloy forging was procured to be used for the trial diffusion bonding runs. Samples to be bonded were used to simulate and attempt to solve problem areas envisioned during fabrication of the actual impeller. The configuration shown provided for the following:

- Simulated inner shroud curved surface
- Simulated outer shroud curved surface
- Four impeller vanes spaced @ 90°
- Use of different restrainer materials to hold total tool part assemblage
- Vertical and horizontal bond joints
- Desired front and rear joint radii
- Simple geometry to allow determination of volumes and various pre-bond and post-bond measurements
- Variations of internal tooling

TRIAL SAMPLE CONFIGURATION

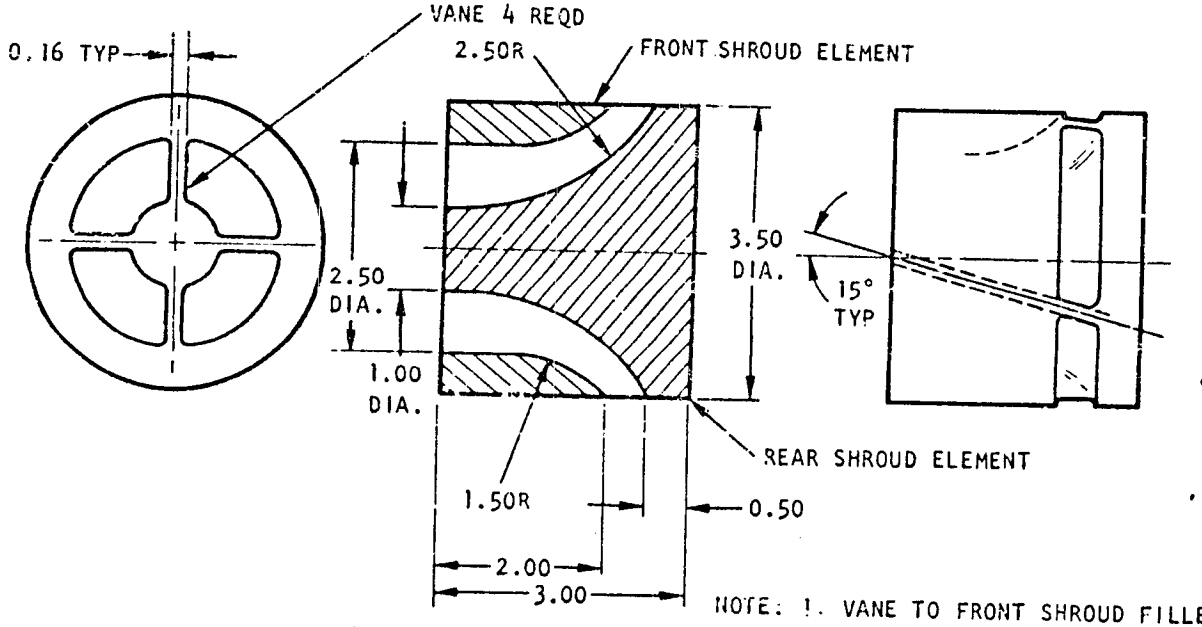

NOTE: 1. VANE TO FRONT SHROUD FILLET R 0.08R
2. VANE TO REAR SHROUD FILLET R 0.112R
3. VANE HT TO HAVE EXCESS MATL TO FILL VANE TO SHROUD FILLETS

Three sample impellers and their tooling were fabricated and the impellers bonded to develop the necessary procedures for the full scale impeller fabrication.

The effects studied were:

Die fill, flash and fillet formation

Completeness of bonding

Tooling behavior and dimensional changes

Volume and configuration control

Tool removal effectiveness

Mechanical and metallurgical effects

Effect of core splitting

Bonding conditions (temperature, pressure, time)

Shown here is the final simulated impeller sample along with complete bond assembly before lay-up.

Bonding is accomplished by sealing the parts to be bonded in a retort, placing the retort assembly in a restrainer, applying a vacuum to the retort and then applying the bonding pressure. After bonding the cores are removed by leaching in an acid bath and the part is then chemical milled to remove any interaction layer from the cores. The simulated impeller after core removal and chem-milling is shown and full fillets can be plainly seen at both the junction of the vanes and hub and vanes and outer shroud.

FINAL SIMULATED IMPELLER SAMPLE SHOWING COMPLETE BOND ASSEMBLY BEFORE LAY UP

330-401
3-71

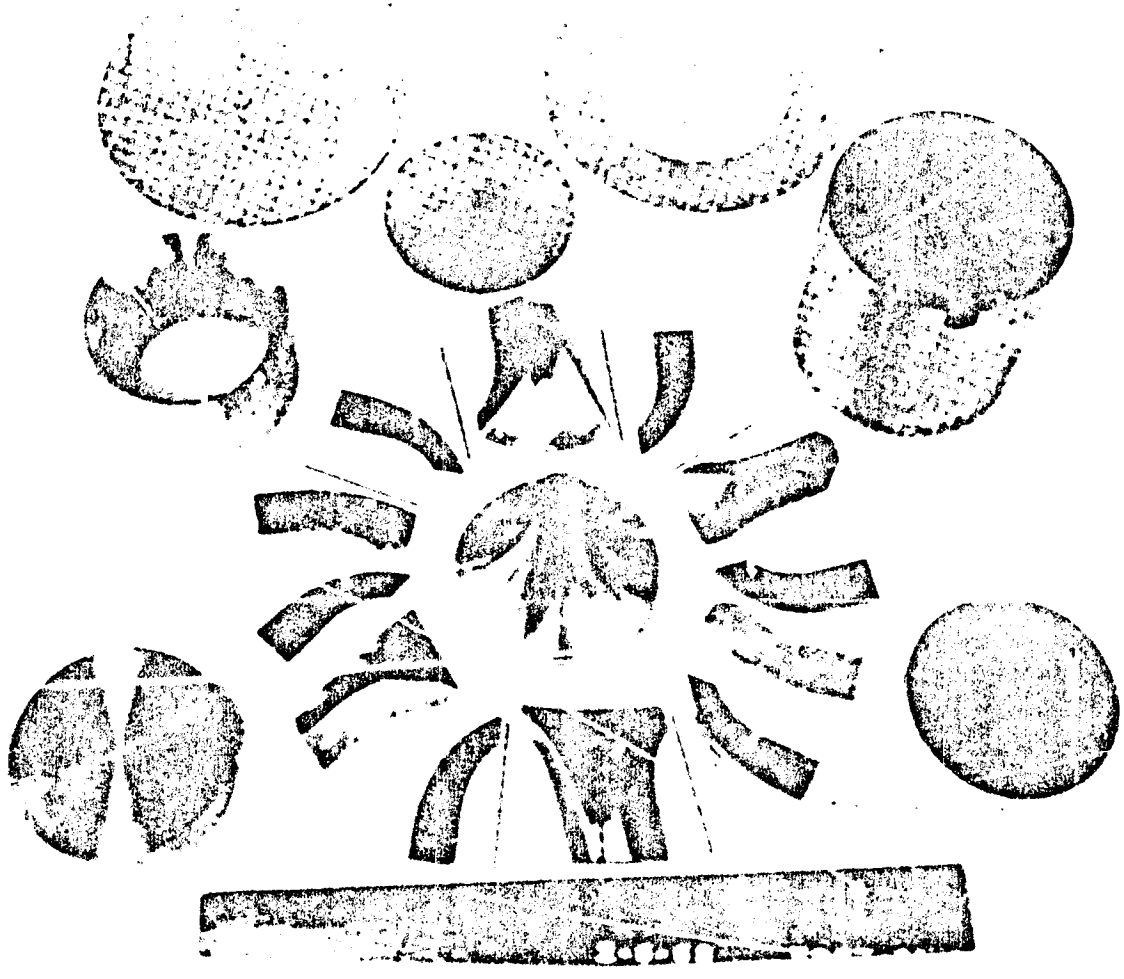

Rocketdyne
North American Rockwell

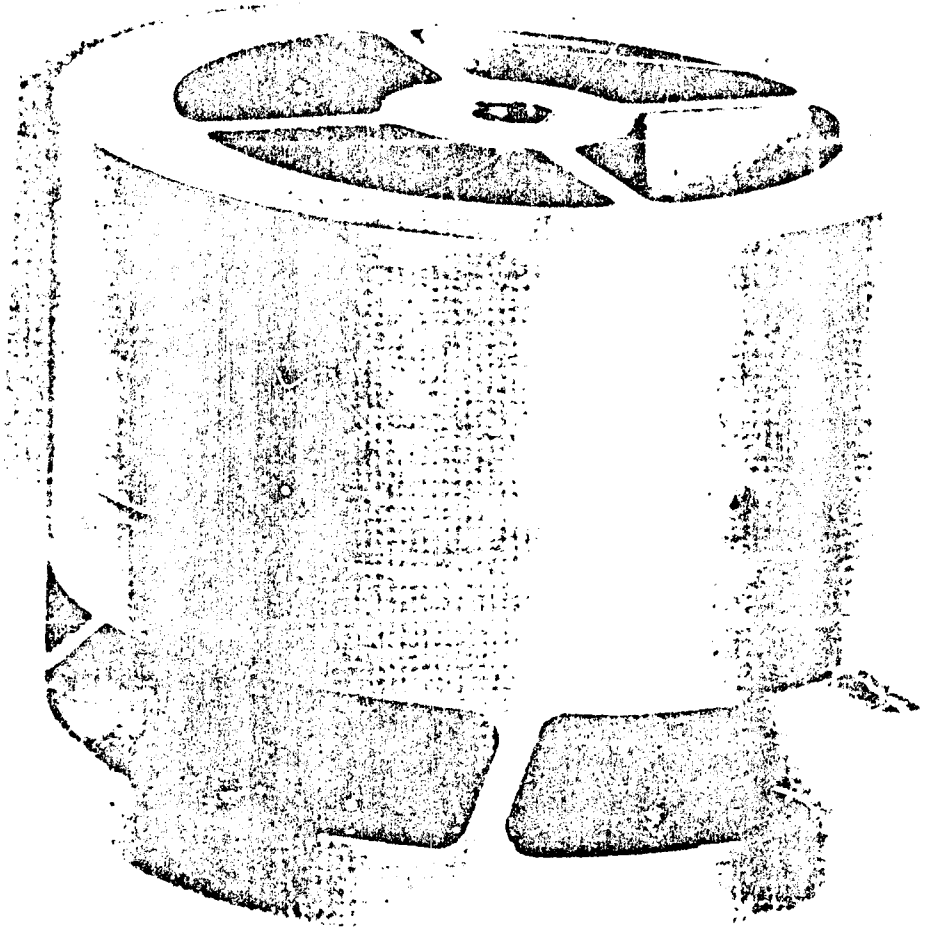

Rocketdyne
North American Rockwell

"FINAL SIMULATED IMPELLER SHOWING DISCHARGE AREA"

(0.020 OF AN INCH OF MATERIAL REMOVED FROM ALL SURFACES BY CHEM-MILLING)

Photo-micrographs and tensile specimens were taken from the impeller and a section of the bond area at magnifications of 50X and 250X respectively is shown. As may be observed, no indication of the bond joint is visible. A photo-micrograph of the non-bonded area at a magnification of 250X is also shown and in comparing them, no significant differences can be found between bonded and non-bonded areas. The photo-micrographs shown were taken of specimens from the impeller inlet.

As a comparison, the grain structure of the titanium material in an as received and after bonding condition at a magnification of 250X is also reproduced. It can be seen that grain growth occurred during the bonding process. Wrought titanium alloys, as received, have variations in properties. The diffusion bonding cycle produces a fully annealed structure with more uniform properties.

The three tensile specimens shown were taken from the impeller inlet and stressed in tension to failure with results shown in Table I.

TABLE I

SPECIMEN NO.	ULTIMATE LOAD LBS	ULTIMATE STRENGTH KSI	ELONGATION $\frac{1}{2}$ in.-%
1	762	122.5	15
2	843	124.3	15
3	567	122.1	20

"PHOTO-MICROGRAPH OF BONDED AREA"

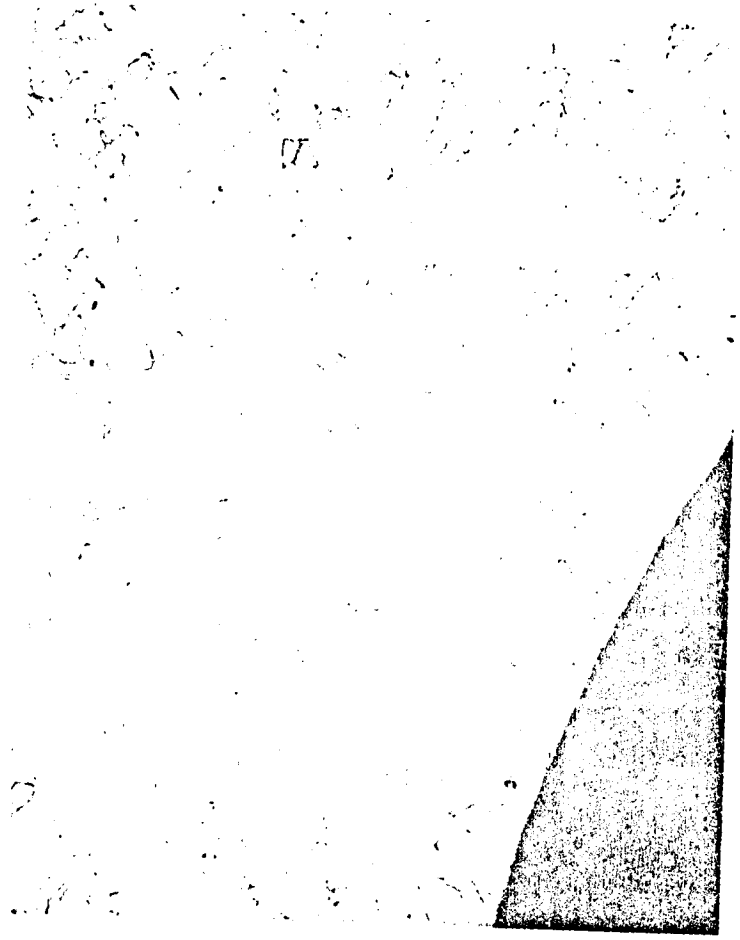

50X

250X

Rocketdyne
North American Rockwell

PHOTO MICROGRAPH OF NON BOND AREA

330-405
3-71

"GRAIN STRUCTURE"

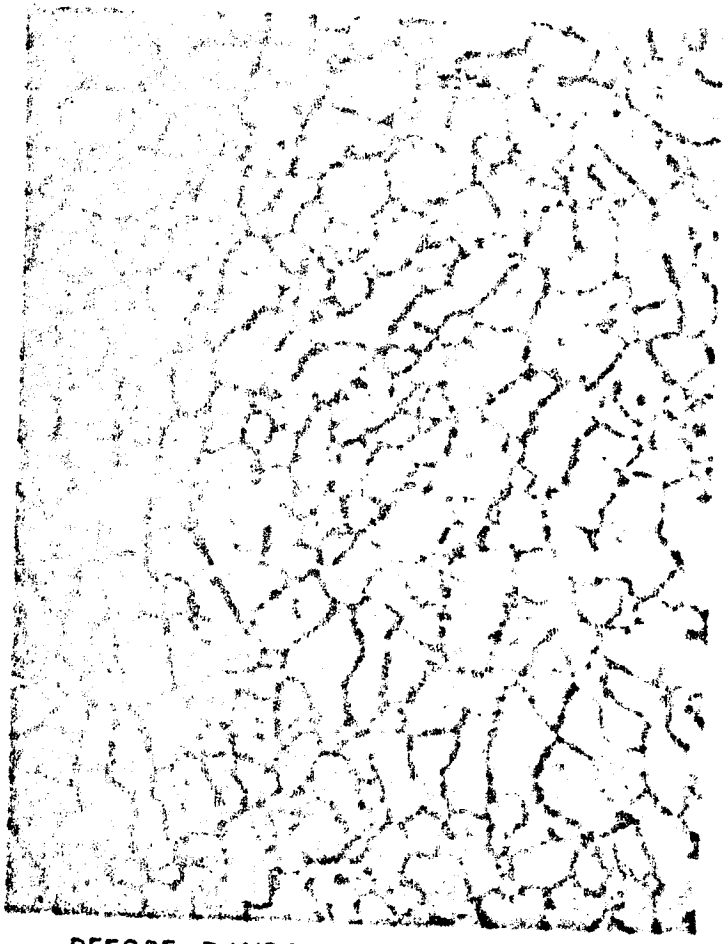

BEFORE BONDING OR AS RECEIVED

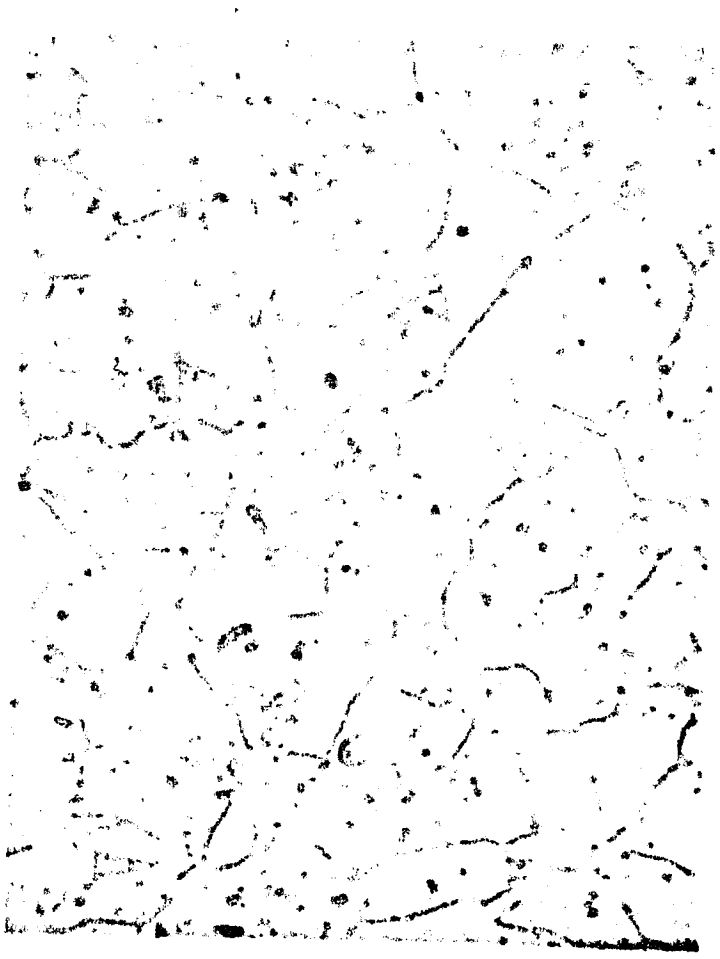

AFTER BONDING

Rocketdyne
North American Rockwell

TENSILE SPECIMENS TAKEN FROM SIMULATED IMPELLER AREA

330-406
3-71

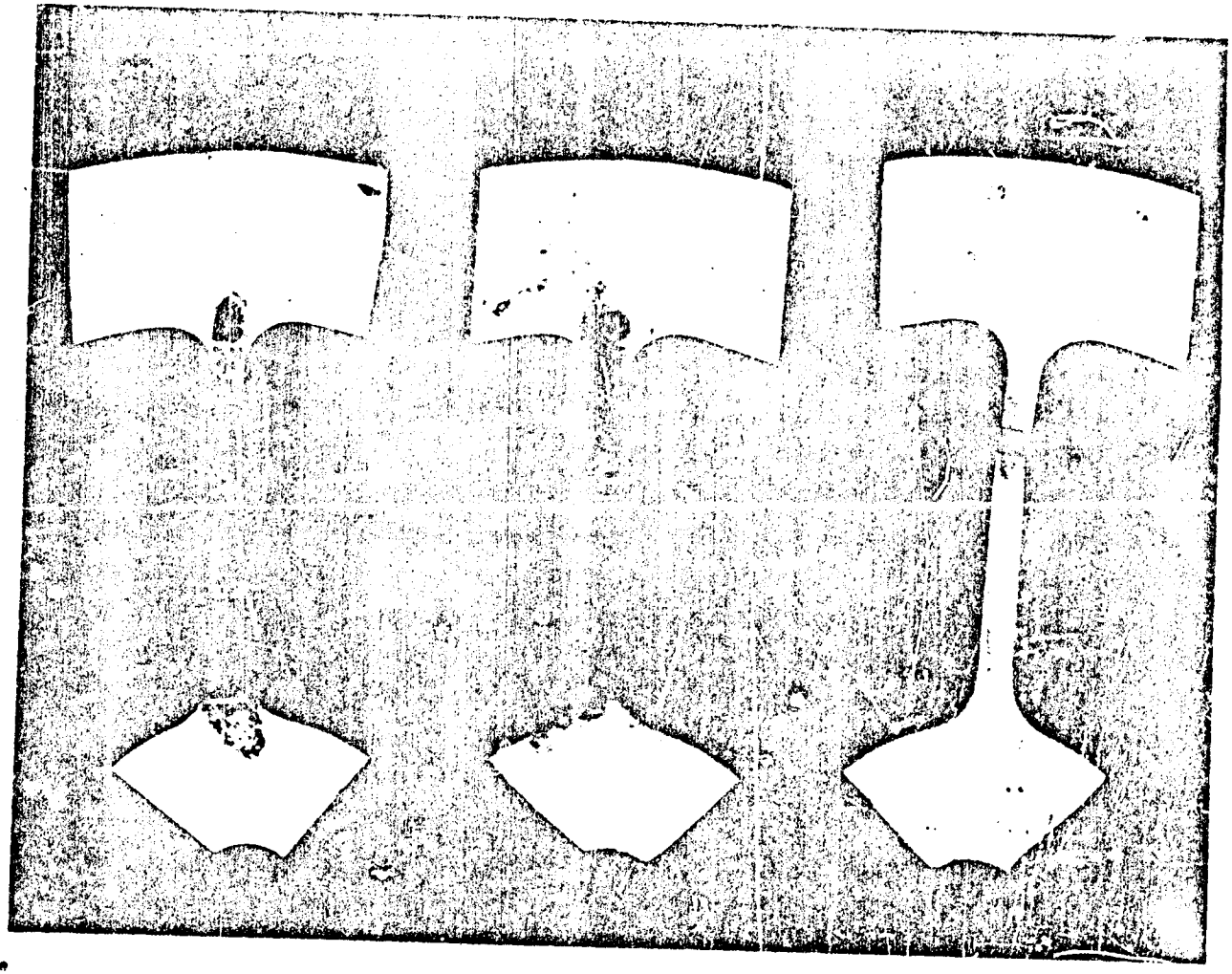

Rocketdyne
North American Rockwell

The values of ultimate strength and elongation are typical for titaniu_ alloy at room temperature. As can be seen, failure occurred well below the fillet area.

Based on the sample evaluation program, core design considerations and both hydrodynamic and stress analysis, a 7 full plus 7 partial vane impeller with 45 degree skewed vanes was selected as the final configuration for fabrication. The head, flow operating speed, inlet blade angles and impeller shroud profiles are identical to those of the existing Mark 29 fuel pump. A comparison is shown in Table II.

TABLE II

DESIGN PARAMETERS OF IMPELLER COMPARED TO MK 29 DESIGN

		MARK 29	NEW DESIGN
Headrise (Pump Overall)	ft	46,100	46,100
Flowrate	gpm	9,754	9,754
Speed	rpm	29,800	29,800
Tip Diameter	inches	11.5	12.0
Blade Discharge Angle	degrees	60	37
Number of Vanes	full	6	7
	long splitter	6	7
	short splitter	12	
Blade Inlet Angles	hub, degrees	21	21
	mean, degrees	16	16
	tip, degrees	13	13
Vane Shape		Const Thickness	Tapered
Vane Discharge Configuration		Axial	45° Skew

Fabrication of the titanium impeller components was accomplished using conventional machining methods and the impeller components are shown in the accompanying photographs. Shown first is a full set of impeller vanes (seven full vanes and seven partial vanes). The next photo shows the finish machined impeller hub and vane shroud. The cores which are used to position and support the vane elements during bonding, a complete set of impeller components ready for the bond sequence, is also shown.

The next photograph shows the pre-bond lay-up of the complete impeller assembly, which includes the front impeller shroud, the core assembly, which includes the impeller vanes; and the impeller back plate and shaft. Another view of the pre-bond lay-up in which the core locks, the rings which hold the vanes and cores together to form the core assembly is also shown.

After bonding the core locks were machined off, the steel cores were removed from the bonded impeller by leaching in a hot nitric acid solution and .040 inch was removed from the impeller surfaces by chemical-milling. One of the bonded impellers is shown.

Following chemical-milling both impellers were visually and dye penetrant inspected, then finish machined balanced and spin tested at room temperature in a spin pit to 31,000 rpm for two minutes. Final machined impeller is also shown.

The highly successful results obtained during this phase of the program which established the feasibility of utilizing the diffusion bonding technique to fabricate high tip speed impellers resulted in the initiation of Phase II of the program to evaluate the limits of the method by stress coat, burst and pump testing of the two diffusion bonded impellers.

IMPELLER COMPONENTS

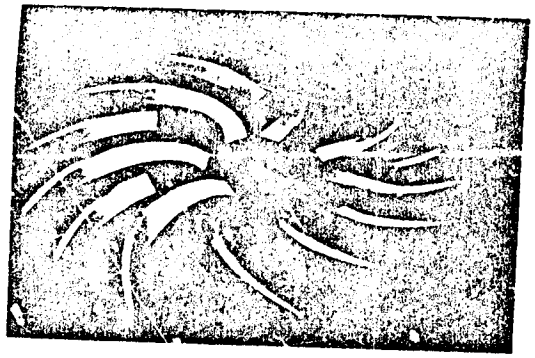

FULL SET OF VANES
(PARTIAL AND FULL)

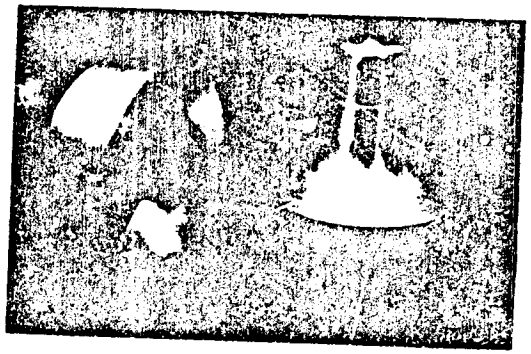

IMPELLER HUB AND SHROUD

IMPELLER CORES

IMPELLER COMPONENTS READY FOR BONDING

330-408
3-71

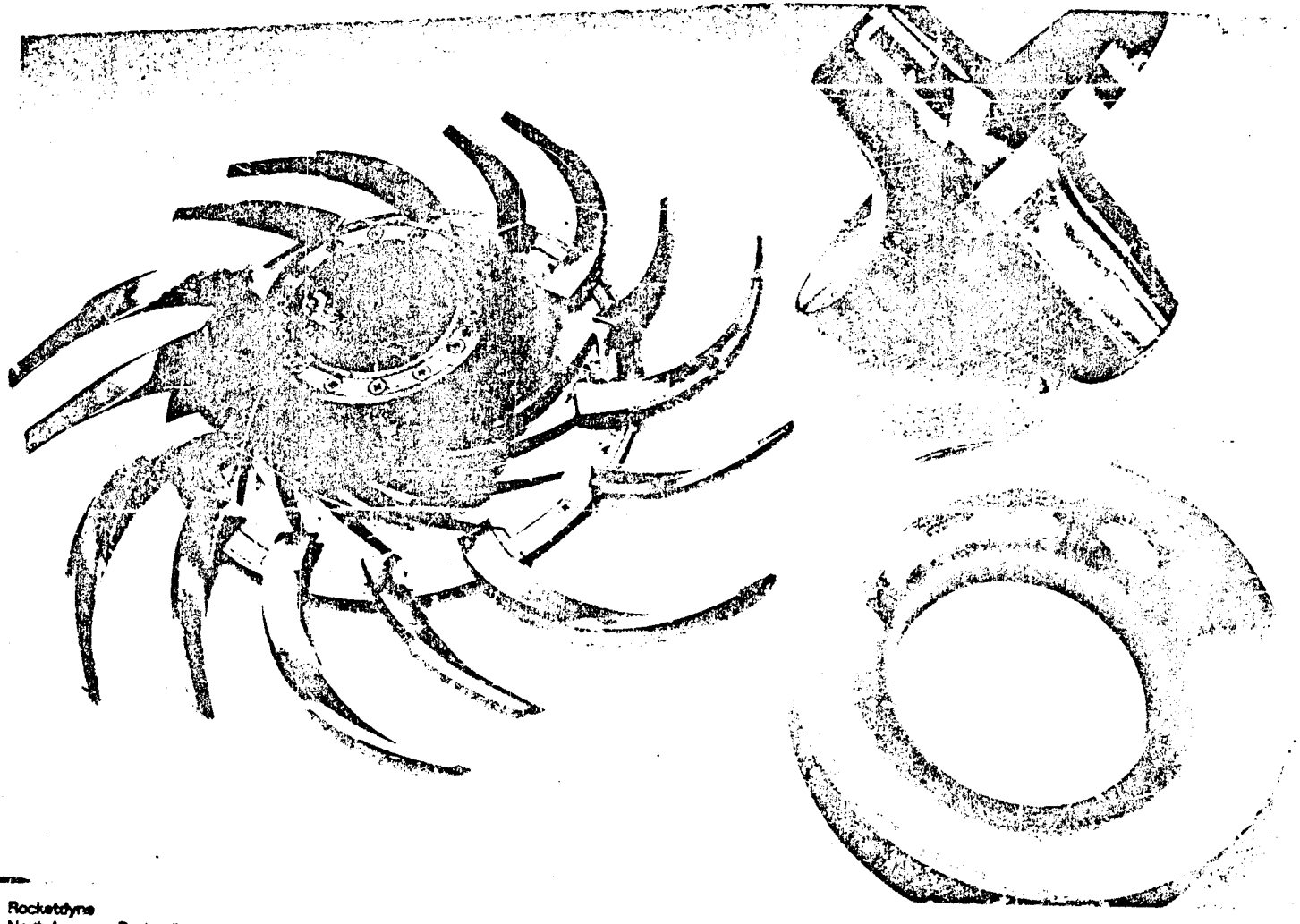

Rocketdyne
North American Rockwell

PREBOND LAYUP OF COMPLETE IMPELLER ASSEMBLY

330-41C
3-71

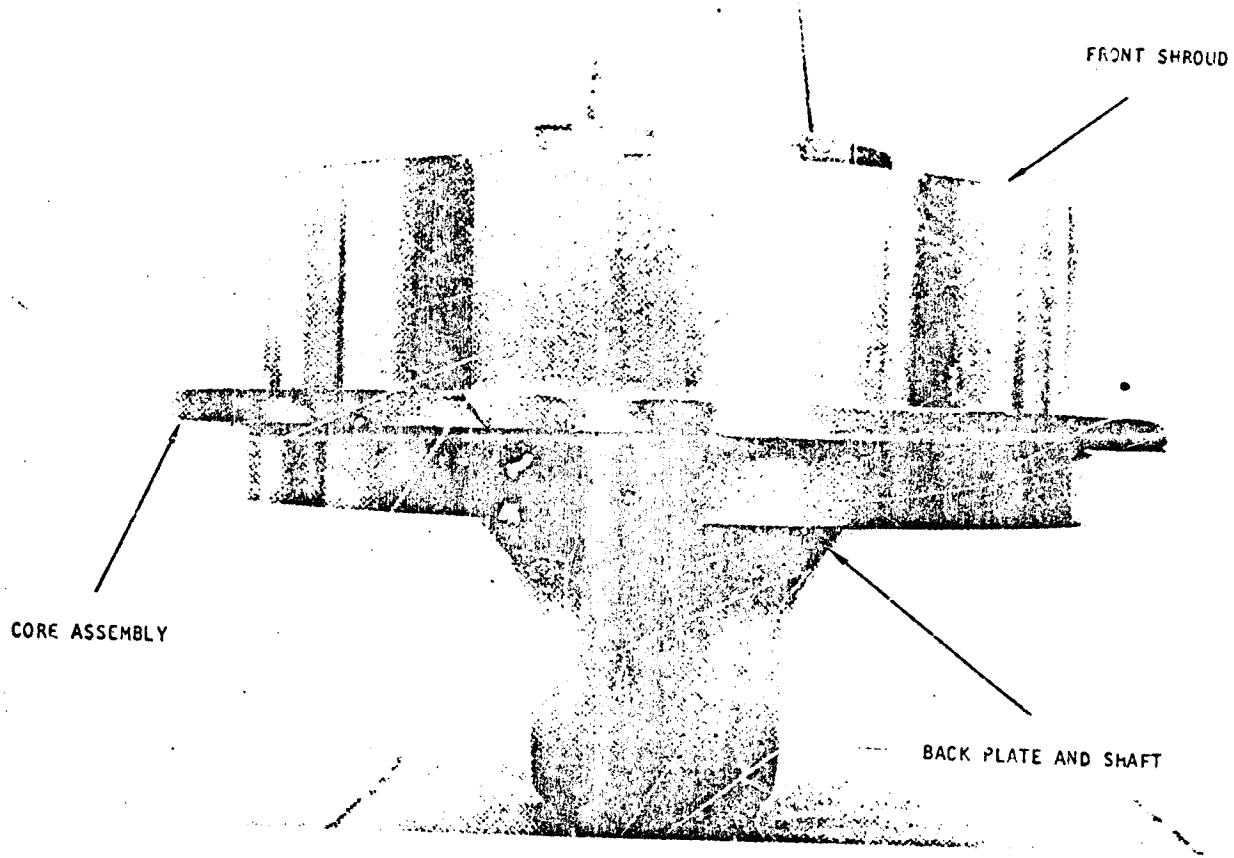

Rocketdyne
North American Rockwell

PREBOND LAYUP

330-409
3-71

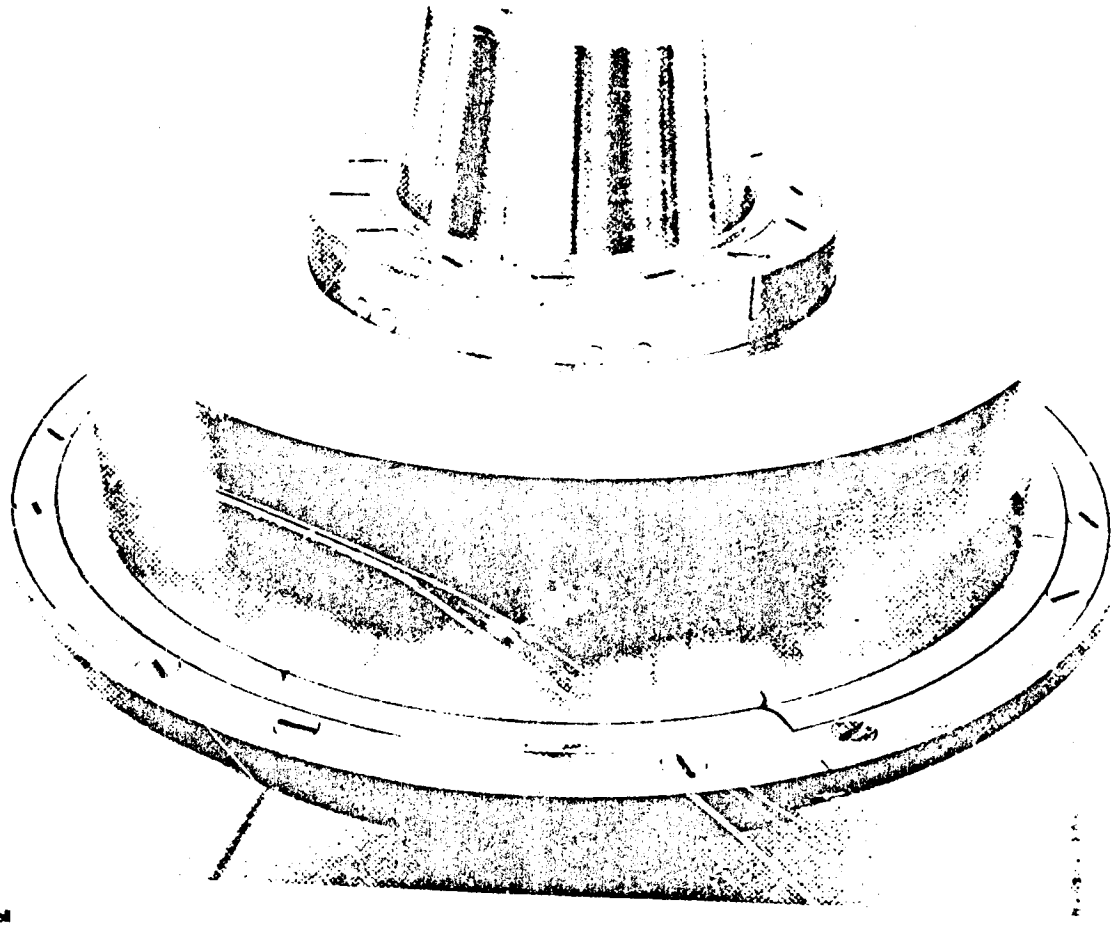

Rocketdyne
North American Rockwell

COMPLETED DIFFUSION BONDED SHROUDED TITANIUM IMPELLER

330-412
3-71

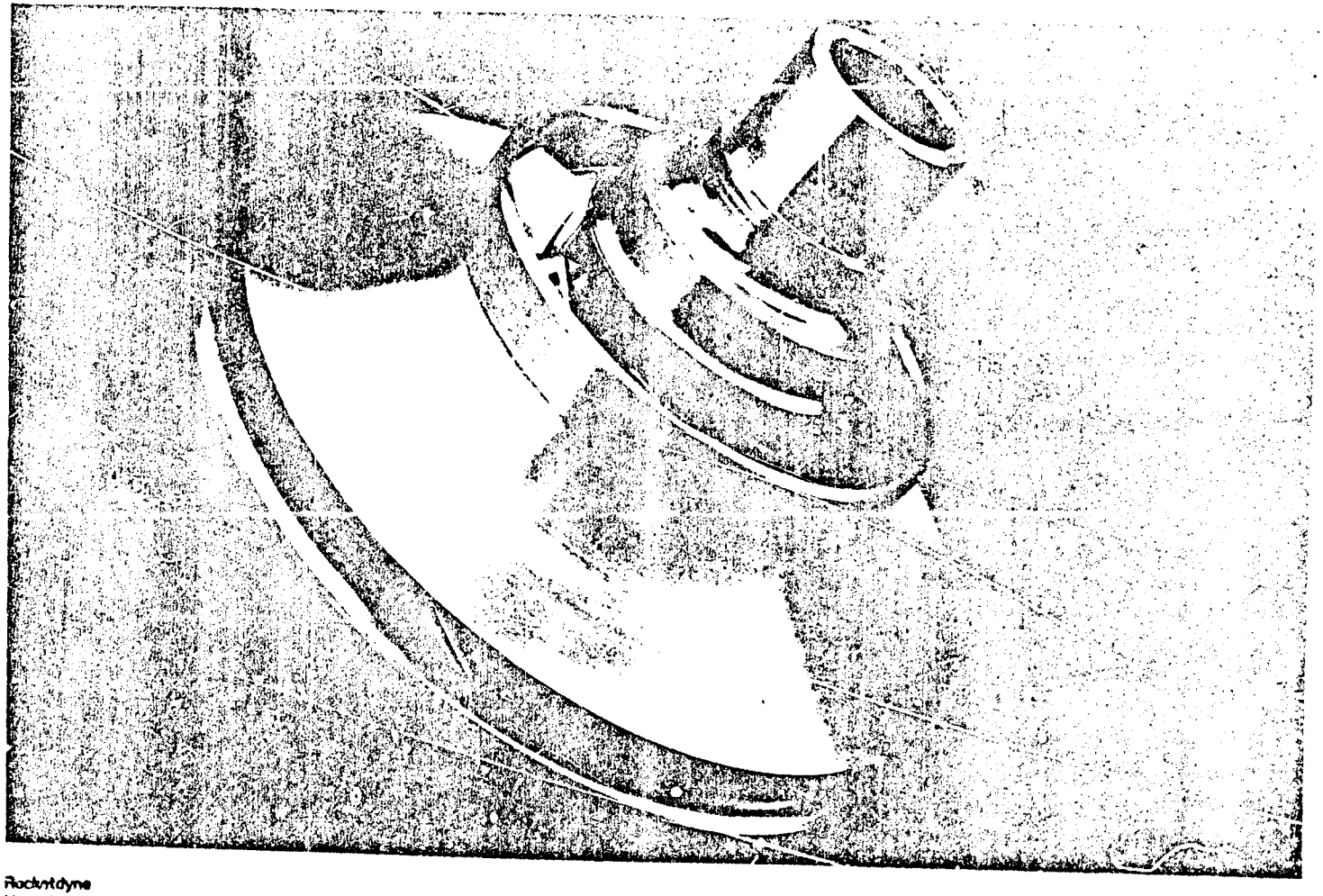

Rocketdyne
North American Rockwell

IMPELLER AFTER CHEMICALLY MILLED

330-411
3-71

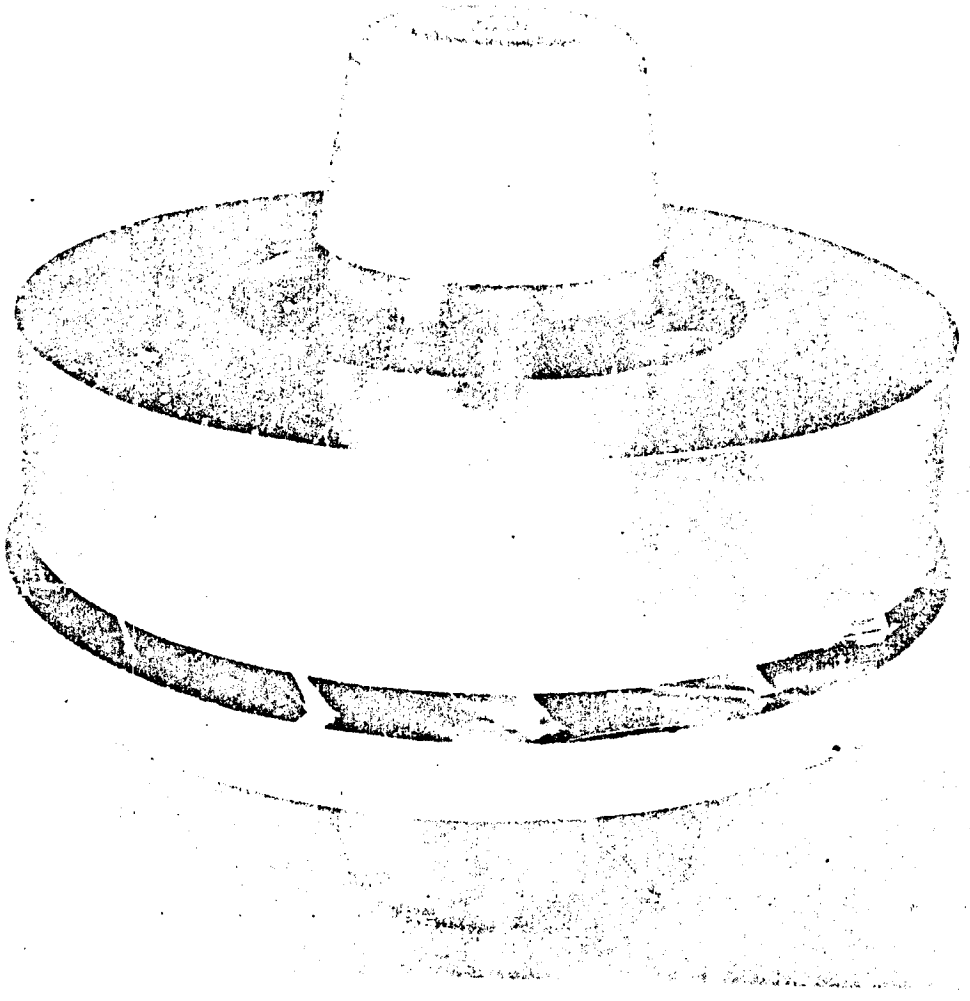

Rocketdyne
North American Rockwell

PHASE II

Ceramic Stresscoat, Burst and Pump Testing

In order to further evaluate the diffusion bonding process, the two impellers fabricated in Phase I were subjected to stress coat, burst and performance testing.

Stress coat testing was performed to determine the magnitude and distribution of the centrifugal stresses in the impeller and also to compare the stresses to those in a similar conventionally machined impeller (MK 29f).

Stresscoat testing consists of spraying the impeller with a ceramic coating that develops cracking at a known strain as determined by calibration standards on test bars. The impeller is subjected to increasing levels of centrifugal stress by spinning and observing the impeller for coating cracks at each step.

Some significant results of the stresscoat testing is shown in Table III.

TABLE III

Stresscoat Cracking Location	Test Speed rpm	Diffusion bonded Impeller Calc. Stress at Operating Speed 31,000 rpm (psi)	2 Piece Machined MK 29F Impeller Assy Calc. Stress at 31,000 rpm (psi)
Leading Edge of Vanes	12,850	48,400	77,000
Impeller Shroud	15,200	34,600	50,400
Impeller Backplate	16,910	28,000	50,400
Vane Trailing Edge	17,900	24,900	67,300

Test results clearly indicate significantly lower stresses for the diffusion bonded design as compared to the two-piece machined impeller. Shown is a composite average of all seven vanes illustrating the stress boundaries that were observed due to the increasing speed increments.

MAGNITUDE AND DISTRIBUTION OF VANE STRESSES ADJUSTED AS THE SQUARE OF THE SPEEDS TO 31,000 RPM OPERATING SPEED

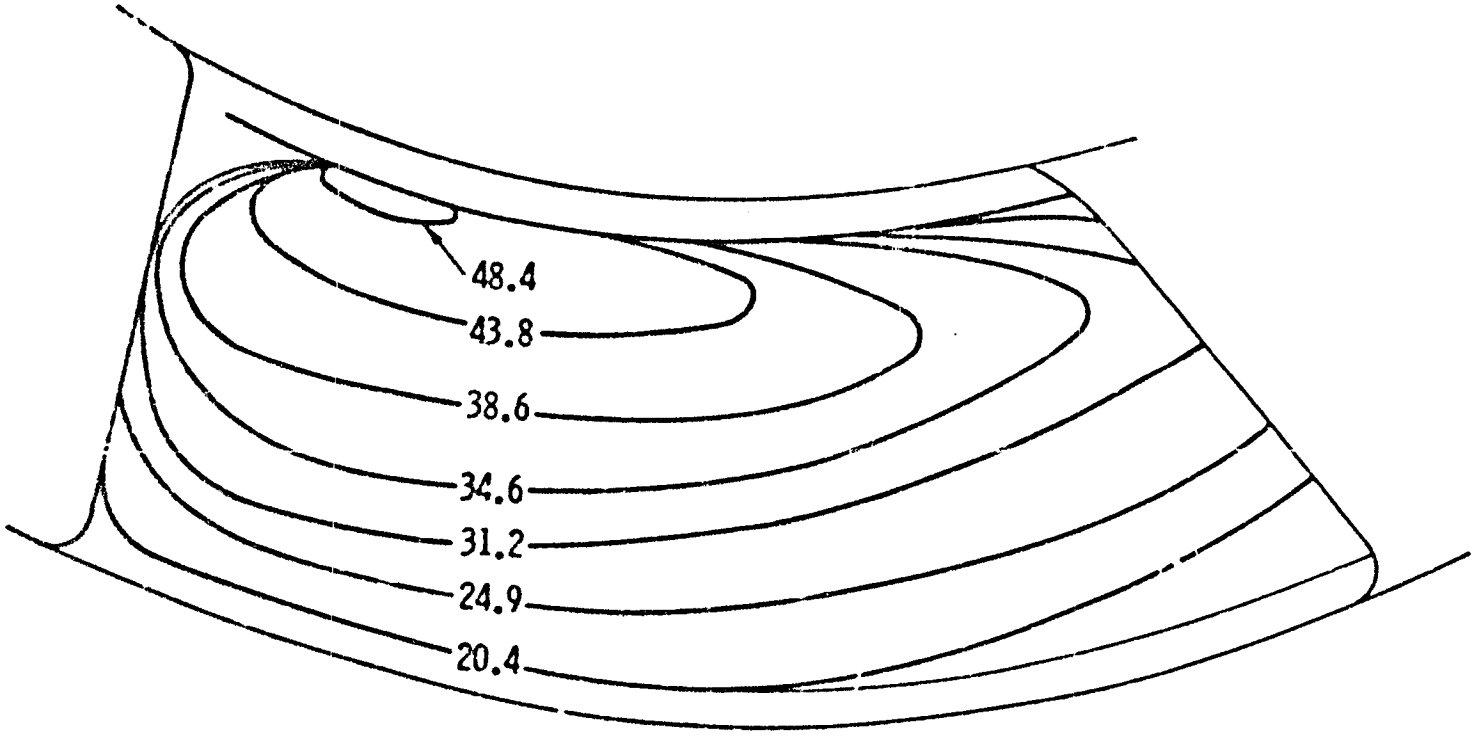

STRESS IN Ksi

The diffusion bonded impeller was spun in a vacuum at 70°F to failure which occurred at 49,000 rpm (vane tip speeds of 2560 ft/sec). This corresponds to a failure speed of 59,800 rpm (vane tip speed of 3120 ft/sec) for typical material properties at the -370°F operating temperature.

The primary mode of failure was separation of the shroud along the diffusion bond line in the impeller inlet region.

The second diffusion bonded impeller fabricated in Phase I was finish machined and installed in a Mark 29 fuel pump shown and performance of the impeller was determined in liquid hydrogen. Tests were run at flows ranging from 30 percent to 135 percent of nominal at 12,000 rpm and 80 percent to 110 percent of nominal at 24,000 and 28,000 rpm. Results of this testing are presented in the accompanying H-Q curve.

To show a comparison with the Mark 29-F performance the Rocketdyne centrifugal pump loss isolation computer program was used to allow for a diffuser matched to the diffusion bonded impeller angle of 37°. This comparison is shown and results agree closely with the test data.

MK-29 FUEL PUMP

330-414
3-71

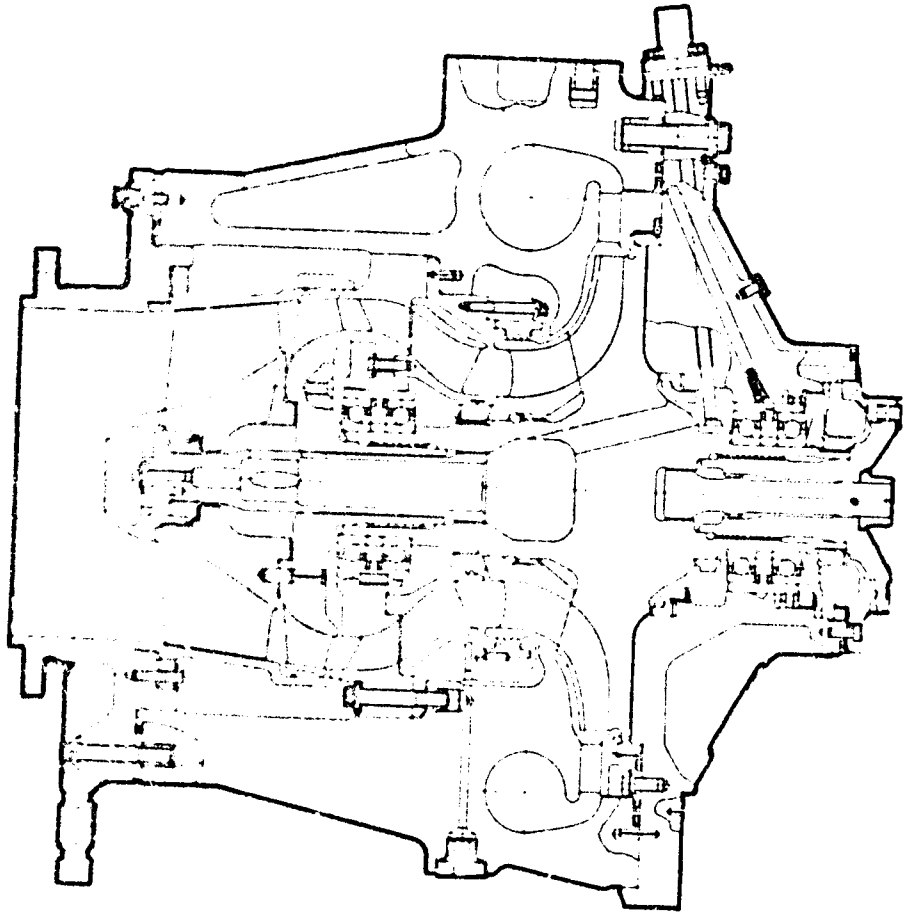

Rocketdyne
North American Rockwell

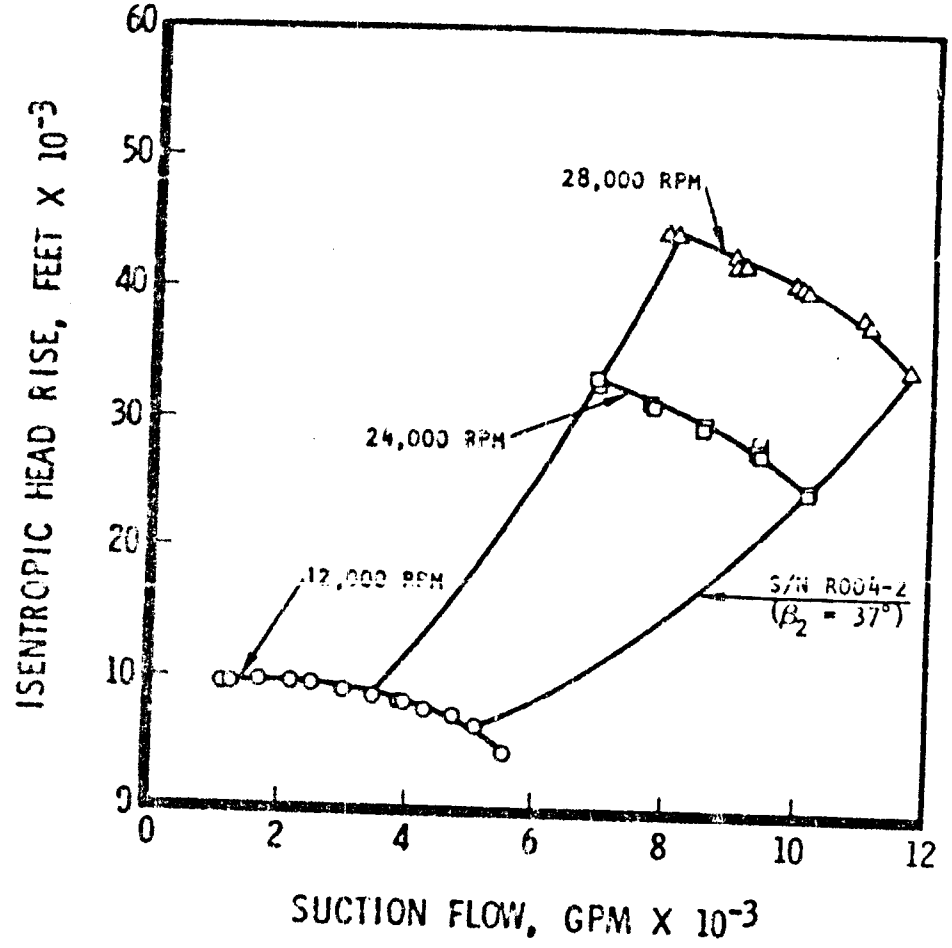

MARK 29 FUEL PUMP PERFORMANCE WITH DIFFUSION BONDED TITANIUM IMPELLER BASED ON TESTS OF PUMP

(S/N-R004 2)

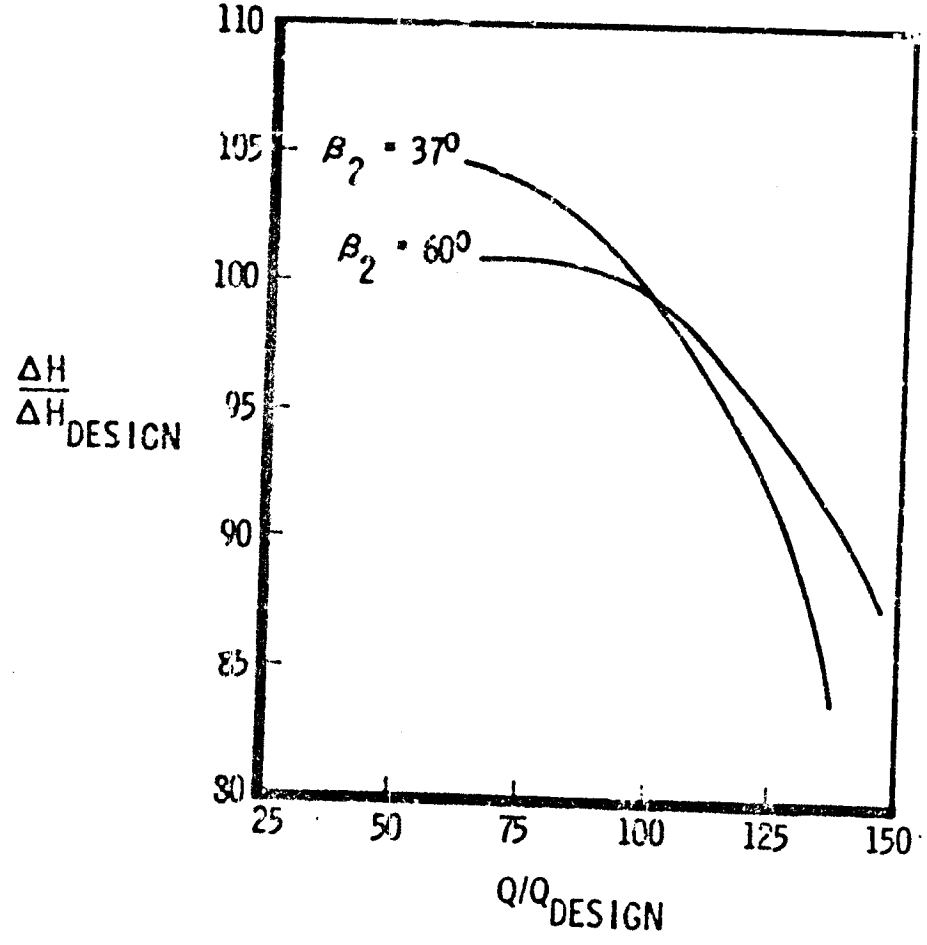

PREDICTED MK 29F PUMP PERFORMANCE

PREDICTED MK-29F PUMP PERFORMANCE WITH MARK 29F IMPELLER & DIFFUSION BONDED TITANIUM IMPELLER USING THE CENTRIFUGAL PUMP LOSS ISOLATION PROGRAM

N = 28,000 RPM

Rocketdyne
North American Rockwell

CONCLUSIONS

1. The ceramic stress coat testing indicated a significant reduction in centrifugal stresses relative to the geometrically similar two piece machined Mark 29F shrouded impeller assembly.

2. The room temperature burst test to 49,000 rpm represents a vane tip speed of 2560 ft/sec which was higher than that of the Mark 29F impeller assembly at 2510 ft/sec.

   The room temperature test corresponds to a speed of 59,800 rpm (vane tip speed of 3,120 ft/sec) for typical material properties at the -370 F operating temperature.

3. The measured H-Q performance of the diffusion bonded titanium impeller shows good agreement with predicted performance and demonstrates the practicality of this method of fabrication. This allows shrouded titanium impellers to be fabricated based on hydrodynamic considerations instead of being limited by machining methods.

"ADVANCED THRUST CHAMBER (NON-TUBULAR)"

D. L. FULTON

ROCKETDYNE

TECHNICAL MANAGER

C. D. PENN

USAF, ROCKET PROPULSION LABORATORY

TITLE: INVESTIGATION OF THERMAL FATIGUE IN NON-TUBULAR REGENERATIVELY COOLED THRUST CHAMBERS

CONTRACT: F04611-70-C-0014

AUTHORS: D. L. FULTON PROJECT DEVELOPMENT ENGINEER (ROCKETDYNE)
C. D. PENN PROJECT ENGINEER (AIR FORCE)

COMPANY: ROCKETDYNE DIVISION OF NORTH AMERICAN ROCKWELL

AIR FORCE PROJECT ENGINEER: C. D. PENN

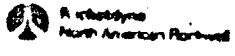

INTRODUCTION

The next generation of high performance regeneratively cooled liquid rocket engines will employ non-tubular construction. The fabricability, performance and cooling characteristics of several typical chamber materials have been demonstrated. However, one major area required of this next generation of chambers, i.e., long life, has not been explored to any depth. It is the intent of this program to analytically and experimentally evaluate this aspect of non-tubular regeneratively cooled thrust chambers with the goal of establishing an accurate analytical procedure that can be used in predicting the thermal fatigue characteristics of such chambers.

This effort, currently underway at Rocketdyne is sponsored by the Air Force Rocket Propulsion Laboratory, Edwards Air Force Base, California.

TYPICAL APPLICATIONS FOR LONG LIFE ENGINES

The primary applications for long life thrust chambers include the various engines required for the Space Transportation System. The SSME must be capable of 100 thermal cycles and 7.5 hours of operation before overhaul. The requirements for the OOS engines are 300 cycles and 10 hours of operation. The auxiliary propulsion engines are in a different regime, with life requirements of 10^6 cycles and 50 hours.

The work described in this program specifically addresses the problems of low cycle fatigue, as represented by engines with cycle requirements like those of the OOS and SSME.

TYPICAL APPLICATIONS

- ORBIT TO ORBIT SHUTTLE (OOS)
- SPACE SHUTTLE MAIN ENGINE (SSME)
- SPACE SHUTTLE AUXILIARY PROPULSION SYSTEM (APS)
- SPACE SHUTTLE ORBITAL MANEUVERING SYSTEM (OMS)

OBJECTIVE

It is the objective of this program to define design criteria for determining the thermal cycling capability of non-tubular regeneratively cooled thrust chambers. This is to be accomplished in two phases as described below:

Phase I consists of an analytical and experimental (laboratory testing) effort to establish design criteria. Included are, in depth heat transfer and structural analysis of non-tubular chambers, material property determination and isothermal fatigue testing of candidate materials. This effort will culminate in the definition of an analytical approach to predicting cyclic life capability.

Phase II will be a demonstration of the thermal fatigue capability of regeneratively cooled chambers designed using the results of Phase I. This effort consists of the fabrication, hot fire cyclic testing and post test analysis of chambers. Materials of interest for the hot gas wall of these chambers include: wrought Nickel-200, NARloy-Z, Zirconium Copper and sintered nickel.

OBJECTIVE:

DEFINE DESIGN CRITERIA FOR THERMAL CYCLING CAPABILITY ON NON-TUBULAR THRUST CHAMBERS AND DEMONSTRATE THERMAL CYCLING CAPABILITY OF SELECTED FABRICATION CONCEPTS AND MATERIALS

SCOPE:

PHASE I: DEVELOPMENT OF DESIGN CRITERIA

PHASE II: THERMAL CYCLING DEMONSTRATION

APPROACH:

PHASE I: ANALYTICAL AND EXPERIMENTAL EVALUATION OF 4 MATERIALS

PHASE II: HOT FIRE CYCLIC TEST OF 4 MATERIALS

THRUST CHAMBERS TO BE TESTED

The operational parameters and physical size of the chamber to be hot fire cyclic tested are shown on this chart. A total of four chambers, one each of the materials listed, are to be tested by the Air Force Rocket Propulsion Laboratory. A thermal cycle will consist of "on" time of three seconds steady state chamber pressure, followed by three seconds "off" with the hydrogen coolant continuing to flow.

Following testing the chambers will be returned to Rocketdyne for post test non-destructive and destructive analysis as required.

THRUST CHAMBERS TO BE HOT FIRE CYCLIC TESTED

- THRUST VACUUM LBS — 3300
- CHAMBER PRESSURE, PSIA — 750
- PROPELLANTS — O_2/H_2
- MIXTURE RATIO — 6:1
- THERMAL CYCLES (GOAL) — 750

- HOT GAS WALL MATERIALS
  - NARloy-Z
  - ZIRCONIUM COPPER
  - NICKEL 200
  - SINTERED NICKEL

- TESTING TO BE ACCOMPLISHED AT THE AFRPL

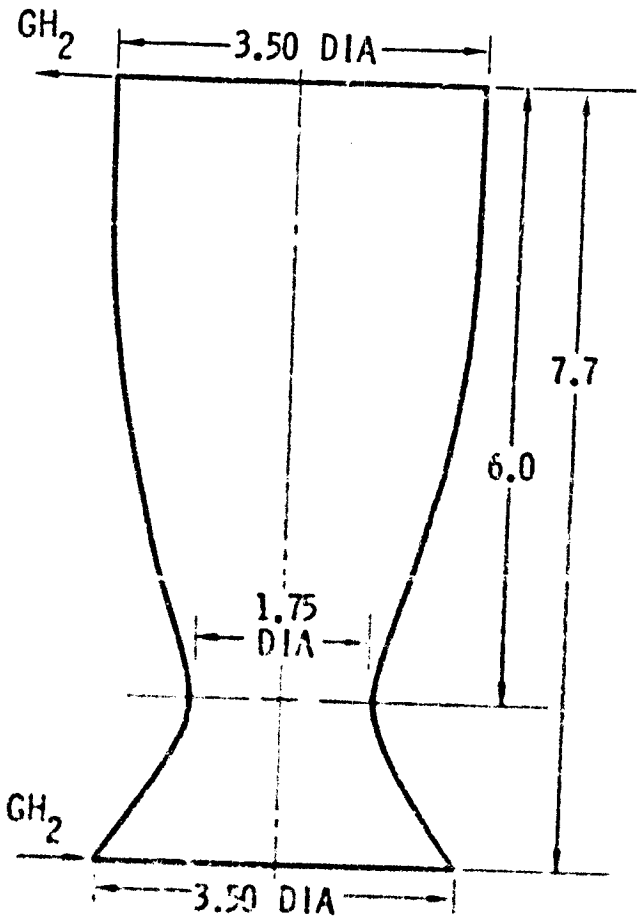

FABRICATION CONCEPTS (SPUN/MACHINED/ELECTROFORMED)

The fabrication concept used for three of the chambers to be hot cyclic tested utilizes spun and machined liners with an electroformed nickel closure.

First, a disk of the material (Nickel 200, NARloy-Z and/or Zirconium-Copper) is spun into the chamber shape. This liner is then machined on the inner and outer surfaces and longitudinal coolant passages machined into the outer surface.

An electroformed nickel closure is then deposited onto this machined liner to close out the coolant circuit and to provide the necessary structure to contain chamber pressure and to transmit thrust.

Post-electroforming machining and flange/manifold joining are accomplished followed by proof pressure testing and flow calibration of the coolant passages.

SPUN LINER WITH ELECTROFORMED NICKEL CLOSURE

327-347
2-69

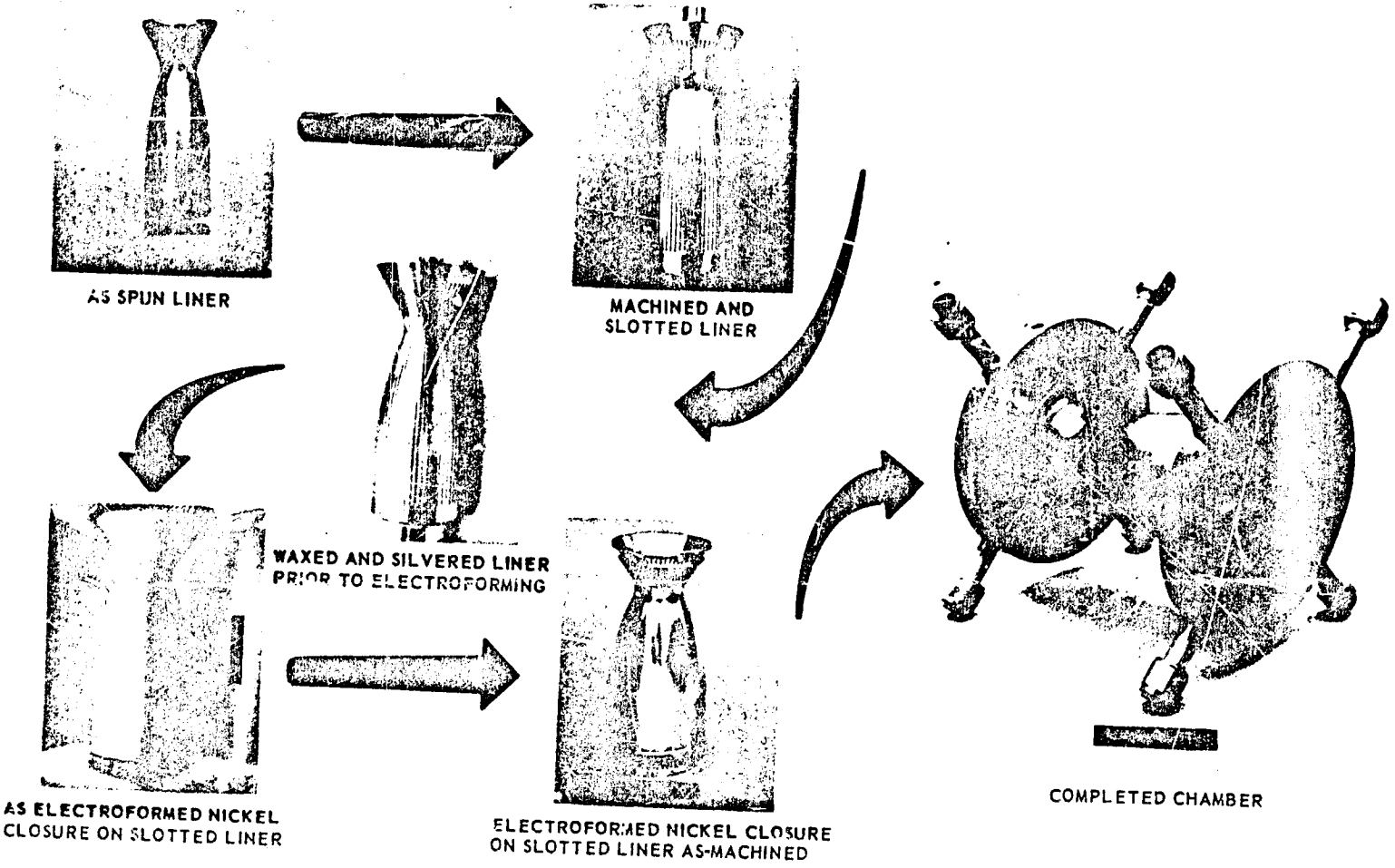

FABRICATION CONCEPTS/POWDER METALLURGY NICKEL

The fourth thrust chamber is residual hardware from Contract F04611-68-C-0061 and is fabricated using the Rocketdyne powder metallurgy process.

A special blend of pure nickel powders is pressed around a hard steel mandrel. This as-pressed liner is then machined to the prescribed thickness forming the hot gas wall of the chamber. Disposable cores, cast to the configuration of the coolant passages, are stacked around this liner and additional nickel pressed in place; forming the lands between the coolant passages and the back wall. This as-pressed body is then machined on the outer surface to prescribed dimensions, the disposable cores flushed out with hot water and steam, the internal mandrel removed and the entire unit sintered as a free standing part in the furnace. Subsequently, flanges and manifolds are attached followed by proof pressure testing and coolant passage flow calibration.

327-346
7-69

POWDER METAL NICKEL BELL CHAMBER

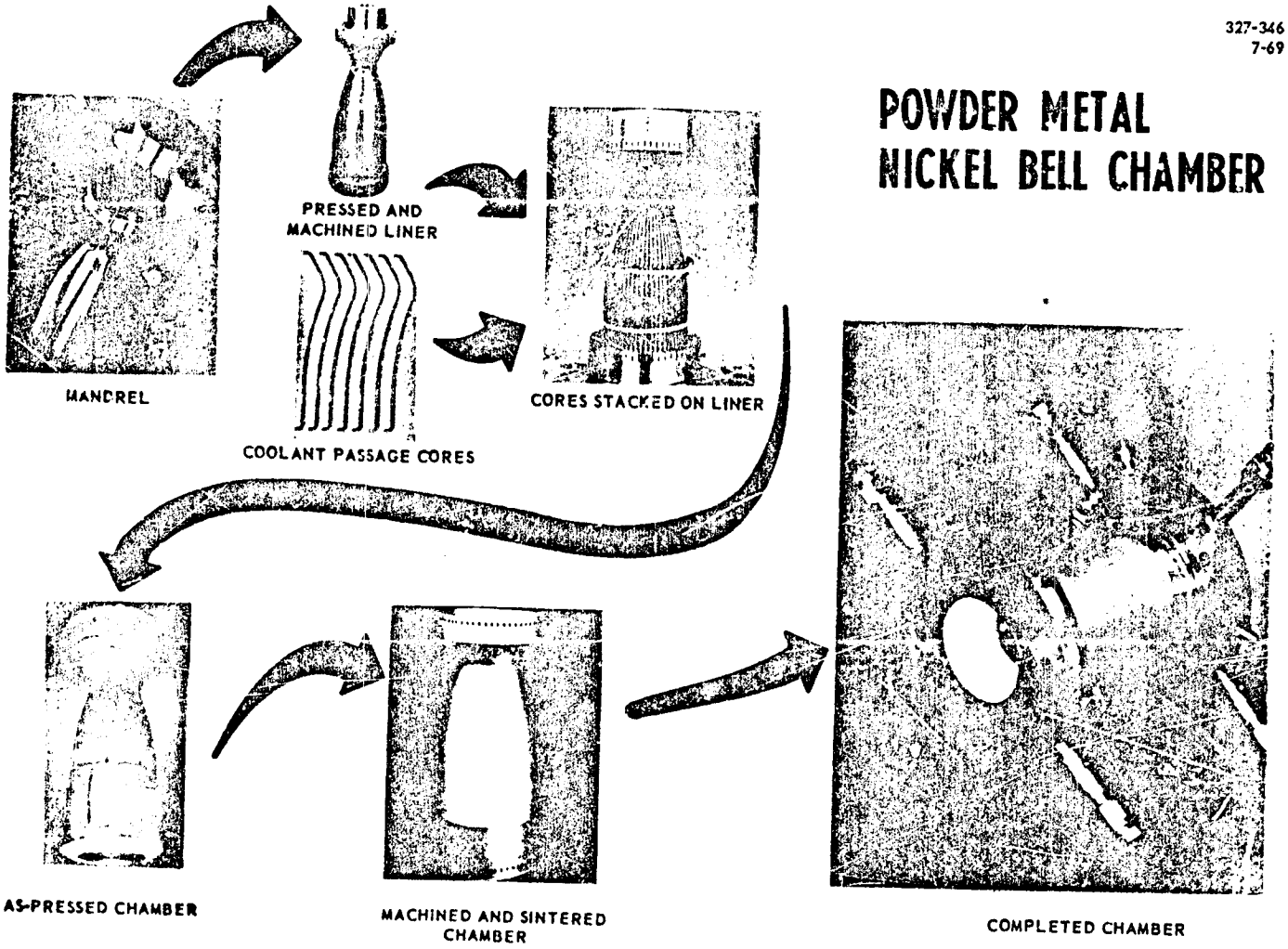

REPRESENTATIVE PARAMETERS IN NON-TUBULAR CHAMBERS

This chart depicts parameters of typical regeneratively cooled thrust chambers. Two classes of materials are represented for the hot gas wall, (1) pure nickel in wrought and sintered (fabricated by the powder metallurgy process) form with its moderate thermal conductivity and (2) copper and copper alloys with their high thermal conductivity. Heat transfer analysis has established the operating temperatures and hot gas wall thickness for a regeneratively cooled thrust chamber operating at 750 psia. Coolant is hydrogen and coolant jacket pressure drop ($\epsilon \approx 60$ to the injector end) is approximately 200 psi. These temperature differentials established a strain range of $\sim$ 1.0 percent for the copper alloy chambers and of $\sim$ 2.2 percent for the nickel chambers. This strain range is then used in the cyclic life analysis as will be shown on subsequent charts. Also, calculated was a typical strain rate for the hot gas wall, (shown to be quite high). This is based on a typical start sequence for regeneratively cooled chambers where chamber pressure and hot gas wall temperature build up to steady state values within milliseconds. Experimental laboratory tests at Rocketdyne have shown strain rate to have an effect on the cyclic life of the candidate materials. This is illustrated in a subsequent chart.

REPRESENTATIVE PARAMETERS OF REGENERATIVELY COOLED NON-TUBULAR WALL THRUST CHAMBERS

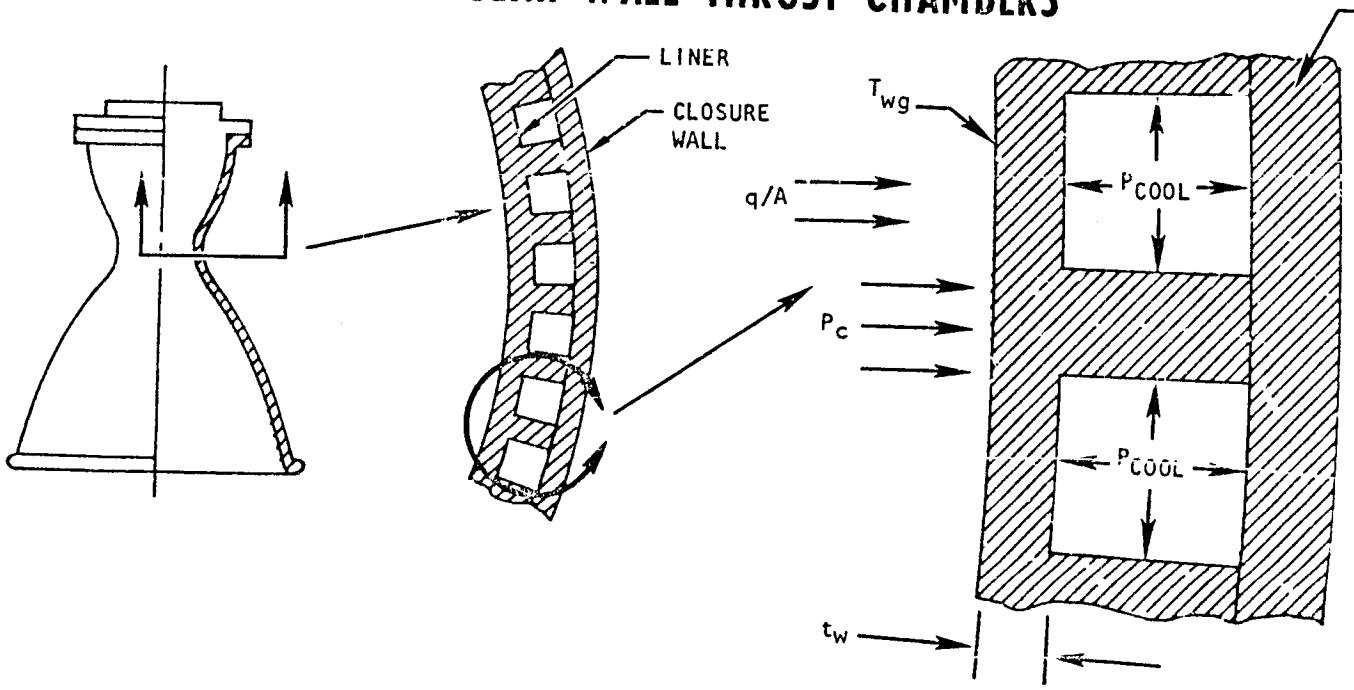

HOT GAS WALL MATERIAL	CHAMBER PRESSURE, PSIA	NO. OF CYCLES	FIRING DURATION, HOURS	HOT GAS WALL TEMPERATURE, (T_{wg}), F	CLOSURE WALL TEMPERATURE, (T_{wg}) F	STRAIN RANGE, PERCENT	STRAIN RATE, IN./IN./SEC	HOT GAS WALL THICKNESS, (t_w), IN.
NICKEL 200	750	750	5	1400 TO 1600	200 TO 300	~ 2.2	UP TO 0.2	0.020 TO 0.030
COPPER ALLOYS				800 TO 1000	350 TO 450	~ 1.0		0.030 TO 0.050

Rocketdyne
North American Rockwell

THERMAL FATIGUE LIFE ANALYSIS (SUMMARY)

The approach to analyzing a rocket engine thrust chamber for thermal fatigue life capability consists of the sequential events summarized on this chart and presented in detail on the next chart. The operational parameters of the chamber (as shown on previous chart) are used to construct structural models of the chamber as a function of station. The most critical, usually located in the throat region is then analyzed to determine its fatigue life capability. This analysis is divided into two parts, that consisting of fatigue damage (cyclic testing) and that associated with creep (time at temperature). Damage fractions of each are determined and the two summed to determine total damage. Fatigue cracking is predicted to occur when the total damage equals 1.

It should be emphasized that the analysis does not predict the service life capability of the thrust chamber but rather crack initiation on the hot gas wall. Experience has shown that non-tubular chambers can perform quite satisfactorily with cracks. Therefore, determination of the service life of a chamber is dependent on other operational factors such as performance, combustion stability, start and shutdown transients, etc. As defined in this paper, however, fatigue life capability really means until initiation of cracking.

THERMAL FATIGUE LIFE ANALYSIS

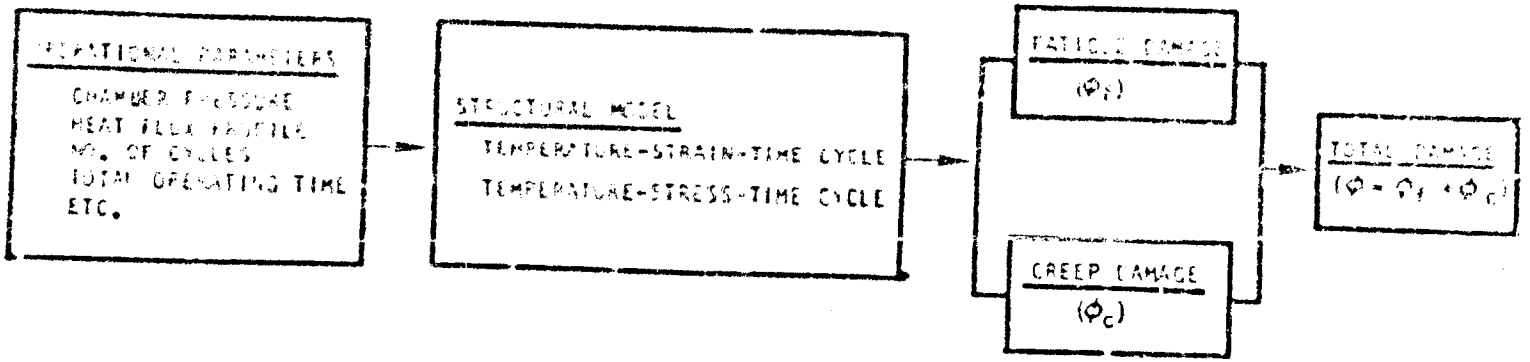

THERMAL FATIGUE LIFE ANALYSIS (DETAILED)

FATIGUE DAMAGE DETERMINATION

Initially a strain-time cycle is calculated for the hot gas wall at the most critical location by considering the hot gas wall temperature (T_{WG}), coolant side wall temperature (T_{WC}) and closure on back wall temperature (T_{WB}) (established through transient and steady state heat transfer analyses). These calculated strain values are then used to determine incremental cyclic life capability at each point in time through the use of material capability data sheets which reflect cyclic life capability as a function of strain range and temperature. These material capability data are based on experiemental isothermal fatigue data or by the use of the Universal Slopes Equation when no isothermal fatigue data are available. (Each of these are discussed in more detail in subsequent charts.) Next, the incremental damage for each thermal cycle is determined by dividing the required cyclic capability under those operating conditions by the material cyclic life capability under those conditions, as determined by the ϵ VS N_f. Finally, these damage fractions are summed up for the total duty cycle requirements of the engine as defined by operation at steady state, throttled, thrust-up and/or off mixture ratio conditions.

CREEP DAMAGE DETERMINATION

In a like manner the damage due to creep is determined by constructing predicted stress-time cycles for the hot gas wall, imputing to experimental stress rupture data and determining the incremental time damage due to creep. This is accomplished by dividing calculated time at a given stress level by the experimentally determined time to rupture at that stress level. These are then summed up for the various duty cycles that the engine is exposed to.

TOTAL DAMAGE

Total damage to the hot gas wall is then determined by summing up the damages due to fatigue and creep. When this sum equals 1, the life limit (occurrence of cracks in the hot gas wall) has been reached.

THERMAL FATIGUE LIFE ANALYSIS

329-983
3-71

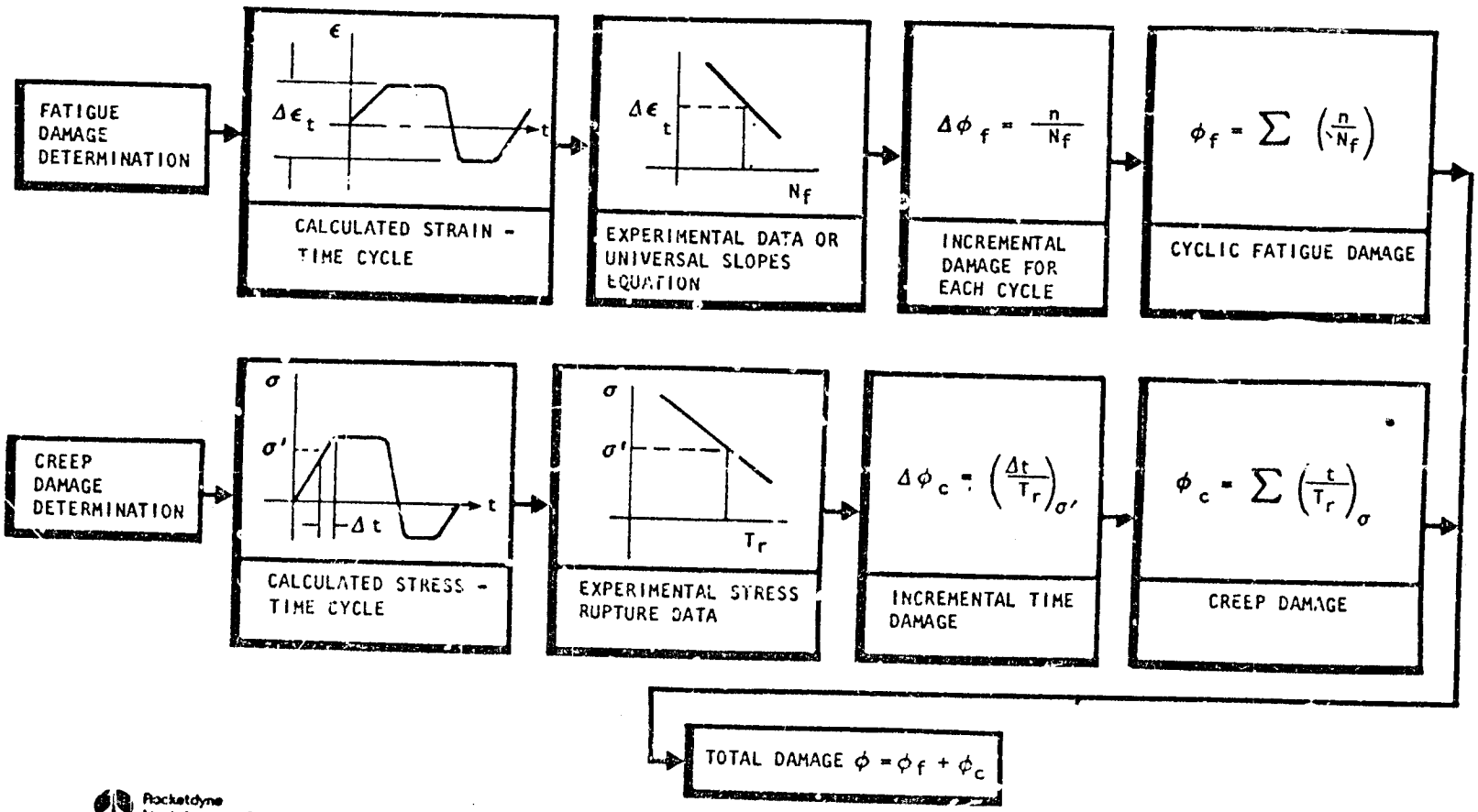

Rocketdyne
North American Rockwell

CYCLIC LIFE ANALYSIS EQUATION

Preliminary predictions of the cyclic fatigue capability of the materials of interest are made using the Universal Slopes Equation developed by Dr. Manson at NASA LeRC [1]. This equation is based on an assimilation of all available isothermal fatigue data as reported in the literature and/or measured by Dr. Manson and his associates. However, due to the variations in test techniques, specimen configuration, strain rate, etc., this equation is considered as a preliminary tool only and is currently being replaced by experimental isothermal fatigue data. These data are being generated for this program under closely controlled conditions, simulating as nearly as possible the structural and thermal environment of rocket engine thrust chambers. Test technique and specimen design are discussed in subsequent charts.

---

[1] Manson, S. S. and G. Halford; "A Method of Estimating High Temperature Low-Cycle Fatigue Behavior of Materials".

CYCLIC LIFE ANALYSIS EQUATION

UNIVERSAL SLOPES EQUATION (MANSON)

- $\epsilon_t = 3.5 \frac{\sigma_u}{E} N_f^{-.12} + D^{.6} N_f^{-.6}$

WHERE

- ϵ_t = TOTAL STRAIN RANGE
- σ_u = MATERIAL ULTIMATE TENSILE STRENGTH
- E = MODULUS OF ELASTICITY
- D = FRACTURE DUCTILITY, $\ln \frac{100}{100 - RA}$
- RA = REDUCTION OF AREA IN PERCENT
- N_f = CYCLIC LIFE

EFFECT OF OPERATIONAL PARAMETERS ON CYCLIC LIFE CAPABILITY

This chart qualitatively reflects the effect that operational parameters (chamber pressure and coolant pressure) have on cyclic life capability. For any given coolant circuit geometry (coolant channel width and hot gas wall thickness, cyclic life capability is affected by operating pressure. At low to moderate chamber pressures, damage due to creep is not sustained until high hot gas wall temperatures are experienced. However, at high chamber pressures, creep damage becomes an important part of the overall life capability at lower temperatures.

EFFECT OF OPERATIONAL PARAMETERS ON CYCLIC LIFE CAPABILITY

329-985
3-71

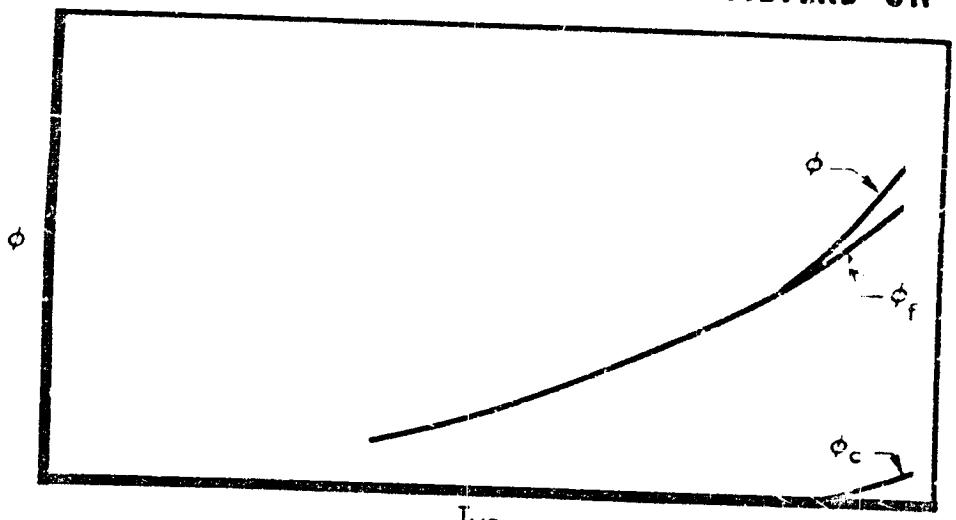

MODERATE CHAMBER PRESSURE
AND COOLANT PRESSURE

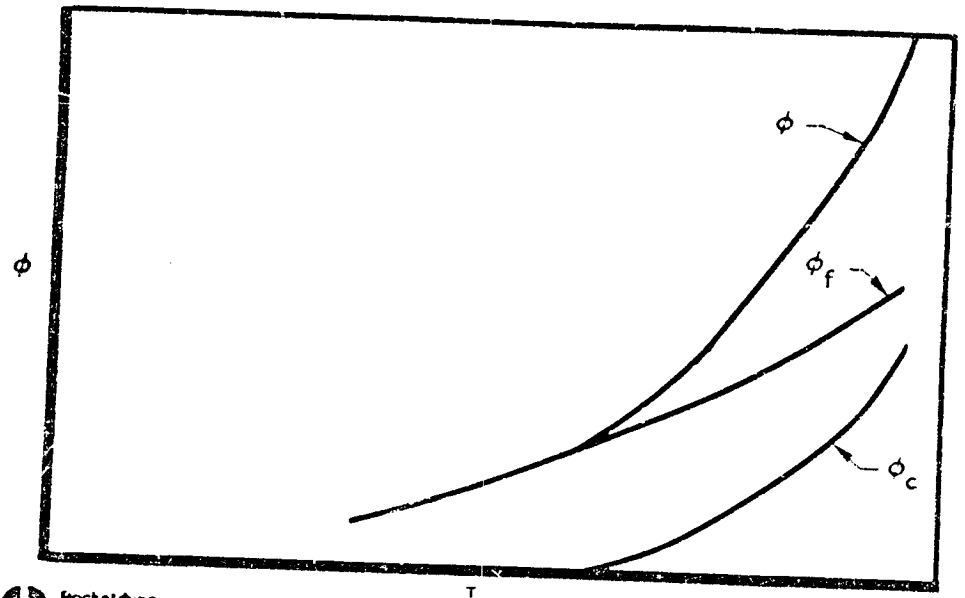

HIGH CHAMBER PRESSURE
AND COOLANT PRESSURE

Rocketdyne
North American Rockwell

TYPICAL EXAMPLE - LIFE ANALYSIS OF POINT DESIGN (THROAT PLANE)

The previous qualitative presentation is illustrated here for one of the chambers of this program. This chamber is constructed with a spun and machined NARloy-Z liner and has an electroformed nickel back wall. Analysis of this chamber (750 psia chamber pressure, 750 cycles, 5 hours life requirement) has shown that for the selected coolant channel geometry (channel width = 0.055 inches, wall thickness = 0.035 inches) no creep damage is experienced until extremely high operating temperatures ($\sim$1200 F) are reached. At the nominal operating temperature of $\sim$ 900 F, the total damage fraction is < 0.4 indicating a life capability well in excess of the design goal.

TYPICAL EXAMPLE-LIFE ANALYSIS OF POINT DESIGN (THROAT PLANE)

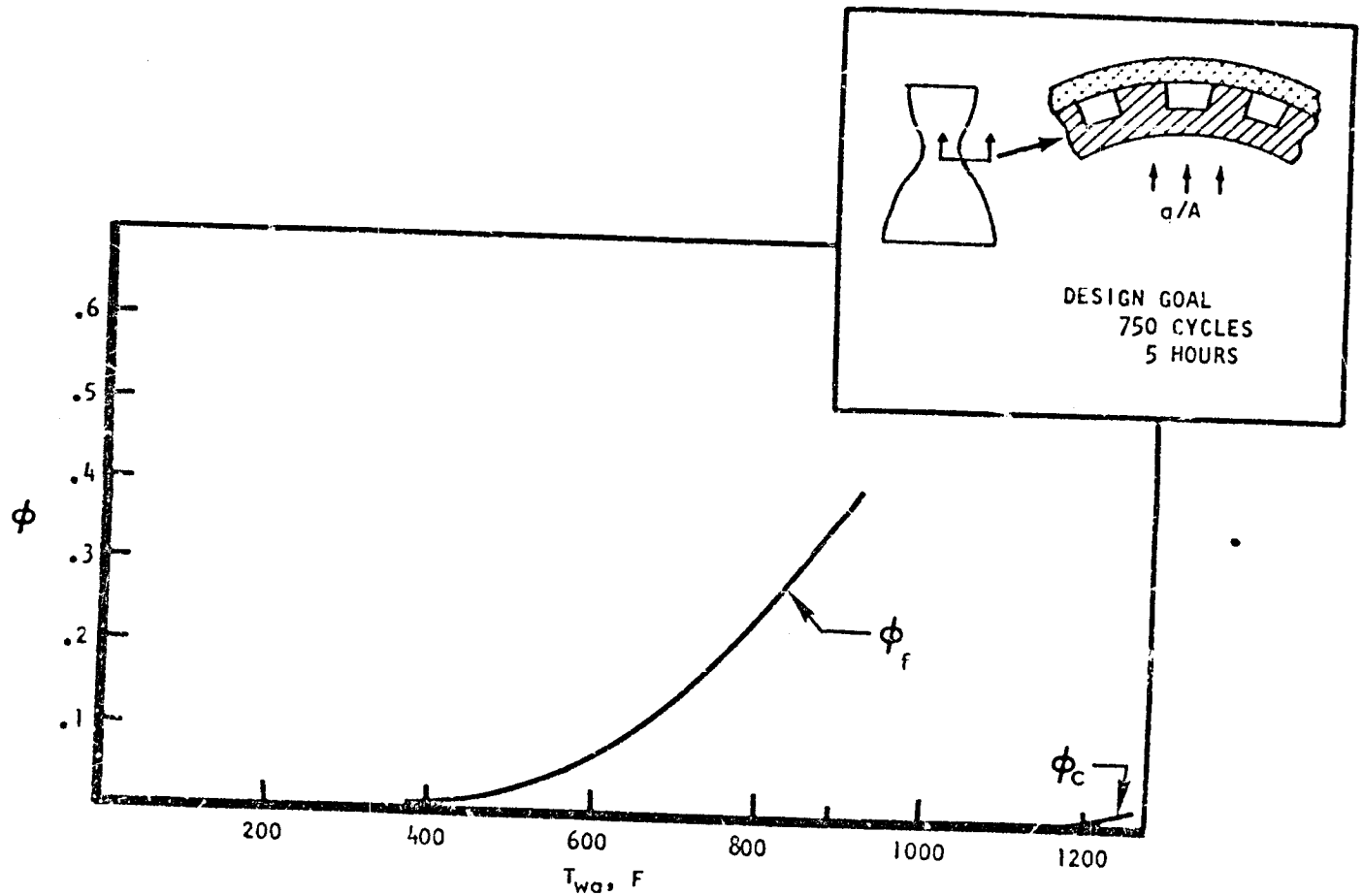

Rocketdyne
North American Rockwell

ISOTHERMAL FATIGUE TESTS

Isothermal fatigue test activity underway at Rocketdyne on this program is accomplished using the specimen shown. Button head specimens (eliminating creep which can occur with threaded specimens) are gripped in a very accurately aligned holding fixture, radiantly heated to a preselected test temperature and cyclically strained mechanically until failure. The specimens are hollow, with a wall thickness approximately equal to that of the thrust chambers; thus representing as nearly as possible the conditions a thrust chamber hot gas wall is exposed to during operation.

Strain range is determined by the use of an extensometer attached to the specimen at the "V" grooves just outside of the test gage region. The extensometer is calibrated at room temperature and 400 F by the use of strain gages attached to the specimen in the test gage specimen. A minimum of two strain gages, located 90 degrees apart are used for maximum accuracy. Temperature is determined and controlled by thermocouples on the specimen and furnace.

Direct readouts are obtained of cyclic strain range, load, temperature and machine stroke. Test variables are illustrated and explained in detail on the next chart.

ISOTHERMAL FATIGUE TESTS

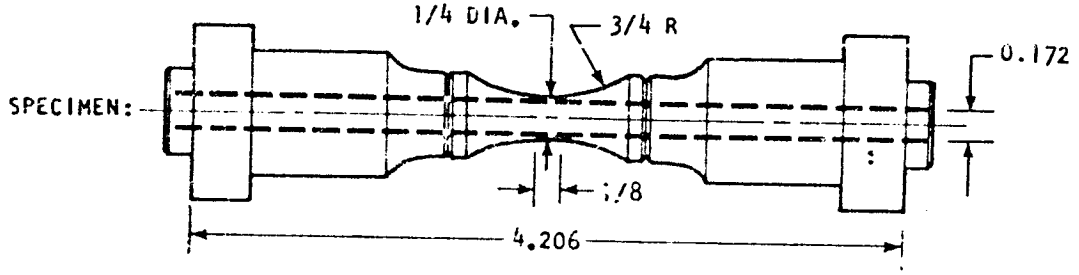

TEST CONDITION: MECHANICALLY STRAIN SPECIMEN AT SELECTED TEMPERATURE

TEST VARIABLES:

- STRAIN RANGE - 0.5 TO 2.5 PERCENT
- STRAIN RATE - 0.005 IN./IN./SEC TO 0.20 IN./IN./SEC
- HOLD TIME - COMPRESSION AND/OR TENSION (0 TO 5 MINUTES)
- TEMPERATURE - AMBIENT TO 1600 F

TEST VARIABLES - ISOTHERMAL FATIGUE TESTS

Four types of isothermal fatigue tests are being used to evaluate the effect that strain rate and creep have on the thermal fatigue characteristics of the materials being evaluated. Initially, a series of fast strain rate tests, comparable to that experienced by the hot gas wall of a regeneratively cooled thrust chamber are completed. Variables include strain range (0.5 to 2.5 percent) and temperature (ambient to 1500 F). Next, selective tests are conducted at reduced strain rate to determine any affect on life capability. These tests should prove useful in correlating isothermal fatigue data with basic material properties such as ultimate strength and reduction of area since these tests are normally conducted at very low strain rates ($\sim$0.005 in/in/sec as compared to strain rates on a thrust chamber in the range of 0.1 to 0.2 in/in/sec). The next series of tests will evaluate the effect of hold time in compression (creep) has on material life capability. This is accomplished by cycling specimens at a selected strain rate and holding for extended periods (possibly as long as 5 minutes). Hold times will be defined based on experimental strain relaxation data on each material. Finally, a limited number of tests incorporating both compression and tension hold times will be undertaken at selected strain ranges, strain rates and temperatures.

TEST VARIABLES-ISOTHERMAL FATIGUE TESTS

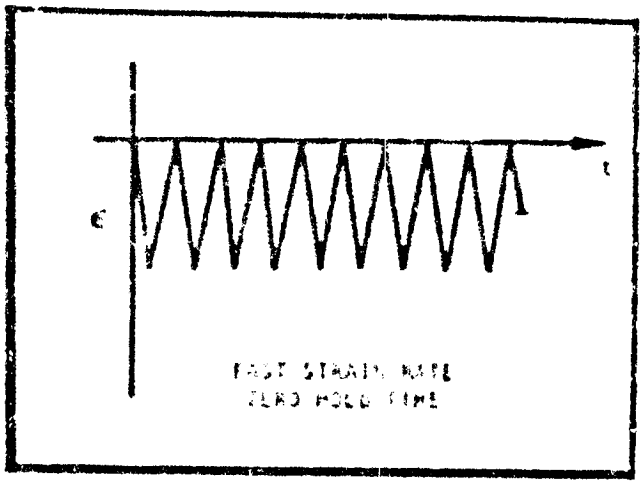

FAST STRAIN RATE
ZERO HOLD TIME

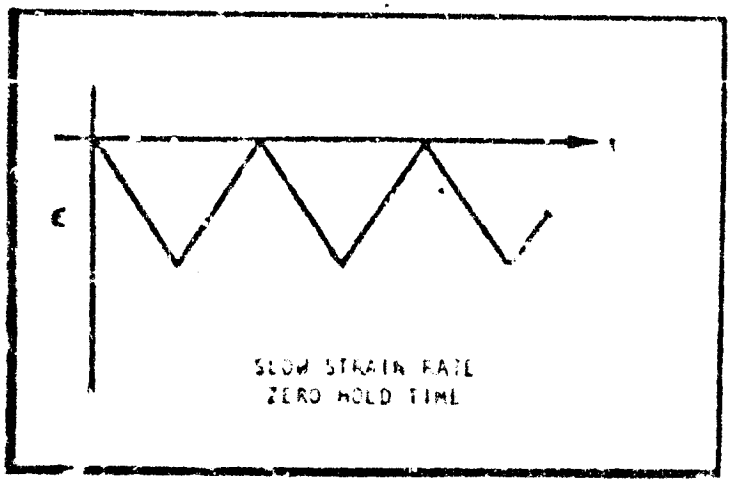

SLOW STRAIN RATE
ZERO HOLD TIME

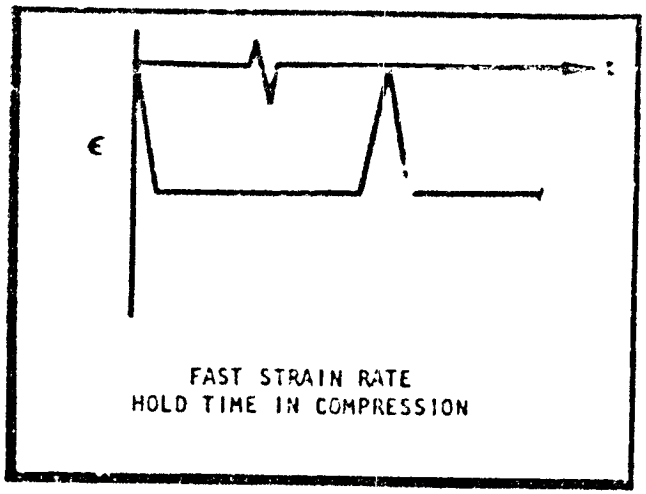

FAST STRAIN RATE
HOLD TIME IN COMPRESSION

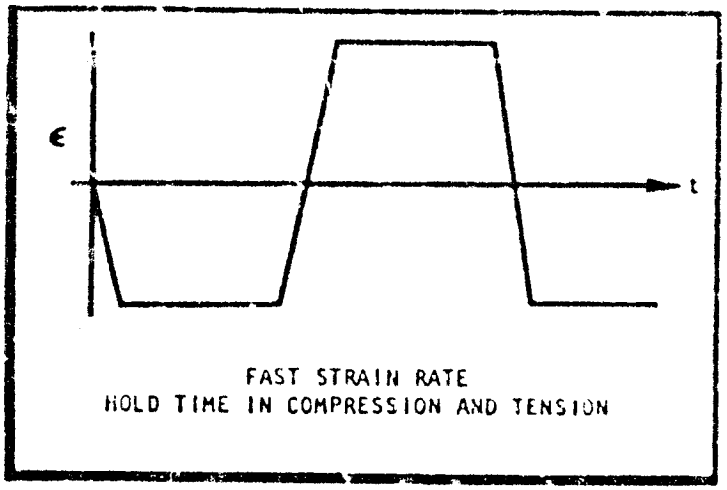

FAST STRAIN RATE
HOLD TIME IN COMPRESSION AND TENSION

Rocketdyne
North American Rockwell

TESTS CONDUCTED AT VARIOUS STRAIN RANGES AND TEMPERATURES

USE OF ISOTHERMAL FATIGUE DATA TO PREDICT FATIGUE CHARACTERISTICS

The data generated on the isothermal fatigue tests described on the previous chart will then be plotted as shown on the figure at the left to reflect N_f vs ϵ for various conditions (temperature, strain rate, with and without hold time). The walls of a regeneratively cooled thrust chamber go from some pre-fire temperature condition to elevated temperature and back down at shutoff; therefore, this data must be converted to "equivalent" temperature data for use in the life analysis. This is accomplished by analyzing and replotting the data through an incremental stress-strain-time-cycles to failure technique. These data are then used to determine the cyclic fatigue damage fraction, replacing the Universal Slopes Equation discussed previously.

USE OF ISOTHERMAL FATIGUE TEST DATA TO PREDICT THERMAL FATIGUE CHARACTERISTICS OF THRUST CHAMBERS

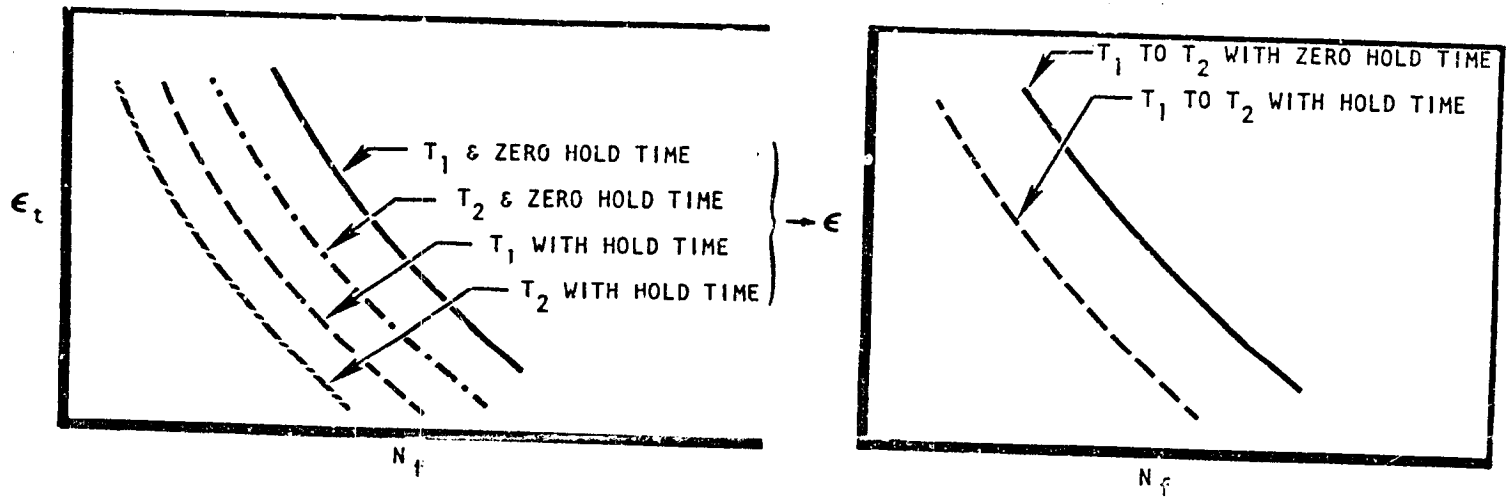

ISOTHERMAL FATIGUE DATA

EQUIVALENT THERMAL FATIGUE DATA

CONVERSION OF ISOTHERMAL FATIGUE DATA TO EQUIVALENT THERMAL FATIGUE DATA ACCOMPLISHED THROUGH INCREMENTAL ANALYSIS OF STRESS-STRAIN-TIME HISTORY

STRAIN VS CYCLES TO FAILURE

Preliminary typical isothermal fatigue data on wrought Nickel 200 are shown on this chart. These data, generated at 1400 F and for a strain range of 2 percent show the relative effect of strain rate and hold time.

Additional data on Nickel 200, sintered nickel, NARloy-Z and Zirconium Copper are currently being generated.

STRAIN vs CYCLES TO 10% LOAD DROP

Ni 200 AT 1400 F, $\Delta\epsilon_t = 2\%$

329-990
3-71

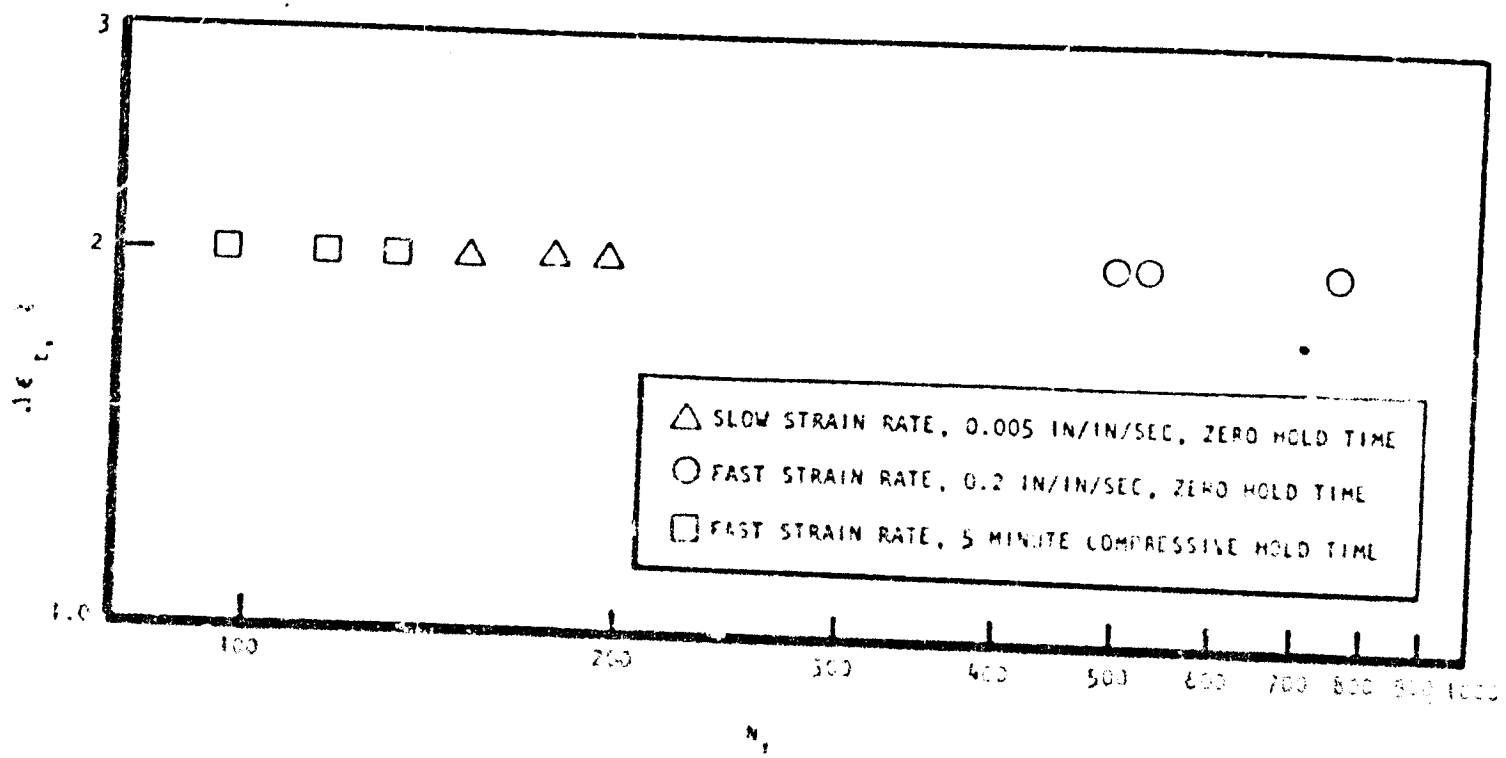

SUMMARY

The analytical and laboratory test effort are continuing on all four materials. Thrust chambers of each are to be hot fire cyclic tested at the AFRPL later this year. Goal is to accumulate 750 thermal cycles on each and to use these results along with the isothermal fatigue data and basic materials property data to finalize the analytical technique for predicting thrust chamber cyclic life capability.

SUMMARY

- ANALYTICAL EFFORT IS CONTINUING AND WILL BE FINALIZED USING LABORATORY TEST DATA AND HOT FIRING RESULTS
- LABORATORY EFFORT (ISOTHERMAL FATIGUE TESTS) UNDERWAY AND YIELDING HIGHLY SATISFACTORY RESULTS
- HOT FIRE TESTING EFFORT PLANNED FOR SPRING AND SUMMER OF 1971 (TEST AT AFRPL).

"HIGH PRESSURE HYDROGEN EFFECTS ON MATERIALS"

W. Mc PHERSON

MARSHALL SPACE FLIGHT CENTER

HIGH-PRESSURE HYDROGEN EFFECTS ON METALS

By

W. B. McPHERSON

MATERIALS DIVISION

MARSHALL SPACE FLIGHT CENTER

FIGURE 1

Until recently, high-pressure gaseous hydrogen (GH_2) at room temperature was not recognized widely as an aggressive environment on metals. The influence of the GH_2 environment is more readily observed by a reduction of strength in the notched tensile tests. As illustrated in the table for the ratio of notched strength in hydrogen to that in helium, the degree of embrittlement or degradation generally increases as the strength of the alloy increases. Alloys could be classified as severely embrittled, including the high strength steels and high strength nickel alloys; moderately embrittled, covering the structural steels, pure nickel, and titanium alloys; and slightly embrittled, including pure titanium, nonstable austenitic stainless steel, and beryllium copper. Hydrogen had almost no influence on stable austenitic stainless steel, precipitation hardened austenitic stainless steel, aluminum alloys, and OFHC copper.

NOTCHED STRENGTH RATIO (H_2/He) FOR VARIOUS ALLOYS IN 10,000 PSI HYDROGEN AT 77°F (25°C)

250 MARAGING STEEL — 0.12

410 S.S. — 0.22

1042 Q&T — 0.22

17-7 PH (TH 1050) — 0.23

Fe-9Ni-4Co — 0.24

H-11 STEEL — 0.25

RENE 41 — 0.27

EF NICKEL — 0.31

4140 STEEL — 0.40

INCONEL 718 — 0.46

440C S.S. — 0.50

Ti-6Al-4V STA — 0.58

430F S.S. — 0.68

NICKEL 270 — 0.70

A515-G70 STEEL — 0.73

HY 100 STEEL — 0.73

A372-IV STEEL — 0.74

1042 (NORMALIZED) — 0.75

A517-F (T-1 STEEL) — 0.77

A533-B STEEL — 0.78

Ti-6Al-4V (ANN.) — 0.79

1020 STEEL — 0.79

HY 80 STEEL — 0.80

Ti-5Al-2.5Sn — 0.81

ARMCO IRON — 0.86

304L S S — 0.87

305 S S — 0.89

Be Cu (ALLOY 25) — 0.93

310 S S — 0.93

TITANIUM C P — 0.95

A-286 S S — 0.97

7075 T73 AL — 0.98

6061-T6 AL — 1.00

1100 0 AL — 1.00

OFHC COPPER — 1.00

316 S S — 1.00

IGURE 2

Property degradation in the GH_2 environment is dependent on two variables - pressure and temperature, as illustrated in Figure 2 for electroformed (EF) nickel, the notched strength decreases as the GH_2 pressure increases. This variation with pressure also depends somewhat on the specific alloy and strength level of the alloy.

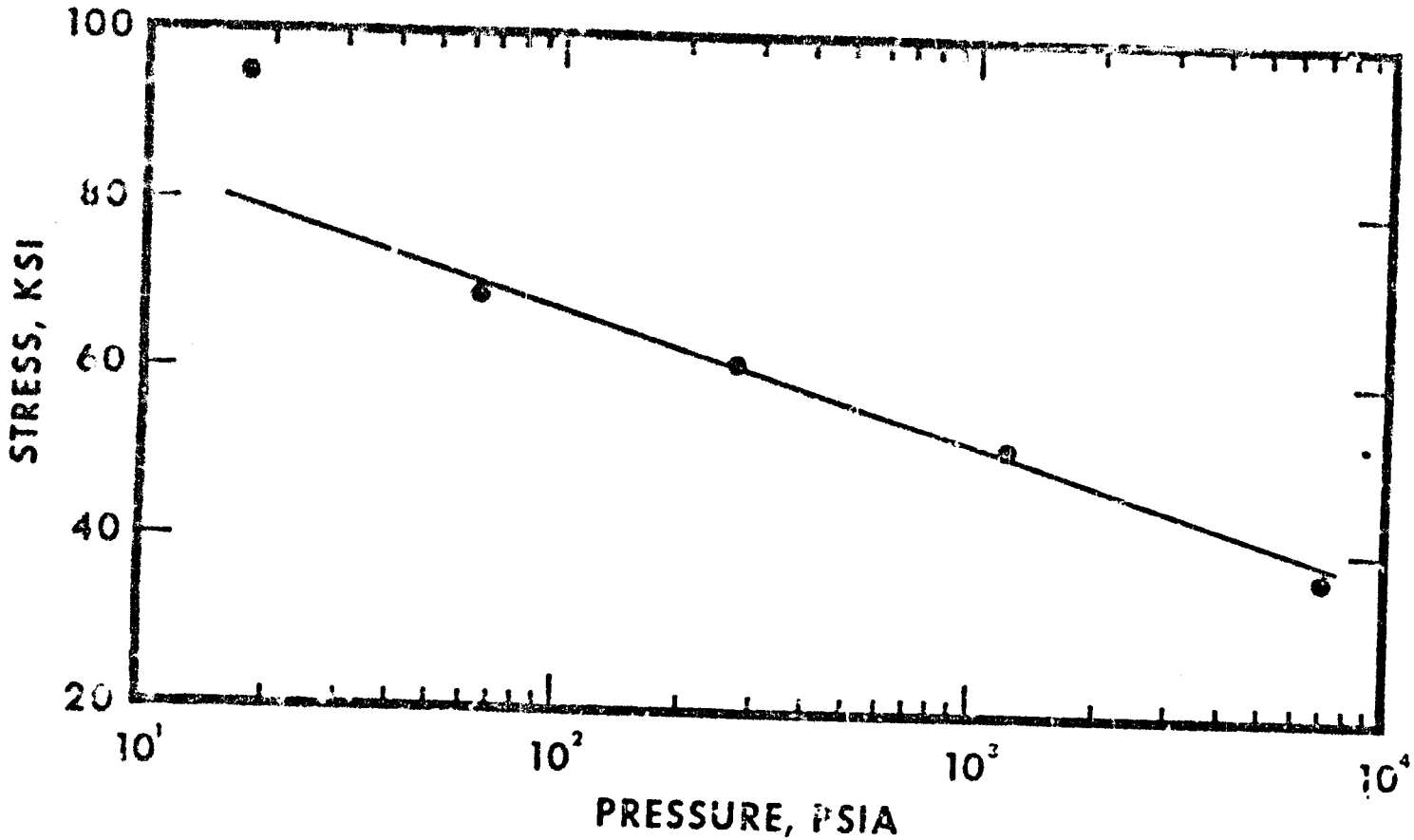

NOTCHED STRENGTH (K_t=6) VS H_2 PRESSURE FOR EF NICKEL

FIGURE 3

As illustrated by the notched strength of EF nickel tested in 1200 psi GH_2, the maximum reduction of strength occurs at room temperature. The low temperature at which GH_2 ceases to influence strength seems to be between -300°F and -200°F for most alloys. The elevated temperature at which this occurs depends upon the specific alloy.

Exposure time has not been overlooked although this variable has been held constant in the recent GH_2 environment test programs. Generally, the maximum reduction in notch strength has been obtained when the test is begun as soon as the test chamber is pressurized. This does not necessarily mean than longer exposure times may not influence some of the alloys, but it does show that the mere presence of the GH_2 environment is sufficient to cause degradation.

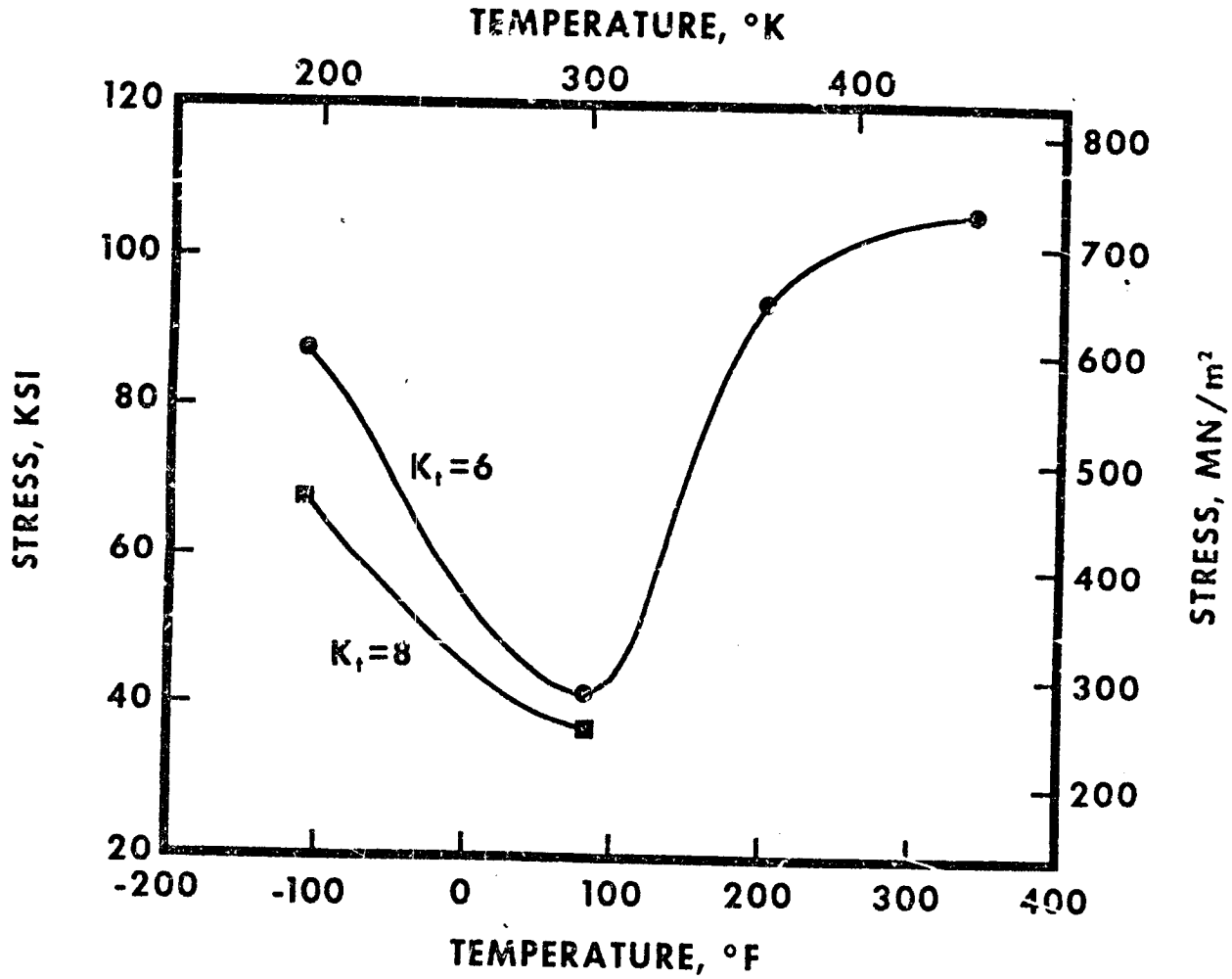

NOTCHED STRENGTH VS TEMPERATURE FOR EF NICKEL IN 1200 psi H_2

FIGURE 4

A few investigations on GH_2 purity have shown that somewhat less than 1 percent oxygen will inhibit the deleterious effect of GH_2. Propellant grade LH_2 used in rocket engines has less than 1 ppm oxygen which would produce almost a maximum aggressiveness for the GH_2 environment at room temperature. Since introduction of oxygen into a GH_2 system for inhibition may not be desirable, a few coatings have been investigated to act as protective surfaces in the GH_2 environment. As illustrated in the accompanying table, copper and gold coatings on EF nickel fully restored the ductility of smooth tensile specimens. In the case of the notched tests, the specimens did not recover their complete strength; however, the coated specimens were almost three times the strength of the uncoated ones.

ELECTROFORMED NICKEL
ROOM TEMPERATURE TESTS

ENVIRONMENT	ULTIMATE STRENGTH KSI	RA %	REMARKS
	SMOOTH TENSILE		
AIR	76	65	AS PLATED
He 1200	78	90	AS PLATED
H_2 1200	71	50	AS PLATED
H_2 1200	76	90	.0012 Cu
H_2 1200	77	89	.003 Au
	NOTCHED TENSILE (K_t=6)		
AIR	124		AS PLATED
H_2 1200	42		AS PLATED
AIR	138		.005 Cu
H_2 1200	106		.003 Cu
H_2 1200	113		.003 Au

FIGURE 5

On an experimental cast copper alloy rocket engine combustion chamber, EF nickel is used to close the hydrogen cooling channels. Small samples of the copper alloy were made with 2-inch long slots to investigate the effectiveness of a thin copper barrier to protect the EF nickel from the GH_2 environment. The results of the burst tests are listed in the accompanying table. The burst pressure of unprotected EF nickel is reduced 80% by the GH_2. Although the copper was beneficial, it does not completely inhibit the degradation by GH_2. For GH_2 service, components either must be designed to account for the strength reduction by GH_2 or a less susceptible alloy used.

SIMULATED CHANNEL BURST TESTS

PLATING THICKNESS, INCH	BURST PRESSURE, PSI
WATER	
.040 Ni	16,000
.012 Cu + .050 Ni	14,200 *
.020 Cu + .050 Ni	15,100 *
HYDROGEN	
.040 Ni	2,950
.005 Cu + .035 Ni	6,200
.012 Cu + .033 Ni	8,200
.030 Cu + .010 Ni	7,550
.012 Cu + .050 Ni	8,300 *
.020 Cu + .050 Ni	11,400 *

* 1 SLOT, .365 WIDE. ALL OTHERS, 2 SLOTS .165 WIDE

FIGURE 6

In a high-pressure hydrogen-oxygen rocket engine such as the type being developed for the space shuttle, the turbomachinery is driven by hot gases composed of hydrogen and water vapor. It was anticipated that the water vapor might act as an inhibitor. As illustrated by limited notched tensile tests on Udiment 700 nickel alloy, this is not the case. The 5% improvement promoted by the water vapor is not very significant considering the total strength reduction.

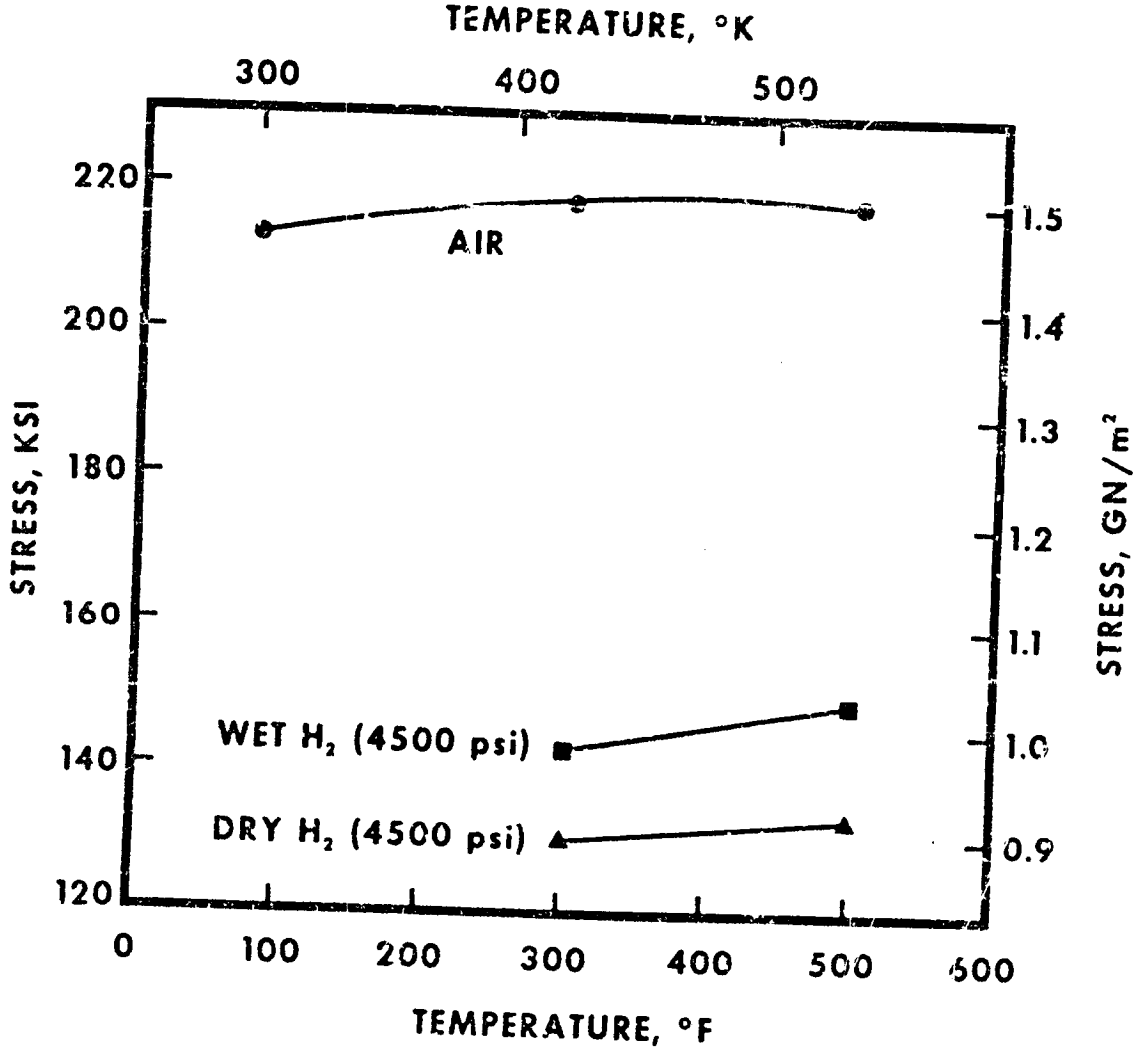

NOTCHED STRENGTH (K_t=8) VS TEMPERATURE FOR UDIMET 700

SUMMARY

DEGREE OF GH_2 DEGRADATION:

- INCREASES WITH GH_2 PRESSURE
- MAXIMUM NEAR ROOM TEMPERATURE
- INCREASES WITH GH_2 PURITY
- INDEPENDENT OF TIME IN THE ENVIRONMENT